



# UNIVERSIDAD NACIONAL AUTÓNOMA DE MÉXICO

---

---

## PROGRAMA DE POSGRADO EN CIENCIAS DE LA TIERRA

ESTUDIO GEOLÓGICO-ESTRUCTURAL TECTÓNICO DEL ÁREA DE XAYACATLÁN  
DEL COMPLEJO ACATLÁN, PUEBLA, SUR DE MÉXICO

### T E S I S

QUE COMO REQUISITO PARCIAL PARA OBTENER EL GRADO DE:  
DOCTOR EN CIENCIAS DE LA TIERRA

P R E S E N T A

MIGUEL MORALES GÁMEZ

#### JURADO EXAMINADOR

DIRECTOR DE TESIS: DR. JOHN DUNCAN KEPPIE  
PRESIDENTES: DR. GUSTAVO TOLSON JONES  
VOCAL: DR. JESÚS SOLÉ VIÑAS  
SUPLENTE: LUIGI SOLARI LOVATI  
SUPLENTE: MICHELANGELO MARTINI

#### COMITÉ TUTORAL:

DR. JOHN DUNCAN KEPPIE  
DR. FERNANDO ORTEGA GUTIÉRREZ  
DR. GUSTAVO TOLSON JONES  
DRA SUSANA ALANIZ ÁLVAREZ  
DR MARIANO ELÍAS HERRERA



**UNAM – Dirección General de Bibliotecas**

**Tesis Digitales**  
**Restricciones de uso**

**DERECHOS RESERVADOS ©**  
**PROHIBIDA SU REPRODUCCIÓN TOTAL O PARCIAL**

Todo el material contenido en esta tesis está protegido por la Ley Federal del Derecho de Autor (LFDA) de los Estados Unidos Mexicanos (Méjico).

El uso de imágenes, fragmentos de videos, y demás material que sea objeto de protección de los derechos de autor, será exclusivamente para fines educativos e informativos y deberá citar la fuente donde la obtuvo mencionando el autor o autores. Cualquier uso distinto como el lucro, reproducción, edición o modificación, será perseguido y sancionado por el respectivo titular de los Derechos de Autor.

### **Agradecimientos:**

Los estudios de doctorado se realizaron mediante una beca otorgada por el Consejo Nacional de Ciencia y Tecnología, así como parte del proyecto CB-2005-1: 24894, y del Programa de Apoyo a Proyectos de Investigación e Innovación Tecnológica (IN100108-3), y a una beca otorgada por el Instituto de Geología de la UNAM, para la culminación de los estudios.

Quiero agradecer de manera especial al Dr John Duncan Keppie Morehouse le agradezco su tutoría, apoyo y conocimientos, dado que con él aprendí mucha de la bastedad de la geología estructural y tectónica, además de otras áreas del conocimiento geológico.

La revisión final de este trabajo estuvo a cargo de los doctores J. Duncan Keppie M., Gustavo Tolson Jones, Luigi A. Solari Lovati, Jesús Solé Viñas y Michelangelo Martini a quienes quiero agradecer el tiempo invertido, así como las sugerencias y recomendaciones propuestas, las cuales desde luego sirvieron para mejorar substancialmente este trabajo.

Este trabajo fue culminado gracias a la ayuda, crítica, recomendaciones y apoyo de los distintos revisores que tuve a lo largo de mis estudios de doctorado en el posgrado de Ciencias de La Tierra, con sede en el Instituto de Geología, los doctores Fernando Ortega Gutiérrez, Gustavo Tolson Jones, Luigi A. Solari Lovati, Susana A. Alaniz Álvarez, Mariano Elías Herrera y J. Duncan Keppie M., fueron insustituibles en mi formación académica.

Quiero agradecer también los colaboradores en los diferentes artículos publicados que se desprendieron de la investigación y que forman parte de esta tesis.

El trabajo de campo fue más divertido con el apoyo de mis amigos y compañeros del Instituto de Geología a quienes quiero agradecer su compañía, especialmente a Judith Callejas, Mario A Ramos, Diana Medina, Héctor Hinojosa. El trabajo de laboratorio fue más eficiente con los consejos de Barbara Martiny y Consuelo Macías.

Quiero agradecer además a Rosario Flores Ramos y Francisco Montaño Coahuilaz, del área de cómputo, quienes además de brindarme su amistad, también me apoyaron durante toda mi estancia como estudiante en el Instituto de Geología. A los doctores Gustavo Tolson, Elena Centeno, Pedro Corona y a la maestra Aida López que con su apoyo y amistad fueron de mis maestros más estimados durante mi estancia en el posgrado y en otras instancias académicas.

Por otra parte quiero agradecerles a mis amigos del posgrado, Hortencia C. Flores Estrella, Pedro Arredondo, Osbaldo Zamora, Araceli Zamora, Edgar Ángeles, Beatriz A. Díaz, Carlos Ortega, Alejandra Aguilar, Rosalva Pérez, Guillermo Hernández.

Especialmente quiero agradecer a mi familia, mis hermanos, Alejandra, Teresa, Luis Manuel, Leticia, Angélica, y a mis sobrinos, así como a Roberto Cira, dado que sin ellos mis estudios hubieran sido muy complicados, a Ofelia Gámez y Miguel Morales, que me dieron su apoyo desde siempre y ahora donde quiera que se encuentren lo siguen haciendo.

A todos muchas gracias, les debo demasiado ....



## ÍNDICE

<b>Índice</b>	<i>i</i>
<b>Índice de figuras</b>	<i>v</i>
<b>Índice de tablas</b>	<i>xi</i>
<b>Resumen</b>	1
<b>Abstract</b>	3
<b><u>INTRODUCCIÓN</u></b>	5
<b>Descripción de las rocas cartografiadas en la región de Xayacatlán</b>	15
<b>Rocas meta-sedimentarias paleozoicas</b>	15
<i>Unidad Amate</i>	15
<i>Unidad Huerta</i>	17
<i>Unidad Salada</i>	19
<i>Formación Tecomate</i>	20
<b>Rocas meta-ígneas paleozoicas</b>	21
<i>Enjambre de diques Xayacatlán</i>	21
<i>Pegmatitas</i>	22
<i>Diques toleíticos en la unidad Salada</i>	23
<i>Lacolito de Totoltepec</i>	23
<b>Rocas mesozoicas</b>	23
<i>Conglomerado Jurásico</i>	23
<i>Rocas calcáreas</i>	24
<b>Rocas cenozoicas</b>	24
<b><u>Las hipótesis de la evolución geológica en el área de Xayacatlán</u></b>	25
<b>Hipótesis uno</b>	25
<b>Hipótesis dos</b>	25
<b>CAPÍTULO UNO</b>	
<b>Margen pasivo y rift Odovícico-Silúrico en la margen mexicana del océano Rheico sobrejacida por rocas de periarco del Carbonífero-Pérmino: Evidencia en el oriente del Complejo Acatlán, sur de México</b>	27
<b>Resumen</b>	27
<b>1. Introducción</b>	27
<b>2. Área de Xayacatlán</b>	32
<b>2.1. Unidad Huerta (nuevo nombre)</b>	32
<b>2.2. Unidad Amate (nuevo nombre)</b>	32
<b>2.3. Unidad Salada (nuevo nombre)</b>	34
<b>2.4. Formación Tecomate</b>	34
<b>2.5. Lacolito de Totoltepec</b>	34

<i>2.6. Conglomerado jurásico</i>	36
<b>3. Análisis de circones por LA-ICPMS</b>	38
<i>3.1. Procedimiento analítico</i>	38
<b>4. Resultados</b>	38
<b>5. Límites en las edades de las nuevas unidades</b>	39
<i>5.1. Unidad Huerta</i>	39
<i>5.2. Unidad Amate</i>	40
<i>5.3. Unidad Salada</i>	40
<b>6. Procedencia de los circones detriticos</b>	41
<i>6.1. Terminología</i>	42
<b>7. Discusión</b>	43
<b>Agradecimientos</b>	45
<b>Referencias</b>	45
<b>CAPÍTULO DOS</b>	
<b>Diques toléticos del Carbonífero en la Unidad Salada, Complejo Acatlán, sur de México: un registro de extensión en la margen oeste de Pangea</b>	47
<b>Abstract</b>	47
<b>Resumen</b>	47
<b>Introducción</b>	48
<b>Marco geológico</b>	48
<b>Petrografía</b>	50
<b>Geoquímica</b>	50
<b>Discusión</b>	53
<b>Agradecimientos</b>	54
<b>Referencias</b>	55
<b>CAPÍTULO TRES</b>	
<b>Estructuras paleozoicas en el área de Xayacatlán, Complejo Acatlán, sur de México: rift transtensional y deformación relacionada a subducción a lo largo de la margen de Oaxaquia</b>	57
<b>Resumen</b>	57
<b>Introducción</b>	57
<b>Complejo Acatlán</b>	59
<b>Área de Xayacatlán</b>	60
<b>Estructura</b>	63
<i>Fábricas en los diques máficos Xayacatlán ca. 442 Ma y zonas adyacentes (<math>S_A</math>, <math>L_X</math> y <math>F_X</math>)</i>	63
<i>Fábricas en la Unidad Amate (<math>S_A</math>, <math>L_A</math> y <math>F_A</math>)</i>	64
<i>Fábricas en las unidades Huerta y Salada (<math>S_{HS}</math>, <math>L_{HS}</math> y <math>F_{HS}</math>)</i>	65
<i>Fábricas en la formación Tecomate (<math>S_T</math>, <math>L_T</math> y <math>F_T</math>)</i>	66

<i>Fábricas en el intrusivo Totoltepec (<math>S_{Ti}</math>)</i>	69
<b>Geocronología <math>^{40}\text{Ar}/^{39}\text{Ar}</math></b>	69
<i>Métodos analíticos</i>	69
<i>Resultados e interpretación</i>	70
<i>Correlación y límites de edad en las fábricas del Paleozoico tardío</i>	76
<i>Conclusiones</i>	76
<b>Agradecimientos</b>	77
<b>Referencias</b>	79
<b>CAPÍTULO CUATRO</b>	
<b>Toleitas de rift Ordovícico-Silúrico temprano en el Complejo Acatlán, sur de México:</b>	
<b>Evidencias de rifting en la margen sur del océano Rheico</b>	82
<i>Resumen</i>	82
<b>1. Introducción</b>	82
<b>2. Marco geológico</b>	84
<i>2.1. Área de Xayacatlán</i>	86
<i>2.2. Área de Patlanoaya</i>	86
<i>2.3. Área de Cuaujote</i>	88
<b>3. Geocronología U–Pb</b>	88
<i>3.1. Métodos analíticos</i>	88
<i>3.2. Resultados</i>	89
<i>3.3. Procedencia de los circones detriticos</i>	89
<b>4. Geocronología de <math>^{40}\text{Ar}/^{39}\text{Ar}</math></b>	89
<i>4.1. Métodos analíticos</i>	89
<i>4.2. Resultados</i>	89
<b>5. Geoquímica</b>	99
<i>5.1. Técnicas analíticas</i>	99
<i>5.2. Resultados</i>	99
<i>5.3. Enjambre de diques Xayacatlán</i>	99
<i>5.4. Área de Patlanoaya</i>	103
<i>5.5. Área de Cuaujote</i>	104
<b>6. Implicaciones tectónicas</b>	105
<b>Agradecimientos</b>	106
<b>Referencias</b>	107
<b>DISCUSIÓN DE RESULTADOS</b>	109
<b>Terminología</b>	109
<b>Edad y procedencia de los circones</b>	109
<b>Circones en las rocas meta-ígneas</b>	111

<b>Geoquímica del enjambre de diques Xayacatlán</b>	111
<b>Geoquímica de las rocas graníticas</b>	113
<b>Geoquímica de los diques toleíticos en la Unidad Salada</b>	113
<b>Geocronología <math>^{40}\text{Ar}/^{39}\text{Ar}</math></b>	114
<b>Correlación y límites de edad en las fábricas de las rocas paleozoicas tardías</b>	115
<b>Correlación de las rocas máficas ordovícicas de Xayacatlán, Patlanoaya y Cuauhtle</b>	116
<b><u>CONCLUSIONES</u></b>	118
<b>Referencias</b>	124

## Índice de figuras

### Introducción

Figura 1-I. Paleogeografía de los océanos Iapetus y Rheico durante: a, b y c ca. 600 Ma, ca. 545 Ma y ca. 520 Ma respectivamente (Keppie, 2004), d, e y f ca. 480 Ma, ca. 440 Ma y ca. 400 Ma respectivamente (Bozkurt *et al.*, 2008; Linnemann *et al.*, 2003; modificado de C.R. Scotese: Paleomap website: [www.scotese.com](http://www.scotese.com)), g ca. 350 Ma (Keppie, 2004) y h ca. 280 Ma (Bozkurt *et al.*, 2008: redibujado de 'Palaeos: The Trace of Life on Earth'website en <http://www.palaeos.com>). A—Armorica (Britania, Normandía, Macizo Central), B — Barrandiania, C — Carolina, EWI — Inglaterra, Gales, e Ireland del Sur, F — Florida, I — Iberia, IR — Irán, M — Terrenos Mexicanos, NF — New Foundland, NS — Nova Scotia, PA — proto-Alpes, RH — Reno-Hercynian, SX — Saxo-Thuringian, TP — Placa Turca. 10

Figura 2-I. Mapa de Ortega-Gutiérrez (1975) y la sección geológica A-A' fue tomada de Ortega-Gutiérrez *et al.* (1999). La zona estudiada en este trabajo se localiza en la parte centro-norte, recuadro negro extremo superior, solo se muestra la parte sur del área de estudio. 12

Figura 3-I. Mapa geológico del área de Xayacatlán (este trabajo). 16

Figura 4-I. Diagrama espacio y tiempo, se muestran las dos hipótesis relacionadas con la evolución de las rocas del Complejo Acatlán con énfasis en el área de Xayacatlán, basado en el trabajo de Ortega-Gutiérrez *et al.*, 1999, izquierda (hipótesis uno) y el realizado en este trabajo, derecha (hipótesis dos). 26

## CAPÍTULO UNO

Fig. 1. Localización del mapa de Xayacatlán en dónde se muestra en (A) mapa de terrenos de Meso-América (modificado después de Keppie, 2004), y (B) mapa geológico del Complejo Acatlán (modificado después de Keppie *et al.*, 2006). 28

Fig. 2. Diagrama espacio y tiempo en donde se muestra el registro geológico del área de Xayacatlán: (A) después de Ortega-Gutiérrez *et al.* (1999), y (B) este trabajo. 29

Fig. 3. Mapa geológico del área de Xayacatlán. 30

Fig. 4. Análisis de circones por LA-ICPMS por medio de U-Pb de una pegmatita que corta a la Unidad Huerta (Ejemplar HUERTA-1) graficado en (a) un diagrama Tera-Wasserburg y (B) un histograma. 39

Fig. 5. Análisis de circones por LA-ICPMS por medio de U-Pb de una meta-psamita de la Unidad Amate (Ejemplar AMATE-1) graficado en (a) un diagrama Terra-Wasserburg y (B) un histograma. 40

**Fig. 6.** Análisis de circones por LA-ICPMS por medio de U-Pb de un granito que corta a la Unidad Amate (Ejemplar AMATE-2) graficado en (a) un diagrama Terra-Wasserburg y (B) un histograma.

41

**Fig. 7.** Análisis de circones por LA-ICPMS por medio de U-Pb de un dique granítico que corta a la Unidad Amate (Ejemplar SAL-12) graficado en (a) un diagrama Terra- Wasserburg y (B) un histograma.

42

**Fig. 8.** Análisis de circones por LA-ICPMS por medio de U-Pb de una meta-psamita de la Unidad Salada (Ejemplar SAL-11) graficado en (a) un diagrama Terra-Wasserburg y (B) un histograma.

43

**Fig. 9.** Reconstrucción paleogeográfica ordovícica mostrando la localización de las unidades Huerta y Amate en la margen sur del océano Rhéico (modificado después de Keppie, 2004).

44

**Fig. 10** reconstrucción paleogeográfica carbonífera mostrando la localización de la unidad Salada en la margen oeste de Pangea (modificada después de Keppie, 2004).

44

## CAPÍTULO DOS

**Figura 1.** Localización del mapa de Xayacatlán donde se muestra en (a) mapa de terrenos de Meso-America (modificado después de Keppie, 2004), y (b) mapa geológico del Complejo Acatlán (modificado después de Keppie *et al.*, 2008a).

49

**Figura 2.** Diagrama espacio y tiempo en donde se muestra el registro geológico del área de Xayacatlán (después de Morales-Gámez *et al.*, 2008).

50

**Figura 3.** Mapa geológico del área de Xayacatlán en donde se muestran las localidades de los ejemplares de diques máficos para geoquímica.

51

**Figura 4.** Datos geoquímicos para los diques máficos en la Unidad Salada graficados en un diagrama Zr/TiO<sub>2</sub> contra SiO<sub>2</sub> (peso en %) diagrama de Winchester y Floyd (1977). Abreviaturas: Sub-AB: Basalto Subalcalino; AB: Basalto Alcalino; TrAn: Traquiandesita; Bas: Basanita; Trach: Traquita; Neph: Nefelinita.

53

**Figura 5.** (a) FeO\*/MgO contra TiO<sub>2</sub> (% en peso) y (b) FeO\*/MgO contra SiO<sub>2</sub> para los diques en Salada. Las líneas muestran tendencias calco-alcalinas y toleíticas son después de Miyashiro (1974). FeO\* = Fe como FeO.

53

**Figura 6.** Datos geoquímicos de los diques máficos en la Unidad Salada graficados en un diagrama de Pearce (1975) en donde el Cr (ppm) contra Ti (ppm) muestra los campos compositionales para toleítas de arco de isla y basaltos intra-placa (incluyendo basaltos de dorsal centro-oceánica).

54

**Figura 7.** Condrita-normalizada abundancia en REE en los diques máficos de Salada y MORB tipo-N de Sun y McDough (1989). Los valores normalizados son después de Sun y McDonouhg (1989).

54

<b>Figura 8. Datos geoquímicos para los diques máficos en la Unidad Salada y MORB tipo-N</b>	54
graficados en un diagrama de elementos traza manto-normalizado (Sun and McDonough, 1989). Los valores normalizados son de Sun and McDonough (1989).	
<b>Figura 9. Reconstrucción Permo-Carbonífo: (a) después de Talavera-Mendoza <i>et al.</i>, (2005) y</b>	55
Vega-Granillo <i>et al.</i> (2007), y (b) modificado de Keppie <i>et al.</i> (2008a).	
<b>CAPÍTULO TRES</b>	
<b>Figura 1. Localización del mapa de Xayacatlán en donde se muestra (a) mapa de terrenos de Meso-América (modificado después de Keppie 2004), y (b) mapa geológico del Complejo Acatlán (modificado después de Keppie <i>et al.</i>, 2008a).</b>	58
58	
<b>Figura 2. Diagrama tiempo y espacio en donde se muestra el registro geológico del área de Xayacatlán: (a) después de Ortega-Gutiérrez <i>et al.</i> (1999); (b) este artículo.</b>	59
59	
<b>Figura 3. Mapa geológico del área de Xayacatlán en donde se muestran la localización de los datos estructurales y la localización de las figuras subsecuentes y muestras datadas por geocronología de <math>^{40}\text{Ar}/^{39}\text{Ar}</math>.</b>	61
61	
<b>Figura 4. Estructuras en los diques gabróicos en la barranca El Viento: (a) fotografía de parte de los pliegues de forma-Z; (b) bosquejo del mismo pliegue; (c) estereograma de los datos estructurales de este afloramiento.</b>	63
63	
<b>Figura 5. Estructuras en el dique gabróico en la Barranca Las ollas: (a) fotografía y (b)</b>	65
estereograma de los patrones de interferencia tipo hongo en el dique gabróico; (c) fotografía y	
(d) estereograma de los pliegues abiertos en los diques máficos que intrusionan a los diques gabróicos.	
65	
<b>Figura 6. Fotografía de las fábricas de libro rotado y porfiroclastos sigma en la Unidad Amate indicando una cizalla destral en la aureola de contacto de los diques gabróicos localizados en la Barranca Amate.</b>	66
66	
<b>Figura 7. Datos estructurales de la Unidad Amate: (a) foliación <math>S_{A1}</math> y Lineación <math>L_{A1}</math>; (b)</b>	67
Foliación compuesta $S_{A2/1}$ y lineación de estiramiento $L_{A3}$ ; (c) ejes de pliegue $F_{A3}$ en diques pegmatíticos que intrusionan a la Unidad Amate.	
67	
<b>Figura 8. Fotografía del clivaje de solución plegado, <math>S_{HS1}</math>, en la meta-psamita de la Unidad Huerta; (b) Estereograma de los datos del plegamiento de la Unidad Huerta; (c) fotografía de los pliegues plegados en la meta-pelita de la Unidad Huerta; (d) bosquejo de (c).</b>	68
68	
<b>Figura 9. Datos estructurales de las unidades Huerta y Salada: (a) Foliación <math>S_{HS1}</math>, pliegues <math>F_{HS2}</math> y</b>	68
lineaciones $F_{HS2}$ ; (b) foliación $S_{HS2}$ y pliegues $F_{HS3}$ .	
<b>Figura 10. Fotografía de las fábricas en la Formación Tecomate.</b>	69
69	

<b>Figura 11. Estereogramas de las fábricas en la Formación Tecomate: (a) ejes de pliegue <math>F_{T1}</math> y lineaciones; (b) foliación <math>S_{T1}</math> con plegamiento asociado a los ejes <math>F_{T2}</math>; (c) ejes de kink band.</b>	70
<b>Figura 12. (a) fotografía del conglomerado cizallado en la Formación Tecomate en la barranca El Carrizal, (b) el diagrama muestra la relación de ejes longitud/acortamiento de los guijarros contra el <i>plunge</i> de los ejes longitudinales, (c) estereograma de las estructuras y (d) el elipsoide de deformación en los conglomerados se muestra en un diagrama de Flynn.</b>	71
<b>Figura 13. Esterograma de las fábricas en el intrusivo de Totoltepec.</b>	71
<b>Figura 14. Espectros de <math>^{40}\text{Ar}/^{39}\text{Ar}</math> para: (a-c) minerales decusados en la aureola de contacto en los diques de gabro: (a) anfíbol y (c) muscovita; (d) muscovita de la Unidad Salada, (e) roca total filita sericitizada de la Formación Tecomate.</b>	75
<b>Figura 15. Gráfica temperatura contra tiempo usando datos de <math>^{40}\text{Ar}/^{39}\text{Ar}</math> que constriñen los eventos en el área de Xayacatlán.</b>	77
<b>Figura 16. Reconstrucción paleogeográfica para: (A) límite Ordovícico-Silúrico a los ca. 440 Ma (modificado después de Keppie 2004) y (B) reconstrucción del Permo-Carbonífero en la cual se muestra la extrusión del Carbonífero y un arco transtensional del Pérmico medio en el margen oeste de Pangea (modificado después de Keppie <i>et al.</i>, 2008a).</b>	78
<b>CAPÍTULO CUATRO</b>	
<b>Fig. 1. (a) Mapa de terrenos de México (después de Keppie, 2004) en el cual se muestran la localidad del Complejo Acatlán y (b) mapa geológico del Complejo Acatlán (modificado después de Ortega-Gutiérrez <i>et al.</i>, 1999) en el cual se muestran las localidades de las Figs. 3, 4 y 5.</b>	83
<b>Fig. 2. Diagrama tiempo y espacio donde se muestra la historia geológica del Complejo Acatlán.</b>	84
<b>Fig. 3. Mapa geológico del área de Xayacatlán en donde se muestran las localidades muestreadas.</b>	85
<b>Fig. 4. Análisis de los anfiboles cárnicos de los diques gabróicos de Xayacatlán graficados en diagramas: (a) <math>\text{Na}/(\text{Na}+\text{Ca})</math> contra <math>\text{Al}/(\text{Al}+\text{Si})</math>: las envolventes muestran la composición para anfiboles de presión media y baja presión de Dalradian (Escocia), Haast River (Nueva Zelanda) y Abukuma (Japón), respectivamente (Laird and Albee, 1981; Caredda <i>et al.</i>, 2001; y (b) el gráfico de átomos <math>\text{AlIV}</math> contra <math>(\text{Na}+\text{K})</math> (después de Caredda <i>et al.</i>, 2001): los cuadros rellenos representan los miembros de frontera de los anfiboles.</b>	86
<b>Fig. 5. Mapa geológico del área de Patlanoaya en donde se muestran los lugares muestreados.</b>	87
<b>Fig. 6. Mapa geológico del área de Cuauhtépetl en donde se muestran los sitios muestreados.</b>	87
<b>Fig. 7. Datos de U-Pb TIMS de circones en gneisses anfibolíticos de la muestra XAY-3 del Conjunto Xayacatlán graficados en un diagrama de concordia.</b>	88

<b>Fig. 8. Análisis de circones U-Pb LA-ICPMS en muestras psamíticas del área de Patlanoaya graficadas un diagramas de concordia e histogramas: (a) Unidad Las Minas; b) Unidad Ocate; (c) Unidad Malpaso y (d) Unidad Ojo de Agua.</b>	97
<b>Fig. 9. Datos de hornblenda de <math>^{40}\text{Ar}/^{39}\text{Ar}</math> en mantos que cortan los diques Xayacatlán en un espectro de liberación incremental.</b>	99
<b>Fig. 10. Rocas máficas de los diques de Xayacatlán graficados en el diagrama <math>\text{FeO}_{\text{tot}}/\text{mgO}</math> contra <math>\text{TiO}_2</math>. Simbología: grupo 1 (+), grupo 2 (o) y grupo 3 (X). Los vectores para las tendencias toleíticas y calco-alcalinas son después de Miyashiro (1974).</b>	103
<b>Fig. 11. Clasificación de las rocas máficas de los diques de Xayacatlán usando el diagrama de cationes de Jensen (1976). Simbología: grupo 1 (+), grupo 2 (o) y grupo 3 (X). Los campos: TA = andesita toleítica; TD = dacita toleítica; TR = riolita toleítica; CB = basalto calco-alcalino; CA = andesita calco-alcalina; CD = dacita calco-alcalina; CR = riolita calco-alcalina.</b>	103
<b>Fig. 12. Abundancia de elementos de las tierras raras normalizados a Condritas en las rocas meta-ígneas de: (a) rocas máficas de Xayacatlán del grupo 1; (b) rocas máficas de Xayacatlán del grupo 3; (c) rocas félasicas de Xayacatlán. Los valores están normalizados después de Sun y McDonough (1989).</b>	103
<b>Fig. 13. Abundancia de elementos traza incompatibles del manto normalizado en las rocas meta-ígneas de: (a) rocas máficas de Xayacatlán del grupo 1; (b) rocas máficas de Xayacatlán del grupo 3; (c) rocas félasicas de Xayacatlán. Los valores normalizados son después de Sun y McDonough (1989).</b>	104
<b>Fig. 14. Rocas de las áreas de Patlanoaya y Coaulote graficadas en: diagrama de <math>\text{Zr}/\text{TiO}_2</math> contra <math>\text{SiO}_2</math> de Winchester y Floyd (1977). Abreviaciones: Com/Pan =Comendita/Pantellerita; TrAn = traquiandesita. Área de Patlanoaya: Anacahuite (O). Las minas (+) y aureola máfica del granito Palo Liso (círculo relleno y área de Cuahulote (cuadro gris).</b>	104
<b>Fig. 15. Rocas máficas de las áreas de Patlanoaya y Cuauhté graficadas en un diagrama de discriminación Ti-Zr-Y de Pearce and Cann (1973). Área de Patlanoaya: Anacahuite (O), Las minas (+) y aureola máfica del granito Palo Liso (círculo relleno) y área de Cuahulote (cuadro gris).</b>	105
<b>Fig. 16. Rocas máficas de las áreas de Patlanoaya y Cuahulote graficas en un digrama <math>\text{Ti}</math> (ppm) contra <math>\text{Cr}</math> (ppm de Pearce (1975)). Área de Patlanoaya: Anacahuite (O), Las Minas (+) y aureola máfica del granito Palo Liso (círculo relleno) y área de Cuahulote (cuadro gris). Los campos composicionales para toleitas de arco de isla y basaltos intraplaca también son mostrados.</b>	105
<b>Fig. 17. Rocas máficas de las áreas de Patlanoaya y Cuauhté graficadas en: (a) diagrama de <math>\text{FeO}_{\text{tot}}/\text{MgO}</math> contra <math>\text{SiO}_2</math> y (b) diagrama de <math>\text{FeO}_{\text{tot}}/\text{MgO}</math> contra <math>\text{TiO}_2</math>, área de Patlanoaya: Anacahuite (O), Las Minas (+) y aureola máfica del granito Palo Liso (círculo relleno) y área de Cuahulote (cuadro gris). Los vectores para las tendencias toleíticas y calco-alcalinas son después de Miyashiro (1974).</b>	105

**Fig. 18.** Abundancia de elementos de las tierras raras normalizadas a condrita en las rocas metágeas de las áreas de Patlanoaya y Cuaulote: (a) anfibolita Anacahuite; (b) Las Minas; (c) aureola máfica del granito Palo Liso y (d) rocas de Cuaulote. Los valores normalizados son después de Sun y McDonough (1989).

106

**Fig. 19.** Abundancia de elementos traza incompatibles normalizados al Manto en las rocas metágeas de las áreas de Patlanoaya y Cuaulote: (a) anfibolita Anacahuite (b) Las Minas (c) aureola máfica del granito Palo Liso y (d) rocas de Cuaulote. Los valores normalizados son después de Sun y MaDonough (1989).

106

**Fig. 20.** Reconstrucción Paleogeográfica a los 460 Ma en donde se muestra la localización del Conjunto Xayacatlán en el margen afectado por rift de Oaxaquía (modificado después de Keppie, 2004).

106

### Conclusiones

Figura 1-C. Depósito de sedimentos en el océano Iapetus, (A) cerrado por el acoplamiento de terrenos peri-gonwánicos y deformados durante el cierre de este océano (Keppie, 2004), y (B) cerrado por la colisión de Laurentia contra Gondwana durante el Ordovícico medio-tardío, en ambos casos el Complejo Acatlán se forma en una sutura colisional (Ortega-Gutiérrez *et al.*, 1999).

120

Figura 2-C Talavera-Mendoza *et al.* 2005, superior y Vega-Granillo *et al.* (2007), inferior. En ambos modelos se propone que los eventos de deformación, registrados en las rocas del Complejo Acatlán, están asociados a procesos de colisión y que estos ocurrieron tanto en los océanos Iapetus y Rhéico durante una evolución tectónica compleja durante el Paleozoico.

121

Figura 3-C. Keppie *et al.* (2008a) propusieron un modelo paleogeográfico en el cual sugieren que la sedimentación de las rocas del Complejo Acatlán, ocurrió tanto en los océanos Rhéico y Paleopacífico en diferentes etapas y una tectónica extensional durante el Ordovícico y Misisípico, respectivamente.

122

## Índice de Tablas

### CAPÍTULO UNO

<b>Tabla 1.</b> Análisis de U-Pb LA-ICPMS de circones en ejemplar de pegmatita en el área de Xayacatlán, Complejo Acatlán, sur de México: HUERTA-1 (ver Fig. 3 para localización de ejemplares).	31
<b>Tabla 2.</b> Análisis de circones por medio del método U-Pb por LA-ICPMS en un ejemplar de meta-psamita de la Unidad Amate en el área de Xayacatlán, Complejo Acatlán, sur de México: AMATE-1 (ver Fig. 3 para localización de ejemplares).	33
<b>Tabla 3.</b> Análisis de circones por medio de U-Pb con LA-ICPMS en un dique granítico que corta a la Unidad Amate en el área de Xayacatlán, Complejo Acatlán, sur de México: AMATE 2 (ver Fig. 3 para localización de ejemplares).	35
<b>Tabla 4.</b> Análisis U-Pb por medio de LA-ICPMS de circones en un ejemplar de metapsamita de la Unidad Salada en el área de Xayacatlán, Complejo Acatlán, sur de México: SAL-12 (ver Fig. 3 para localización de ejemplares).	36
<b>Tabla 5.</b> Análisis de U-Pb por medio de LA-ICPMS de circones en dique granítico que corta a la Unidad Amate en el área de Xayacatlán, Complejo Acatlán, sur de México: SAL-11 (ver Fig. 3 para localización de ejemplares).	37

### CAPÍTULO DOS

<b>Tabla 1.</b> Datos geoquímicos para los diques máficos que cortan a la Unidad Salada, Complejo Acatlán, sur de México.	52
---	----

### CAPÍTULO TRES

<b>Tabla 1.</b> Datos $^{40}\text{Ar}/^{39}\text{Ar}$ para muestras del área de Xayacatlán, en la parte este del Complejo Acatlán, sur de México.	72
---	----

### CAPÍTULO CUATRO

<b>Tabla 1.</b> Análisis de circones por U-Pb TIMS del dique de Xayacatlán.	88
<b>Tabla 2.</b> Análisis de circones por U-Pb LA-ICPMS en el área de Patlanoaya.	90
<b>Tabla 3.</b> Análisis de $^{40}\text{Ar}/^{39}\text{Ar}$ de hornblenda del dique máfico de Xayacatlán.	98
<b>Tabla 4.</b> Análisis químicos de muestras del Complejo Acatlán.	100

## Resumen

En el área de Xayacatlán del Complejo Acatlán en el sur de México, los paquetes de rocas están limitados por fallas N-S formados por (de oeste a este): (i) psamitas y pelitas intercaladas en facies metamórficas de esquisto verde (Unidad Huerta): el circón detritico concordante más joven en la parte oeste de esta unidad es de  $455\pm4$  Ma; (ii) psamitas y arcosas en facies de esquisto verde-anfibolita (Unidad Amate): el circón detritico concordante más joven da una edad  $^{206}\text{Pb}/^{238}\text{U}$  de  $902\pm14$  Ma, y edades concordantes viejas de ~900-1300 Ma; (iii) mármoles y rocas clásticas de bajo grado metamórfico (Formación Tecomate Pérmica); y (iv) psamitas, pelitas y delgados diques máficos toleíticos con metamorfismo en facies de esquisto verde (Unidad Salada): los circones detriticos concordantes más jóvenes proporcionan una edad  $^{206}\text{Pb}/^{238}\text{U}$  de  $352\pm3$  Ma y edades concordantes más viejas de ~434–485 Ma, 511–630 Ma y 920–1200 Ma. La parte este de la Unidad Huerta es cortada por pegmatitas que proporcionan una edad en circón  $^{206}\text{Pb}/^{238}\text{U}$  casi concordante de  $464\pm4$  (una edad significativa de los cuatro circones casi concordantes más jóvenes es ~485.5 Ma) interpretada como el tiempo de intrusión y circones heredados con edades concordantes de ~530–580 Ma y ~910–1200 Ma. Estos datos sugieren que la Unidad Huerta tiene un rango en edad desde el Ordovícico temprano (posiblemente más viejo)-tardío. La Unidad Amate es cortada por diques graníticos, en los cuales las edades  $^{206}\text{Pb}/^{238}\text{U}$  en circones concordantes son  $452\pm6$  Ma y  $447\pm3$  Ma interpretadas como el tiempo de intrusión, y las edades en circones heredados más viejos con edades  $^{206}\text{Pb}/^{238}\text{U}$  concordantes en un rango de 950-1250 Ma. Las edades intrusivas son similares a la edad U-Pb concordante  $442\pm1$  Ma para los diques máficos que también cortan a la Unidad Amate. Esos datos constriñen la edad de depósito de la Unidad Amate entre ~900 Ma y el Ordovícico tardío. La edad de la Unidad Salada es probablemente carbonífera por que está estructuralmente sobrejacida por la Formación Tecumate Pérmico inferior-medio. La preponderancia de las edades de 510-630 Ma y 900-1250 en ambas edades, detriticas y heredadas en algunos de los datos muestreados sugiere una fuente en el adyacente y subyacente Complejo Maya y Oaxaqueño, respectivamente, aunque una fuente de la roca encajonante xenocristalina no puede ser descartada para las rocas intrusivas. Las intrusiones ígneas han sido interpretadas como parte de una suite relacionada a rift bimodal. Su sincronización con el depósito de la Unidad Huerta (y posiblemente también de la Unidad Amate) sugiere un ambiente de margen pasivo-rift de deposición en la margen sur del océano Rheico. En otro sentido, la Unidad Salada y la Formación Tecumate parecen ser síncronas con un arco magmático desarrollado en el Permo-Triásico en la margen oeste de Pangea.

Un conjunto de diques máficos intrusionan a las meta-pelitas y meta-psamitas polideformadas, con metamorfismo en facies de esquisto verde, de la Unidad Salada. La edad de los diques es constreñida por los circones detriticos más jóvenes en la roca de la encajonante Unidad Salada ( $352\pm3$  Ma) y la edad Pérmico temprano de la sobrejaciente Formación Tecumate, la cual está desprovista de estos diques. Las rocas máficas son generalmente compuestas de anfibol, clorita, feldespato, epidota y minerales opacos accesarios. Su química se parece a toleitas relacionadas a rift con ~50 % en peso  $\text{SiO}_2$  y  $\text{Mg}^{\#}$  ~0.40-0.60. Sus patrones REE normalizadas a condritas se parecen a MORB tipo N con  $(\text{La}/\text{Sm})_n$  principalmente ~0.5-0.6., y sus patrones normalizados al manto son relativamente planos con una anomalía no negativa de Nb y una baja relación Th/La indicando la ausencia tanto de fluidos relacionados a subducción, como a contaminación cortical. Su química parece ser MORB tipo N. Sus relaciones intrusivas con las rocas clásticas derivadas del continente sugieren que ellos fueron

emplazados en una corteza continental adelgazada. La fauna misisípica de agua somera en el adyacente terreno Oaxaquia, con afinidades Meso-Continental (EUA), indica que Pangea estuvo amalgamada para este tiempo. En este contexto, los diques toleíticos se infiere, haberse formado durante la extensión en la margen oeste de Pangea, la cual fue síncrona con la extrusión de rocas de alta presión por encima de una zona de subducción activa.

El área de Xayacatlán fue previamente considerado preservar un contacto por cabalgadura ordovícico-silúrico entre los vestigios del océano Iapetus y la colindante para-autóctona Oaxaquia. Un mapeo detallado indica que las rocas ocurren en cuatro bloques limitados por fallas verticales N-S. Los últimos eventos tectonotérmicos registrados son posteriores a Iapetus y ocurren a lo largo de la margen de los océanos Rhéico (1) y paleo-Pacífico (2 y 3): (1) transtensión desstral acompañada de intrusión de enjambres de diques N-S toleíticos, 442 Ma; (2) deformación penetrativa acompañada por metamorfismo en facies de sub-esquisto verde, durante el Misisípico relacionada a la intrusión de rocas de alta presión, y (3) transtensión desstral N-S acompañada de metamorfismo en facies de sub-esquisto verde, durante la generación de fábricas en el Pérmico medio.

El complejo Acatlán es un vestigio de un océano paleozoico el cual se ha inferido ser tanto el océano Iapetus del Cambro-Ordovícico y/o el Rhéico del Ordovícico-Carbonífero. Los granitoides ordovícicos en el complejo han sido interpretados como el producto de deshidratación del fundido, arco o magmatismo de rift, sin embargo, la geoquímica de las rocas félsicas es no concluyente. La geoquímica de una recientemente descubierta, suite ígnea máfica mayor del Ordovícico-Silúrico temprano asociada con esos granitos, es crítica para definir los conjuntos tectónicos de los eventos ígneos y una reconstrucción paleogeográfica. Algunos datos de tres áreas en el Complejo Acatlán (Xayacatlán, Patlanoaya y Cuauhtle) documentan rocas toleíticas, con características intraplaca con una fuente del manto primitivo o manto previamente modificado por magmatismo relacionado a subducción, posiblemente combinado con contaminación cortical. Así, combinado con su ocurrencia, como es un enjambre de diques intrusionando rocas sedimentarias clásticas en una margen pasiva-rift, indica rifting de una margen continental. Los diques máficos en Xayacatlán proporcionan edades en circones por U-Pb TIMS de  $442 \pm 1$  Ma y una edad  $^{40}\text{Ar}/^{39}\text{Ar}$  de meseta (hornblenda) de  $434 \pm 3$  Ma. La edad del magmatismo en otras localidades es definida por las edades de granitoides asociados e intrusionados ca. 461 Ma y por la edad de los circones detríticos más jóvenes en las rocas encajonantes:  $496 \pm 25$  Ma en Patlanoaya. Los datos publicados previamente sugieren que este evento ígneo pudo haber empezado tempranamente a los  $478 \pm 5$  Ma (Ordovícico temprano). Sin embargo la vida abarcada de los océanos Iapetus y Rhéico tiene puntos en común durante el Ordovícico, la subducción y colisión caracteriza al primero, mientras el segundo consistió en un modo rift-deriva. Así, este magmatismo Ordovícico-Silúrico temprano es más consistente con un rift a lo largo de la margen sur del océano Rhéico. El inicio del rifting es ca. 480 Ma es contemporáneo con la separación de los terrenos peri-gonwánicos, como Avalonia y Carolinia, desde Amazonia-Oaxaquia. Subsecuentemente el rifting pudo ser análogo al oeste de Norteamérica en el Mesozoico-Cenozoico donde la deformación transtensional está relacionada a la dispersión de terrenos (*e.g.* Baja California y Baja British Columbia cretácica) llevando al colapso de la margen continental.

**Palabras clave:** Complejo Acatlán, Geocronología, Geoquímica, Estructura, México, Oaxaquia, Ordovícico, Permo-Carbonífero, Carbonífero, Pangea, Rifting.

## Abstract

In the Xayacatlán area of the Acatlán Complex in southern Mexico, several, N–S, fault-bounded packages of rocks occur (from west to east): (i) greenschist facies, interbedded psammites and pelites (Huerta Unit): the youngest concordant detrital zircon in the western part of the unit is  $455\pm4$  Ma; (ii) greenschist-amphibolite facies arkoses and psammites (Amate Unit): the youngest concordant detrital zircon gave a  $^{206}\text{Pb}/^{238}\text{U}$  age of  $902\pm14$  Ma, and older concordant ages of  $\sim 900$ – $1300$  Ma; (iii) low grade clastic rocks and marbles (Permian Tecolate Formation); and (iv) greenschist facies psammites, pelites and thin tholeiitic mafic slices (Salada Unit): the youngest concordant detrital zircon yielded a  $^{206}\text{Pb}/^{238}\text{U}$  age of  $352\pm3$  Ma and older concordant ages of  $\sim 434$ – $485$  Ma,  $511$ – $630$  Ma, and  $920$ – $1200$  Ma. The eastern part of the Huerta Unit is cut by pegmatite that yielded an almost concordant  $^{206}\text{Pb}/^{238}\text{U}$  zircon age of  $464\pm4$  Ma (a mean age of the four almost concordant young zircons is  $\sim 485.5$  Ma) interpreted as the time of intrusion, and inherited zircons with concordant ages of  $\sim 530$ – $580$  Ma and  $\sim 910$ – $1200$  Ma. These data suggest that the Huerta Unit ranges in age from Early (possibly older) to Late Ordovician. The Amate Unit is cut by granitic dikes, in which the youngest concordant  $^{206}\text{Pb}/^{238}\text{U}$  zircon ages are  $452\pm6$  Ma and  $447\pm3$  Ma interpreted as the time of intrusion, and older inherited zircon ages with concordant  $^{206}\text{Pb}/^{238}\text{U}$  ages in the range of  $950$ – $1250$  Ma. The intrusive ages are similar to the  $442\pm1$  Ma concordant U–Pb age for mafic dikes that also cut the Amate Unit. These data constrain the depositional age of the Amate Unit between  $\sim 900$  Ma and latest Ordovician. The age of the Salada Unit is probably Carboniferous because it is structurally overlain by the Lower–Middle Permian Tecolate Unit. The preponderance of  $510$ – $630$  Ma and  $900$ – $1250$  Ma ages in both the detrital and inherited ages in some of the dated samples suggests a source in the adjacent and subjacent Maya and Oaxacan Complex, respectively, although a xenocrystic host rock source cannot be ruled out for the intrusive rocks. The igneous intrusions have been interpreted as part of a  $480$ – $440$  Ma bimodal rift-related suite. Their synchronicity with deposition of the Huerta Unit (and possibly also the Amate Unit) suggests a rift-passive margin environment of deposition on the southern margin of the Rheic Ocean. On the other hand, the Salada Unit and the Tecolate Formation appear to be synchronous with a Permo-Triassic magmatic arc that developed on the western margin of Pangea.

A suite of mafic dikes intrudes polydeformed, greenschist facies, metapsammites and metapelites of the Salada unit. The age of the dikes is constrained by the youngest detrital zircon in the Salada host rocks ( $352\pm3$  Ma) and the Early Permian age of the overlying Tecolate Formation, which is devoid of such dikes. The mafic rocks are generally composed of amphibole, chlorite, feldspar, epidote and accessory opaque minerals. Their chemistry resembles rift-related tholeiites with  $\sim 50$  wt.% SiO<sub>2</sub> and Mg#  $\sim 0.40$ – $0.60$ . Their chondrite-normalized REE patterns resemble N-type MORB with (La/Sm)<sub>n</sub> mostly  $\sim 0.5$ – $0.6$ , and their mantle-normalized patterns are relatively flat with no negative Nb anomaly and a low Th/La ratio indicating the absence of both subduction-related fluids and crustal contamination. Their chemistry resembles N-type MORB. Their intrusive relationships with the continentally-derived clastic rocks suggest that they were emplaced in thin continental crust. Shallow-water, Mississippian fauna in the adjacent Oaxaquia terrane, with Mid-Continent (USA) affinities, indicate that Pangea had already amalgamated by this time. In this context, the tholeiitic dikes are inferred to have formed during extension on the western margin of Pangea that was synchronous with extrusion of high-pressure rocks above an active subduction zone.

The Xayacatlán area was previously inferred to preserve the Ordovician-Silurian thrust contact between vestiges of the Iapetus Ocean and the para-autochthon bordering Oaxaquia. Detailed remapping indicates that the rocks occur in four vertically-bounded, NS fault blocks. The latter record the following tectonothermal events that post-date Iapetus and occurred along the margins of the Rheic (1) and Pacific (2 and 3) oceans: (1) dextral transtension accompanying intrusion of an NS, tholeiitic dike swarm at 442 Ma; (2) penetrative, greenschist-facies deformation during the Mississippian related to extrusion of high-pressure rocks; and (3) subgreenschist-facies dextral transtension on NS faults during the generation of Middle Permian fabrics.

The Acatlán Complex is a vestige of a Paleozoic Ocean inferred to be either the Cambro-Ordovician Iapetus and/or the Ordovician-Carboniferous Rheic oceans. Ordovician granitoids in the complex have been interpreted as either the products of dehydration melting, arc or rift magmatism, however, the geochemistry of felsic rocks is inconclusive. The geochemistry of a recently discovered, major, Ordovician-earliest Silurian mafic igneous suite associated with these granitoids is critical to defining the tectonic setting of the igneous event, and to paleogeographic reconstructions. Such data from three areas in the Acatlán Complex (Xayacatlán, Patlanoaya, and Cuauhtle) document tholeiitic, within-plate characteristics with a source in either primitive mantle or mantle previously modified by subduction-related magmatism possibly combined with crustal contamination. This, combined with their occurrence as a dike swarm intruding rift-passive margin clastic sedimentary rocks, indicates rifting of a continental margin. Mafic dikes at Xayacatlán yielded a concordant U-Pb TIMS zircon age of  $442 \pm 1$  Ma and a  $^{40}\text{Ar}/^{39}\text{Ar}$  hornblende plateau age of  $434 \pm 3$  Ma. The age of mafic magmatism at other localities is defined by the ages of associated granitoids intruded at ca. 461 Ma and by the age of the youngest detrital zircon in the host rocks:  $496 \pm 25$  Ma at Patlanoaya. Previously published age data suggest that this igneous event may have started earlier at  $478 \pm 5$  Ma (Early Ordovician). Although the life spans of the Iapetus and Rheic oceans overlap during the Ordovician, subduction and collision characterize the former, whereas the latter was in a rift-drift mode. Thus, this Ordovician-earliest Silurian magmatism is more consistent with rifting along the southern margin of the Rheic Ocean. Initiation of rifting at ca. 480 Ma is contemporaneous with separation of peri-Gondwanan terranes, such as Avalonia and Carolina, from Amazonia-Oaxaquia. Subsequent rifting may be analogous to Mesozoic-Cenozoic western North America where transtensional deformation is related to dispersal of terranes (e.g. Baja California and Cretaceous Baja British Columbia) leading to a gradual collapse of the inboard continental margin.

**Keywords:** Acatlán Complex, geochronology, geochemistry, structure, Mexico, Oaxaquia, Ordovician, Permo-Carboniferous, Carboniferous, Pangea, Rifting.

## **INTRODUCCIÓN**

En el Sur de México afloran varios conjuntos litotectónicos (Campa y Coney, 1983; Sedlock *et al.*, 1993; Keppie, 2004) que se han amalgamado paulatinamente desde el Precámbrico-Paleozoico hasta el Cenozoico temprano (Keppie, 2004). En consecuencia; cada uno de estos terrenos ha tenido una evolución tectónica distinta a lo largo del tiempo geológico. Las rocas del basamento del terreno Mixteca son de edad paleozoica (Yañez *et al.*, 1991; Ortega-Gutiérrez *et al.*, 1995) y forman parte de este mosaico de terrenos que actualmente integran esta parte del país.

El sur de México representa, desde el punto de vista geológico, un área compleja donde afloran rocas cuyas edades conocidas se remontan hasta el Proterozoico, las cuales incluyen a los basamentos de los terrenos Oaxaca y Maya (Campa y Coney, 1983; Keppie, 2004), además de las rocas paleozoicas del basamento del terreno Mixteca y terrenos mesozoicos, *e.g.* Juárez y Xolapa (Keppie, 2004). Centeno-García y colaboradores (2008) señalan un basamento permo-triásico del terreno compuesto Guerrero, lo cual ubica a las rocas de este basamento en el límite paleozoico-mesozoico y el cual se localiza en la parte occidental y suroccidental del país. Todos estos terrenos tienen una cobertura cenozoica.

El terreno Mixteca (Campa y Coney, 1983; Sedlock *et al.*, 1993; Keppie, 2004) está compuesto por una sucesión de rocas paleozoicas, que a lo largo de su formación han dado un arreglo estratigráfico y estructural complicado. La cobertura de este terreno está integrada por rocas jurásicas, cretácicas y cenozoicas, y su basamento cristalino lo forman rocas meta-sedimentarias, meta-ígneas y rocas intrusivas.

El terreno Mixteca se ubica en la parte central del sur de México y está limitado al este por el basamento metamórfico grenvilliano de Oaxaquia (Ortega-Gutiérrez *et al.*, 1995), por medio de la falla de Caltepec, cuya edad es de 278 Ma (Elias-Herrera y Ortega-Gutiérrez, 2002), ambos complejos, Acatlán y Oaxaqueño, están cubiertos por rocas de la Formación Matzitzi (Pérmico tardío, Centeno-García *et al.*, 2009). Al sur está

limitado por el Complejo Xolapa, el cual está formado por rocas migmatizadas y deformadas dúctilmente (Pérez-Gutiérrez *et al.*, 2009).

El límite oeste entre estos dos complejos (Acatlán y Xolapa) es la zona de falla de Tierra Colorada, la cual presenta una cinemática normal y lateral izquierda, activa en el Eoceno (Riller *et al.*, 1992; Solari *et al.*, 2007), y por la zona de cizalla Chacalapa en el límite este, con una cinemática predominantemente lateral izquierda y fallas normales con desplazamientos importantes, con actividad desde el Oligoceno hasta el presente (Tolson, 2007). Al oeste las rocas del terreno compuesto Guerrero cabalgan a rocas del terreno Mixteca (Centeno-García *et al.*, 2008). Cerca *et al.*, (2008) sugieren; con base en la deformación de los depósitos continentales Copalillo y Tuzantlan; que el movimiento de esta falla ocurrió en el Terciario temprano, aunque no descartan movimientos previos. El terreno Mixteca es cubierto al norte por rocas de la Faja Volcánica Transmexicana, cuya actividad inicia desde el Mioceno medio-tardío y continua actualmente (Gómez-Tuena *et al.*, 2005).

El basamento metamórfico del terreno Mixteca fue denominado como Complejo Acatlán por Ortega-Gutiérrez (1978), quien identificó regionalmente tres unidades tectónicas, diferenciadas posteriormente en base a estudios de geocronología, geoquímica, litología, estructura y grado metamórfico (Yañez *et al.*, 1991, Ortega-Gutiérrez *et al.*, 1993, Ortega-Gutiérrez *et al.*, 1999, Ramírez-Espinosa, 2001). Las dos unidades principales fueron denominadas como sub-grupos, Petlalcingo y Acateca (Ortega-Gutiérrez, 1978), las cuales son cubiertas por rocas de la Formación Tecolate (Ortega-Gutiérrez *et al.*, 1999).

El sub-Grupo Petlalcingo está compuesto por meta-sedimentos y meta-lavas metamorfosados en facies de esquistos verde. Estos sub-Grupos representan proporcionalmente el área mayor expuesta de dicho basamento, el grupo está integrado por las formaciones Cosoltepec, Chazumba y Magdalena (Ortega-Gutiérrez *et al.*, 1999).

El sub-Grupo Acateca (renombrado como Grupo Piaxtla por Ramírez-Espinosa, 2001) está formado por rocas ultramáficas y máficas eclogitizadas e intercaladas con rocas pelíticas y rocas metasedimentarias silíceas, separado en la Formación Xayacatlán y los granitoides Esperanza (Ortega-Gutiérrez *et al.*, 1999).

La Formación Tecolate originalmente fue incluida por Ortega-Gutiérrez (1978) dentro del Sub-Grupo Acateca como No Diferenciada. Posteriormente Ortega-Gutiérrez *et al.* (1999) la consideraron como una entidad independiente que cubre a los sub-grupos Petlalcingo y Acateca (Piaxtla).

Recientemente el Complejo Acatlán ha sido separado en dos conjuntos litotectónicos (Keppie *et al.*, 2008a) análogos a los descritos en trabajos anteriores (*e.g.* Ortega-Gutiérrez *et al.*, 1999; Ramírez-Espinosa, 2001; Talavera-Mendoza *et al.*, 2005), los cuales se agrupan en:

- (i) rocas de alta presión que son caracterizadas por el Grupo Piaxtla y los granitoides Esperanza, ambos presentan metamorfismo en facies de eclogita/esquistos azules (Ortega-Gutiérrez, 1975; Ortega-Gutiérrez *et al.*, 1999; Ramírez-Espinosa, 2002; Meza-Figueroa *et al.*, 2000; Middleton *et al.*, 2007), y
- (ii) rocas de bajo grado metamórfico, en las que predominan las meta-arcosas, cuarcitas, meta-psamitas y meta-pelitas que previamente fueron incluidas en la Formación Cosoltepec (Ortega-Gutiérrez *et al.*, 1999), y que actualmente es considerada como una unidad compuesta (*e.g.* Morales-Gámez *et al.*, 2008; Ramos-Arias *et al.*, 2008; Hinojosa-Prieto *et al.*, 2008; Grodzicki *et al.*, 2008).

La superficie expuesta (de las rocas) del Complejo Acatlán en el sentido de Ortega-Gutiérrez (1978) es superior a 10 000 km<sup>2</sup>. En este trabajo se estudió un área ~180 km<sup>2</sup> a 16 km al este-noreste de la ciudad de Acatlán, Puebla. En esta región afloran

litologías que han sido correlacionadas con las formaciones Cosoltepec y Tecolate (Ortega-Gutiérrez *et al.*, 1999; Ramírez-Espinosa, 2001), así como la sección tipo de la Formación Xayacatlán en el sentido de Ortega-Gutiérrez (1978).

La historia paleozoica del Complejo Acatlán ha sido correlacionada tanto a la margen continental de Laurentia como a la de Gondwana. En la última década se han postulado varias interpretaciones relacionadas con el origen de las rocas del Complejo Acatlán (*e.g.* Ortega-Gutiérrez *et al.*, 1999, Keppie y Ramos, 1999; Talavera-Mendoza, *et al.*, 2005; Nance *et al.*, 2006; Vega-Granillo *et al.*, 2007, 2009; Keppie *et al.*, 2008a). Las cuales se desprenden de una serie de estudios realizados durante las décadas pasadas (Ortega-Gutiérrez, 1975; De Cerna, 1967; Yañez *et al.* 1991; Ramírez-Espinosa, 2001), y apoyadas por investigaciones recientes en diferentes localidades del Complejo Acatlán (Ortega-Gutiérrez *et al.*, 1999; Elías-Herrera y Ortega-Gutiérrez, 2002; Vachard y Flores de Dios, 2002; Malone *et al.*, 2002; Keppie *et al.*, 2004a,b, 2006; Sánchez-Zavala *et al.*, 2004; Talavera-Mendoza *et al.*, 2005; Nance *et al.*, 2006, 2007; Murphy *et al.*, 2006; Miller *et al.*, 2007; Middleton *et al.*, 2007; Elías-Herrera *et al.*, 2007; Vega-Granillo *et al.*, 2007; Grodzicki *et al.*, 2008, Hinojosa-Prieto *et al.*, 2008, Ramos-Arias *et al.*, 2008, Vega-Granillo *et al.*, 2009; este trabajo).

Las discusiones acerca del origen del Complejo Acatlán se han centrado principalmente en la edad de este complejo y su evolución a lo largo del Paleozoico en diferentes cuencas oceánicas, separadas en tiempo y espacio (Yañez *et al.*, 1991; Ortega-Gutiérrez *et al.*, 1999; Keppie y Ramos 1999; Talavera-Mendoza *et al.*, 2005).

En este sentido cabe señalar por una parte que, durante el Paleozoico inferior evolucionaron al menos dos grandes cuencas oceánicas, la primera relacionada a un proceso de rifting entre las masas continentales del este de Laurentia y la parte oeste de Gondwana, lo que dio origen a la apertura del océano Iapetus durante el Cámbrico temprano, posteriormente el cierre de este océano culminó con el super-continente de Gondwana (McCausland *et al.*, 2007).

Por otra parte también, en el Paleozoico inició, durante un proceso de rifting, la separación de los continentes de Báltica y Avalonia en el norte del gigantesco continente de Gondwana (Murphy *et al.*, 2004), con el desarrollo de un intenso magmatismo asociado a una cuenca marina. Báltica y Avalonia convergieron con Laurentia durante el

Ordovícico-Silúrico, el océano Rhéico se desarrolló a expensas del océano Iapetus durante el cierre de este último, y tuvo su máximo desarrollo durante el Silúrico y su cierre culminó con un proceso de acreción/subducción durante la colisión de Gondwana y Laurasia durante la orogenia Variscana-Alleghaniana (Matte, 2001) durante el ensamblaje Carbonífero del supercontinente de Pangea (Pereira *et al.*, 2008) (Figura 1-1).

Con base en lo anterior se han interpretado varios escenarios tectónicos. Ortega-Gutiérrez *et al.* (1999) plantearon que el Complejo Acatlán está vinculado al cierre del océano Iapetus al final del Silúrico y explican que la orogenia Acateca tuvo lugar durante la colisión entre el noroeste de Gondwana y este de Laurentia. Mientras que Keppie y Ramos (1999) sugieren que las rocas del complejo Acatlán están relacionadas con la apertura del océano Rhéico más que con el cierre del océano Iapetus.

En este sentido Murphy *et al.* (2006) han señalado que las rocas del Complejo Acatlán están relacionadas con la evolución del océano Rheico, el cual se inició durante un proceso de rifting durante el Paleozoico y se desarrolló entre el continente de Gondwana en el sur y los continentes de Báltica y Avalonia al norte, debido al rompimiento de una margen continental neoproterozoica, y su posterior cierre dio lugar al supercontinente Pangea (Nance *et al.*, 2006).

Talavera-Mendoza *et al.* (2005) y Vega-Granillo *et al.* (2007, 2009) publicaron un modelo en el cual colocan a diferentes unidades del Complejo Acatlán en distintos períodos, de esta manera asocian a las rocas de El Rodeo y a los granitoides megacristalinos del Ordovícico inferior, en el noroeste del Complejo Acatlán, entre el este de Laurentia y un arco. A la Formación Xayacatlán la colocan como parte del océano Iapetus, y a la Formación Cosoltepec la relacionan con un margen pasivo que bordeaba a Amazonia.

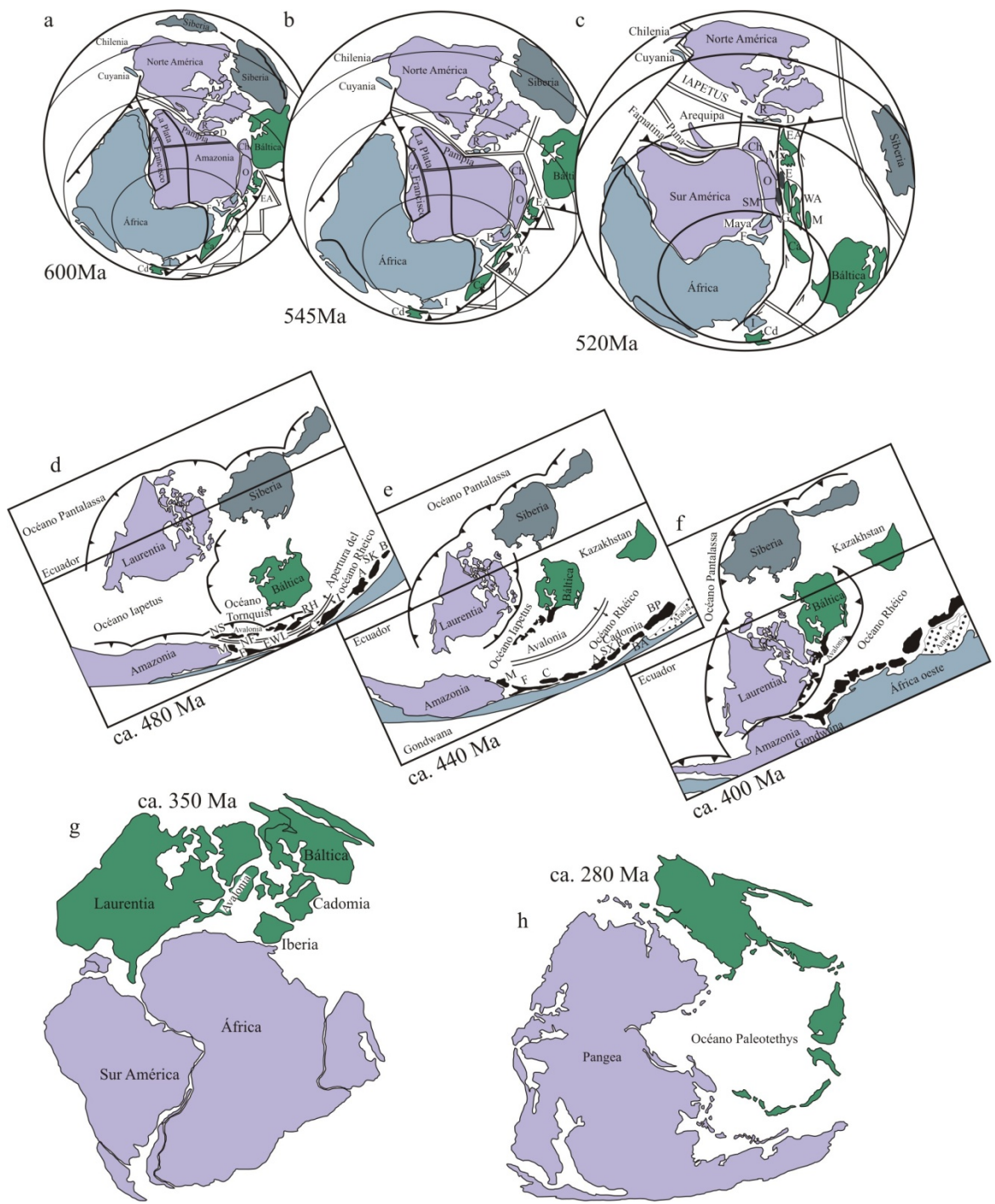


**Figura 1-1.** Paleogeografía de los océanos Iapetus y Rheico durante: a, b y c ca. 600 Ma, ca. 545 Ma y ca. 520 Ma respectivamente (Keppie, 2004), d, e y f ca. 480 Ma, ca. 440 Ma y ca. 400 Ma respectivamente (Bozkurt *et al.*, 2008; Linnemann *et al.*, 2003; modificado de C.R. Scotese: Paleomap website: [www.scotese.com](http://www.scotese.com)), g ca. 350 Ma (Keppie, 2004) y h ca. 280 Ma (Bozkurt *et al.*, 2008; redibujado de ‘Palaeos: The Trace of Life on Earth’website en <http://www.palaeos.com>). A — Armorica (Britania, Normandía, Macizo Central), B — Barrandiania, C — Carolina, EWI — Inglaterra, Gales, e Irlanda del Sur, F — Florida, I — Iberia, IR — Irán, M — Terrenos Mexicanos, NF — New Foundland, NS — Nova Scotia, PA — proto-Alpes, RH — Reno-Hercynian, SX — Saxo-Thuringian, TP — Placa Turca.

Recientemente Keppie *et al.* (2008a) propusieron que el Complejo Acatlán se originó en la margen sur del océano Rheico viajando con Amazonia y al final estuvo relacionado con una margen activa del océano Paleo-Pacífico (Keppie *et al.*, 2008a).

En el presente trabajo se consideró el estudio de la región de Xayacatlán, la cual se considera clave para entender parte de la historia paleozoica del Complejo Acatlán, y donde fue definida anteriormente la sección tipo de la Formación Xayacatlán, la cual forma parte del Grupo Piaxtla (*e.g.* Ortega-Gutiérrez *et al.*, 1999). En el área de estudio afloran así mismo rocas asociadas a las formaciones Cosoltepec y Tecomate (Ortega-Gutiérrez *et al.*, 1999; Talavera-Mendoza, 2005).

En este trabajo se presentan los resultados obtenidos de la investigación llevada a cabo en la región de estudio en cuatro capítulos. Los capítulo están ordenados de tal manera que muestran los resultados obtenidos en cada etapa de la investigación, de esta manera, en primer lugar se hizo una cartografía detallada de las unidades que afloran en la región de estudio y se obtuvieron las edades de rocas meta-sedimentarias y meta-ígneas.

Estos tópicos fueron abordados en primer lugar dados los contrastes litológicos identificados en las rocas que afloran en la región de Xayacatlán, previamente descritas por otros autores, los cuales adoptaron una descripción regional e incluyeron varias unidades litodémicas en formaciones (*e.g.* Ortega-Gutiérrez *et al.*, 1999; Ramírez-Espinosa, 2001).

Por medio de la cartografía a detalle del área de estudio se pudieron definir varias unidades meta-sedimentarias y meta-ígneas paleozoicas, las cuales han sido denominadas como unidades Huerta y Salada, anteriormente consideradas como Formación Cosoltepec (*e.g.* Ortega-Gutiérrez *et al.*, 1999; Ramírez-Espinosa, 2001; Talavera-Mendoza *et al.*, 2005), y la unidad Amate la cual fue integrada, previamente, en las rocas de la Formación Xayacatlán al igual que el aquí descrito como enjambre de diques Xayacatlán, o bien como subgrupo Acateco no diferenciado (Figura 2-I: Ortega Gutiérrez, 1975).

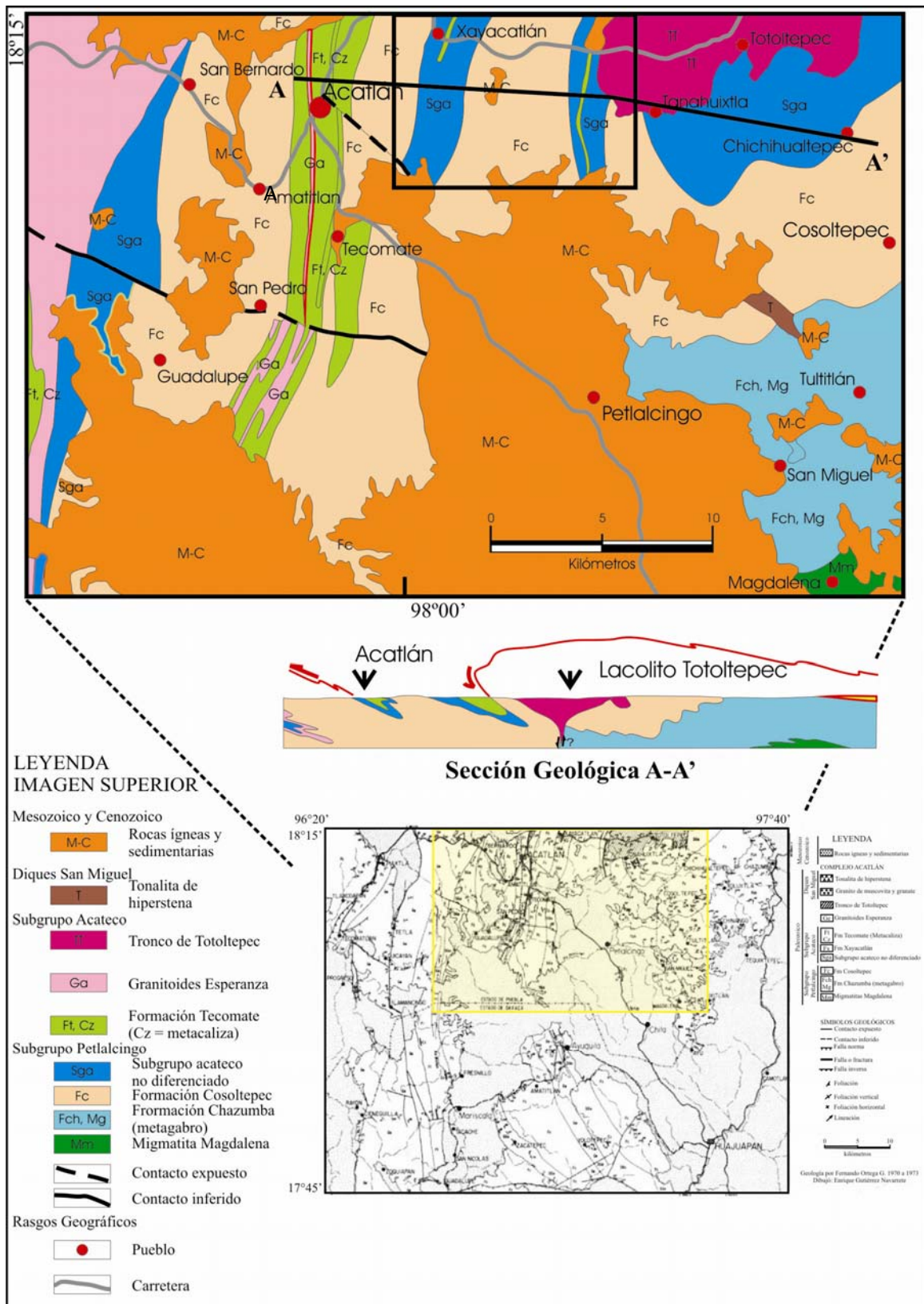


Figura 2-I. Mapa de Ortega-Gutiérrez (1975) y la sección geológica A-A' fue tomada de Ortega-Gutiérrez *et al.* (1999). La zona estudiada en este trabajo se localiza en la parte centro-norte, recuadro negro extremo superior, solo se muestra la parte sur del área de estudio.

Al norte del área de estudio fueron descritas rocas que han sido correlacionadas con la Formación Tecomate, y cubriendo la secuencia rocas más jóvenes que pertenecen a la cobertura del terreno Mixteca. Las diferencias litológicas encontradas en rocas incluidas en un mismo litotipo indicaban ambientes de depósito distintos o bien un contraste cronológico en ellas, de tal manera que se llevaron a cabo dataciones geocronométricas, por medio del método U-Pb (realizadas en RSES-ANU: *Research School of Earth Sciences-Australian National University, Canberra, Australia*), en circones detriticos de las unidades Amate, Huerta y Salada, así como en circones ígneos de las pegmatitas y rocas máficas que intrusionan a las unidades Huerta y Amate.

Las unidades meta-sedimentarias Huerta y Salada presentan elementos litológicos que excluyen a una de la otra, por ejemplo: la primera está intrusionada por pegmatitas y no hay registro de diques máficos emplazados en ella. El segundo tópico consistió en realizar análisis geoquímicos a estos diques. Diez ejemplares, colectados en varios sitios en la Unidad Salada fueron analizados por elementos mayores y trazas (Rb, Sr, Ba, Ga, Zr, Y, Nb, V, Ni, Co y Cr), por medio de espectrometría de fluorescencia de rayos X en el *Department of Earth Sciences of University of Ottawa, Canada*. Ocho ejemplares representativos fueron seleccionados de este conjunto para análisis de otros elementos traza (elementos de las tierras raras [REE, por sus siglas en inglés], Th, Nb, Ta, Zr y Hf) por medio de ICP-MS (Espectrometría de Masas con Fuente de Plasma Acoplado Inductivamente) en el *Department of Earth Sciences, Memorial University of Newfoundland, Canada*. Los análisis estuvieron enfocados en determinar en qué tipo de ambiente tectónico fueron emplazados estos diques, los resultados obtenidos se presentan en el segundo capítulo.

El tercer tópico, tratado en este estudio, es el de la historia de deformación de las diferentes unidades y su relación con los eventos metamórficos registrados en las rocas de la región de Xayacatlán. Los estilos de deformación en las unidades Huerta y Salada han sido descritos como parte de los mismos eventos de deformación (Formación Cosoltepec), mientras que en las unidades Amate y Formación Tecomate presentan etapas de deformación que varían en tiempo y número (Formación Xayacatlán y Formación Tecomate, respectivamente: Malone *et al.*, 2002). En el Complejo Acatlán han sido

descritos múltiples eventos de deformación y metamorfismo (*e.g.* Vega-Granillo 2006; Vega-Granillo *et al.*, 2009), en este sentido el trabajo estructural, en el entendimiento que los estilos de deformación se manifiestan de manera distinta en rocas sometidas a diferentes condiciones de presión y temperatura, así como la composición mineralógica (Alsop y Holdworth, 2004a, b), se enfocó en caracterizar los eventos de deformación observados únicamente en el área de estudio, y su relación con el metamorfismo, para posteriormente compararlos con los eventos de deformación y metamorfismo registrados en otras zonas del complejo (*e.g.* Ramos-Arias *et al.*, 2008; Grodzicki *et al.*, 2008; Hinojosa-Prieto *et al.*, 2008; Vega-Granillo *et al.*, 2009) y de esta manera poder establecer correlaciones cronológicas, geoquímicas y estructurales.

El último capítulo consiste de un artículo enfocado a la geoquímica y geocrontología a las rocas de composición toleíticas en las zonas de Xayacatlán, Patlanoaya y Cuauhtle, el cual a pesar que no es un trabajo netamente realizado en el área de estudio, integra los resultados obtenidos en esta investigación en un contexto tectónico global y en el cual se compila la información disponible en otras áreas del complejo, esto desde luego permite entender la historia tectónica del Complejo Acatlán y la trascendencia del área de Xayacatlán en el entramado geológico del Sur de México y el rol tectónico de sus rocas durante el Paleozoico.

## **Descripción de las rocas cartografiadas en la región de Xayacatlán**

### **Rocas meta-sedimentarias paleozoicas**

En el área de estudio fueron cartografiadas cuatro unidades meta-sedimentarias, incluidas previamente en las formaciones Xayacatlán, Cosoltepec, Tecolate y lacolito de Totoltepec, las cuales forman parte de las rocas paleozoicas del Complejo Acatlán. La región de estudio se separó estructuralmente en bloques (Figura 3-I).

#### *Unidad Amate*

La Unidad Amate ocupa la parte central del área de estudio, dentro del bloque Bravo y está limitada por medio de zonas de cizalla subverticales con una tendencia estructural NNE-SSW y con una cinemática lateral derecha. Al oeste está en contacto con la unidad meta-sedimentaria Huerta dentro del bloque Tizac, por medio de la falla Las Ollas. Al este el contacto es con el bloque Estaca por medio de la falla Carrizal. El bloque Bravo al norte está cubierto por rocas de la formación Tecolate, el contacto tectónico a su vez está plegado. En la parte central del bloque Bravo las rocas meta-calcáreas de la Formación Tecolate están fuertemente deformadas por un cizallamiento lateral derecho, ambos cuerpos son sobreyacidos por caliza de la cobertura mesozoica del terreno Mixteca. Al sur la Unidad Amate está sobreyacida por rocas volcanosedimentarias cenozoicas. La unidad Amate está formada principalmente de meta-arcosas y en menor medida por meta-pelitas, contiene cuarzo, plagioclasa, muscovita, clorita y minerales accesorios como circones y minerales opacos. Estas minerales indican un metamorfismo en facies de esquisto verde y anfibolita (hornfels) cerca de las zonas de intrusión del enjambre de diques de Xayacatlán, en las zonas adyacentes a los diques gabróicos (hornfels) los cristales de clinozoicita y muscovita tienen una fábrica decusada.

Se colectaron tres muestras en la Unidad Amate cerca de las zonas de contacto con los diques gabróicos en el bloque Bravo. La edad de enfriamiento obtenida para el ejemplar AMATE-GA3/D-644 (anfibol, N $18^{\circ}16.442'$ , W $97^{\circ}54.852'$ ), muestra una edad de meseta de  $404\pm2$  Ma, con una temperatura de cierre inferior *ca.* 480°C. Los ejemplares REP-1/AOR-1016 (muscovita,  $18^{\circ}15.508'$ ,  $97^{\circ}58.090'$ ) y AMATE-4/AOR-1018 (muscovita,  $18^{\circ}13.735'$ ,  $97^{\circ}58.947'$ ) muestran espectros discordantes con edades de meseta de  $357\pm6$  Ma y  $278\pm2$  Ma, respectivamente, con edades mínimas de enfriamiento probablemente *ca.* 370-380°C.

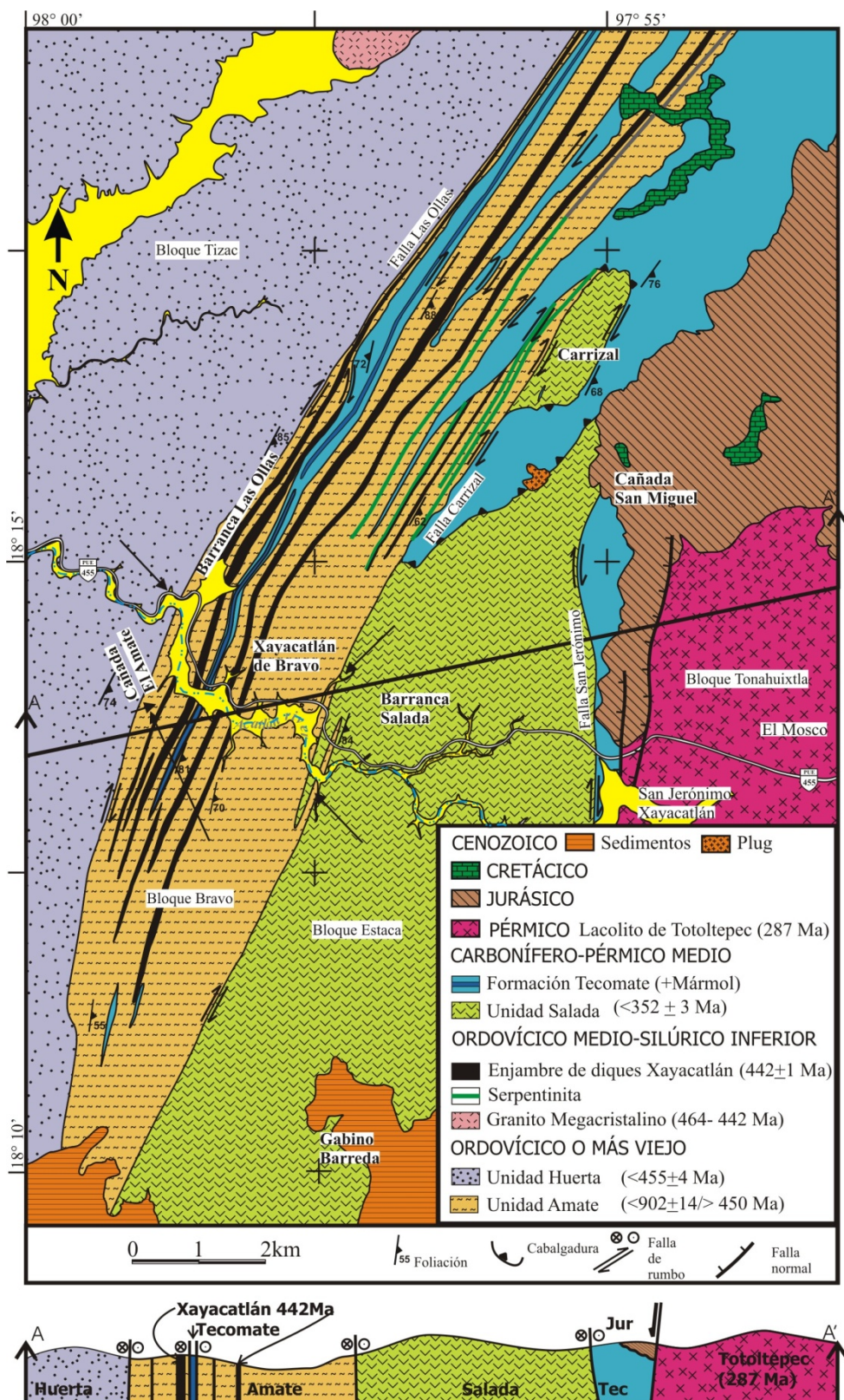


Figura 3-I. Mapa geológico del área de Xayacatlán (este trabajo).

En la meta-psammita feldespática en la Unidad Amate (AMATE-1, N $18^{\circ}$  13.793', W $97^{\circ}$  58.965') se obtuvieron edades en los circones detriticos de esta unidad en un rango de 847 Ma a 1325 Ma. Las edades concordantes más viejas están dentro de un periodo que comprende un rango de ~900 Ma a 1300 Ma. No obstante, la edad concordante más joven en esta unidad es de 902±14 Ma. El depósito de la Unidad Amate está constreñido en un lapso que es posterior a 904±14 Ma (edad de los circones detriticos concordantes más jóvenes) y previo a las edades de 447±3Ma, 452±6Ma (las edades intrusivas de los diques graníticos que cortan a esta unidad) y a 442±1 Ma (edad del intrusivo de composición gabróica que corta a esta unidad).

La Unidad Amate preserva una estratificación relictica la cual se observa como una alternancia de bandas de cuarcita y meta-pelita. Este bandeadimiento es paralelo al clivaje S<sub>A1</sub>, el cual está definido por cristales de muscovita y clorita alineados. En las aureolas de contacto de la meta-arcosa con el gabro se definen lineaciones de clorita y muscovita, lo cual indica un metamorfismo en facies de esquisto verde, sobreimpuesto al metamorfismo en facies de anfibolita de los metagabros de los diques de Xayacatlán, acompañado por una deformación lateral derecha.

Los indicadores cinemáticos, en las zonas de cizalla lateral derecha, incluyen fábricas tipo libro rotado (*bookshelf fabrics*) (Tolson, 1996), lineación de estiramiento subhorizontal y estructuras sigma que indican movimientos destrales. El clivaje, S<sub>A1</sub> está deformado por pliegues cerrados con una orientación de sus planos axiales hacia el NNE-SSW y los ejes de pliegue varían de subverticales a subhorizontales, acompañados por lineación de estiramiento subhorizontal, L<sub>A2</sub>, y el desarrollo de un clivaje de crenulación planar axial, S<sub>A2</sub>, el cual es observable en las litologías meta-pelíticas y en las zonas de falla que limitan al bloque Bravo. Todas estas estructuras están localmente deformadas por pliegues abiertos, con un buzamiento N-S sub-horizontal, F<sub>A3</sub>.

### *Unidad Huerta*

La unidad Huerta aflora en la parte occidental del área de estudio y está contenida dentro del bloque estructural Tizac. Las líneas que definen la orientación de las estructuras de cizalla tienen una dirección NNE-SSW. Al este, el bloque Tizac está en contacto, por medio de la falla Las Ollas, con el bloque Bravo. La unidad Huerta, en este bloque (Tizac), en la parte norte del área, está intrusionada por un granito megacristalino,

el cual está débilmente deformado. La edad que se asume en este trabajo para dichas rocas es del Ordovícico-Silúrico, consistente con muchos granitoides descritos por Miller *et al.* (2007), Keppie et al. (2008a) y *circa* de Xayacatlan (este estudio). Al oeste el contacto es con rocas de la Formación Tecomate (fuera del área cartografiada), mientras que al norte y sur el contacto es cubierto discordantemente por rocas mesozoicas y cenozoicas, respectivamente (fuera del área cartografiada).

La Unidad Huerta está integrada por bandas deformadas de meta-psamitas y meta-pelitas con metamorfismo en facies de esquisto verde. Las meta-psamitas y meta-pelitas consisten de cuarzo, moscovita, clorita, circones y minerales opacos. Esta unidad es intrusionada intensamente por vetas de cuarzo en la parte oeste, mientras que en la parte este predominan las vetas de pegmatitas de composición cuarzo-feldespáticas. La edad concordante más joven obtenida en circones detríticos en la parte occidental de esta unidad es de  $455\pm4$  Ma y presenta picos en  $\sim 600$  Ma y  $\sim 1-1.2$  Ga (Keppie *et al.*, 2006).

Las rocas de esta unidad muestran una intensa deformación polifásica, que incluye el desarrollo de pliegues de vaina en condiciones metamórficas de facies de esquisto verde (*e.g.* Malone *et al.*, 2002). Los rasgos estructurales de la unidad Huerta son análogos a los observados en la unidad Salada, la cual será descrita más adelante:

(*i*) en este sentido la estratificación,  $S_0$ , se preserva como una alternancia de horizontes psamíticos y pelíticos metamorfizados;

(*ii*) las estructuras de clivaje,  $S_{HS1}$ , varían de un clivaje de presión solución en las meta-psamitas a un clivaje filítico en las meta-pelitas: este clivaje es sub-paralelo a la estratificación en las meta-pelitas y es refractado en las meta-psamitas. Estructuras de plegamiento para esta fase de deformación no fueron observadas. El clivaje es definido por una lineación de muscovita y clorita, indicando que esta deformación tuvo lugar bajo un metamorfismo en facies de esquisto verde;

(*iii*) un grupo de estructuras incluye pliegues isoclinales y raramente pliegues de funda (Malone *et al.*, 2002,  $F_{HS2}$ ), presenta un clivaje ( $S_{HS2}$ ) y una fuerte lineación de estiramiento en cuarzo ( $L_{HS2}$ ). El clivaje  $S_{HS2}$  varía de un clivaje de solución en las meta-psamitas a un clivaje filítico en muscovitas, cloritas, fengitas y lineación de estiramiento en cuarzo, que es generalmente un clivaje compuesto,  $S_{HS1+2}$ . Esta asociación mineral

indica una deformación bajo condiciones de facies de esquisto verde. El clivaje generalmente tiene una orientación N-S con un buzamiento subvertical, mientras que la lineación es generalmente horizontal. Los planos axiales de los ejes son generalmente sub-verticales, mientras que los ejes de los pliegues son predominantemente sub-horizontales; y

(iv) Un grupo de estructuras deforman a  $S_{HS1}$  y  $S_{HS2}$  y producen pliegues, tanto abiertos como apretados, los pliegues verticales y la crenulación tienen una inclinación superficial el N ( $N25^{\circ}E$  a  $N10^{\circ}W$ ), los ejes de los pliegues tienen un *plunge* entre  $0^{\circ}$  y  $25^{\circ}$  al N ( $F_{HS3}$ ). Los cristales de muscovita son plegados en las charnelas de los pliegues, mientras que la clorita parece recristalizada en segmentos rectos y cortos, sugiriendo condiciones de metamorfismo en facies de esquistos verde-baja.

#### *Unidad Salada*

La Unidad Salada está formada por meta-psamitas y meta-pelitas en facies de esquisto verde que afloran dentro del bloque Estaca, el cual se localiza en la parte centro-oriental del área de estudio. El bloque Estaca está en contacto tectónico, al oeste, por medio de la falla Carrizal con el bloque Bravo, y al este con el Bloque Tonahuixtla por medio de la falla San Jerónimo, la cual pone en contacto por medio de una zona de falla lateral derecha rocas de la Formación Tecolate y el Lacolito de Totoltepec ubicados en el bloque Tonahuixtla.

La unidad Salada originalmente fue cartografiada como parte de la Formación Cosoltepec junto con la unidad Huerta, mencionada anteriormente, ambas unidades presentan los mismos estilos de deformación. Sin embargo, la unidad Salada presenta bandas delgadas de diques máficos toleíticos, con una orientación estructural NNE, estos diques cortan a la roca encajonante.

En sección delgada los diques muestran arreglos mineralógicos de anfíbol, clorita, feldespato, epidota y minerales opacos accesorios. Las rocas meta-sedimentarias están compuestas de cuarzo, muscovita, clorita y minerales opacos accesorios. Las asociaciones minerales observadas tanto en la roca de caja como en los diques muestran un metamorfismo en facies de esquisto verde. La edad concordante en el circón detrítico más joven, obtenida por medio de  $^{206}\text{Pb}/^{238}\text{U}$ , es de  $352\pm3$  Ma, mientras que las edades

concordantes más viejas varían de ~434–485 Ma, 511–630 Ma, y 920–1200 Ma (muestra SAL-11: 18° 14.077, 97° 57.341').

La edad de enfriamiento  $^{40}\text{Ar}/^{39}\text{Ar}$  obtenida en la muestra W3-SAL (muscovita, 18°16.952', 97°54.852') de la Unidad Salada, proporciona datos discordantes con una edad de meseta de  $324 \pm 2$  Ma. Esta edad representa una edad mínima de enfriamiento *ca.* 400°C. Estas edades limitan la deposición de la Unidad Salada en el Misisípico.

#### *Formación Tecomate*

La Formación Tecomate en el área de Xayacatlán es tectónicamente yuxtapuesta a las unidades meta-sedimentarias en los bloques Bravo y Estaca. Las rocas de esta formación están en contacto por medio de falla con el Lacolito de Totoltepec y está cubierta por rocas sedimentarias continentales jurásicas en la parte este. Las cuales a su vez están cubiertas discordantemente por rocas calcáreas cretácicas, esta relación se observa en algunas áreas en el norte del área de estudio. También está intrusionada por cuellos volcánicos cuya edad considerada es cenozoica.

La Formación Tecomate consiste de meta-arcosas, meta-psamitas, pizarras, meta-conglomerados y bandas de mármoles. Las rocas clásticas consisten principalmente de cuarzo, feldespato, muscovita, clorita, epidota y minerales opacos. Los conglomerados contienen diversos guijarros que proceden de granitoides y rocas volcánicas, meta-psamitas y vetas de cuarzo. Los guijarros derivados de los granitoides, obtenidos de un meta-conglomerado, a ~20 km al sureste del área de Xayacatlán han dado edades en U-Pb de ~290 Ma y se ha inferido que son derivados del Lacolito de Totoltepec (Yañez *et al.*, 1991; Keppie *et al.*, 2004b), el cual se expone a lo largo de la margen oriental de la zona de estudio.

Las rocas calcáreas en la sección tipo de la Formación Tecomate están expuestas al sur del pueblo de Acatlán, y contienen microfósiles del Pensilvánico tardío-Pérmino temprano (Keppie *et al.*, 2004a). La deformación en las rocas correlacionadas con la Formación Tecomate en el área de Xayacatlán, presenta dos etapas.

La estratificación se preserva en algunas zonas ligeramente deformadas donde se observa la alternancia de areniscas, pizarras/filitas, conglomerado y capas de caliza/mármol. Las rocas de esta formación están deformadas por una serie de pliegues

abiertos isoclinales, subhorizontales y pliegues de funda (Malone *et al.*, 2002), dicho plegamiento se identifica con el evento de deformación ( $F_{T1}$ ). Los planos axiales son paralelos al clivaje definido por muscovita y clorita,  $S_{T1}$ , la lineación asociada,  $L_{T1}$ , varía desde una lineación de intersección a una lineación de estiramiento subhorizontal en las zonas de cizalla. La forma prolada de los fragmentos en los conglomerados indica que la deformación fue transtensional destral sobrepuesta a las deformaciones previas en la zona de estudio.

La segunda etapa de deformación,  $F_{T2}$ , deforma a las estructuras  $S_{T1}$  por medio de pliegues abiertos, clivaje de crenulación y *kink bands*, este plegamiento está asociado con el crecimiento de clorita. Se fechó por medio del método  $^{40}\text{Ar}/^{39}\text{Ar}$  un esquisto (sericitita en roca total) de la formación Tecomate (AxTT-366-TCC,  $18^{\circ}15.582'$ ,  $97^{\circ}56.223'$ ), el cual proporcionó un espectro discordante con una edad aparente de  $263 \pm 3$  Ma (Pérmico temprano-tardío). El grado de metamorfismo que se infiere para esta formación varía de facies sub-esquisto verde a facies de esquisto verde-baja (Malone *et al.*, 2002).

### Rocas meta-ígneas paleozoicas

Las rocas meta-ígneas cartografiadas en el área de estudio son: (i) diques gabróicos del Enjambre de Xayacatlán que intrusionan a la unidad Amate, (ii) diques pegmatíticos que intrusionan a la unidad Huerta, y (iii) diques tholeíticos emplazados en la unidad Salada y el Lacolito de Totoltepec, este último en la porción oriental del área de estudio.

#### *Enjambre de diques Xayacatlán*

Originalmente las rocas meta-gabróicas fueron incluidas en la Formación Xayacatlán por Ortega-Gutiérrez (1975). Estas rocas afloran como un enjambre de diques verticales, con una orientación  $\sim\text{N-S}$ , afectados por múltiples eventos de deformación y por metamorfismo retrógrado, resultando esquistos de clorita y serpentinita. La edad obtenida en circones por medio del método U-Pb de estos diques es de  $442 \pm 1$  Ma (muestra XAY-3,  $N18^{\circ}15.150$ ,  $W97^{\circ}58.287$ , Keppie *et al.*, 2008b).

Los diques tienen anchos variables, siendo el de mayor anchura de  $\sim 100$  m y su extensión es de varios kilómetros (Figura 3-I), tienen una textura de gneisses anfibolíticos foliados y presentan, en afloramiento, bandas de composición anfibolítica a leucocrática

(principalmente plagioclasa). Los anfíboles son de verde pardo a hornblendas café, con pleocroismo distintivo. Los cristales elongados tienen un rango usualmente de 0.1 mm a ~3 mm. El anfibol tiene una composición de magnesio-hornblenda a edenita (Keppie *et al.*, 2008b). Los anfíboles son localmente remplazados por tremolita mientras la plagioclasa es reemplazada por sericitas.

Los diques meta-gabróicos están intrusionados por delgados diques máficos plegados y con el mismo estilo de foliación que la roca encajonante, metamorfosados en facies de anfibolita y afectados por un metamorfismo retrogrado en facies de esquisto verde. El cual se manifiesta en las aureolas de contacto con la presencia de clorita, los diques máficos son de pocos centímetros de espesor, pero llegan a tener un desarrollo longitudinal de varios metros dentro de las bandas de metagrabros.

Los diques máficos presentan alteraciones a serpentina, principalmente en las zonas de alta deformación por cizalla, y en menores proporciones feldespato-K. Las edades de enfriamiento obtenidas de la relación de  $^{40}\text{Ar}/^{39}\text{Ar}$  en hornblenda (XAY-13: N18°15.150, W97°58.275) da un edad de 434 Ma que se asocia al enfriamiento debajo de 550°C (Keppie *et al.*, 2008b). La geoquímica indica que los diques son toleíticos y se ha interpretado que se emplazaron durante un periodo de extensión, (Keppie *et al.*, 2008b).

### *Pegmatitas*

Los cuerpos de pegmatitas intrusionan a las unidades meta-sedimentarias Amate y Huerta, así como al enjambre de diques de Xayacatlán, en la parte oeste del área de estudio. Las pegmatitas que cortan a los diques máficos están compuestas de cuarzo, feldespato-K, plagioclásas alteradas a sericitas y minerales accesorios de circón, apatito y minerales opacos.

Las pegmatitas a su vez están foliadas y plegadas. Los resultados del análisis de circones por medio del método U-Pb proporcionaron edades en rangos desde 427 Ma hasta 2531 Ma, mientras que el promedio de cuatro edades concordantes es de ~485.5 Ma. Otras dos poblaciones se registran en circones heredados con edades concordantes de ~530-580 Ma y ~910-1200 Ma. Las pegmatitas que intrusionan la parte este presentan edades U-Pb en circones en un rango entre 427 Ma y 2531 Ma, las edades más jóvenes casi concordantes en circones son de 464±4 Ma.

### *Diques toleíticos en la Unidad Salada*

Los diques máficos, que intrusionan a meta-pelitas y meta-psamitas polideformadas de la Unidad Salada (Figura 3-I), presentan un metamorfismo en facies de esquisto verde. Estos diques están compuestos por anfíbol, clorita, feldespato, epidota y minerales opacos.

La geoquímica indica que los diques son toleíticos. Las relaciones de campo indican que estos diques son simultáneos o posteriores al depósito de las psamitas/pelitas de la Unidad Salada, pero son previos a los eventos de deformación, por otra parte estos diques no cortan a las rocas correlacionadas con la Formación Tecomate.

### *Lacolito de Totoltepec*

El Lacolito de Totoltepec aflora a lo largo de la margen este del área de Xayacatlán (Figura 3-I), tiene una composición de gabro (hornblenda, plagioclasa, epidota y clorita) a granito (cuarzo, feldespato-K, muscovita, plagioclasa alterada a sericita). Las edades obtenidas de los cuerpos máficos y félsicos en circones es de *ca.* 288 Ma (Yañez *et al.*, 1991; Keppie *et al.*, 2004b).

La fábrica tectónica identificada en el intrusivo es una foliación plegada con lineación mineral, y ha sido interpretada en términos de intrusiones sin-tectónicas durante un cabalgamiento con vergencia al sur (Malone *et al.*, 2002). El cuerpo intrusivo muestra una geoquímica calcoalcalina sugiriendo que forma parte de un arco Pérmico que corrió a lo largo de la margen oeste de México (Malone *et al.*, 2002).

## **Rocas mesozoicas**

### *Conglomerado jurásico*

En la porción nororiental del área de estudio, descansan discordantemente rocas sedimentarias continentales sobre rocas correlacionadas con la formación Tecomate, y están compuestas de conglomerados rojos, arenisca y ocasionalmente capas pizarrosas. En las capas pizarrosas se observan impresiones de hojas, por medio de ellas se ha determinado la edad jurásica para estos sedimentos, (Malone *et al.*, 2002; R. Weber, comunicación personal, 2005). Los conglomerados contienen guijarros de esquistos en la

base de la secuencia y gravas de feldespato y cuarzo. Esas rocas están deformadas por un basculamiento suave con buzamiento al norte asociado a una falla normal (Figura 3-I).

#### *Rocas calcáreas*

Al norte y cubriendo discordantemente a las rocas metamórficas paleozoicas y conglomeráticas jurásicas afloran tres cuerpos de caliza masiva no deformada ni metamorfizada, con espesores de pocas decenas de metros (Figura 3-I). En algunos afloramientos se observan concentraciones de organismos fosilizados, principalmente gasterópodos y corales. La edad cretácica de la caliza se ha determinado por correlación estratigráfica con las sucesiones de caliza que afloran al noreste y suroeste del área de estudio (SGM, 2001).

#### **Rocas cenozoicas**

Las rocas cenozoicas afloran principalmente en la parte sur del área de estudio, en esta zona consisten principalmente de sucesiones de rocas volcanosedimentarias que cubren discordantemente a las rocas paleozoicas. Esta relación se observa cerca del poblado de Gabino Barreda, la composición de los depósitos es andesítica y de edad paleógeno (SGM, 2001). Al norte las rocas terciarias se limitan a pequeños afloramientos relacionados con cuellos volcánicos, al oeste de la cañada San Miguel, la textura de estas rocas volcánicas es afanítica y presentan una composición andesítica (Figura 3-I).

## **Las hipótesis de la evolución geológica en el área de Xayacatlán**

### **Hipótesis uno**

La historia geológica del Complejo Acatlán ha sido inferida básicamente en dos sentidos (Figura 4-Ia y b), uno relacionado a un choque continental de las márgenes del océano Iapetus durante el Paleozoico, en este sentido se ha planteado la siguiente hipótesis:

- i) Depósito durante el Cambro-Ordovícico de siliciclastos pertenecientes al Grupo Petlalcingo (Magdalena, formaciones Chazumba y Cosoltepec: Ortega-Gutiérrez *et al.*, 1999) y la formación Xayacatlán de naturaleza oceánica [renombrada como Grupo Piaxtla o Suite Piaxtla por Ramírez-Espinosa (2001) y Middleton *et al.* (2007), respectivamente].
- ii) Metamorfismo en facies de eclogita durante el Ordovícico tardío-Silúrico, deformaciones múltiples y emplazamiento del Grupo Piaxtla sobre el Grupo Petlalcingo en facies de esquisto verde durante la orogenia Acateca (Ortega-Gutiérrez *et al.*, 1999) u orogenias Taconiana-Saliniana (Talavera-Mendoza *et al.*, 2005; Vega-Granillo *et al.*, 2007): la fusión por descompresión es inferida para explicar los granitoides megacristalinos Esperanza (Ortega-Gutiérrez *et al.*, 1999).
- iii) Depósito de la formación Tecomate cuya edad asignada es del Silúrico-Devónico (Ortega-Gutiérrez *et al.*, 1999).
- iv) Deformación y metamorfismo en facies de esquisto verde durante la orogenia Mixteca del Devónico tardío (Ortega-Gutiérrez *et al.*, 1999; Sánchez-Zavala *et al.*, 2000).

### **Hipótesis dos**

Durante la última década se han llevado a cabo múltiples investigaciones en el Complejo Acatlán y por los datos aportados, se ha planteado otra hipótesis relacionada con la apertura del océano Rhéico (Keppie *et al.* 2008a, y este trabajo).

- 1) Depósito Ordovícico de rocas clásticas de margen pasivo relacionada a rift (Huerta y Amate) y emplazamiento de un magmatismo bimodal (granitoides megacristalinos y diques Xayacatlán).

2) Depósito de rocas sedimentarias del Devónico-Carbonífero (Unidad Salada) durante un metamorfismo en facies de eclogita (Piaxtla), deformación polifásica atribuida a la rápida exhumación de las rocas de alta presión durante el Misisípico.

3) Intrusión de plutones (Totoltepec) durante el Pérmico temprano relacionados a un arco en rocas sedimentarias de peri-arco (incluyendo la formación Tecolate) síncrona con una deformación polifásica de bajo grado.

4) Depósito de rocas siliciclásticas del Pérmico tardío-Triásico de rocas (unidades Chazumba y Magdalena) en un *foredeep* en el frente de una cabalgadura con vergencia hacia el sur.

5) Migmatización jurásica asociada con la deformación polifásica de las unidades Chazumba y Magdalena.

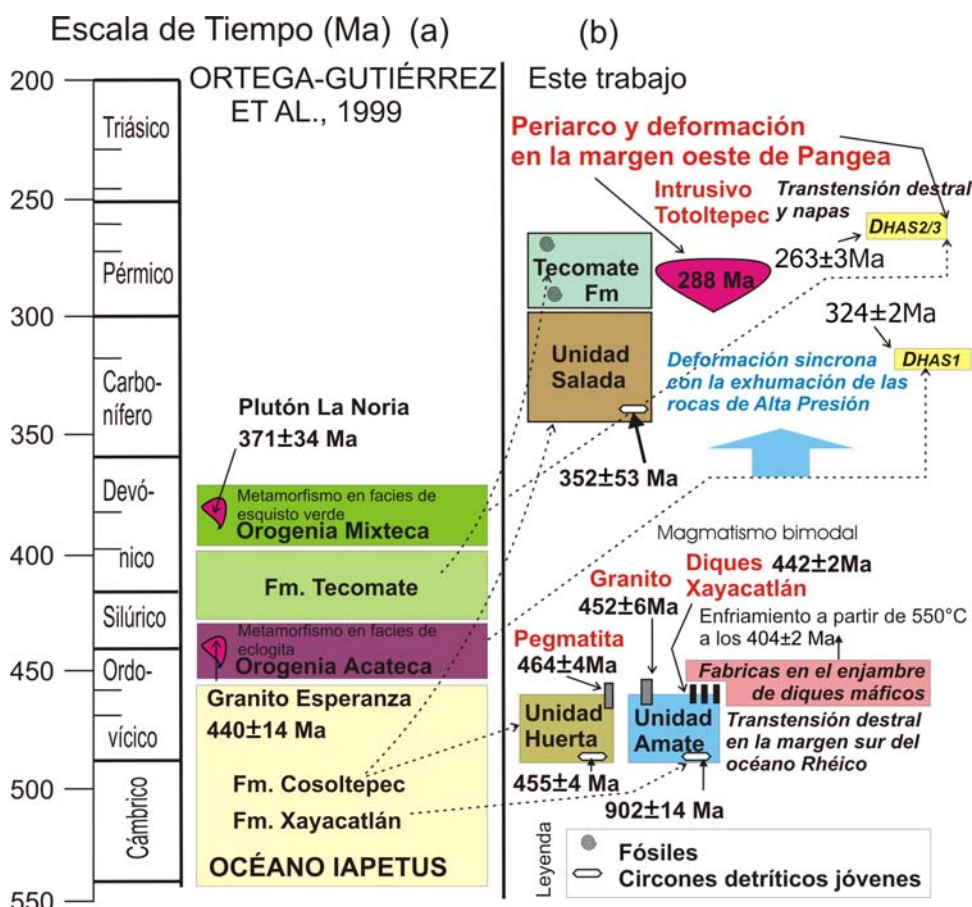


**Figura 4-I.** Diagrama espacio y tiempo, se muestran las dos hipótesis relacionadas con la evolución de las rocas del Complejo Acatlán con énfasis en el área de Xayacatlán, basado en el trabajo de Ortega-Gutiérrez *et al.*, 1999, izquierda (hipótesis uno) y el realizado en este trabajo, derecha (hipótesis dos).



# Ordovician–Silurian rift-passive margin on the Mexican margin of the Rheic Ocean overlain by Carboniferous–Permian periarc rocks: Evidence from the eastern Acatlán Complex, southern Mexico

Miguel Morales-Gámez <sup>a</sup>, J. Duncan Keppie <sup>a,\*</sup>, Marc Norman <sup>b</sup>

<sup>a</sup> Departamento de Geología Regional, Instituto de Geología, Universidad Nacional Autónoma de México, C.P. 04510 México D.F., Mexico

<sup>b</sup> Research School of Earth Sciences, Australian National University, Mills Road, Building 61, Canberra, ACT 0200, Australia

Received 16 May 2007; received in revised form 22 October 2007; accepted 25 January 2008

Available online 8 February 2008

## Abstract

In the Xayacatlán area of the Acatlán Complex in southern Mexico, several, N–S, fault-bounded packages of rocks occur (from west to east): (i) greenschist facies, interbedded psammites and pelites (Huerta Unit): the youngest concordant detrital zircon in the western part of the unit is  $455 \pm 4$  Ma; (ii) greenschist-amphibolite facies arkoses and psammites (Amate Unit): the youngest concordant detrital zircon gave a  $^{206}\text{Pb}/^{238}\text{U}$  age of  $902 \pm 14$  Ma, and older concordant ages of  $\sim 900$ – $1300$  Ma; (iii) low grade clastic rocks and marbles (Permian Tecolate Formation); and (iv) greenschist facies psammites, pelites and thin tholeiitic mafic slices (Salada Unit): the youngest concordant detrital zircon yielded a  $^{206}\text{Pb}/^{238}\text{U}$  age of  $352 \pm 3$  Ma and older concordant ages of  $\sim 434$ – $485$  Ma,  $511$ – $630$  Ma, and  $920$ – $1200$  Ma. The eastern part of the Huerta Unit is cut by pegmatite that yielded an almost concordant  $^{206}\text{Pb}/^{238}\text{U}$  zircon age of  $464 \pm 4$  Ma (a mean age of the four almost concordant young zircons is  $\sim 485.5$  Ma) interpreted as the time of intrusion, and inherited zircons with concordant ages of  $\sim 530$ – $580$  Ma and  $\sim 910$ – $1200$  Ma. These data suggest that the Huerta Unit ranges in age from Early (possibly older) to Late Ordovician. The Amate Unit is cut by granitic dikes, in which the youngest concordant  $^{206}\text{Pb}/^{238}\text{U}$  zircon ages are  $452 \pm 6$  Ma and  $447 \pm 3$  Ma interpreted as the time of intrusion, and older inherited zircon ages with concordant  $^{206}\text{Pb}/^{238}\text{U}$  ages in the range of  $950$ – $1250$  Ma. The intrusive ages are similar to the  $442 \pm 1$  Ma concordant U–Pb age for mafic dikes that also cut the Amate Unit. These data constrain the depositional age of the Amate Unit between  $\sim 900$  Ma and latest Ordovician. The age of the Salada Unit is probably Carboniferous because it is structurally overlain by the Lower–Middle Permian Tecolate Unit. The preponderance of  $510$ – $630$  Ma and  $900$ – $1250$  Ma ages in both the detrital and inherited ages in some of the dated samples suggests a source in the adjacent and subjacent Maya and Oaxacan Complex, respectively, although a xenocrystic host rock source cannot be ruled out for the intrusive rocks. The igneous intrusions have been interpreted as part of a  $480$ – $440$  Ma bimodal rift-related suite. Their synchronicity with deposition of the Huerta Unit (and possibly also the Amate Unit) suggests a rift-passive margin environment of deposition on the southern margin of the Rheic Ocean. On the other hand, the Salada Unit and the Tecolate Formation appear to be synchronous with a Permo-Triassic magmatic arc that developed on the western margin of Pangea.

© 2008 Elsevier B.V. All rights reserved.

**Keywords:** Acatlán Complex; Mexico; Ordovician; Permo–Carboniferous; Geochronology

## 1. Introduction

The Xayacatlán area is located in the eastern part of the Acatlán Complex (Fig. 1) (designated the Mixteca terrane by

Campa and Coney, 1983). The Acatlán Complex has been interpreted to be a vestige of a Paleozoic ocean, however, which ocean is presently a matter of debate. Ortega-Gutiérrez et al. (1999) suggested that it was part of the Cambro-Ordovician Iapetus Ocean, whereas Keppie and Ramos (1999) proposed that it was part of the Ordovician–Devonian Rheic Ocean. Subsequently, Talavera-Mendoza et al. (2005) and Vega-Granillo (2007) published a model that placed parts of the

\* Corresponding author. Fax: +52 555 622 4290.

E-mail addresses: moruz@yahoo.com (M. Morales-Gámez), duncan@servidor.unam.mx (J.D. Keppie).

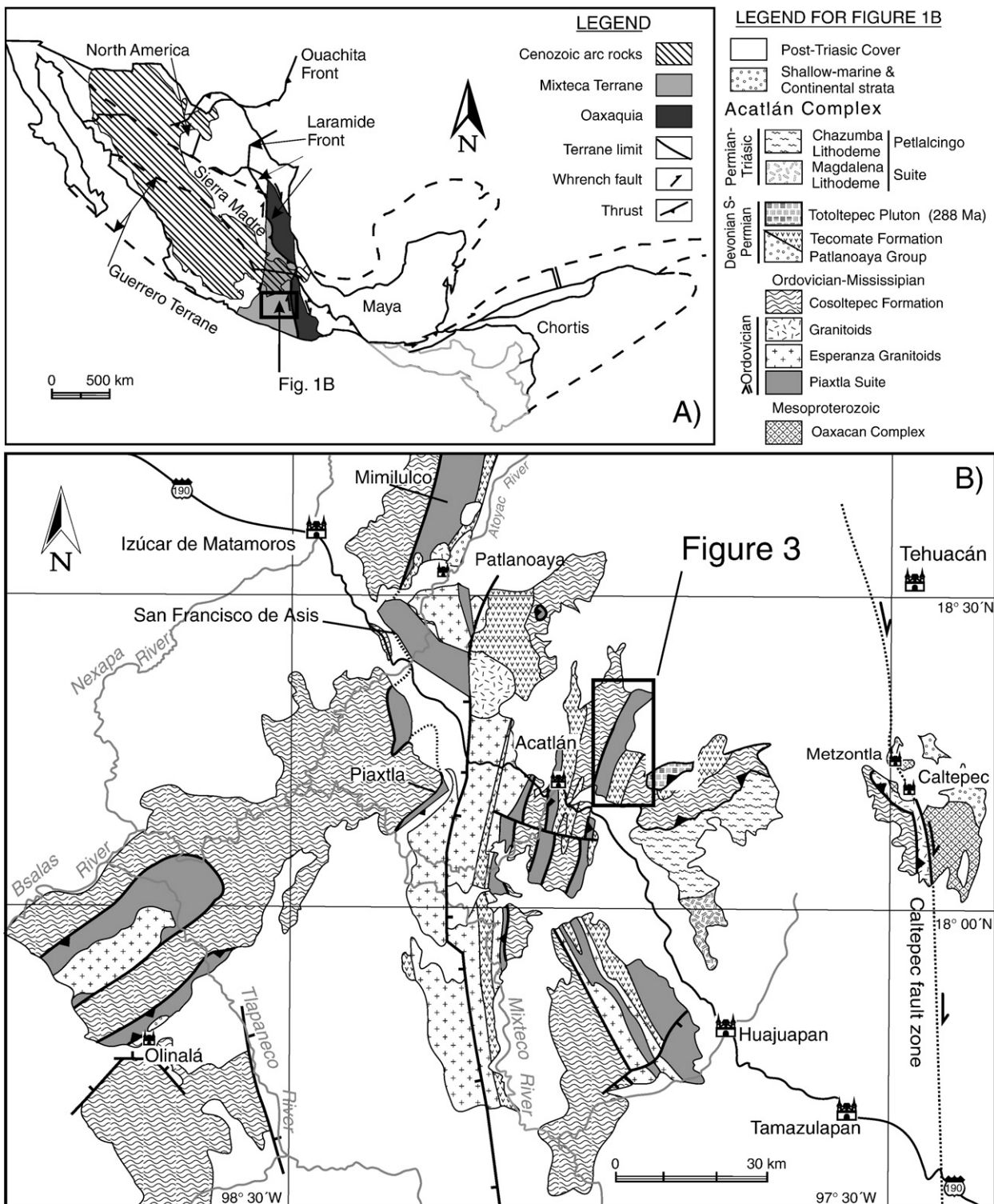


Fig. 1. Location of the Xayacatlán map shown on (A) terrane map of Middle America (modified after Keppie, 2004), and (B) geological map of the Acatlán Complex (modified after Keppie et al., 2006).

Acatlán Complex in three oceans: the El Rodeo unit and Lower Ordovician megacrystic granitoids were placed in the Bay Verte seaway between eastern Laurentia and an arc, the Xayacatlán Formation was attributed to the Iapetus Ocean, and the

Cosoltepec Formation was envisaged as a passive margin bordering Amazonia. A recent synthesis by Keppie et al. (2008a) proposes that the Acatlán Complex originated on the southern margin of the Rheic Ocean traveling with Amazonia to

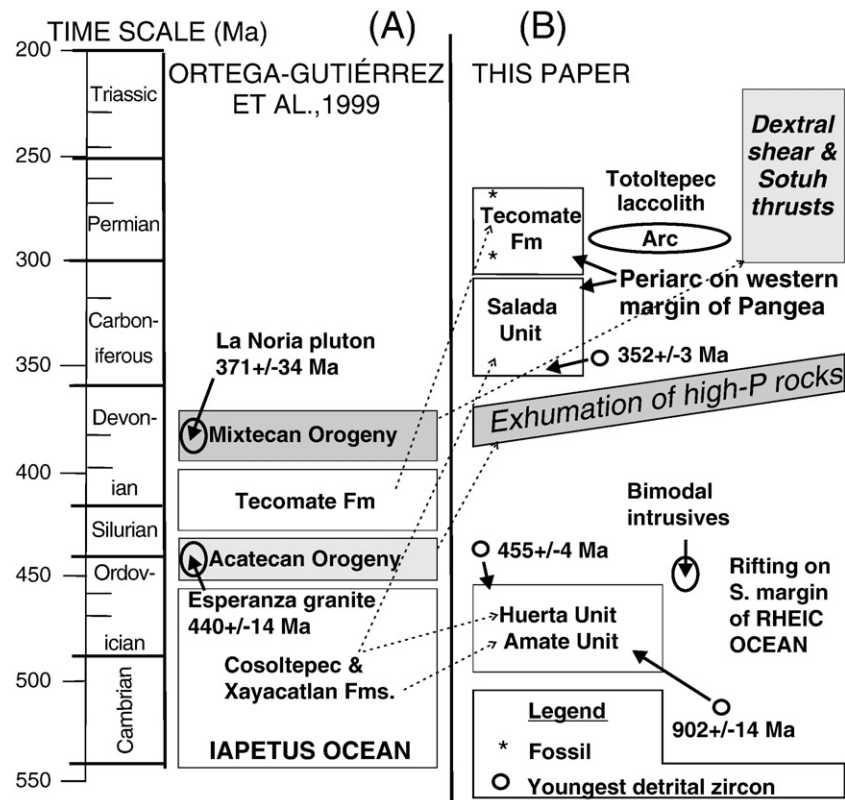


Fig. 2. Time-and-space diagram showing geological record of the Xayacatlán area: (A) after Ortega-Gutiérrez et al. (1999), and (B) this work.

end up on the active margin of the paleo-Pacific Ocean (Keppie et al., 2008a).

The Xayacatlán area is critical to resolution of this debate because it is the type area of the Xayacatlán Formation (Ortega-Gutiérrez, 1975). Ortega-Gutiérrez (1975) described the Xayacatlán Formation as an assemblage of metapsammites, metapelites, metagabbros, amphibolites, and serpentinite associated with megacrystic granitoids (Esperanza granitoids) that had undergone eclogite facies metamorphism (Fig. 2A). This high pressure metamorphism was believed to be late Ordovician based on the inference that the megacrystic granitoids were decompression melts that yielded a lower intercept U–Pb age of  $440 \pm 14$  Ma (Ortega-Gutiérrez et al., 1999). During this tectonothermal event, the Xayacatlán Formation was believed to have been thrust over the low grade Petlalcingo Group consisting of the Magdalena Migmatite at the base, the Chazumba Formation, and the Cosoltepec Formation at the top. Following exhumation, these rocks were unconformably overlain by the Tecolate Formation (of supposedly Siluro-Devonian age), which was intruded by arc-related rocks of Devonian age (based on a lower intercept age of  $371 \pm 34$  Ma (poorly defined lower intercept U–Pb TIMS zircon age: Yañez et al., 1991) during a Middle–Upper Devonian orogeny called the Mixtecan Orogeny (Sánchez-Zavala et al., 2000). This was followed by deposition of Carboniferous and Permian rocks unconformably on the older rocks.

However, the eclogite facies metamorphism has since been dated directly as Mississippian in the northern part of the Acatlán Complex (Middleton et al., 2007; Elías-Herrera et al.,

2007), whereas the megacrystic granitoids are almost exclusively of Ordovician age (Sánchez-Zavala et al., 2004; Talavera-Mendoza et al., 2005; Miller et al., 2007). Furthermore, the fossils and dated granitic pebbles in Tecolate Formation show it to be Early–Middle Permian, possibly extending into the Carboniferous in undated underlying rocks (Keppie et al., 2004a). The Magdalena and Chazumba units contain detrital zircons as young as Permian and Triassic, whereas the youngest detrital zircons in units included in the Cosoltepec Formation of the eastern Acatlán Complex are either Ordovician ( $\sim 455$  Ma: Keppie et al., 2004b, 2006) or Devonian–Carboniferous ( $\sim 410$  and/or  $\sim 374$  Ma: Talavera-Mendoza et al., 2005). This has led to a revision of the geological history of the Acatlán Complex that has been summarized by Nance et al. (2006, 2007) and Keppie et al. (2008a) involving:

- (i) deposition of ?Cambro-Ordovician rift-passive margin sediments associated with intrusion of bimodal, rift-related igneous rocks (Miller et al., 2007; Keppie et al., 2008b; Ramos-Arias et al., 2008);
- (ii) deposition of latest Devonian–Permian–Triassic continental-shallow marine rocks (Vachard et al., 2000) that was synchronous with Mississippian exhumation of the high pressure rocks (Middleton et al., 2007), extensional and dextral shear on listric normal zones and N–S vertical zones (Elías-Herrera and Ortega-Gutiérrez, 2002; Ramos-Arias et al., 2008), and Permo-Triassic arc magmatism (Torres et al., 1999; Malone et al., 2002).

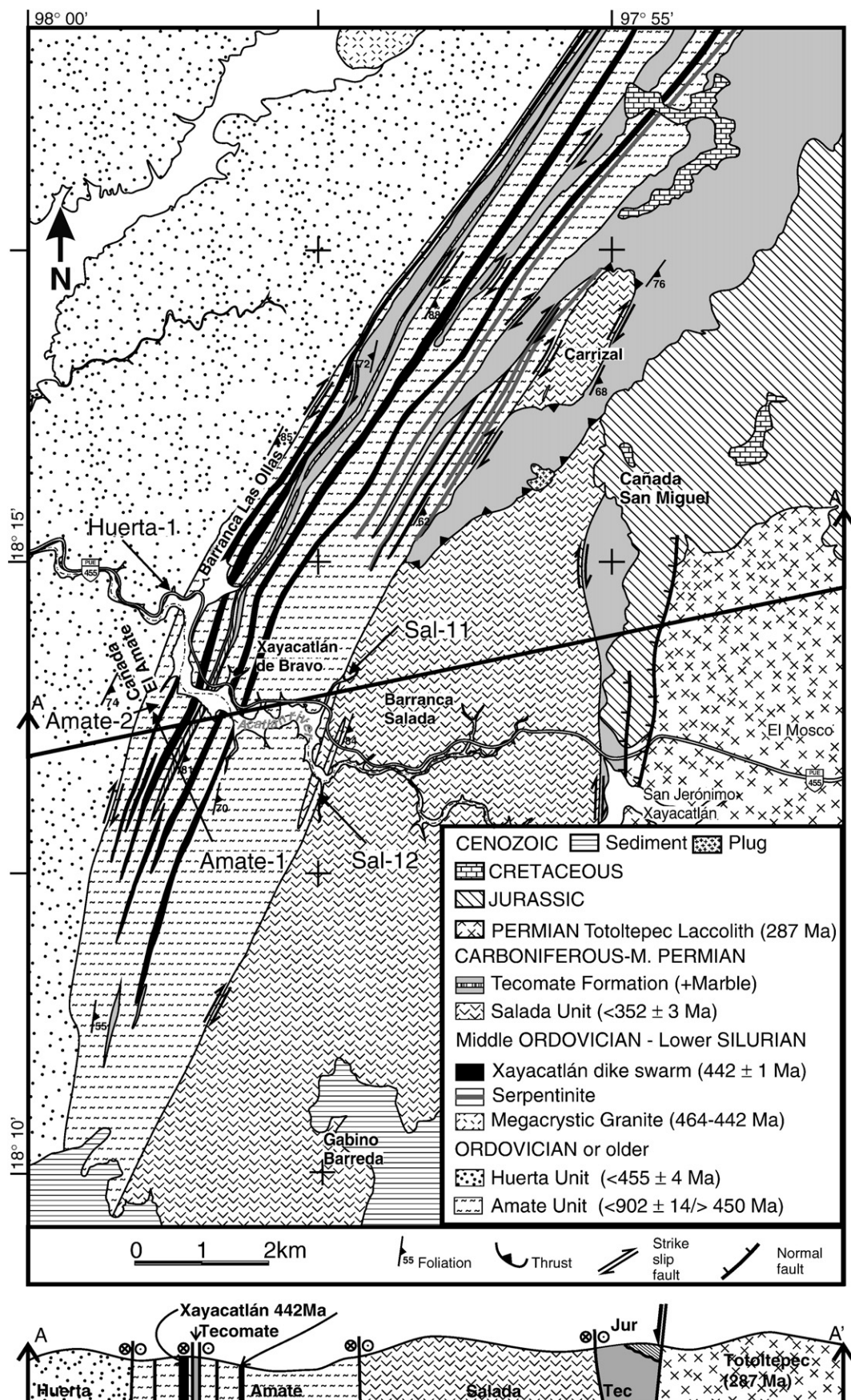


Fig. 3. Geological map of the Xayacatlán area.

Table 1  
U–Pb LA-ICPMS analyses of zircons in a pegmatite sample in the Xayacatlán area, Acatlán Complex, southern Mexico: HUERTA-1 (see Fig. 3 for sample locations)

Sample/analysis	$^{206}\text{Pb}/^{238}\text{U}$	Percentage error	$^{207}\text{Pb}/^{235}\text{U}$	Percentage error	$^{207}\text{Pb}/^{206}\text{Pb}$	Percentage error	Age, Ma $^{206}\text{Pb}/^{238}\text{U}$	(2σ)	$^{207}\text{Pb}/^{235}\text{U}$	(2σ)	$^{207}\text{Pb}/^{206}\text{Pb}$	(2σ)
<i>HUERTA-1</i>												
ap05e10rim	0.1079	0.00086	0.9355	0.0092	0.06287	0.00062	659	10	671	10	702	42
ap05e11core	0.1513	0.00123	1.4791	0.0213	0.07091	0.00078	908	14	922	17	954	44
ap05e12	0.197	0.0014	2.297	0.0372	0.08458	0.00132	1150	19	1211	23	1304	60
ap05e13	0.0912	0.0007	0.7578	0.0213	0.06028	0.00189	565	14	573	25	612	134
ap05e14	0.117	0.0007	1.0857	0.0125	0.06732	0.00077	708	9	746	12	846	48
ap05e15	0.0913	0.00041	0.7574	0.0081	0.06019	0.00062	563	5	573	9	610	44
ap05e16	0.1127	0.00034	0.9879	0.0056	0.0636	0.00035	687	4	698	6	728	22
ap05f05	0.4287	0.0021	9.4091	0.0452	0.1592	0.00089	2299	20	2379	9	2446	20
ap05f06dark rim.	0.0938	0.0004	0.7637	0.0082	0.05907	0.00066	578	5	576	9	568	48
ap05f07mottled.core.	0.1249	0.00055	1.1849	0.0111	0.06883	0.00062	757	7	794	10	892	38
ap05f08	0.0855	0.00037	0.686	0.0062	0.05819	0.00056	529	5	530	7	536	40
ap05f09	0.0905	0.0009	0.7327	0.0155	0.05873	0.00143	563	16	558	18	556	106
ap05f10	0.3966	0.00238	8.5912	0.0481	0.15713	0.00074	2160	25	2296	10	2424	16
ap05f11	0.1165	0.00076	1.0801	0.0095	0.06726	0.00057	710	9	744	9	844	34
ap05f12	0.1746	0.00066	1.8474	0.0176	0.07673	0.00071	1036	8	1063	12	1114	38
ap05f13	0.1006	0.00056	0.8499	0.0097	0.0613	0.00067	617	7	625	11	648	48
ap05f14	0.0897	0.00045	0.7378	0.0081	0.05963	0.00069	554	6	561	9	590	50
ap05f15	0.0778	0.00036	0.6137	0.0071	0.05724	0.00065	483	5	486	9	500	50
ap05f16	0.4805	0.00221	12.3109	0.0665	0.18584	0.00095	2531	21	2628	10	2704	18
ap05g05	0.1732	0.00132	1.8143	0.0318	0.07599	0.00131	1030	16	1051	23	1094	70
ap05g06	0.092	0.00036	0.8328	0.0082	0.06569	0.00064	563	5	615	9	796	42
ap05g07	0.1685	0.00113	1.9705	0.0211	0.08484	0.00088	997	13	1105	14	1310	40
ap05g08	0.0933	0.00081	0.777	0.0184	0.06041	0.00154	575	10	584	21	618	110
ap05g09	0.1516	0.00091	1.4613	0.0178	0.06991	0.00073	911	11	915	15	924	44
ap05g10d.rim	0.08	0.00035	0.6243	0.0066	0.05662	0.00061	496	4	493	8	476	48
ap05g11.core	0.0804	0.00042	0.6502	0.0075	0.05864	0.00071	499	5	509	9	552	52
ap05g12	0.1042	0.00048	0.9385	0.0135	0.06536	0.00093	636	6	672	14	784	60
ap05g13	0.1057	0.00035	0.9022	0.0076	0.06193	0.00053	648	4	653	8	670	36
ap05g14	0.0937	0.00046	0.7813	0.0111	0.06048	0.00084	576	5	586	13	620	60
ap05g15	0.0904	0.00098	0.8729	0.0357	0.07007	0.00294	551	13	637	39	930	174
ap05g16	0.3259	0.00147	4.9909	0.0359	0.11108	0.00083	1820	18	1818	12	1816	28
ap05h05	0.2037	0.00065	2.2638	0.0152	0.08062	0.00052	1197	8	1201	9	1212	26
ap05h06	0.0851	0.00083	0.6911	0.0254	0.05889	0.00225	529	11	533	31	562	168
ap05h07	0.1748	0.00072	1.9479	0.0265	0.08084	0.00104	1030	9	1098	18	1216	52
ap05h08	0.205	0.00133	3.628	0.0395	0.12836	0.001	1205	15	1556	17	2074	28
ap05h09	0.18	0.00074	1.8704	0.0172	0.07538	0.00077	1069	9	1071	12	1078	40
ap05h10	0.1713	0.00081	1.7546	0.0223	0.07428	0.00091	1021	10	1029	16	1048	48
ap05h11	0.0746	0.00031	0.5913	0.0052	0.05748	0.00051	464	4	472	7	510	38
ap05h12	0.1381	0.00062	1.3176	0.009	0.06923	0.00046	832	8	853	8	904	28
ap05h13	0.0962	0.00047	0.787	0.0127	0.05935	0.00095	591	6	589	14	580	70
ap05h14	0.1546	0.00056	1.5503	0.0116	0.07273	0.00051	920	7	951	9	1006	28
ap05h15	0.095	0.00065	0.7901	0.0145	0.06036	0.00113	583	11	591	16	616	82
ap05h16	0.1179	0.00101	1.0652	0.024	0.06556	0.00146	716	12	736	24	792	94
ap05i05	0.4544	0.00204	11.5921	0.0545	0.18502	0.00104	2396	21	2572	9	2698	18
ap05i06	0.2908	0.00125	4.1756	0.0263	0.10415	0.00055	1645	14	1669	10	1698	20
ap05i07	0.2028	0.0014	2.2418	0.0365	0.08017	0.00135	1189	18	1194	23	1200	68
ap05i08	0.0686	0.00045	0.569	0.0075	0.06017	0.00079	427	6	457	10	608	56
ap05i09	0.1699	0.00093	1.7583	0.0222	0.07508	0.00104	1009	12	1030	16	1070	56
ap05i10	0.5104	0.00327	16.3265	0.1339	0.23201	0.00174	2614	32	2896	16	3064	22
ap05i11	0.1769	0.00115	1.8844	0.0249	0.07727	0.00104	1051	14	1076	18	1128	54
ap05i12	0.0732	0.00063	0.605	0.0097	0.05995	0.00098	453	9	480	12	600	72
ap05i13core	0.1549	0.0009	1.5343	0.023	0.07183	0.00119	924	11	944	18	980	68
ap05i14rim	0.0875	0.00044	0.7191	0.0065	0.05964	0.00052	541	5	550	8	590	38
ap05i15	0.1966	0.00077	2.1807	0.0177	0.08047	0.00058	1156	9	1175	11	1208	28
ap05i16	0.0909	0.00035	0.7429	0.0079	0.05929	0.00065	562	4	564	9	576	48
ap05j05	0.3835	0.0013	6.8902	0.0496	0.13033	0.00083	2092	13	2097	13	2102	22
ap05j06	0.1625	0.00065	1.8017	0.0092	0.08042	0.00039	971	8	1046	7	1206	20
ap05j07	0.177	0.00074	1.8419	0.0151	0.07546	0.00057	1052	9	1061	11	1080	30
ap05j08	0.1283	0.00059	1.2004	0.0096	0.06786	0.00058	771	7	801	9	864	34
ap05j09	0.0876	0.00084	0.7361	0.011	0.06093	0.00101	535	10	560	13	636	70
ap05j10	0.2448	0.00118	3.5992	0.0328	0.10666	0.00094	1399	13	1549	14	1742	32

(continued on next page)

Table 1 (continued)

Sample/analysis	$^{206}\text{Pb}/^{238}\text{U}$	Percentage error	$^{207}\text{Pb}/^{235}\text{U}$	Percentage error	$^{207}\text{Pb}/^{206}\text{Pb}$	Percentage error	Age, Ma $^{206}\text{Pb}/^{238}\text{U}$	(2 $\sigma$ )	$^{207}\text{Pb}/^{235}\text{U}$	(2 $\sigma$ )	$^{207}\text{Pb}/^{206}\text{Pb}$	(2 $\sigma$ )
<i>HUERTA-1</i>												
ap05j11	0.0907	0.00079	0.6987	0.0234	0.05588	0.0018	561	11	538	28	446	142
ap05j12	0.0908	0.00047	0.7568	0.0104	0.06045	0.00081	560	6	572	12	618	58
ap05j13core	0.108	0.00048	0.8978	0.0086	0.06027	0.00064	661	6	651	9	612	46
ap05j14rim	0.101	0.00051	0.8343	0.007	0.0599	0.00053	619	6	616	8	598	38
ap05j15	0.1678	0.00057	1.7281	0.0137	0.07468	0.00062	999	7	1019	10	1058	34
ap05j16	0.0949	0.0005	0.7955	0.0086	0.06077	0.00067	584	6	594	10	630	48

- (iii) a tectonothermal event during the Jurassic that may be related to a mantle plume (Keppie et al., 2004b);
- (iv) deposition of Mesozoic platformal rocks and Cenozoic arc-related rocks.

Our reexamination of the Xayacatlán area involving mapping and zircon geochronology shows that: (i) whereas some of the units are Ordovician or older others are post-Devonian (probably Carboniferous and Permian); (ii) high grade (amphibolite facies) metamorphism is restricted to syntectonic gabbroic intrusions and their contact aureoles intruded during transtensional deformation (none of the rocks have undergone eclogite facies metamorphism); and (iii) most of the N–S striking contacts between the units are vertical shear zones (not thrusts as previously inferred). These data are then applied to paleogeographic reconstructions and we suggest that whereas the Ordovician rocks formed on the southern margin of the Rheic Ocean, the Carboniferous and Permian rocks formed on the active Pacific margin of Pangea.

## 2. Xayacatlán area

The Xayacatlán area was originally mapped by Ortega-Gutiérrez (1975), who recognized two units: retrograded eclogites of the Xayacatlán Formation that was thrust over the low grade Cosoltepec Formation (Fig. 2A). The Xayacatlán Formation was subsequently included in the eclogitic Piaxtla Group (Ramírez-Espinosa, 2001) and renamed the Piaxtla Suite by Middleton et al. (2007). However, the absence of eclogite facies metamorphism in the Xayacatlán area makes its inclusion in the Piaxtla Suite uncertain. Furthermore, correlation of the low grade rocks in the vicinity of Xayacatlán with the type Cosoltepec Formation are also uncertain because detrital zircon suites have different ages (c.f. Talavera-Mendoza et al., 2005; Keppie et al., 2006). In view of these problems, we define new names for most of the units in the Xayacatlán area (Figs. 2B and 3). The structure, metamorphism and geochemistry of the various units forms part of separate papers (e.g. Keppie et al., 2008b).

### 2.1. Huerta Unit (new name)

The Huerta Unit occurs with a N–S trending fault block that is bounded on its western side by sub-greenschist facies rocks assigned to the Tecomate Formation, and on its eastern side by

rocks of the Amate Unit where the contact is a dextral shear zone formed under greenschist facies metamorphic conditions (Fig. 3). A megacrystic granite is exposed along the northern margin of the Xayacatlán area, however, its contact with the Huerta Unit is not exposed. It is composed of interbedded metapsammites and metapelites consisting of quartz, muscovite, chlorite and accessory zircon and opaque minerals. The unit is pervasively intruded by veins that gradually change in mineralogy from quartz veins in the west to pegmatites in the east. All of these rocks have undergone intense polyphase deformation at least three sets of folds including sheath folds under greenschist facies metamorphic conditions (Malone et al., 2002; and paper in preparation by authors). In view of this, it is impossible to measure a type section. However, the road between Xayacatlán and Acatlán provides an excellent cross-section of the unit. A sample from the western part of this unit has yielded detrital zircons, the youngest of which yielded a concordant age of  $455 \pm 4$  Ma with older population age peaks at  $\sim 600$  Ma and  $\sim 1\text{--}1.2$  Ga (Keppie et al., 2006). A pegmatite sample (Fig. 3: HUERTA-1:  $18^\circ 14.758'$ ,  $97^\circ 58.727'$ ) was collected in the eastern part of the fault block for U–Pb detrital zircon analysis (Fig. 3).

### 2.2. Amate Unit (new name)

The Amate Unit occurs in the central N–S trending fault block (Fig. 3). All the contacts with other rock units are dextral shear zones. The Amate Unit is mainly composed of metaarkose, metapsammite, and metapelite that are intruded by mafic and felsic dikes. The metasedimentary rocks generally consist of quartz, muscovite, feldspar, and chlorite with accessory zircon and opaque minerals. However, adjacent to the largest mafic dike, the rocks are hornfelsed and contain large decussate muscovite and clinzoisite crystals. The petrography, geochemistry and geochronology of the mafic (gabbro and diabase) and felsic (granite and pegmatite) rocks have been described by Keppie et al. (2008b). They are mainly mafic amphibolitic gneisses with ultramafic and anorthositic bands with a continental tholeiitic signature cut by medium grained mafic dikes and granitic pegmatites. In places, these mafic dikes have undergone intense shearing associated with retrogressive metamorphism that produced serpentinite and chlorite schist. The rocks of the Amate Unit have been deformed by at least three sets of folds generally developed under greenschist facies metamorphic conditions (detailed in a paper in preparation by authors). As a

Table 2

U-Pb LA-ICPMS analyses of zircons in a metapsammite sample of the Amate Unit in the Xayacatlán area, Acatlán Complex, southern Mexico: AMATE-1 (see Fig. 3 for sample locations)

Sample/analysis	$^{206}\text{Pb}/^{238}\text{U}$	Percentage error	$^{207}\text{Pb}/^{235}\text{U}$	Percentage error	$^{207}\text{Pb}/^{206}\text{Pb}$	Percentage error	Age, Ma $^{206}\text{Pb}/^{238}\text{U}$	(2σ)	$^{207}\text{Pb}/^{235}\text{U}$	(2σ)	$^{207}\text{Pb}/^{206}\text{Pb}$	(2σ)
<i>AMATE-1</i>												
ap03h05	0.1959	0.0007	2.1751	0.0126	0.08053	0.0005	1151	8	1173	8	1208	26
ap03h06	0.2068	0.0008	2.3453	0.0178	0.08225	0.0005	1211	9	1226	11	1250	26
ap03h07	0.151	0.0005	1.4568	0.0079	0.06998	0.0003	906	6	913	6	926	18
ap03h08	0.2138	0.0011	2.4633	0.0227	0.08357	0.0009	1248	12	1261	13	1282	40
ap03h09	0.1692	0.0009	1.767	0.0186	0.07573	0.0008	1006	10	1033	14	1088	42
ap03h10	0.1823	0.0011	1.8743	0.0337	0.07456	0.0013	1079	12	1072	24	1056	70
ap03h11	0.1542	0.0018	1.4552	0.0469	0.06845	0.0025	923	21	912	39	882	154
ap03h12	0.1664	0.0007	1.6448	0.0176	0.07169	0.0008	992	8	988	13	976	44
ap03h13	0.1592	0.0006	1.5677	0.0121	0.07142	0.0005	953	8	958	10	968	28
ap03h14	0.2091	0.0017	2.4126	0.0396	0.0837	0.0012	1222	18	1246	24	1284	56
ap03h15	0.1965	0.0008	2.1623	0.0132	0.07982	0.0006	1157	9	1169	8	1192	28
ap03h16	0.1589	0.0006	1.683	0.0076	0.07679	0.0003	952	7	1002	6	1114	16
ap03i05	0.1716	0.0009	1.7676	0.017	0.0747	0.0007	1021	10	1034	12	1060	36
ap03i06	0.1805	0.0008	1.8891	0.0134	0.0759	0.0004	1069	9	1077	9	1092	24
ap03i07	0.1723	0.0007	1.7778	0.0135	0.07482	0.0006	1025	8	1037	10	1062	30
ap03i08	0.1642	0.0022	1.908	0.0277	0.08429	0.0004	978	26	1084	19	1298	20
ap03i09	0.1902	0.0012	2.1003	0.0269	0.0801	0.0011	1120	15	1149	18	1198	56
ap03i10	0.1501	0.0012	1.4315	0.0269	0.06916	0.0013	900	14	902	22	902	78
ap03i11	0.1411	0.0006	1.3589	0.0121	0.06987	0.0007	847	7	871	10	924	38
ap03i12	0.195	0.0013	2.1476	0.0288	0.07987	0.0011	1147	15	1164	19	1192	54
ap03i13	0.1945	0.0007	2.1055	0.0116	0.07849	0.0004	1147	7	1151	8	1158	20
ap03i14	0.2046	0.0014	2.2091	0.0258	0.07832	0.0009	1205	15	1184	16	1154	48
ap03i15	0.1725	0.0006	1.7495	0.0121	0.07357	0.0005	1027	6	1027	9	1028	26
ap03i16	0.2112	0.0009	2.4046	0.0137	0.08257	0.0005	1235	9	1244	8	1258	24
ap03j05	0.2149	0.0012	2.3879	0.0224	0.08061	0.0008	1256	13	1239	14	1210	38
ap03j06	0.1877	0.0008	2.0741	0.0091	0.08015	0.0003	1111	8	1140	6	1200	14
ap03j07	0.2015	0.0007	2.2795	0.0125	0.08206	0.0004	1180	8	1206	8	1246	20
ap03j08	0.1536	0.0008	1.61	0.0079	0.076	0.0003	924	10	974	6	1094	20
ap03j09	0.156	0.0011	1.5346	0.0273	0.07136	0.0014	933	13	944	22	966	78
ap03j10	0.2282	0.0009	2.7648	0.0182	0.08789	0.0006	1325	9	1346	10	1380	26
ap03j11	0.1699	0.0007	1.7146	0.0111	0.0732	0.0006	1013	8	1014	8	1018	32
ap03j12	0.1724	0.0009	1.8003	0.0247	0.07573	0.0011	1025	10	1046	18	1086	58
ap03j13	0.2011	0.0007	2.1895	0.0204	0.07898	0.0008	1182	8	1178	13	1170	40
ap03j14	0.1894	0.002	2.0413	0.0274	0.07818	0.0008	1116	22	1129	18	1150	40
ap03j15	0.1698	0.0005	1.7364	0.0099	0.07417	0.0004	1011	6	1022	7	1046	22
ap03j16	0.1585	0.0011	1.5431	0.0201	0.07064	0.0009	948	12	948	16	946	50
ap03k05	0.1932	0.0007	2.1011	0.0118	0.07887	0.0004	1138	8	1149	8	1168	20
ap03k06	0.1832	0.0008	1.9052	0.0105	0.07543	0.0005	1084	9	1083	7	1078	26
ap03k07	0.156	0.0009	1.5089	0.0243	0.07017	0.0013	936	11	934	20	932	76
ap03k08	0.1702	0.0012	1.7423	0.0211	0.07427	0.0008	1013	14	1024	16	1048	44
ap03k09	0.1854	0.0008	1.9556	0.0198	0.07651	0.0008	1098	9	1100	14	1108	42
ap03k10	0.1921	0.0008	2.0666	0.0118	0.07803	0.0004	1134	9	1138	8	1146	22
ap03k11	0.1968	0.0006	2.4169	0.0126	0.0891	0.0003	1151	7	1248	7	1406	14
ap03k12	0.1721	0.0007	1.7297	0.0164	0.0729	0.0007	1024	8	1020	12	1010	40
ap03k13	0.1743	0.0005	1.7838	0.01	0.07421	0.0004	1036	6	1040	7	1046	20
ap03k14	0.1678	0.0007	1.6805	0.0096	0.07264	0.0004	1000	7	1001	7	1004	22
ap03k15	0.1896	0.0009	2.1294	0.023	0.08147	0.0009	1116	10	1158	15	1232	46
ap03k16	0.2207	0.0009	2.6476	0.0191	0.08701	0.0006	1285	10	1314	11	1360	24
ap03l05	0.1697	0.001	1.7163	0.0156	0.07335	0.0006	1010	11	1015	12	1022	34
ap03l06	0.1762	0.0011	1.8235	0.0352	0.07506	0.0015	1049	14	1054	25	1070	82
ap03l07	0.1596	0.0008	1.6017	0.0178	0.07277	0.0008	951	10	971	14	1006	48
ap03l08	0.1578	0.0006	1.5676	0.0152	0.07207	0.0008	945	7	957	12	986	42
ap03l09	0.1877	0.0008	2.187	0.0103	0.08451	0.0004	1105	10	1177	7	1304	16
ap03l10	0.2089	0.0008	2.3823	0.0157	0.08273	0.0006	1223	9	1237	9	1262	26
ap03l11	0.2148	0.0009	2.5011	0.0133	0.08446	0.0004	1251	11	1272	8	1302	20
ap03l12	0.1756	0.0008	1.7631	0.0153	0.07282	0.0006	1043	9	1032	11	1008	32
ap03l13	0.1649	0.0016	1.6489	0.0424	0.07253	0.002	985	19	989	32	1000	110
ap03l14	0.2224	0.0009	3.5857	0.0384	0.11693	0.0012	1243	15	1546	17	1908	36
ap03l15	0.158	0.001	1.5318	0.0201	0.07031	0.0008	946	12	943	16	936	48
ap03l16	0.143	0.001	1.4067	0.0255	0.07133	0.0013	856	12	892	22	966	78

(continued on next page)

Table 2 (continued)

Sample/analysis	$^{206}\text{Pb}/^{238}\text{U}$	Percentage error	$^{207}\text{Pb}/^{235}\text{U}$	Percentage error	$^{207}\text{Pb}/^{206}\text{Pb}$	Percentage error	Age, Ma $^{206}\text{Pb}/^{238}\text{U}$	(2 $\sigma$ )	$^{207}\text{Pb}/^{235}\text{U}$	(2 $\sigma$ )	$^{207}\text{Pb}/^{206}\text{Pb}$	(2 $\sigma$ )
<i>AMATE-1</i>												
ap03m05	0.1631	0.0007	1.6395	0.009	0.07289	0.0003	974	8	986	7	1010	16
ap03m06	0.1874	0.0014	1.9049	0.037	0.07371	0.0014	1106	16	1083	26	1032	76
ap03m07	0.1751	0.0012	1.7998	0.0149	0.07455	0.0008	1040	14	1045	11	1056	46
ap03m08	0.1663	0.0008	1.7034	0.0121	0.07428	0.0005	988	10	1010	9	1048	28
Ap03m09	0.2021	0.0012	2.1879	0.0234	0.07851	0.0008	1187	13	1177	15	1158	42
Ap03m10	0.2232	0.0008	2.5847	0.0194	0.08398	0.0006	1299	9	1296	11	1292	26
Ap03m11	0.2099	0.0011	2.3755	0.0283	0.08207	0.0009	1228	12	1235	17	1246	44
Ap03m12	0.1701	0.0007	1.7071	0.0142	0.0728	0.0007	1012	9	1011	11	1008	38
Ap03m13	0.2032	0.0009	2.2199	0.0173	0.07925	0.0007	1192	10	1187	11	1178	38
Ap03m14	0.2012	0.001	2.1713	0.0154	0.07826	0.0005	1184	12	1172	10	1152	28
Ap03m15	0.1607	0.0014	1.5535	0.0259	0.0701	0.0014	963	17	952	21	930	80
Ap03m16	0.2001	0.0009	2.228	0.0118	0.08077	0.0004	1175	11	1190	7	1214	18
Ap03n05	0.2141	0.001	2.4366	0.0239	0.08255	0.0008	1252	12	1253	14	1258	36
Ap03n06	0.1834	0.0007	1.955	0.0174	0.07732	0.0007	1082	9	1100	12	1128	34
Ap03n07	0.1494	0.0006	1.5046	0.0129	0.07302	0.0006	896	8	932	10	1014	34
Ap03n08	0.2004	0.001	2.2346	0.0183	0.08087	0.0006	1176	11	1192	11	1218	30
Ap03n09	0.1472	0.0005	1.471	0.0078	0.07246	0.0004	884	6	919	6	998	24
Ap03n10	0.1924	0.0009	2.1696	0.0165	0.08178	0.0006	1120	12	1171	11	1240	28
Ap03n11	0.1547	0.0011	1.5071	0.0213	0.07064	0.001	926	13	933	17	946	56
Ap03n12	0.173	0.0007	1.7662	0.014	0.07404	0.0005	1029	9	1033	10	1042	30
Ap03n13	0.2089	0.0008	2.3261	0.017	0.08074	0.0006	1221	9	1220	10	1214	28
Ap03n14	0.1688	0.0012	1.6488	0.0251	0.07085	0.0013	1006	14	989	19	952	78
Ap03n15	0.1709	0.0007	1.7168	0.011	0.07285	0.0005	1017	9	1015	8	1008	26
Ap03n16	0.1749	0.001	1.7606	0.0178	0.07302	0.0009	1039	12	1031	13	1014	50

consequence of the polyphase deformation, no stratigraphic section is available for a type section: the Amate River provides the best section of the unit (Fig. 3). Three samples were collected for U–Pb zircon analyses (Fig. 3): one from a feldspathic psammite (AMATE-1,  $18^{\circ} 13.793'$ ,  $97^{\circ} 58.965'$ ), and the other two from cross-cutting foliated granitic dikes (AMATE-2:  $18^{\circ} 13.772'$ ,  $97^{\circ} 58.963'$ ; SAL-12:  $18^{\circ} 13.247'$ ,  $97^{\circ} 57.608'$ ).

### 2.3. Salada Unit (new name)

The Salada Unit occurs in a N–S trending fault block in the eastern part of the area. It is bounded on its western side by a dextral shear zone that juxtaposes it against the Tecomate Formation, on its northern side by an E–W trending, shallow N-dipping shear zone, above which lies the Tecomate Formation, and to the south it is unconformably overlain by Cenozoic rocks (Fig. 3). It consists mainly of metapelites, metapsammites and thin, tectonically intercalated mafic lenses. The metasedimentary rocks made up of quartz, muscovite, chlorite and accessory opaque minerals. The mafic rocks are composed of amphibole, chlorite, feldspar, epidote and accessory opaque minerals. A metapsammite sample was collected for U–Pb zircon analysis (Fig. 3: SAL-11:  $18^{\circ} 14.077'$ ,  $97^{\circ} 57.341'$ ).

### 2.4. Tecomate Formation

The Tecomate Formation in the Xayacatlán area is tectonically juxtaposed against all the previously described units, either along N–S trending dextral shear zones or above gently

N-dipping shear zones with gently N-plunging stretching lineations (Malone et al., 2002; paper in preparation by authors) (Fig. 3). In the north, it is overlain unconformably by Mesozoic rocks, whereas in the southeast it is faulted against the Totoltepec laccolith (Fig. 3). The Tecomate Formation consists predominantly of meta-arkoses, metapsammites, slates, metaconglomerates, and marbles. The clastic rocks consist mainly of quartz, feldspar, muscovite, chlorite, epidote and opaque minerals. The conglomerates contain a diverse assemblage of pebbles: granitoid and volcanic rocks, metapsammite, and vein quartz. Granitoid pebbles from a conglomerate ~20 km to the east of the Xayacatlán area have yielded U–Pb ages of ~290 Ma and are inferred to have been derived from the Lower Permian Totoltepec laccolith (Yañez et al., 1991; Keppie et al., 2004b), which is exposed along the eastern margin of Fig. 3. On the other hand, marbles in the type section of the Tecomate Formation exposed to the south of the town of Acatlán (Fig. 1B), have yielded latest Pennsylvanian–Early Permian microfossils (Keppie et al., 2004a). Deformation in the Tecomate Formation in the Xayacatlán area varies from almost undeformed to polyphase involving three sets of folds (Malone et al., 2002; and paper in preparation by authors). The grade of metamorphism varies from sub-greenschist facies to lower greenschist facies (Malone et al., 2002).

### 2.5. Totoltepec laccolith

The Totoltepec laccolith crops out along the eastern margin of the Xayacatlán area (Fig. 3). It has yielded concordant U–Pb zircon ages of ~288 Ma (Yañez et al. et al., 1991; Keppie et al.,

Table 3

U–Pb LA-ICPMS analyses of zircons in a granitic dike cutting the Amate Unit in the Xayacatlán area, Acatlán Complex, southern Mexico: AMATE-2 (see Fig. 3 for sample locations)

Sample/analysis	$^{206}\text{Pb}/^{238}\text{U}$	Percentage error	$^{207}\text{Pb}/^{235}\text{U}$	Percentage error	$^{207}\text{Pb}/^{206}\text{Pb}$	Percentage error	Age, Ma $^{206}\text{Pb}/^{238}\text{U}$	(2σ)	$^{207}\text{Pb}/^{235}\text{U}$	(2σ)	$^{207}\text{Pb}/^{206}\text{Pb}$	(2σ)
<i>AMATE-2</i>												
Ap05k05	0.0737	0.0006	0.5643	0.013	0.05554	0.00118	457	8	454	17	434	94
Ap05k06	0.2138	0.0014	2.5109	0.0271	0.0852	0.00085	1252	17	1275	16	1318	38
Ap05k07	0.0745	0.0005	0.5894	0.0136	0.05741	0.00134	462	7	470	17	506	104
Ap05k08	0.0717	0.0002	0.5543	0.0022	0.05606	0.0002	447	3	448	3	454	16
Ap05k09	0.071	0.0002	0.5598	0.0029	0.05721	0.00027	444	3	451	4	498	20
ap05k10	0.0808	0.0004	0.74	0.0081	0.06646	0.00073	495	5	562	10	820	46
ap05k11	0.1871	0.0007	2.0692	0.0174	0.08023	0.00054	1102	8	1139	11	1202	26
ap05k12	0.0702	0.0004	0.525	0.0104	0.05427	0.00112	437	6	428	14	382	92
ap05k13	0.071	0.0006	0.5561	0.018	0.05677	0.00194	442	8	449	23	482	152
ap05k14	0.2115	0.0013	2.3549	0.0162	0.08077	0.00058	1235	15	1229	10	1214	30
ap05k15	0.2128	0.0008	2.4141	0.0176	0.08227	0.00064	1244	9	1247	11	1250	30
ap05k16	0.1794	0.0012	1.838	0.0298	0.07432	0.00115	1061	14	1059	21	1050	62
ap05l05	0.1579	0.0012	1.5687	0.0207	0.07205	0.00104	944	14	958	16	986	60
ap05l06	0.192	0.0013	2.0882	0.0232	0.0789	0.00082	1132	15	1145	15	1168	40
ap05l07	0.1708	0.0006	1.8449	0.0116	0.07833	0.00052	1018	7	1062	8	1154	26
ap05l08	0.072	0.0003	0.6143	0.0045	0.0619	0.00048	447	4	486	6	670	32
ap05l09	0.0723	0.0003	0.5715	0.0034	0.05729	0.00037	449	3	459	4	502	28
ap05l10	0.1523	0.001	1.5168	0.0155	0.07226	0.00059	914	12	937	13	992	32
ap05l11	0.1588	0.0008	1.5635	0.0152	0.07139	0.00066	950	9	956	12	968	38
ap05l12	0.0734	0.0004	0.5574	0.0093	0.05505	0.00088	458	5	450	12	414	70
ap05l13	0.0709	0.0005	0.5503	0.0144	0.05628	0.00154	442	7	445	19	462	122
ap05l14	0.0693	0.0005	0.5402	0.0077	0.05653	0.00083	432	6	439	10	472	64
ap05l15	0.1225	0.0006	1.187	0.0094	0.07028	0.00067	745	7	795	9	936	38
ap05l16	0.073	0.0006	0.6545	0.0107	0.06506	0.0007	451	7	511	13	776	46
ap05m05	0.0706	0.0006	0.5539	0.013	0.05688	0.0014	440	8	448	17	486	110
ap05m06rim	0.0744	0.0002	0.5863	0.0029	0.05713	0.00026	462	3	469	4	496	20
ap05m07core	0.1217	0.0005	1.118	0.0111	0.06662	0.00061	740	6	762	11	824	38
ap05m08	0.1343	0.0006	1.2545	0.0133	0.06777	0.00072	809	7	825	12	860	44
ap05m09	0.0764	0.0004	0.6006	0.0069	0.05702	0.00064	476	5	478	9	492	50
ap05m10	0.1674	0.0007	1.6782	0.0123	0.07272	0.00057	997	8	1000	9	1006	30
ap05m11	0.1959	0.0009	2.143	0.0238	0.07936	0.00084	1154	10	1163	15	1180	40
ap05m12	0.2101	0.0007	2.3772	0.0138	0.08205	0.00053	1230	8	1236	8	1246	26
ap05m13	0.0711	0.0004	0.5631	0.0091	0.05743	0.00097	442	5	454	12	508	74
ap05m14	0.0723	0.0005	0.5602	0.0103	0.05617	0.00112	450	6	452	13	458	88
ap05m15	0.1639	0.0006	1.6294	0.0116	0.0721	0.00055	978	7	982	9	988	32
ap05m16	0.2099	0.0009	2.3427	0.0225	0.08096	0.00075	1228	11	1225	14	1220	36
ap05n05	0.0279	0.0003	0.2063	0.0069	0.05365	0.00193	177	4	190	12	356	162
ap05n06	0.1935	0.0016	2.1068	0.0356	0.07898	0.00132	1140	19	1151	23	1170	66
ap05n07	0.1923	0.0013	2.1478	0.0247	0.08099	0.00081	1134	15	1164	16	1220	40
ap05n08	0.0694	0.0004	0.5338	0.0075	0.05582	0.00087	433	5	434	10	444	68
ap05n09	0.0697	0.0007	0.5297	0.0122	0.05515	0.00116	435	9	432	16	418	94
ap05n10	0.071	0.0004	0.5539	0.0089	0.05658	0.00094	442	6	448	12	474	74
ap05n11	0.0697	0.0004	0.524	0.0088	0.05455	0.00087	434	6	428	12	392	72
ap05n12core	0.0705	0.0003	0.5318	0.006	0.0547	0.00066	439	4	433	8	400	54
ap05n13rim	0.0711	0.0003	0.5513	0.004	0.05621	0.00043	443	4	446	5	460	34
ap05n14rim	0.0749	0.0004	0.589	0.0074	0.05707	0.00074	466	5	470	9	494	58
ap05n15core	0.0709	0.0003	0.5573	0.0065	0.05705	0.00068	441	4	450	8	492	52
ap05n16	0.0962	0.0006	0.7973	0.0237	0.06012	0.00177	594	9	595	27	606	128
ap05o05	0.199	0.001	2.4302	0.0277	0.08856	0.00094	1163	12	1252	16	1394	40
ap05o06	0.1482	0.0014	1.387	0.0226	0.0679	0.00101	890	16	883	19	864	62
ap05o07	0.072	0.0003	0.5789	0.0042	0.05833	0.00043	447	4	464	5	542	32
ap05o08	0.1651	0.0009	1.6873	0.0202	0.07413	0.00089	985	11	1004	15	1044	48
ap05o09core	0.1955	0.001	2.1556	0.0181	0.07998	0.00078	1151	11	1167	12	1196	38
ap05o10rim	0.0725	0.0003	0.6449	0.0104	0.06451	0.00095	447	4	505	13	758	62
ap05o11core	0.1599	0.0012	1.583	0.0258	0.07179	0.00116	954	15	964	20	978	66
ap05o12rim	0.0742	0.0003	0.6091	0.0044	0.05957	0.00042	459	3	483	6	586	30

2004b). It varies from mafic (hornblende, epidote, chlorite) to felsic (quartz, feldspar, muscovite) and has a calc-alkaline geochemistry interpreted in terms of arc magmatism (Malone

et al., 2002). The laccolith contains a folded foliation with a N-plunging mineral lineation interpreted in terms of syntectonic intrusion during S-vergent thrusting (Malone et al., 2002).

Table 4  
U-Pb LA-ICPMS analyses of zircons in a metapsammite sample of the Salada Unit in the Xayacatlán area, Acatlán Complex, southern Mexico: SAL-12 (see Fig. 3 for sample locations)

Sample/analysis	$^{206}\text{Pb}/^{238}\text{U}$	Percentage error	$^{207}\text{Pb}/^{235}\text{U}$	Percentage error	$^{207}\text{Pb}/^{206}\text{Pb}$	Percentage error	Age, Ma $^{206}\text{Pb}/^{238}\text{U}$	(2σ)	$^{207}\text{Pb}/^{235}\text{U}$	(2σ)	$^{207}\text{Pb}/^{206}\text{Pb}$	(2σ)
<i>SAL-12</i>												
ap05a05	0.1393	0.0006	1.3007	0.0144	0.06772	0.00076	839	7	846	13	860	46
ap05a06	0.0753	0.0003	0.5968	0.0034	0.05745	0.0003	468	4	475	4	508	24
ap05a07	0.074	0.0004	0.5933	0.0043	0.05818	0.00048	460	5	473	5	536	36
ap05a08	0.2085	0.0008	2.3722	0.0119	0.08254	0.00043	1224	9	1234	7	1258	20
ap05a09	0.0745	0.0004	0.5829	0.0078	0.05674	0.00073	463	5	466	10	480	56
ap05a10	0.0497	0.0004	0.4598	0.0051	0.06704	0.00052	313	6	384	7	838	32
ap05a11	0.2053	0.0008	2.2962	0.017	0.08112	0.0005	1204	9	1211	10	1224	24
ap05a12	0.1712	0.0007	1.7477	0.0147	0.07406	0.00069	1019	8	1026	11	1042	36
ap05a13	0.2104	0.0007	2.3278	0.0242	0.08023	0.00081	1232	8	1221	15	1202	40
ap05a14	0.0737	0.0003	0.579	0.0058	0.05695	0.00056	459	4	464	7	488	44
ap05a15	0.0746	0.0003	0.5904	0.0045	0.05744	0.0004	463	4	471	6	508	30
ap05a16	0.0741	0.0003	0.6635	0.0064	0.06495	0.00066	456	3	517	8	772	42
ap05b05	0.2104	0.001	2.3768	0.0209	0.08195	0.00074	1231	11	1236	13	1244	34
ap05b06	0.2014	0.0009	2.2188	0.0131	0.07991	0.00051	1184	11	1187	8	1194	24
ap05b07	0.0761	0.0004	0.6075	0.0046	0.05791	0.00043	473	5	482	6	526	34
ap05b08	0.1744	0.001	1.7986	0.0214	0.0748	0.00102	1035	12	1045	16	1062	56
ap05b09	0.158	0.0008	1.5908	0.0232	0.07301	0.00103	946	9	967	18	1014	58
ap05b10	0.0751	0.0003	0.6156	0.0057	0.05947	0.00056	466	4	487	7	584	42
ap05b11	0.2019	0.001	2.2455	0.0171	0.08068	0.00058	1186	11	1195	11	1212	28
ap05b12	0.1151	0.0008	1.0693	0.0145	0.0674	0.00096	683	11	738	14	850	58
ap05b13	0.1384	0.001	1.581	0.0207	0.08288	0.001	822	12	963	16	1266	46
ap05b14	0.1368	0.0009	1.3218	0.0169	0.07008	0.00102	822	11	855	15	930	60
ap05b15	0.0759	0.0003	0.6231	0.006	0.05958	0.00058	469	3	492	8	588	42
ap05b16core	0.091	0.0007	0.8237	0.0078	0.06565	0.00069	560	9	610	9	794	44
ap05c05rim	0.0887	0.0003	0.808	0.0051	0.06604	0.00045	543	4	601	6	806	28
ap05c06	0.0748	0.0003	0.6124	0.0044	0.05936	0.00047	463	4	485	6	580	34
ap05c07	0.0723	0.0004	0.616	0.0056	0.06179	0.00048	448	5	487	7	666	34
ap05c08main	0.0694	0.0005	0.7175	0.0067	0.075	0.00053	424	7	549	8	1068	28
zone												
ap05c09rim?	0.0728	0.0002	0.5733	0.0038	0.05715	0.00037	452	3	460	5	496	28
ap05c10	0.0711	0.0003	0.9512	0.009	0.09711	0.0009	422	6	679	9	1568	36
ap05c11	0.078	0.0004	0.6415	0.0061	0.05967	0.00061	482	5	503	8	590	44
ap05c12	0.0783	0.0003	0.6511	0.0077	0.0603	0.00072	486	4	509	9	614	50
ap05c13	0.1697	0.0008	1.8473	0.0168	0.07896	0.00076	1001	9	1062	12	1170	36
ap05c14core	0.0726	0.0004	0.5647	0.0067	0.05639	0.00061	452	6	455	9	466	48
ap05c15rim	0.0735	0.0004	0.5659	0.008	0.05582	0.00078	457	5	455	10	444	60
ap05c16	0.1299	0.0011	1.287	0.0257	0.07189	0.00129	765	15	840	23	982	74
ap05d05	0.1661	0.0005	1.6569	0.0101	0.07236	0.00045	991	6	992	8	994	26
ap05d06	0.0743	0.0003	0.5738	0.006	0.05603	0.00054	463	4	460	8	452	44
ap05d07	0.1822	0.0011	1.9441	0.0247	0.07741	0.00098	1076	13	1096	17	1130	50
ap05d08	0.0721	0.0003	0.6582	0.0047	0.06622	0.00045	445	4	514	6	812	28
ap05d09	0.1518	0.0008	1.4925	0.0161	0.07132	0.00081	912	9	927	13	966	46
ap05d10	0.0737	0.0003	0.7233	0.0073	0.0712	0.00077	451	4	553	9	962	44
ap05d11	0.2747	0.0012	3.7626	0.026	0.09936	0.00062	1565	12	1585	11	1612	22
ap05d12	0.2208	0.0012	2.606	0.0305	0.08561	0.00104	1280	14	1302	17	1328	48
ap05d13	0.0747	0.0003	0.5832	0.0045	0.05662	0.0004	465	4	467	6	476	32
ap05d14	0.0746	0.0004	0.586	0.0064	0.05697	0.00063	463	5	468	8	490	48
ap05d15	0.1821	0.001	2.0148	0.025	0.08025	0.00101	1076	12	1121	17	1202	48
ap05d16	0.0743	0.0004	0.5703	0.0094	0.05567	0.00097	463	5	458	12	438	76
ap05e05	0.0764	0.0003	0.7428	0.0065	0.07055	0.00068	467	4	564	8	944	38
ap05e06	0.0741	0.0004	0.5804	0.0059	0.05677	0.00052	461	5	465	8	482	40
ap05e07	0.149	0.0004	1.4563	0.0063	0.0709	0.00026	895	5	912	5	954	16
ap05e08	0.1832	0.0008	2.2745	0.015	0.09004	0.0005	1077	9	1204	9	1426	22
ap05e09	0.0735	0.0003	0.8316	0.0063	0.08209	0.00065	444	5	615	7	1246	30

## 2.6. Jurassic conglomerate

Lying unconformably upon the Tecomate Formation in the northeastern part of the area are a sequence of red conglomer-

ates, sandstones and occasional shaly layers (Fig. 3). Leaf impressions recovered from this sequence are probably Jurassic (R. Weber, pers. comm., 2005). The conglomerates contain pebbles of schist and large feldspar and quartz grains. These

Table 5

U-Pb LA-ICPMS analyses of zircons in a granitic dike cutting the Amate Unit in the Xayacatlán area, Acatlán Complex, southern Mexico: SAL.11 (see Fig. 3 for sample locations)

Sample/analysis	$^{206}\text{Pb}/^{238}\text{U}$	Percentage error	$^{207}\text{Pb}/^{235}\text{U}$	Percentage error	$^{207}\text{Pb}/^{206}\text{Pb}$	Percentage error	Age, Ma $^{206}\text{Pb}/^{238}\text{U}$	(2σ)	$^{207}\text{Pb}/^{235}\text{U}$	(2σ)	$^{207}\text{Pb}/^{206}\text{Pb}$	(2σ)
<i>SAL-11</i>												
ap03a05	0.5925	0.0023	19.7945	0.0673	0.24231	0.00073	3000	19	3081	7	3134	8
ap03a06	0.1097	0.0005	0.9668	0.0079	0.0639	0.00048	671	6	687	8	738	32
ap03a07	0.1689	0.0006	1.7389	0.0144	0.07468	0.00063	1008	7	1023	11	1058	34
ap03a08	0.1997	0.0013	2.3	0.0455	0.08352	0.00159	1174	16	1212	28	1280	74
ap03a09	0.5024	0.0022	11.8614	0.0474	0.17123	0.00067	2628	19	2594	8	2568	14
ap03a10	0.098	0.0005	0.8209	0.0069	0.06076	0.00058	602	6	609	8	630	42
ap03a11	0.0871	0.0005	0.7168	0.0116	0.05967	0.00092	538	6	549	14	590	68
ap03a12	0.1045	0.0005	0.8922	0.0062	0.06194	0.00046	641	5	648	7	670	32
ap03a13	0.3512	0.0012	12.1767	0.0426	0.25151	0.0007	1940	11	2618	7	3194	10
ap03a14	0.2776	0.0012	4.1555	0.0258	0.10858	0.00073	1566	13	1665	10	1774	26
ap03a15	0.0851	0.0006	0.7059	0.0077	0.06015	0.00067	527	8	542	9	608	48
ap03a16	0.0973	0.0005	0.7968	0.01	0.05942	0.00078	599	6	595	11	582	58
ap03b05	0.134	0.0007	1.2375	0.0099	0.06697	0.00051	812	8	818	9	836	32
ap03b06	0.3057	0.002	5.1402	0.0334	0.12198	0.00059	1717	21	1843	11	1984	16
ap03b07	0.3356	0.0012	5.2714	0.0285	0.11394	0.00062	1869	13	1864	9	1862	20
ap03b08	0.1777	0.0009	1.8322	0.0114	0.07479	0.0004	1055	11	1057	8	1062	20
ap03b09	0.2049	0.0008	2.3866	0.0155	0.0845	0.00046	1198	8	1239	9	1304	22
ap03b10	0.14	0.0006	1.3963	0.0101	0.07235	0.00046	839	7	887	8	994	26
ap03b11	0.1022	0.0004	0.8567	0.0072	0.06078	0.00051	629	5	628	8	630	36
ap03b12	0.2012	0.0008	2.1772	0.0155	0.0785	0.00057	1184	10	1174	10	1158	28
ap03b13	0.1025	0.0006	0.9125	0.0115	0.06455	0.00077	627	7	658	12	758	50
ap03b14	0.302	0.0009	4.4817	0.0134	0.10763	0.00042	1699	10	1728	5	1758	14
ap03b15	0.0829	0.0007	1.2626	0.0758	0.11048	0.00514	483	14	829	68	1806	168
ap03b16	0.2202	0.0084	16.4658	0.7014	0.54224	0.00672	492	220	2904	82	4000	0
ap03c05	0.1496	0.0047	2.9584	0.0846	0.14347	0.00194	847	60	1397	43	2268	46
ap03c06	0.1	0.0008	1.1146	0.0308	0.08087	0.00215	604	12	760	30	1218	104
ap03c07	0.1533	0.0007	1.493	0.0094	0.07063	0.00037	919	8	928	8	946	20
ap03c08	0.0724	0.0003	0.5811	0.0035	0.05823	0.00037	450	4	465	4	538	28
ap03c09	0.0617	0.0003	0.6057	0.0072	0.07117	0.00088	380	5	481	9	962	50
ap03c10	0.1779	0.0007	1.8184	0.0156	0.07413	0.00066	1056	9	1052	11	1044	36
ap03c11	0.0872	0.0004	0.7705	0.0065	0.06408	0.00062	544	5	580	7	744	42
ap03c12	0.3317	0.001	5.1702	0.0248	0.11305	0.00047	1848	10	1848	8	1848	16
ap03c13	0.1044	0.0005	0.991	0.0076	0.06884	0.00049	639	6	699	8	892	30
ap03c14	0.1481	0.0015	1.9885	0.0169	0.09736	0.00152	875	18	1112	11	1574	58
ap03c15	0.149	0.0006	1.7949	0.0179	0.0874	0.00087	876	8	1044	13	1368	38
ap03c16	0.065	0.0003	0.7303	0.0067	0.08152	0.00088	395	5	557	8	1232	42
ap03d05	0.0753	0.0002	0.5968	0.0054	0.05748	0.00056	469	3	475	7	508	42
ap03d06	0.0685	0.0004	0.5218	0.0078	0.05524	0.0008	434	7	426	10	422	66
ap03d07	0.0842	0.0004	0.6861	0.0096	0.05913	0.00079	521	6	530	12	570	58
ap03d08	0.1016	0.0005	0.8589	0.0071	0.06134	0.00059	624	7	630	8	650	40
ap03d09	0.1009	0.0005	0.8772	0.0113	0.06304	0.00093	620	6	639	12	708	64
ap03d10	0.5241	0.0023	13.6093	0.049	0.18836	0.00068	2710	21	2723	7	2726	12
ap03d11	0.0971	0.0006	0.8556	0.0076	0.06392	0.00062	597	7	628	8	738	40
ap03d12	0.1221	0.0004	1.0863	0.0086	0.06451	0.00049	742	5	747	8	758	32
ap03d13	0.1032	0.0007	0.9907	0.0141	0.06964	0.0011	626	9	699	14	916	66
ap03d14	0.1008	0.0004	0.8459	0.0087	0.06089	0.00062	621	5	622	10	634	44
ap03d15	0.0534	0.0003	0.4393	0.0066	0.05968	0.00089	334	4	370	9	592	66
ap03d16	0.0832	0.0012	0.9478	0.0181	0.08259	0.00249	500	16	677	19	1258	118
ap03e05	0.1246	0.0007	1.1595	0.0256	0.06749	0.00115	754	9	782	24	852	72
ap03e06	0.1456	0.0006	1.8269	0.011	0.09099	0.00056	885	8	1055	8	1446	24
ap03e07	0.1905	0.001	2.1608	0.0212	0.08227	0.00079	1122	12	1169	14	1250	38
ap03e08	0.0872	0.0004	0.7177	0.0093	0.05967	0.00083	539	5	549	11	590	60
ap03e09	0.3321	0.0024	8.2825	0.0654	0.1809	0.00166	1822	28	2262	14	2660	32
ap03e10	0.0824	0.0004	0.6537	0.0093	0.05755	0.00079	511	6	511	11	512	62
ap03e11	0.2037	0.0008	2.2611	0.0154	0.0805	0.00049	1195	10	1200	10	1208	24
ap03e12	0.056	0.0002	0.4169	0.0042	0.05398	0.00062	352	3	354	6	370	52
ap03e13	0.1016	0.0004	0.8675	0.0107	0.06192	0.00074	623	6	634	12	670	52
ap03e14	0.1165	0.0005	1.0567	0.0123	0.06581	0.00083	709	7	732	12	800	54
ap03e15	0.0736	0.0004	0.5859	0.0057	0.05772	0.00055	459	5	468	7	518	42
ap03e16	0.0783	0.0004	0.6278	0.007	0.05819	0.00066	485	5	495	9	536	50

(continued on next page)

Table 5 (continued)

Sample/analysis	$^{206}\text{Pb}/^{238}\text{U}$	Percentage error	$^{207}\text{Pb}/^{235}\text{U}$	Percentage error	$^{207}\text{Pb}/^{206}\text{Pb}$	Percentage error	Age, Ma $^{206}\text{Pb}/^{238}\text{U}$	(2 $\sigma$ )	$^{207}\text{Pb}/^{235}\text{U}$	(2 $\sigma$ )	$^{207}\text{Pb}/^{206}\text{Pb}$	(2 $\sigma$ )
<i>SAL-11</i>												
ap03f05	0.1581	0.0006	1.9772	0.0091	0.09068	0.00052	918	9	1108	6	1438	22
ap03f06	0.1646	0.0011	1.7427	0.0197	0.07677	0.0009	973	14	1024	15	1114	48
ap03f07	0.1534	0.0013	1.5557	0.0219	0.07355	0.00088	918	16	953	17	1028	48
ap03f08	0.1578	0.0006	1.6096	0.0106	0.074	0.00046	943	7	974	8	1040	26
ap03f09	0.1332	0.0012	1.2409	0.045	0.06758	0.00219	801	16	819	41	854	134
ap03f10	0.0992	0.0006	0.8582	0.0094	0.06278	0.00082	608	7	629	10	700	56
ap03f11	0.1048	0.0008	0.9372	0.0378	0.06487	0.00288	640	11	671	40	770	188
ap03f12	0.3579	0.0017	5.9463	0.0416	0.1205	0.00081	1974	19	1968	12	1962	24
ap03f13	0.203	0.0009	2.337	0.0236	0.08352	0.00071	1190	10	1224	14	1280	32
ap03f14	0.3538	0.0029	7.712	0.0671	0.15812	0.00059	1936	31	2198	16	2434	12
ap03f15	0.1801	0.0009	1.903	0.0124	0.07662	0.00056	1065	10	1082	9	1110	28
ap03f16	0.0887	0.0009	0.7442	0.0258	0.06085	0.0022	546	11	565	30	632	156
ap03g05	0.0908	0.0003	0.8468	0.007	0.06768	0.00057	554	5	623	8	858	34
ap03g06	0.0868	0.0006	0.7051	0.0113	0.05893	0.00098	536	7	542	13	564	74
ap03g07	0.0917	0.0005	0.7766	0.0077	0.06142	0.00073	566	6	584	9	652	50
ap03g08	0.0572	0.0002	0.4342	0.0066	0.05508	0.00089	358	3	366	9	414	72
ap03g09	0.0564	0.0002	0.4184	0.0033	0.05377	0.00042	352	3	355	5	360	36
ap03g10	0.0766	0.0004	0.6183	0.0098	0.05852	0.00105	476	6	489	12	548	80
ap03g11	0.0966	0.0005	0.8187	0.009	0.06146	0.00061	593	6	607	10	654	44
ap03g12	0.1022	0.0004	0.8782	0.0056	0.06234	0.00043	627	5	640	6	684	30
ap03g13	0.1485	0.0009	1.4725	0.0141	0.0719	0.00079	889	11	919	12	982	44
ap03g14	0.0916	0.0004	0.8903	0.0112	0.07052	0.00089	559	6	647	12	942	52
ap03g15	0.1826	0.0005	1.9295	0.0125	0.07664	0.00055	1082	6	1091	9	1110	30
ap03g16	0.3392	0.0013	5.4985	0.0302	0.11758	0.00061	1882	14	1900	9	1918	18

rocks are gently dipping to the north and post-date all but normal faulting.

### 3. LA-ICPMS zircon analyses

#### 3.1. Analytical procedures

Preparation of the five samples was carried at Instituto de Geología, UNAM. About 15 kg of each of the selected samples for zircon dating was crushed with a jaw crusher and pulverized in a Bico disk mill. The heavy minerals were concentrated on a Wifley table and were then passed through a Frantz magnetic separator. A current up to 1.5 A is used to generate a magnetic field for samples to concentrate zircons suitable for LA-ICPMS dating. Further separation by passing non-magnetic fractions through heavy liquids (bromoform), ensured a nearly pure zircon concentration.

Zircons from all five samples were mounted in epoxy and polished for age determinations on individual grains by LA-ICPMS. All grains were photographed using transmitted and reflected light optical microscopy, and the internal structures of the grains imaged using SEM-CL. U-Pb isotopic compositions of individual zircon grains were determined at RSES-ANU, Canberra, Australia, using an ArF excimer laser system (193 nm, Lambda Physik) coupled to an Agilent 7500 quadrupole ICPMS (Eggins et al., 1998). Ablation was done under a He atmosphere in a custom-built sample chamber using a 40-micron diameter spot and a laser repetition rate of 4 Hz. Data were reduced relative to the reference zircon FC1 (1099 Ma, Paces and Miller 1993), with gas backgrounds collected before each analysis and subtracted from net intensities measured for each isotope. Internal precision of

measured  $^{207}\text{Pb}/^{206}\text{Pb}$  and  $^{206}\text{Pb}/^{238}\text{U}$  ratios typically was  $\sim 0.5\%$  1 $\sigma$  relative standard deviation for individual analyses. The samples were analyzed in two sessions; replicate analyses of the FC1 zircon from each session indicate external reproducibilities of 0.9% ( $n=30$ ) and 0.8% ( $n=32$ ), respectively, on the measured  $^{207}\text{Pb}/^{206}\text{Pb}$  ratios, 1.1% and 0.8%, respectively, on the measured  $^{206}\text{Pb}/^{238}\text{U}$  ratios, and 1.2% and 1.6%, respectively, on the  $^{208}\text{Pb}/^{232}\text{Th}$  ratios (1 $\sigma$  relative standard deviation). These errors are not included in the quoted uncertainties for individual analyses of the analyzed zircons. The data are provided in Tables 1–5 and the corrected  $^{206}\text{Pb}/^{238}\text{U}$  data are plotted on Terra–Wasserburg diagrams (Figs. 4–8).

### 4. Results

A pegmatite cutting the eastern part of the Huerta Unit (HUERTA-1) consists of K-feldspar, quartz and muscovite with accessory zircon, apatite and opaque minerals. Zircons yielded  $^{206}\text{Pb}/^{238}\text{U}$  ages ranging from 427 Ma to 2531 Ma, however the youngest, almost concordant  $^{206}\text{Pb}/^{238}\text{U}$  zircon age is  $464 \pm 4$  Ma and a mean age of the four almost concordant young zircons is  $\sim 485.5$  Ma (Fig. 4; Table 1): these are interpreted as dating the time of intrusion. Two population of older, inherited zircons with concordant ages have ages of  $\sim 530$ –580 Ma and  $\sim 910$ –1200 Ma.

Three samples were collected from the Amate Unit: one feldspathic metapsammite (AMATE-1) and two cross-cutting, foliated granitic dikes (AMATE-2 and SAL-12). The metapsammite is composed mainly of quartz, K-feldspar and muscovite. It yielded detrital zircons with  $^{206}\text{Pb}/^{238}\text{U}$  ages ranging from 847 Ma to 1325 Ma, however, the youngest concordant detrital zircon gave

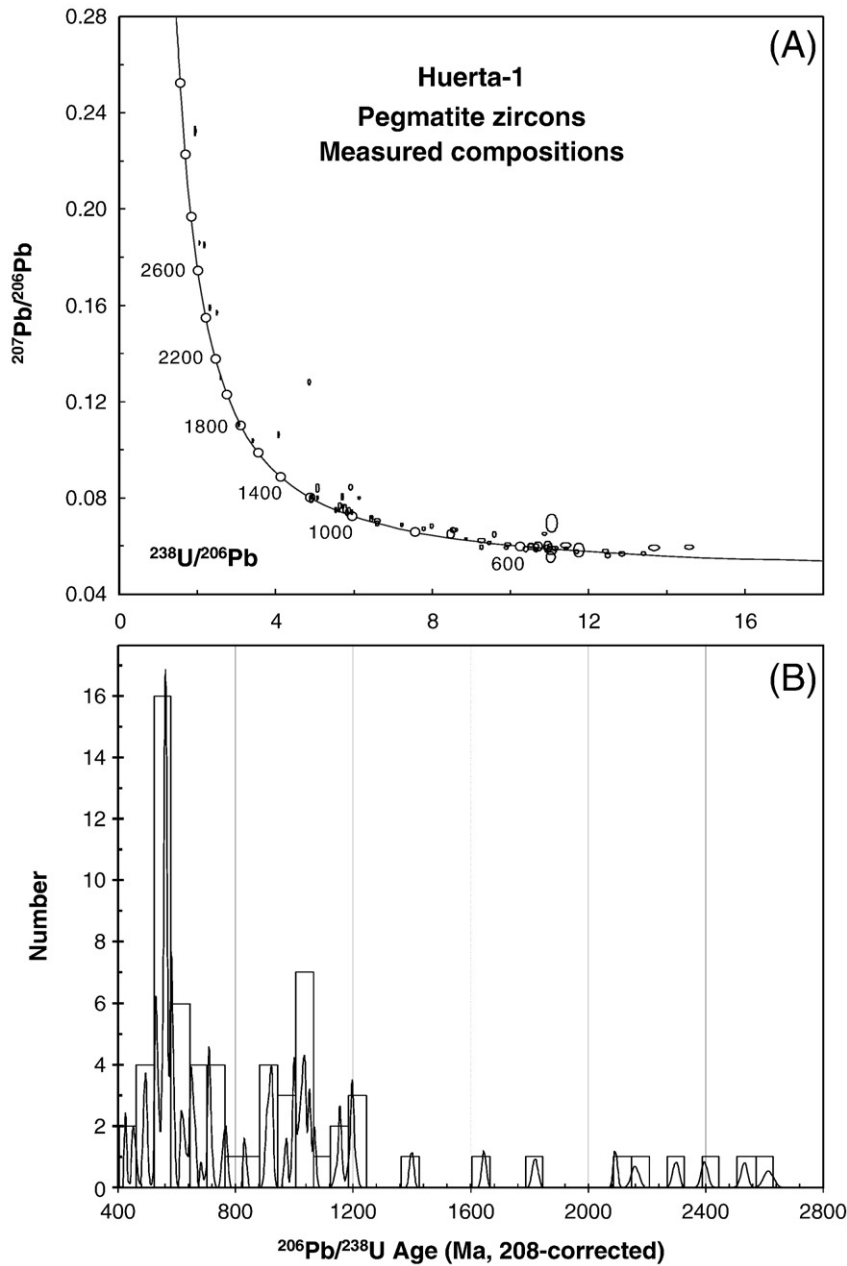


Fig. 4. U–Pb LA-ICPMS zircon analyses from pegmatite cutting the Huerta Unit (sample HUERTA-1) plotted on (A) a Terra–Wasserburg diagram, and (B) a histogram.

a  $^{206}\text{Pb}/^{238}\text{U}$  age of  $902 \pm 14$  Ma, and older concordant ages in the range of  $\sim 900$  Ma to 1300 Ma (Fig. 5; Table 2).

The foliated granite dike (AMATE-2) consists of quartz, feldspar, muscovite, and accessory zircon, apatite, and opaque minerals. The  $^{206}\text{Pb}/^{238}\text{U}$  ages range from 432 Ma to 1252 Ma with the youngest concordant  $^{206}\text{Pb}/^{238}\text{U}$  zircon age being  $447 \pm 3$  Ma (Fig. 6, Table 3). Older inherited zircon ages with concordant  $^{206}\text{Pb}/^{238}\text{U}$  ages in the range of 950–1230 Ma.

Another foliated and folded granitic dike (SAL-12) intruding the eastern part of the Amate Unit yielded  $^{206}\text{Pb}/^{238}\text{U}$  zircon ages ranging from 422 Ma to 1565 Ma, however the youngest concordant age is  $452 \pm 6$  Ma interpreted as the time of intrusion (Fig. 7, Table 4). Older inherited zircons gave concordant  $^{206}\text{Pb}/^{238}\text{U}$  ages in the range of 912–1280 Ma with single concordant ages at  $839 \pm 7$  Ma and  $1565 \pm 12$  Ma.

Detrital zircons in a metapsammite of the Salada Unit (SAL-11) yielded a  $^{206}\text{Pb}/^{238}\text{U}$  ranging from 352 Ma to 3000 Ma with the youngest concordant detrital zircon yielded a  $^{206}\text{Pb}/^{238}\text{U}$  age of  $352 \pm 3$  Ma (Fig. 8, Table 5). Older concordant ages of  $\sim 434$ –485 Ma, 511–630 Ma, and 920–1200 Ma.

## 5. Constraints on the ages of the new units

### 5.1. Huerta Unit

Deposition of the Huerta Unit is constrained by the  $455 \pm 4$  Ma age of the youngest detrital zircon (Keppe et al., 2006) and  $464 \pm 4$  Ma intrusive age of a cross-cutting pegmatite. The ages are similar within analytical error and suggest that deposition was synchronous with intrusion. However, the two dated samples were collected

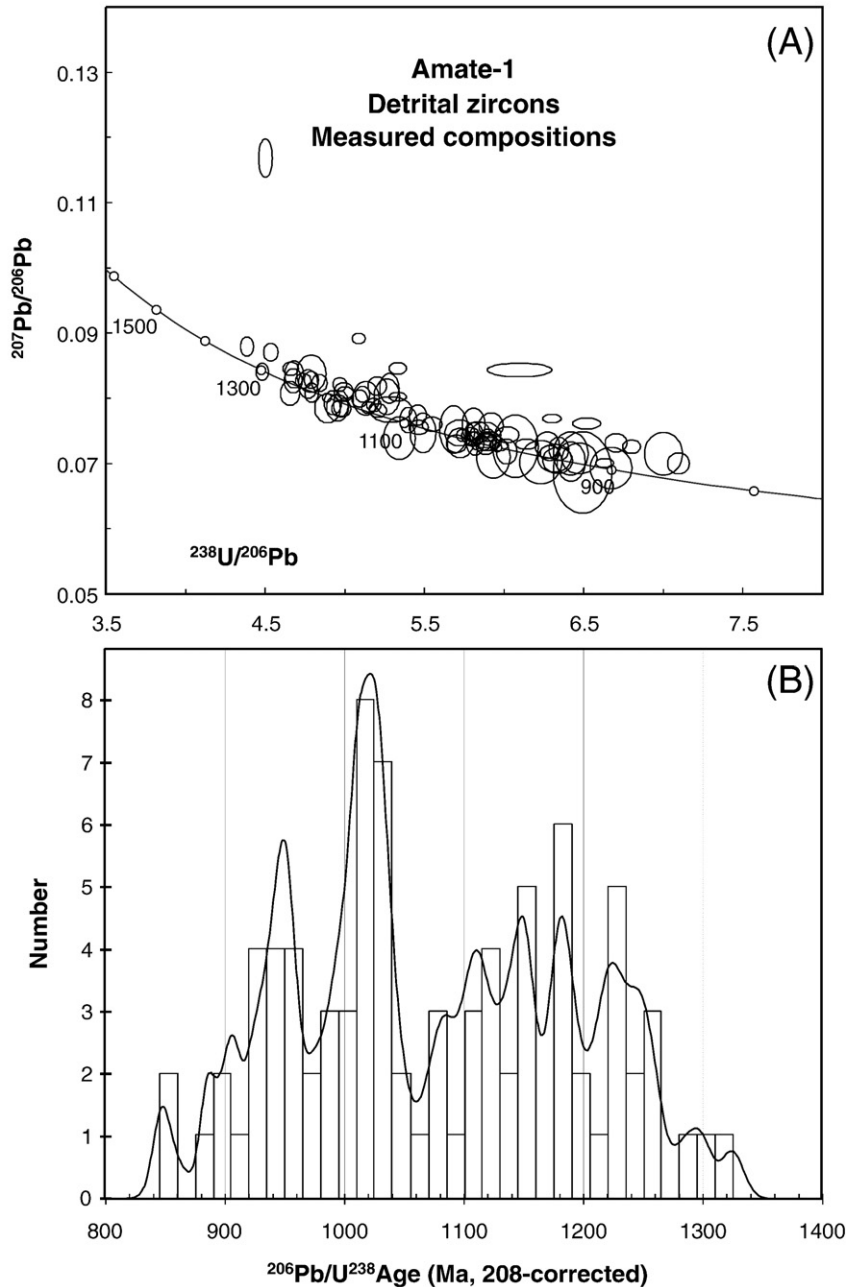


Fig. 5. U-Pb LA-ICPMS zircon analyses from metapsammite of the Amate Unit (sample AMATE-1) plotted on (A) a Terra-Wasserburg diagram, and (B) a histogram.

10 km apart from western and eastern parts of the Huerta Unit, respectively. Thus deposition of rocks in the eastern part of the unit that are cut by the pegmatite may be somewhat older than ~455 Ma. The polyphase deformation of the unit probably means that this problem cannot be ascertained by further mapping: further detrital zircon dating is required. Nevertheless, deposition of the unit probably took place during the Ordovician.

### 5.2. Amate Unit

Deposition of the Amate Unit is less tightly constrained: post-902±14 Ma (youngest concordant detrital zircon) and pre-447±3 Ma, pre-452±6 Ma (the intrusive ages of cross-cutting granite dikes: this paper), and pre-442±1 Ma (the intrusive age

of a cross-cutting gabbro dike: [Keppie et al., 2008b](#)). The absence of late Neoproterozoic ages in the Amate Unit, where they are present in the Huerta Unit, suggests either that the units are of different ages or that the provenance changed. The latter situation is apparent in the Ordovician units of the Patlanoaya area ([Keppie et al., 2008b](#)) and in the Tecomate Formation ([Sánchez-Zavala et al., 2004](#)). However, at this stage, one cannot rule out a difference in the time of deposition.

### 5.3. Salada Unit

An older limit on the time of deposition of the Salada Unit is provided by the 352±3 Ma age of the youngest detrital zircon. A younger limit is not directly available. The Tecmome

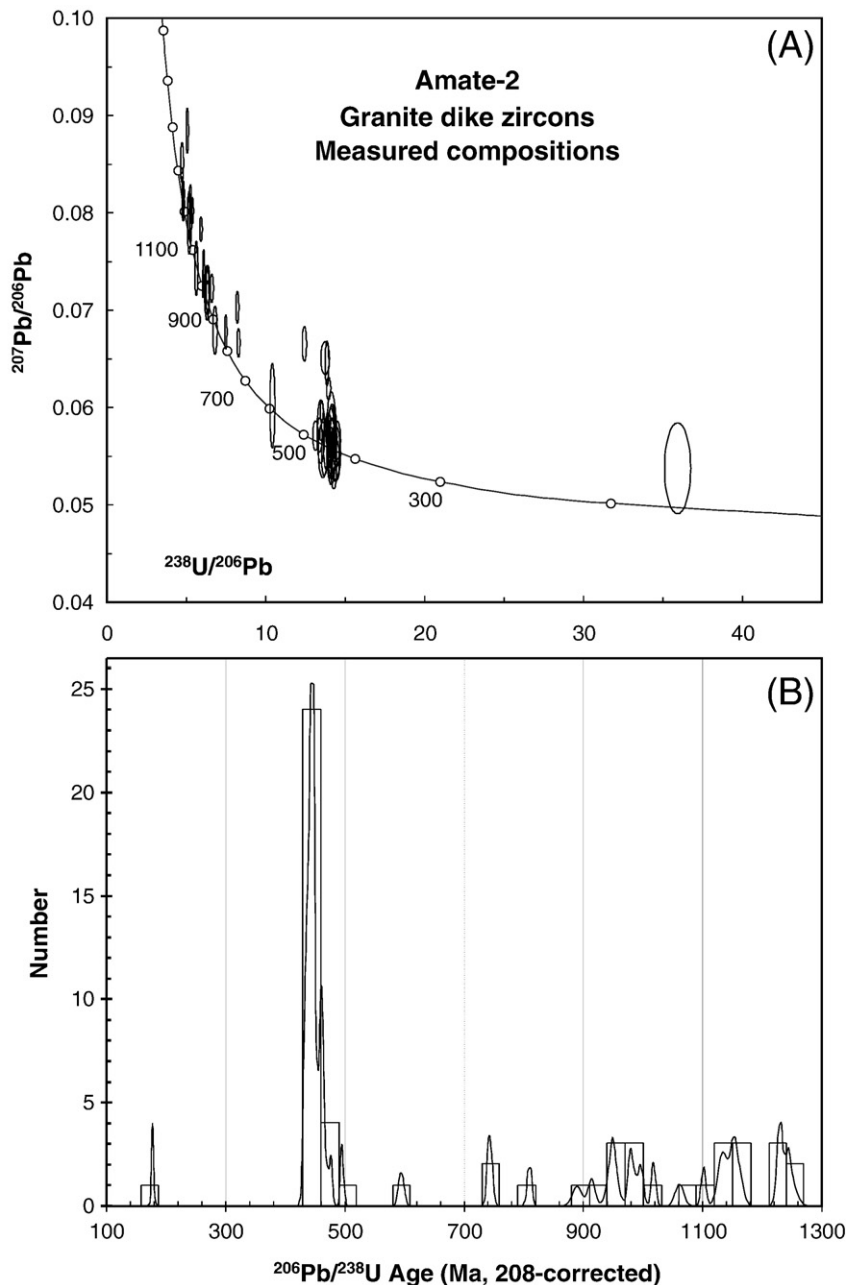


Fig. 6. U–Pb LA-ICPMS zircon analyses from granitic dike cutting the Amate Unit (sample AMATE-2) plotted on (A) a Terra–Wasserburg diagram, and (B) a histogram.

Formation is everywhere in tectonic contact with the Salada Unit, however, the lithologies are markedly distinct and the dated parts of the Tecomate Formation are latest Pennsylvanian to Middle Permian (Keppie et al., 2004a). Furthermore, it is lithologically distinct from the Permo-Triassic Chazumba and Magdalena units, which also have distinctly younger detrital zircon populations (Keppie et al., 2006). Thus its age is most likely to be Carboniferous.

#### 6. Provenance of the detrital zircons

Whereas both the Huerta and Amate units both contain a 900–1300 Ma detrital zircon population, ~460 Ma and ~510–

640 Ma populations are only recorded in the Huerta Unit. The 900–1300 Ma population is probably of local provenance in the neighbouring Oaxacan Complex (Fig. 1B), which has yielded ages ranging from 920 Ma to 1300 Ma (Keppie et al., 2003; Solari et al., 2003; Ortega-Obregón et al., 2003). A local source for the ~460 Ma detrital zircons is also likely in the Ordovician granitoids of the Acatlán Complex (Fig. 1B)(Sánchez-Zavala et al., 2004; Talavera-Mendoza et al., 2005; Miller et al., 2007). On the other hand a more distal source for the ~510–640 Ma zircons may be found in either the basement beneath the Yucatan Peninsula, the Brasiliano orogens of Amazonia, or Avalonia (which separated from Oaxaca/Amazonia at ~480 Ma) (Keppie, 2004; Keppie et al., 2006; Nance et al., 2006).

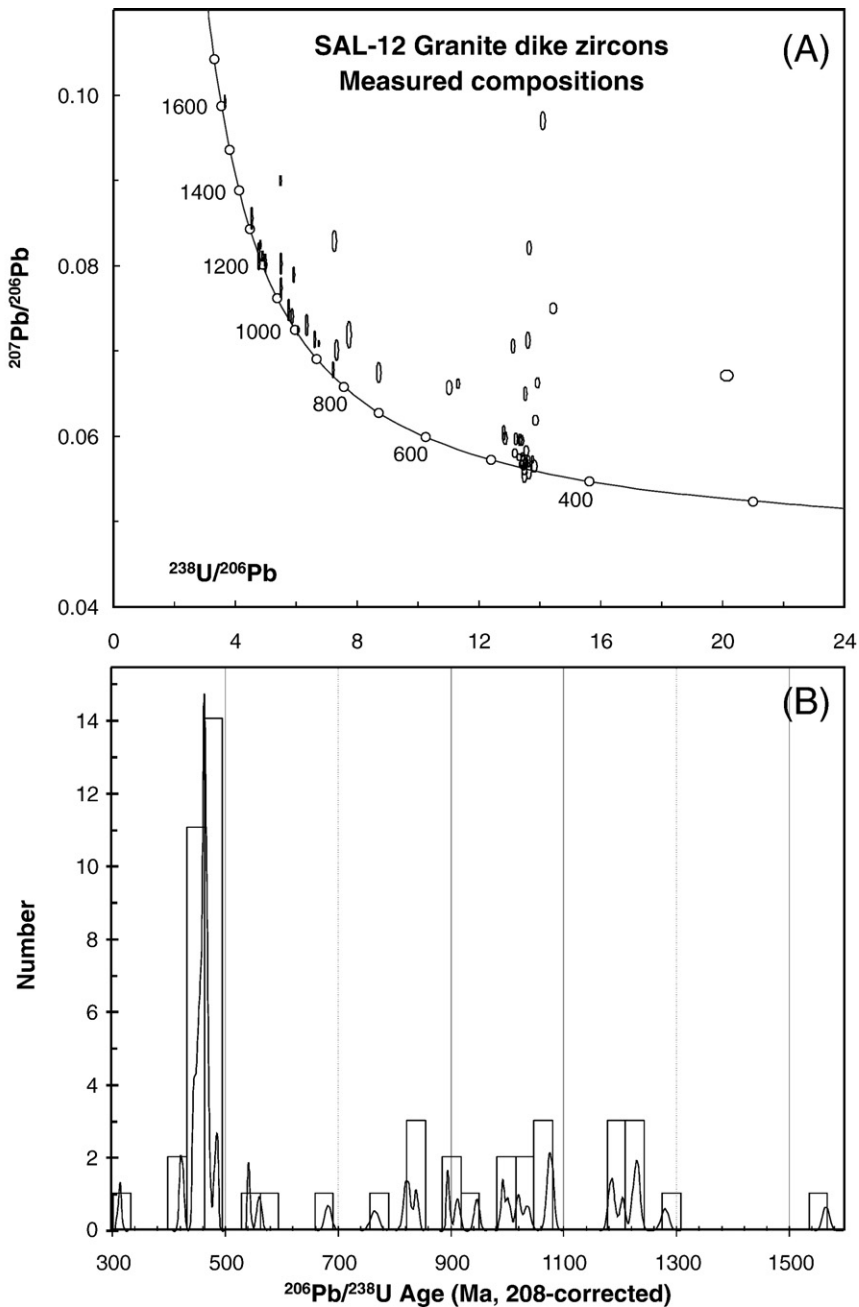


Fig. 7. U–Pb LA-ICPMS zircon analyses from granitic dike cutting the Amate Unit (sample SAL-12) plotted on (A) a Terra–Wasserburg diagram, and (B) a histogram.

The Salada Unit, in addition to these latter populations also contains ~352 Ma detrital zircons. Such ages (353–346 Ma) have been recorded in the zircons from eclogites of the Piaxtla Suite in the central part of the Acatlán Complex (Middleton et al., 2007; Elías-Herrera et al., 2007), where they have been related to exhumation of subduction-related rocks. Thus a local source is likely, however by this time, Pangea had amalgamated and thus more distal sources are also possible.

#### 6.1. Terminology

The absence of eclogite facies metamorphism in the Xayacatlán area precludes inclusion of the units in this area in

the Piaxtla Suite. Furthermore, the term Xayacatlán is so inextricably linked to the Piaxtla Suite (e.g. Vega-Granillo et al., 2007, and references therein) that we introduce the name, Amate Unit, for the sedimentary rocks previously included in the Xayacatlán Formation. Also the differences in ages of the Huerta and Salada units, both of which were previously assigned to the Cosoltepec Formation (Ortega-Gutiérrez, 1975), justifies their separation and redefinition. A sample of the Cosoltepec Formation type section yielded a similar detrital zircon age population to the Salada Unit, however, the youngest  $^{206}\text{Pb}/^{238}\text{U}$  age reported from the type Cosoltepec Formation is ~376 Ma (discordant data: Talavera-Mendoza et al., 2005), slightly older than the 352 Ma age in the Salada Unit. Both the

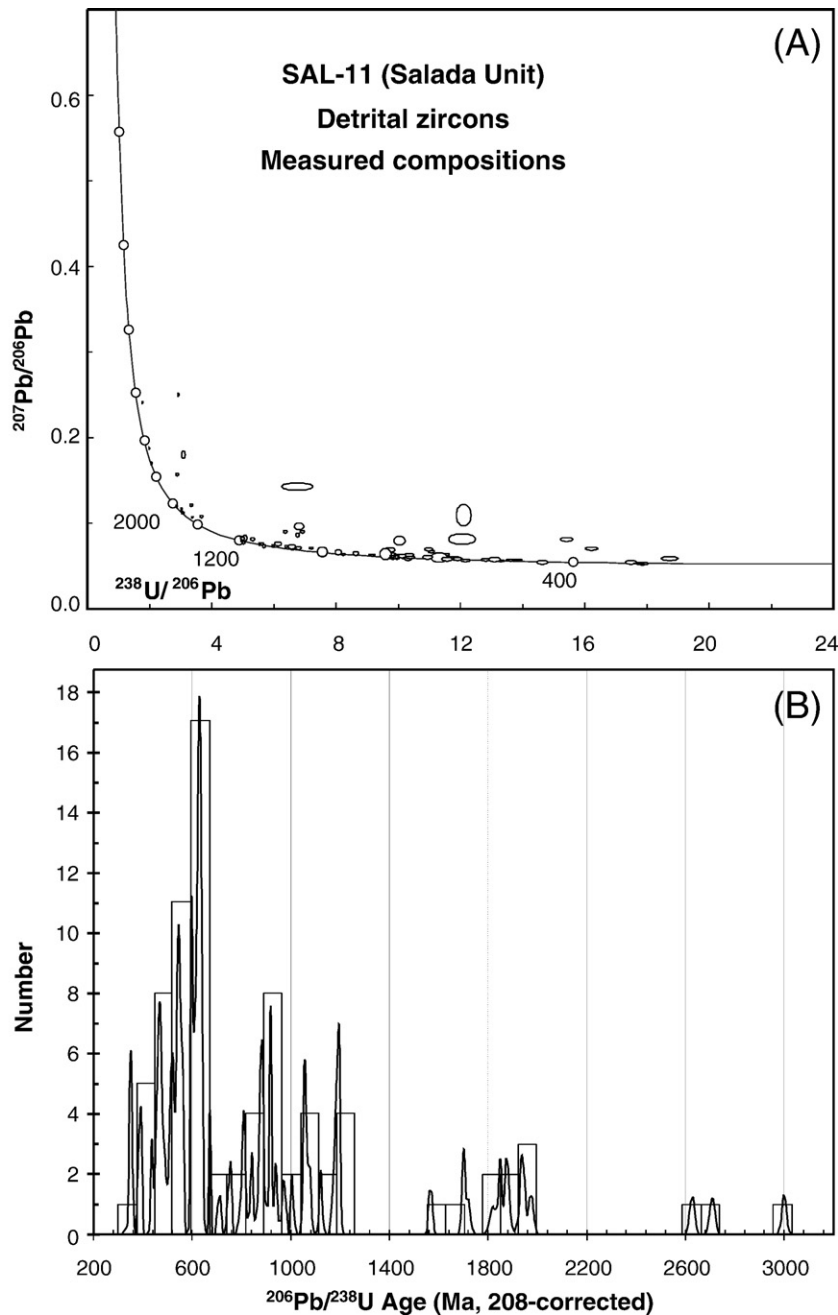


Fig. 8. U–Pb LA-ICPMS zircon analyses from metapsammite of the Salada Unit (sample SAL-11) plotted on (A) a Terra–Wasserburg diagram, and (B) a histogram.

Salada Unit and the type Cosoltepec Formation contain mafic igneous lenses and appear to be continuous along strike from one another (Fig. 1B). However, until mapping and further data confirms their continuity, it is better to maintain the Salada Unit as a distinct unit.

## 7. Discussion

The younger granitoid rocks dated in the Xayacatlán area, which range from  $464 \pm 4$  Ma to  $447 \pm 3$  Ma age, are very similar to the  $442 \pm 1$  Ma age of a gabbroic dike cutting the Amate Unit (Keppie et al., 2008b). As granitic dikes and pegmatites also cut this mafic dike, it indicates that magmatism in the Xayacatlán

area lasted from  $\sim 464$  Ma to 442 Ma. These igneous rocks are bimodal and the mafic dikes are continental rift tholeiites (Keppie et al., 2008b), and appear to form part of a more widespread  $\sim 480$ –440 Ma magmatic event in the Acatlán Complex. The Huerta Unit appears to have been deposited during this same time interval, and thus it probably represents a rift setting on the margin of Oaxaca (Fig. 9). The Oaxacan Complex is inferred to have underlain the Acatlán Complex during the Ordovician (Keppie, 2004), an interpretation that is consistent with the  $\sim 1$  Ga inherited zircons in the pegmatite cutting the Huerta Unit. The same interpretations probably also apply to the Amate Unit, however, it may be somewhat older. The rifted continental margin setting inferred for all of these

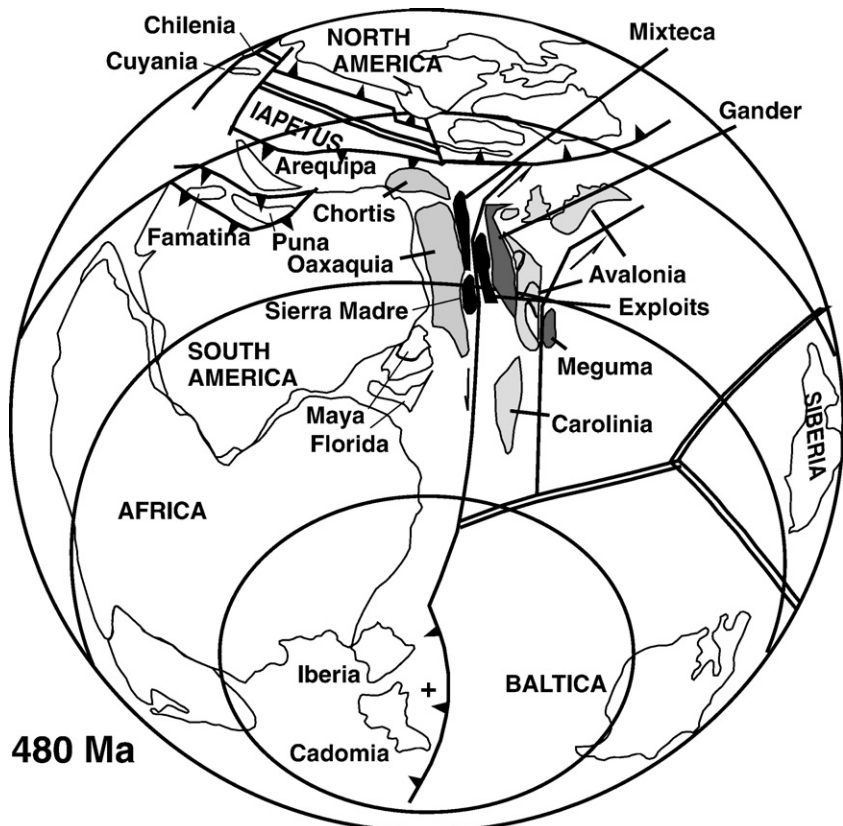


Fig. 9. Ordovician paleogeographic reconstruction showing the location of the Huerta and Amate units on the southern margin of the Rheic Ocean (modified after Keppie, 2004).

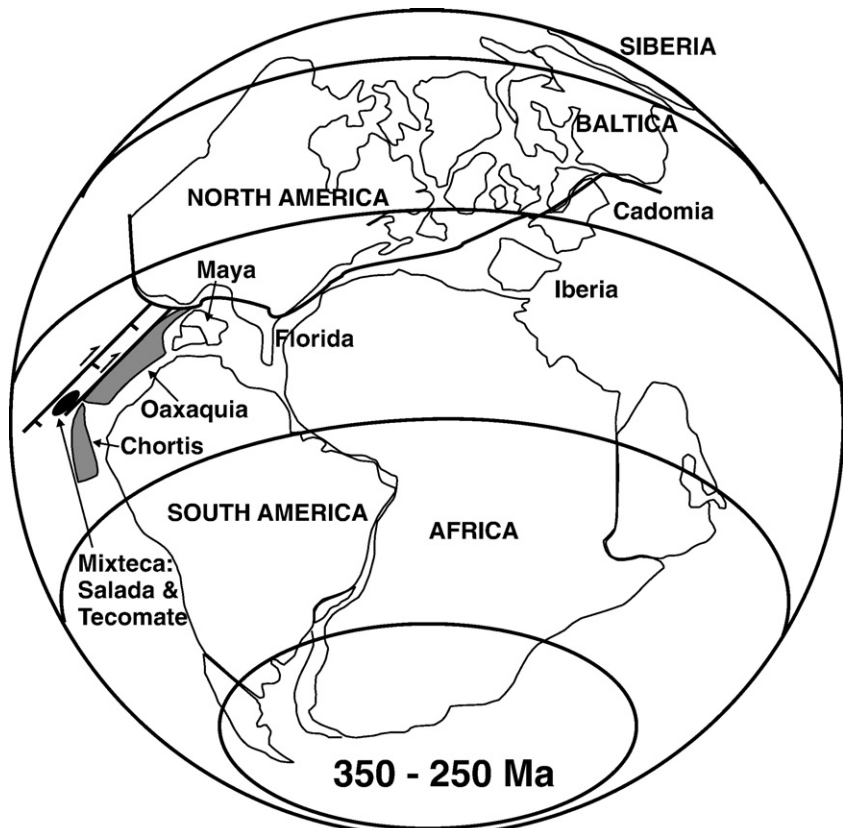


Fig. 10. Carboniferous paleogeographic reconstruction showing the location of the Salada Unit on the western margin of Pangea (modified after Keppie, 2004).

Ordovician (and possibly older) rocks is more consistent with the deposition along the rift-drift southern margin of the Rheic Ocean (Fig. 9), because the Iapetus Ocean was closing during the Ordovician and it was bordered by active margins. Furthermore, all the detrital zircons in these two units could have been derived from Oaxaquia and Amazonia: the Neoproterozoic zircons are incompatible with the derivation from Laurentia.

The presumed Carboniferous age of the Salada Unit suggests that its deposition was synchronous with the older parts of the latest Devonian–Early Permian Patlanaoya Group (Vachard et al., 2000), which was synchronous with extensional deformation and easterly dipping subduction (Ramos-Arias et al., 2008). The overlying Permian Tecomate Formation was synchronous with arc magmatism (Torres et al., 1999), including the Totoltepec laccolith. That these rocks formed on the western margin of Pangea (Fig. 10) is indicated by the Midcontinent (USA) faunal affinity of fossils in the Mississippian rocks lying on top of the Oaxacan Complex (Navarro-Santillan et al., 2002).

## Acknowledgements

We would like to acknowledge a Papiit grant (IN103003) and a CONACyT grant (CB-2005-1: 24894) to JDK. CONACyT contributed to studies for MMG. We are grateful for constructive reviews by Drs. Peter A. Cawood and José R. Martínez Catalán.

## References

- Campa, M.F., Coney, P.J., 1983. Tectono-stratigraphic terranes and mineral distributions in Mexico. Canadian Journal of Earth Science 20, 1040–1051.
- Egging, S.M., Kinsley, L.P.J., Shelley, J.M.G., 1998. Deposition and element fractionation processes during atmospheric pressure laser sampling for analysis by ICP-MS. Applied Surface Science 127/129, 278–286.
- Elías-Herrera, M., Ortega-Gutiérrez, F., 2002. Caltepec fault zone: an Early Permian dextral transpressional boundary between the Proterozoic Oaxacan and Paleozoic Acatlán complexes, southern Mexico, and regional implications. Tectonics 21 (3). doi:10.1029/200TC001278.
- Elías-Herrera, M., Macías-Romo, C., Ortega-Gutiérrez, F., Sánchez-Zavala, J.L., Iriondo, A., Ortega-Rivera, A., 2007. Conflicting stratigraphic and geochronologic data from the Acatlán Complex: “Ordovician” granites intrude metamorphic and sedimentary rocks of Devonian–Permian age. Eos Transactions of the American Geophysical Union 88 (23) Joint Assembly Supplement, Abstract T41A-12.
- Keppie, J.D., 2004. Terranes of Mexico revisited: a 1.3 billion year odyssey. International Geology Review 46, 765–794.
- Keppie, J.D., Ramos, V.S., 1999. Odyssey of terranes in the Iapetus and Rheic Oceans during the Paleozoic. In: Keppie, J.D., Ramos, V.A. (Eds.), Laurentia–Gondwana Connections Before Pangea. Geological Society of America Special Paper, vol. 336, pp. 267–276.
- Keppie, J.D., Dostal, J., Cameron, K.L., Solari, L.A., Ortega-Gutiérrez, F., Lopez, R., 2003. Geochronology and geochemistry of Grenvillian igneous suites in the northern Oaxacan Complex, southern México: tectonic implications. Precambrian Research 120, 365–389.
- Keppie, J.D., Sandberg, C.A., Miller, B.V., Sánchez-Zavala, J.L., Nance, R.D., Poole, F.G., 2004a. Implications of latest Pennsylvanian to Middle Permian paleontological and U–Pb SHRIMP data from the Tecomate Formation to re-dating tectonothermal events in the Acatlán Complex, southern Mexico. International Geology Review 46, 745–753.
- Keppie, J.D., Nance, R.D., Powell, J.T., Mumma, S.A., Dostal, J., Fox, D., Muise, J., Ortega-Rivera, A., Miller, B.V., Lee, J.W.K., 2004b. Mid-Jurassic tectonothermal event superposed on a Paleozoic geological record in the Acatlán Complex of southern Mexico: hotspot activity during the breakup of Pangea. Gondwana Research 7, 239–260.
- Keppie, J.D., Nance, R.D., Fernández-Suárez, J., Storey, C.D., Jeffries, T.E., Murphy, J.B., 2006. Detrital zircon data from the eastern Mixteca terrane, southern Mexico: evidence for an Ordovician–Mississippian continental rise and a Permo-Triassic clastic wedge adjacent to Oaxaquia. International Geology Review 48, 97–111.
- Keppie, J.D., Dostal, J., Murphy, J.B., Nance, R.D., 2008a. Synthesis and tectonic interpretation of the westernmost Paleozoic Variscan orogen in southern Mexico: from rifted Rheic margin to active Pacific margin. Tectonophysics.
- Keppie, J.D., Dostal, J., Ramos-Arias, M.A., Morales-Gámez, M., Miller, R.D., Nance, Murphy, J.B., Ortega-Rivera, A., Lee, J.W.K., 2008b. Ordovician rift tholeites in the Acatlán Complex, southern Mexico: evidence of rifting on the southern margin of the Rheic Ocean. Tectonophysics.
- Malone, J.W., Nance, R.D., Keppie, J.D., Dostal, J., 2002. Deformational history of part of the Acatlán Complex: Late Ordovician–Early Silurian and Early Permian orogenesis in southern Mexico. Journal of South American Earth Sciences 15, 511–524.
- Middleton, M., Keppie, J.D., Murphy, J.B., Miller, B.V., Nance, R.D., Ortega-Rivera, A., Lee, J.W.K., 2007. P–T–t constraints on exhumation following subduction in the Rheic Ocean from eclogitic rocks in the Acatlán Complex of southern Mexico. In: Linnemann, U., Nance, R.D., Kraft, P., Zulauf, G. (Eds.), The Evolution of the Rheic Ocean: From Avalonian–Cadmian Active Margin to Alleghenian–Variscan Collision. Geological Society of America Special Paper, vol. 423, pp. 489–509.
- Miller, B.V., Dostal, J., Keppie, J.D., Nance, R.D., Ortega-Rivera, A., Lee, J.W.K., 2007. Ordovician calc-alkaline granitoids in the Acatlán Complex, southern Mexico: geochemical and geochronological data and implications for tectonic of the Gondwanan margin of the Rheic Ocean. In: Linnemann, U., Nance, R.D., Zulauf, G., Kraft, P. (Eds.), The Evolution of the Rheic Ocean: From Avalonian–Cadmian Active Margin to Alleghenian–Variscan Collision. Geological Society of America Special Paper, vol. 423, pp. 465–475.
- Nance, R.D., Miller, B.V., Keppie, J.D., Murphy, J.B., Dostal, J., 2006. The Acatlán Complex, southern Mexico: record of Pangea assembly to breakup. Geology 34, 857–860.
- Nance, R.D., Miller, B.V., Keppie, J.D., Murphy, J.B., Dostal, J., 2007. Vestige of the Rheic Ocean in North America: the Acatlán Complex of southern México. In: Linnemann, U., Nance, R.D., Zulauf, G., Kraft, P. (Eds.), The Evolution of the Rheic Ocean: From Avalonian–Cadmian Active Margin to Alleghenian–Variscan Collision. Geological Society of America Special Paper, vol. 423, pp. 437–452.
- Navarro-Santillan, D., Sour-Tovar, F., Centeno-Garcia, E., 2002. Lower Mississippian (Osagean) brachiopods from the Santiago Formation, Oaxaca, Mexico: stratigraphic and tectonic implications. Journal of South American Earth Sciences 15, 327–336.
- Ortega-Gutiérrez, F., 1975. The pre-Mesozoic geology of the Acatlán area, south Mexico: Ph.D. thesis, Leeds University, U.K. 166 pp.
- Ortega-Gutiérrez, F., Elias-Herrera, M., Reyes-Salas, M., Macias-Romo, C., López, R., 1999. Late Ordovician–Early Silurian continental collision orogeny in southern Mexico and its bearing on Gondwana–Laurentia connections. Geology 27, 719–722.
- Ortega-Obregón, C., Keppie, J.D., Solari, L.A., Ortega-Gutiérrez, F., Dostal, J., López, R., Ortega-Rivera, A., Lee, J.W.K., 2003. Geochronology and geochemistry of the ~917 Ma, calc-alkaline Etla granitoid pluton (Oaxaca, southern México): evidence of post-Grenvillian subduction along the northern margin of Amazonia. International Geology Review 45, 596–610.
- Paces, J.B., Miller, J.D., 1993. Precise U–Pb ages of the Duluth Complex and related mafic intrusions, northeastern Minnesota: geochronological insights to physical, petrogenetic, paleomagnetic, and tectonomagmatic processes associated with the 1.1 Ga Midcontinent Rift System. Journal of Geophysical Research 98, 13997–14013.
- Ramírez-Espinosa, J., 2001. Tectono-magmatic evolution of the Paleozoic Acatlán Complex in southern Mexico, and its correlation with the Appalachian system: Ph.D. thesis, University of Arizona, 170 p.
- Ramos-Arias, M.A., Keppie, J.D., Ortega-Rivera, A., Lee, J.W.K., 2008. Extensional deformation on the western margin of Pangea, Patlanoaya area, Acatlán Complex, southern Mexico. Tectonophysics.

- Sánchez-Zavala, J.L., Ortega-Gutiérrez, F., Elías-Herrera, M., 2000. La orogenia Mixteca del Devónico del complejo Acatlán, sur de México. GEOS Unión Geofísica Mexicana, Boletín Informativo Época II, 20, No. 3, pp. 321–322.
- Sánchez-Zavala, J.L., Ortega-Gutiérrez, F., Keppie, J.D., Jenner, G.A., Belousova, E., Macías-Romo, C., 2004. Ordovician and Mesoproterozoic zircons from the Tecolate Formation and Esperanza granitoids, Acatlán Complex, southern Mexico: local provenance in the Acatlán and Oaxacan complexes. *International Geology Review* 46, 1005–1021.
- Solari, L.A., Keppie, J.D., Ortega-Gutiérrez, F., Cameron, K.L., Lopez, R., Hames, W.E., 2003. ~990 and ~1,100 Grenvillian tectonothermal events in the northern Oaxacan Complex, southern Mexico: roots of an orogen. *Tectonophysics* 365, 257–282.
- Talavera-Mendoza, O., Ruiz, J., Gehrels, G.E., Meza-Figueroa, D.M., Vega-Granillo, R., Campa-Uranga, M.F., 2005. U–Pb geochronology of the Acatlán Complex and implications for the Paleozoic paleogeography and tectonic evolution of southern Mexico. *Earth and Planetary Science Letters* 235, 682–699.
- Torres, R., Ruiz, J., Patchett, P.J., Grajales-Nishimura, J.M., 1999. Permo-Triassic continental arc in eastern Mexico; tectonic implications for reconstructions of southern North America. In: Bartolini, C., Wilson, J.L., Lawton, T.F. (Eds.), *Mesozoic Sedimentary and Tectonic History of North-central Mexico*. Geological Society of America Special Paper, vol. 340, pp. 191–196.
- Vega-Granillo, R., Talavera-Mendoza, O., Meza-Figueroa, D., Ruiz, J., Gehrels, G.E., López-Martínez, M., de La Cruz-Vargas, J.C., 2007. Pressure–temperature–time evolution of Paleozoic high-pressure rocks of the Acatlán Complex (southern Mexico): implications for the evolution of the Iapetus and Rheic Oceans. *Geological Society of America Bulletin* 119, 1249–1264.
- Vachard, D., Flores de Dios, A., Pantoja, J., Buitrón, B.E., Arellano, J., Grajales, M., 2000. Les fusulines du Mexique, une revue biostratigraphique et paléogéographique. *Geobios* 33, 655–679.
- Yañez, P., Ruiz, J., Patchett, J.P., Ortega-Gutiérrez, F., Gehrels, G.E., 1991. Isotopic studies of the Acatlán Complex, southern Mexico: implications for Paleozoic North American tectonics. *Geological Society of America Bulletin* 103, 817–828.

# Carboniferous tholeiitic dikes in the Salada unit, Acatlán Complex, southern Mexico: a record of extension on the western margin of Pangea

**Miguel Morales-Gámez<sup>1,2\*</sup>, J. Duncan Keppie<sup>3</sup>, and Jaroslav Dostál<sup>4</sup>**

<sup>1</sup>Posgrado en Ciencias de la Tierra, Instituto de Geología, Universidad Nacional Autónoma de México, Ciudad Universitaria, Del. Coyoacán, 04510 México D.F., Mexico.

<sup>2</sup>Present address: Instituto Tecnológico Superior de Tacámbaro, Departamento de Ingeniería Geológica, Av. Tecnológico #201, Zona El Gigante. 61650 Tacámbaro, Mich., Mexico.

<sup>3</sup>Departamento de Geología Regional, Instituto de Geología, Universidad Nacional Autónoma de México, Ciudad Universitaria, Del. Coyoacán, 04510 México D.F., Mexico.

<sup>4</sup>Department of Geology, St. Mary's University, 923 Robie Street, Halifax, Nova Scotia, Canada B3H 3C3.  
\* mgmsgz@gmail.com

## ABSTRACT

*A suite of mafic dikes intrudes polydeformed, greenschist facies, metapsammites and metapelites of the Salada unit in the eastern part of the Acatlán Complex, southern Mexico. The age of the dikes is constrained by the youngest detrital zircon in the Salada host rocks ( $352 \pm 3$  Ma) and the Early Permian age of the overlying Tecomate formation, which is devoid of such dikes. The mafic rocks are generally composed of amphibole, chlorite, feldspar, epidote and accessory opaque minerals. Their chemistry resembles rift-related tholeiites with ~50 wt.% SiO<sub>2</sub> and Mg# ~0.40–0.60. Their chondrite-normalized REE patterns resemble N-type MORB with (La/Sr)n mostly ~0.5–0.6, and their mantle-normalized patterns are relatively flat with no negative Nb anomaly and a low Th/La ratio indicating the absence of both subduction-related fluids and crustal contamination. Their chemistry resembles N-type MORB. Their intrusive relationships with the continentally-derived clastic rocks suggests that they were emplaced in thin continental crust. Shallow-water, Mississippian fauna in the adjacent Oaxaquia terrane, with Mid-Continent (USA) affinities, indicate that Pangea had already amalgamated by this time. In this context, the tholeiitic dikes are inferred to have formed during extension on the western margin of Pangea that was synchronous with extrusion of high-pressure rocks above an active subduction zone.*

*Key words:* Acatlán Complex, geochemistry, Pangea, Carboniferous, Mexico.

## RESUMEN

*Se estudia una serie de diques máficos que intruyen metapelitas y metapsamitas polideformadas de la unidad Salada y que se hallan en condiciones metamórficas de esquistos verdes. Esta unidad aflora en el sector oriental del complejo Acatlán, en el sur de México. La edad de los diques está limitada por los circones detriticos más jóvenes de las rocas de caja de la unidad Salada ( $352 \pm 3$  Ma) y por la edad del Pérmico Temprano de la formación Tecumate sobreyacente, en la cual no se ha hallado ese tipo de diques. Los diques máficos están compuestos generalmente por anfibol, clorita, feldespato, epidota y minerales opacos. Su composición geoquímica los clasifica como rocas toleíticas originadas por extensión (rift) con contenidos de silice en torno al 50% en peso y Mg# entre 40 y 60. Los espectros de tierras*

*raras normalizados a valores condriticos indican que son de tipo N-MORB con (La/Sm)m entre 0.5 y 0.6, mientras que los espectros normalizados a valores del manto son planos, no presentan anomalía de Nb y tienen una baja relación de Th/La, lo que indica la ausencia tanto de fluidos derivados de procesos de subducción como de contaminación cortical. Su similitud con rocas de tipo N-MORB y su relación de intrusión en rocas clásicas de afinidad continental sugiere que estos diques se emplazaron en una corteza continental adelgazada. La presencia de fauna misisipiense de aguas someras, con afinidad al Mid-Continent (EUA), en el colindante terreno de Oaxaquia indica que Pangea pudo estar amalgamada entonces. De esta manera, se puede inferir que los diques toleíticos se formaron debido a la extensión en el margen occidental de Pangea, que fue coetánea con la exhumación de rocas de alta presión en un ambiente de margen activa.*

*Palabras clave:* Complejo Acatlán, geoquímica, Pangea, Carbonífero, México.

## INTRODUCTION

The mafic dikes that form the topic of this paper occur in the Xayacatlán area within the eastern part of the Acatlán Complex, Mixteca terrane (Figure 1). They intrude metapsammites and metapelites that were polydeformed under greenschist facies conditions. They were previously assigned to the Cosoltepec Formation, which was interpreted as a Cambro-Ordovician accretionary prism by Ortega-Gutiérrez *et al.* (1999, and references therein). However, the presence of Devonian detrital zircons (youngest detrital zircon age of ~376 Ma or ~410 Ma youngest population) in the type Cosoltepec Formation led Talavera-Mendoza *et al.* (2005) and Vega-Granillo *et al.* (2007) to suggest that the Cosoltepec Formation was deposited as a Devonian-Carboniferous passive margin bordering Gondwana and that it was subsequently caught in the collision zone between Gondwana and Laurentia during the amalgamation of Pangea. On the other hand, Keppie *et al.* (2008a, and references therein) have proposed that the Mixteca terrane lay on the active western margin of Gondwana during the Carboniferous. In an attempt to shed light on the Late Paleozoic tectonic setting of the Mixteca terrane, we present geochemical data for some Carboniferous mafic dikes in the eastern part of the Acatlán Complex.

## GEOLOGICAL SETTING

The Acatlán Complex (Mixteca terrane) is bounded on three sides by faults and shear zones (Figure 1a): 1) along its eastern side the north-trending, Permian, dextral Caltepec fault zone separates it from the ~1 Ga Oaxacan Complex (Elias-Herrera and Ortega-Gutiérrez, 2002), which forms the basement of the Oaxacan (Oaxaquia) terrane (Keppie, 2004); 2) to the south, the east-west, Cenozoic, dextral La Venta-Chacalapa Fault (Tolson, 2007; Solari *et al.*, 2007) juxtaposes it against the Xolapa terrane; and 3) to the west, the NNE-trending, late Mesozoic-early Cenozoic, westerly-vergent Papalutla thrust places the Acatlán Complex on top

of the Cretaceous Morelos platform (Cerca *et al.*, 2007). The northern boundary of the Mixteca terrane is obscured by overlain Mesozoic-Cenozoic rocks of the Mixteca terrane cover and the Trans-Mexican Volcanic Belt (Gómez-Tuena *et al.*, 2007) (Figure 1a). The geological history of the eastern Acatlán Complex has recently been summarized by Keppie *et al.* (2008a) as follows (Figure 2):

- 1) Ordovician deposition of rift-passive margin clastic rocks and intrusion of a rift-related, bimodal suite of igneous rocks;
- 2) latest Devonian-Carboniferous, polyphase deformation attributed to rapid exhumation of the high pressure (HP) rocks that was synchronous with deposition of sedimentary rocks, including the Salada unit; Mississippian eclogite facies (HP) metamorphism and polyphase deformation;
- 3) Early Permian intrusion of arc-related plutons into periacr sedimentary rocks (including the Tecolote formation) synchronous with low grade polyphase deformation; and
- 4) Late Permian-Triassic deposition of the siliciclastic rocks (Chazumba and Magdalena units) in a foredeep in front of S-vergent thrusts; and
- 5) Jurassic migmatization associated with polyphase deformation of the Chazumba and Magdalena units.

Remapping of the Xayacatlán area has distinguished three greenschist facies, clastic units (Figure 3), from west to east (Morales-Gámez *et al.*, 2008): 1) the Ordovician Huerta unit composed of polydeformed metapsammites and metapelites; 2) the pre-450 Ma Amate unit consisting of polydeformed meta-arkoses and metapelites; and 3) the Carboniferous Salada unit made up of metapsammites and metapelites cut by mafic dikes. An older limit for the age of the mafic dikes that intrude the Salada unit is provided by the  $352 \pm 3$  Ma age of the youngest detrital zircon (Morales-Gámez *et al.*, 2008). These dikes do not occur in the overlying, Lower Permian Tecolote formation. A reconnaissance of the geochemical characteristics of mafic rocks associated with the greenschist facies clastic rocks revealed that they are predominantly tholeiitic MORB-type rocks associated with minor alkalic varieties of uncertain age (Keppie *et al.*,

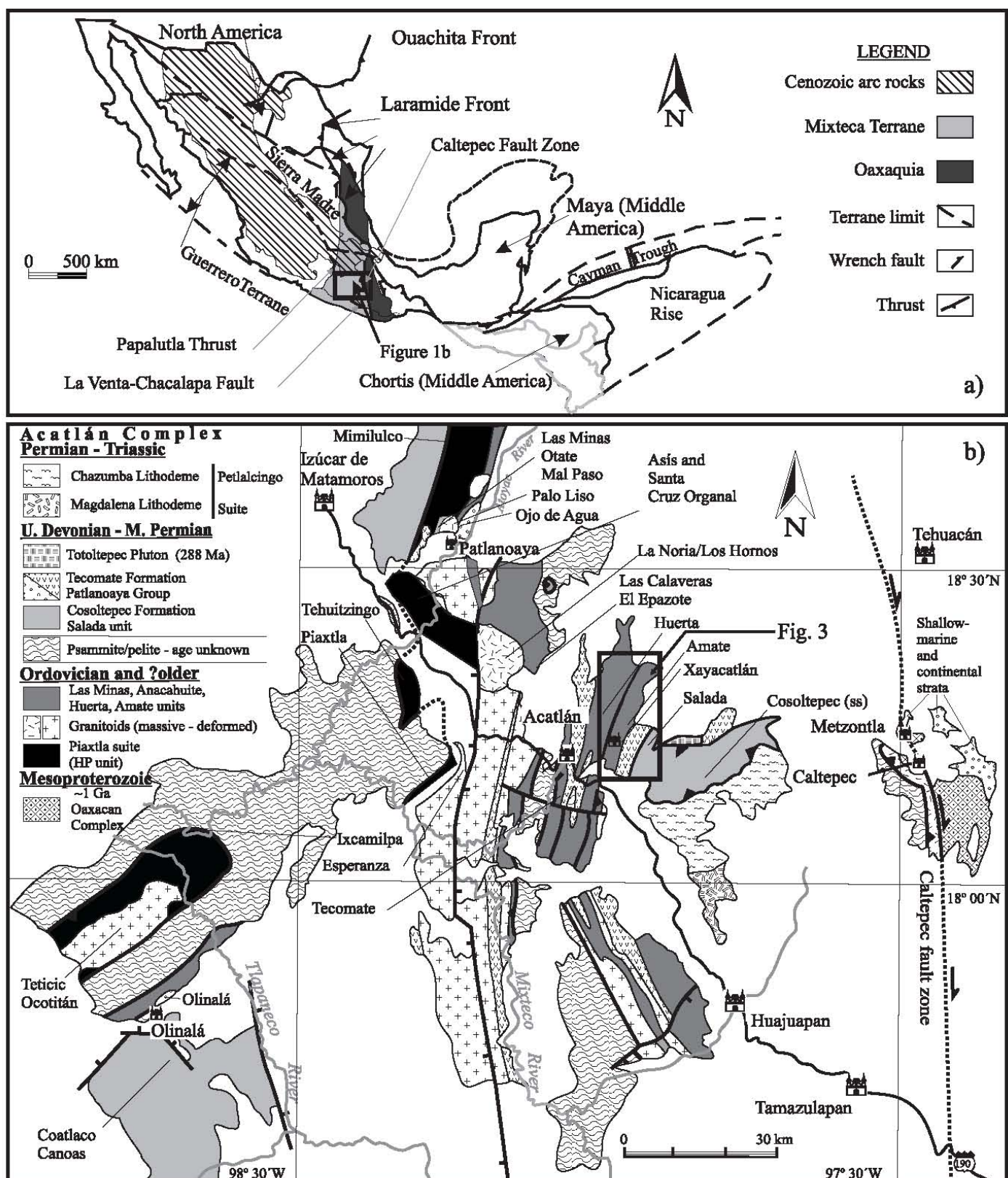


Figure 1. Location of the Xayacatlán map shown on (a) terrane map of Middle America (modified after Keppie, 2004), and (b) geological map of the Acatlán Complex (modified after Keppie *et al.*, 2008a).

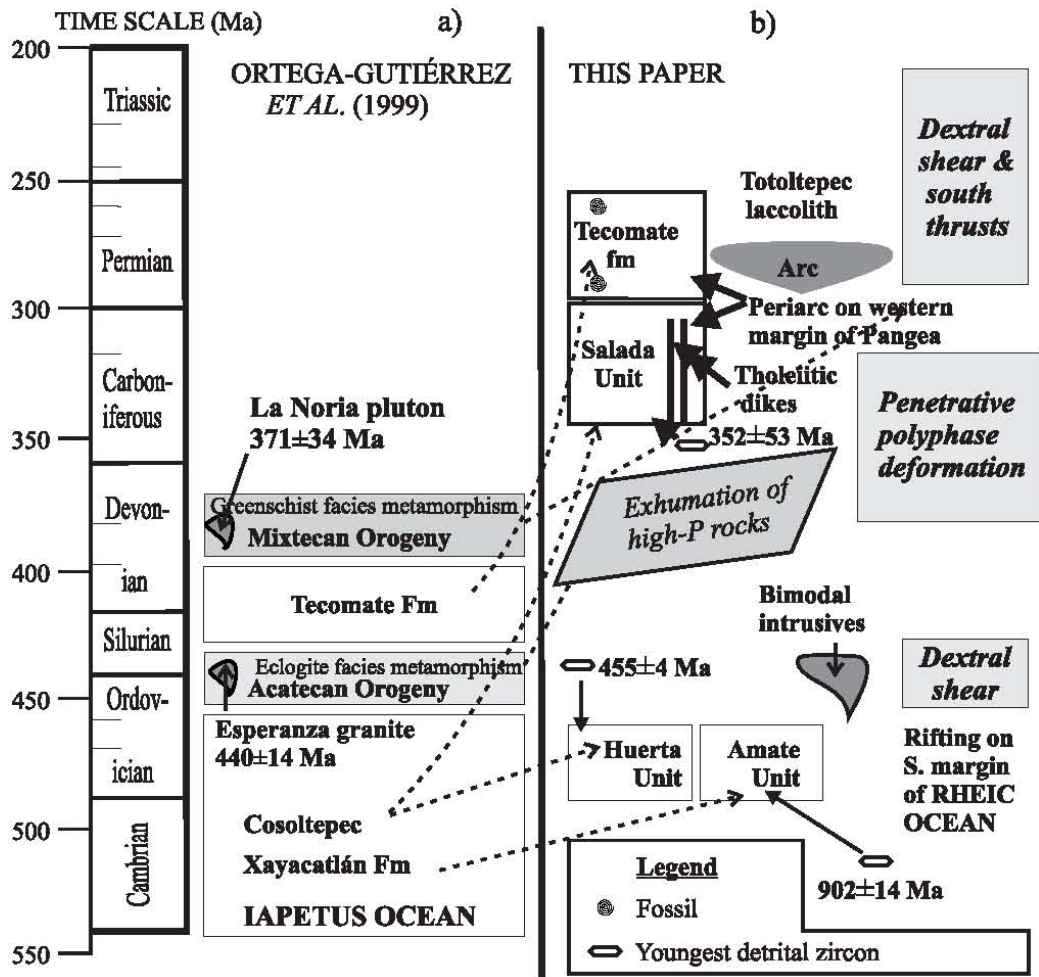


Figure 2. Time and space diagram showing the geological record of the Xayacatlán area (after Morales-Gámez *et al.*, 2008).

2007). Further research has indicated that the clastic rocks can be assigned to, at least, two different ages: Ordovician (Huerta and Amate units and correlative) and Carboniferous (Salada unit and correlative) (Keppie *et al.*, 2008a; Ramos-Arias *et al.*, 2008; Morales-Gámez *et al.*, 2008; Grodzicki *et al.*, 2008; Hinojosa-Prieto *et al.*, 2008). Mafic dikes and flows associated with the Ordovician clastic rocks appear to be continental rift tholeiites formed in a rift-passive margin environment (Keppie *et al.*, 2008b). The Carboniferous mafic pillow lavas in the western Acatlán Complex also have within-plate tholeiitic affinities (Grodzicki *et al.*, 2008). In order to determine the tectonic environment during the Carboniferous (passive or active margin), the geochemistry of mafic dikes that intrude the Salada unit was undertaken and is presented in this paper.

## PETROGRAPHY

Nine geochemical samples of the Salada Unit were collected in the northern part of the area, and one sample from the south (Figure 3). All the samples are from different NNE-trending mafic dikes and display the same structural history as the host rocks. In places, the dikes cut the bed-

ding in the host rocks. In thin section the mafic rocks are composed of amphibole, chlorite, feldspar, epidote and accessory opaque minerals. The metasedimentary rocks are made up of quartz, muscovite, chlorite and accessory opaque minerals. These mineral associations indicate metamorphism under greenschist facies conditions. The fact that the amphiboles are aligned indicates that this metamorphism was synchronous with deformation.

## GEOCHEMISTRY

Ten samples were analyzed for major and some trace elements (Rb, Sr, Ba, Ga, Zr, Y, Nb, V, Ni, Co and Cr) by X-ray fluorescence spectrometry in the Department of Earth Sciences of University of Ottawa, Canada. Eight representative samples were selected from this set for analysis of other trace elements (rare-earth elements [REE], Th, Nb, Ta, Zr and Hf) by ICP-MS at the Department of Earth Sciences, Memorial University of Newfoundland. The analytical error of the trace element determinations is 2–10 % and <2% for major elements. Where available, ICP-MS data were preferred because of their better quality at low concentration levels.

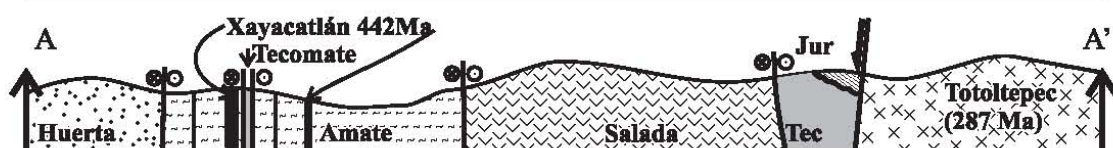
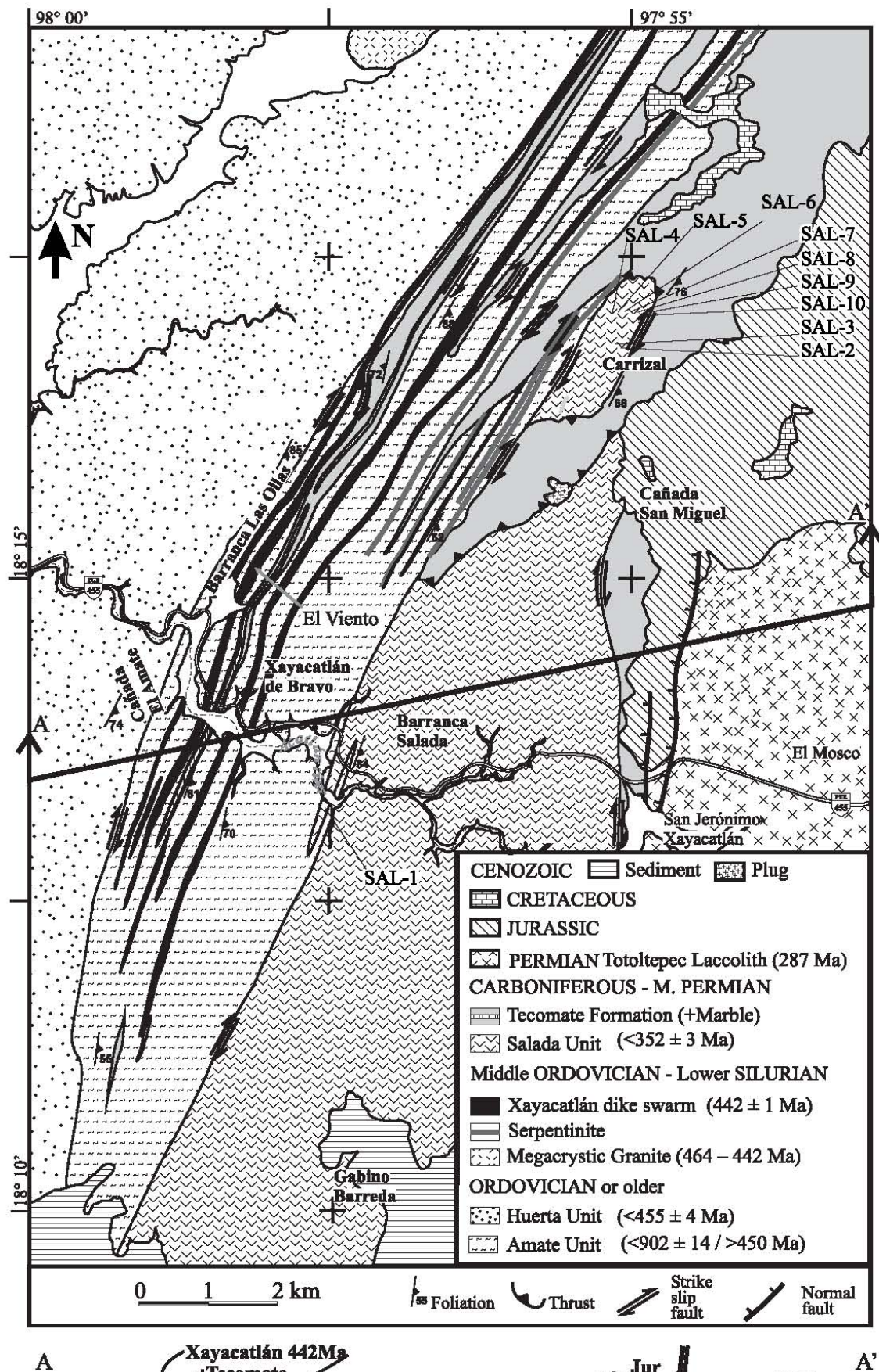


Figure 3. Geological map of the Xayacatlán area showing locations of mafic dikes sampled for geochemistry.

Table 1. Geochemical data for mafic dikes cutting the Salada unit, Acatlán Complex, southern Mexico.

Sample	SAL-1	SAL-2	SAL-3	SAL-4	SAL-5	SAL-6	SAL-7	SAL-8	SAL-9	SAL-10
Long.	97°57'39"	97°55'29"	97°55'28	97°55'11"	97°55'03"	97°55'00"	97°54'54"	97°54'51"	97°54'48"	97°54'46"
Lat.	18°13'16"	18°16'44"	18°16'44	18°17'04"	18°17'05"	18°17'06"	18°17'02"	18°17'02"	18°17'04"	18°17'05"
SiO <sub>2</sub> (wt.%)	47.66	45.39	45.34	44.93	46.28	43.67	46.50	45.27	47.44	49.21
TiO <sub>2</sub>	0.99	1.59	1.31	2.43	1.23	1.48	1.49	2.06	1.44	1.24
Al <sub>2</sub> O <sub>3</sub>	16.40	14.96	12.94	14.86	15.03	15.44	14.58	11.66	13.62	13.47
Fe <sub>2</sub> O <sub>3</sub> <sup>T</sup>	10.33	12.03	10.25	13.28	11.47	11.56	12.01	13.61	13.30	12.21
MnO	0.16	0.19	0.19	0.20	0.18	0.29	0.21	0.23	0.19	0.18
MgO	6.63	8.86	5.54	6.51	8.66	7.79	8.31	4.54	7.59	7.84
CaO	9.93	8.03	13.31	11.06	8.01	9.01	10.49	11.09	9.35	8.63
Na <sub>2</sub> O	3.07	2.64	2.89	1.13	1.80	1.78	2.03	3.16	2.75	2.77
K <sub>2</sub> O	0.02	0.10	0.25	0.04	0.17	0.39	0.14	0.13	0.08	0.19
P <sub>2</sub> O <sub>5</sub>	0.08	0.13	0.12	0.22	0.10	0.12	0.11	0.33	0.13	0.11
LOI	4.10	6.00	7.30	5.40	7.40	9.20	3.50	8.00	4.70	4.40
Total	99.37	99.92	99.44	100.06	100.32	100.73	99.37	100.08	100.59	100.25
Mg#	0.56	0.59	0.52	0.49	0.60	0.57	0.58	0.40	0.53	0.56
Cr (ppm)	234	360	167	261	221	126	244	43	170	175
Ni	98	84	78	62	122	98	99	20	90	66
Co	44	45	41	40	47	49	49	46	55	50
V	251	321	275	400	275	290	304	325	359	333
Zn	72	88	74	93	85	97	90	114	100	91
Rb	3	6	13	5	12	19	9	10	8	15
Ba	32	32	39	26	39	55	37	56	66	45
Sr	371	148	153	226	119	166	190	76	123	97
Ga	16	17	14	19	14	17	16	15	16	14
Ta	0.28	0.14	0.10	0.24	0.08	-	0.14	-	0.22	0.21
Nb	4.2	2.4	1.8	4.4	1.5	-	2.1	-	4.0	3.4
Hf	1.66	2.46	1.87	4.45	1.82	-	2.45	-	2.11	1.71
Zr	64	98	75	117	68	91	93	152	82	70
Y	17	29	24	48	22	38	29	46	25	23
Th	0.27	0.17	0.17	0.53	0.08	-	0.10	-	0.19	0.16
La	3.29	2.95	2.37	5.44	2.05	-	2.59	-	2.82	2.41
Ce	7.77	9.32	6.86	16.33	6.15	-	8.16	-	7.94	6.79
Pr	1.25	1.66	1.25	2.86	1.10	-	1.49	-	1.33	1.20
Nd	6.51	9.29	7.20	15.78	6.22	-	8.71	-	7.54	6.74
Sm	2.10	3.11	2.45	5.23	2.19	-	2.90	-	2.58	2.34
Eu	0.83	1.21	0.92	1.77	0.83	-	1.18	-	0.96	0.87
Gd	2.86	4.58	3.73	7.52	3.55	-	4.61	-	4.09	3.71
Tb	0.51	0.84	0.67	1.34	0.63	-	0.82	-	0.78	0.68
Dy	3.46	5.78	4.64	9.18	4.36	-	5.76	-	5.30	4.80
Ho	0.67	1.19	0.96	1.93	0.87	-	1.20	-	1.04	0.94
Er	2.04	3.53	2.89	5.73	2.65	-	3.48	-	3.06	2.74
Tm	0.286	0.514	0.422	0.823	0.399	-	0.502	-	0.449	0.413
Yb	1.99	3.37	2.83	5.41	2.60	-	3.29	-	3.10	2.72
Lu	0.284	0.472	0.394	0.761	0.357	-	0.452	-	0.479	0.425

Fe<sub>2</sub>O<sub>3</sub><sup>T</sup> = total Fe as Fe<sub>2</sub>O<sub>3</sub>; Mg# = Mg/(Mg+Fe<sup>T</sup>).

Analytical results for these rocks are presented in Table 1. The major and trace element compositions of these rocks are similar to those of modern volcanic rocks. This suggests that the rocks are the metamorphic equivalents of such rocks and that they retain, to a large degree, their magmatic composition. Unlike sedimentary rocks, they have high Cr/Th (>400) and low Th/La (<0.1) ratios (Rollinson, 1993), and according to a procedure of Leake (1964), they resemble metamorphosed basalts. The rocks

have a composition corresponding to subalkaline basalts (Figure 4) with SiO<sub>2</sub> (volatile-free basis) ranging between 47.5 and 51.5 wt. % and Mg# (=Mg/Mg+Fe<sub>tot</sub>) between 0.40 and 0.60, and display tholeiitic characteristics (Figure 5). According to their normative compositions, the rocks are mostly olivine-normative tholeiites. Cr and Ti abundances are typical of rift-related tholeiites (Figure 6). The chondrite-normalized REE patterns of most of the rocks show a minor depletion of light REE (Figure 7) and their patterns

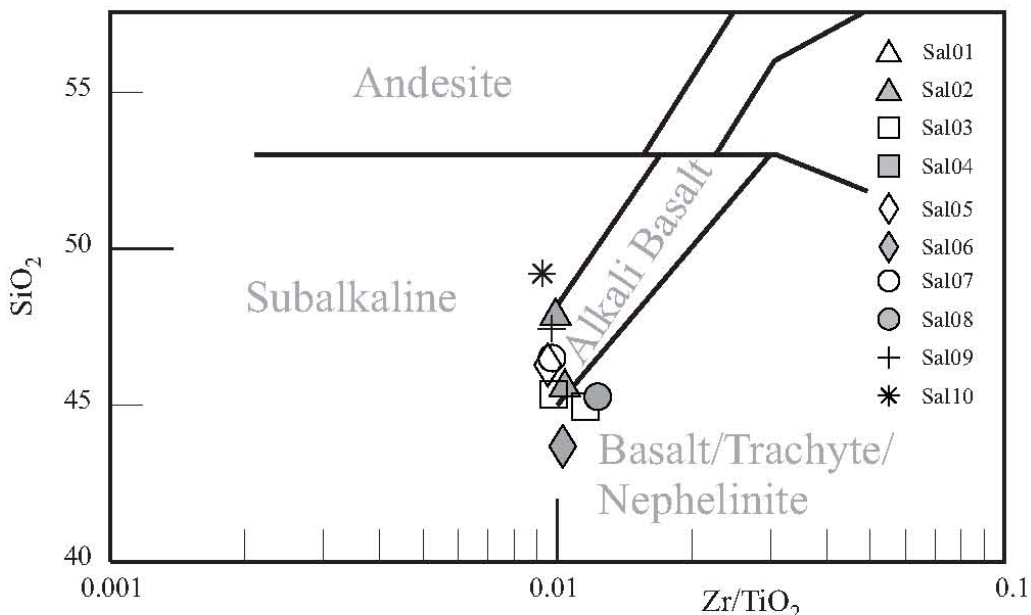


Figure 4. Geochemical data for the Salada mafic dikes plotted on the  $Zr/TiO_2$  versus  $SiO_2$  (wt.%) diagram of Winchester and Floyd (1977). Abbreviations: Sub-AB: subalkaline basalt; AB: alkaline basalt; TrAn: trachyandesite; Bas: basanite; Trach: trachyte; Neph: nepheline.

are similar to N-type MORB with  $(La/Sm)_n$  mostly  $\sim 0.5\text{--}0.6$ . The absolute concentration of REE varies slightly but the shape of the patterns remains the same: these variations are consistent with low-pressure fractional crystallization. The mantle-normalized trace element patterns of the rocks (Figure 8) are relatively flat without a Nb depletion relative to La and Th suggesting that the rocks have not been modified by subduction-related fluids and that the rocks were not significantly contaminated by crustal material. The absence of a Nb anomaly and a low Th/La ratio suggest an asthenospheric source without any suprasubduction imprint or crustal contamination. The high Ti and Cr content also rules out formation in an arc environment. The rocks resemble N-type MORB. The geochemical characteristics suggest that the rocks are either rift-related oceanic basalts or continental tholeiite emplaced in rather thin crust without significant crustal contamination: the latter is most likely as the mafic dikes intrude continentally-derived clastic rocks.

## DISCUSSION

The Carboniferous, rift-related tholeiitic dikes in the Xatacatlán area may be correlated with within-plate, rift-related tholeiitic pillow basalts interbedded with clastic metasedimentary rocks (Coatlaco unit) in the western part of the Acatlán Complex, which have yielded a  $357 \pm 35$  Ma detrital zircon age (Grodzicki *et al.*, 2008). Deposition of the Salada and Coatlaco units was also contemporaneous with deposition of the Patlanoaya Group, which, in turn, was synchronous with exhumation and deformation of high-pressure rocks (Ramos-Arias *et al.*, 2008), and the earliest

deformation of the Salada unit (Morales-Gámez *et al.*, in press). This deformation has been related to extrusion of the high-pressure rocks into the upper plate above an active subduction zone (Keppie *et al.*, 2008a).

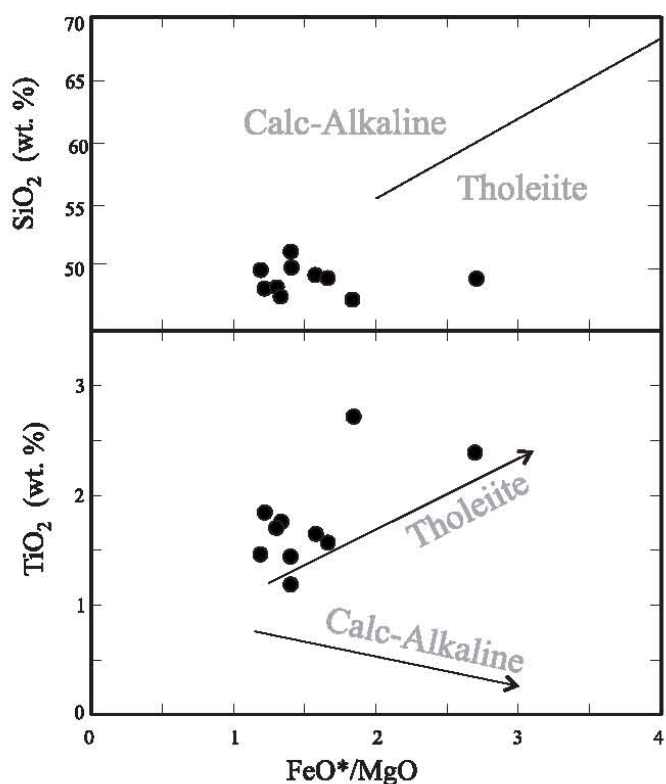


Figure 5. (a)  $FeO^*/MgO$  versus  $TiO_2$  (wt%) and (b)  $FeO^*/MgO$  versus  $SiO_2$  for Salada dikes. The lines showing calc-alkaline and tholeiitic trends are after Miyashiro (1974).  $FeO^*$  = total Fe as  $FeO$ .

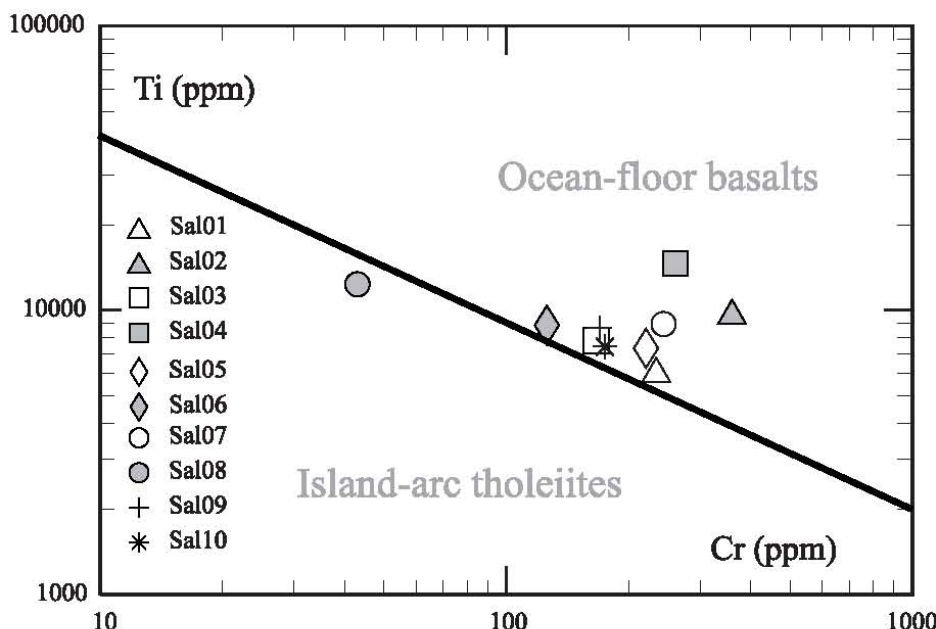


Figure 6. Geochemical data for the Salada mafic dikes plotted on the Cr (ppm) versus Ti (ppm) diagram of Pearce (1975) showing the compositional fields for island arc tholeiites and within-plate basalts (including mid-ocean ridge basalts).

Talavera-Mendoza *et al.* (2005) and Vega-Granillo *et al.* (2007) place the Mixteca terrane in the collisional suture zone between southern Laurentia and Gondwana (Figure 9a). That this collision had already taken place by the Mississippian is suggested by the presence of shallow water Mid-Continent (USA) fauna in the Santiago Formation that lies above the ~1 Ga Oaxacan Complex in the adjacent Oaxaquia terrane (Navarro-Santillan *et al.*, 2002). Although the presence of Carboniferous, within-plate, rift-related tholeiites could be explained by gravitational collapse of a collisional orogen, it is inconsistent with paleomagnetic data, which indicate that, in the Permian, the Mixteca terrane lay roughly at its present position relative to Laurentia (Alva-Valdivia *et al.*, 2002). The latter position places the Mixteca terrane on the Pacific margin of Pangea (Figure 9b). On the other hand, Carboniferous rift-related tholeiites synchronous with deformation, and extrusion of high-pressure rocks in an active margin setting, is more consistent with a location along the western margin of Pangea, well south of the Laurentia-Gondwana suture zone (Figure 9b) (Elias-Herrera and Ortega-Gutiérrez, 2002; Keppie *et al.*, 2008a).

## ACKNOWLEDGMENTS

We would like to acknowledge a PAPIIT grant (IN100108-3) and a CONACyT grant (CB-2005-1: 24894) to JDK and a NSERC discovery grant to JDS that facilitated the fieldwork and chemical analyses. CONACyT contributed to studies for MMG. We are grateful to Dr. J.B. Murphy for detailed reviews that have allowed for improvement of the manuscript.

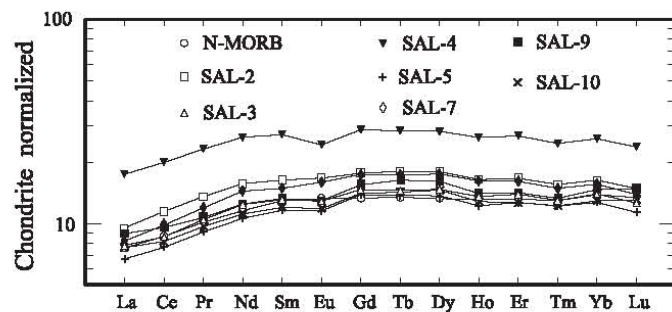


Figure 7. Chondrite-normalized REE abundances in the Salada mafic dikes and N-type MORB of Sun and McDonough (1989). Normalizing values are after Sun and McDonough (1989).

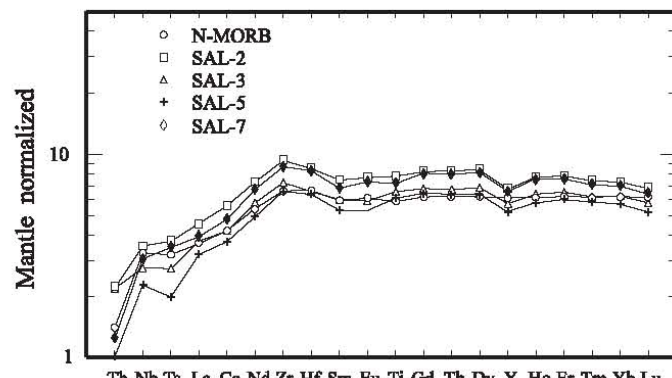


Figure 8. Geochemical data for the Salada mafic dikes and N-type MORB plotted on the mantle-normalized trace element diagram (Sun and McDonough, 1989). Normalizing values after Sun and McDonough (1989).

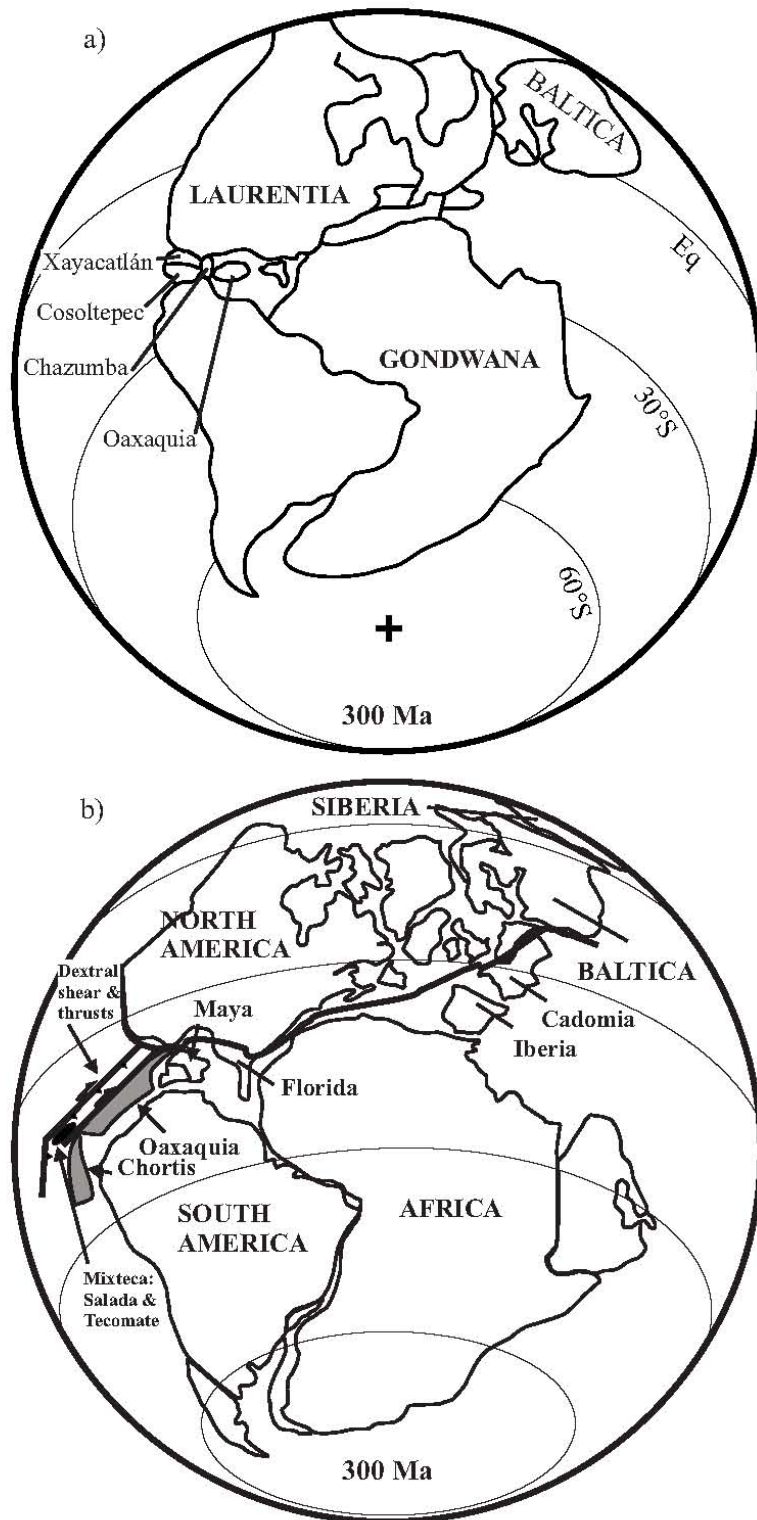


Figure 9. Permo-Carboniferous reconstructions: (a) after Talavera-Mendoza *et al.* (2005) and Vega-Granillo *et al.* (2007), and (b) modified from Keppie *et al.* (2008a).

## REFERENCES

- Alva-Valdivia, L.M., Goguitchaichvili, A., Grajales, M., Flores de Dios, A., Urrutia-Fucugauchi, J., Rosales C., Morales, J., 2002, Further constraints for Permo-Carboniferous magnetostratigraphy: case study of the sedimentary sequence from San Salvador-Patlanoaya (Mexico): Compte Rendus Geoscience, 334, 1-7.
- Cerca, M., Ferrari, L., Lopez, M., Martiny, B., Iriondo, A., 2007, Late Cretaceous shortening and early Tertiary shearing in the central Sierra Madre del Sur, southern Mexico: Insights into the evolution of the Caribbean-North American plate interaction: Tectonics, 26, TC3007, doi:10.1029/2006TC001981.
- Elías-Herrera, M., Ortega-Gutiérrez, F., 2002, Caltepec fault zone: an Early Permian dextral transpressional boundary between the Proterozoic

- Oaxacan and Paleozoic Acatlán complexes, southern Mexico, and regional implications: *Tectonics*, 21(3), 10.1029/200TC001278.
- Gómez-Tuena, A., Langmuir, C.H., Goldstein, S.L., Straub, S.M., Ortega-Gutiérrez, F., 2007, Geochemical evidence for slab-melting in the Trans-Mexican Volcanic Belt: *Journal of Petrology*, 48(3), 537–562.
- Grodzicki, K.R., Nance, J.D., Keppie, J.D., Dostal, J., Murphy, J.B., 2008, Structural, geochemical and geochronological analysis of metasedimentary and metavolcanic rocks of the Coatlaço area, Acatlán Complex, southern Mexico: *Tectonophysics*. doi:10.1016/j.tecto.2008.01.016.
- Hinojosa-Prieto, H.R., Nance, R.D., Keppie, J.D., Dostal, J.V., Ortega-Rivera, A., Lee, J.K.W., 2008, Ordovician and Late Paleozoic-Early Mesozoic tectonothermal history of the La Noria area, northern Acatlán Complex, southern Mexico: Record of convergence in the Rheic and paleo-Pacific Oceans: *Tectonophysics*. doi: 10.1016/j.tecto.2008.06.002
- Keppie, J.D., 2004, Terranes of Mexico revisited: a 1.3 billion year odyssey: *International Geology Review*, 46, 765–794.
- Keppie, J.D., Dostal, J., and Elias-Herrera, M., 2007, Ordovician-Devonian oceanic basalts in the Cosoltepec Formation, Acatlán Complex, Mixteca terrane, southern Mexico: vestiges of the Rheic Ocean, in Linnemann, U., Kraft, P., Nance, R.D., Zulauf, G. (eds.), *The Geology of Peri-Gondwana*: Geological Society of America, Special Paper 423, 477-487.
- Keppie, J.D., Dostal, J., Murphy, J.B., Nance, R.D., 2008a, Synthesis and tectonic interpretation of the westernmost Paleozoic Variscan orogen in southern Mexico: from rifted Rheic margin to active Pacific margin: *Tectonophysics*, doi:10.1016/j.tecto.2008.01.012.
- Keppie, J.D., Dostal, J., Miller, B.V., Ramos-Arias, M.A., Morales-Gámez, M., Nance, R.D., Murphy, J.B., Ortega-Rivera, A., Lee, J.W.K., Housh, T., Cooper, P., 2008b, Ordovician-earliest Silurian rift tholeiites in the Acatlán Complex, southern Mexico: evidence of rifting on the southern margin of the Rheic Ocean: *Tectonophysics*, doi:10.1016/j.tecto.2008.01.010.
- Leake, B.E., 1964, The chemical distinction between ortho- and para-amphibolites: *Journal of Petrology*, 5, 238–254.
- Miyashiro, A., 1974, Volcanic rock series in island arcs and active continental margins: *American Journal of Science*, 274, 321–355.
- Morales-Gámez, M., Keppie, J. D., Norman, M., 2008, Ordovician-Silurian rift-passive margin on the Mexican margin of the Rheic Ocean overlain by Permian periarc rocks: evidence from the Acatlán Complex, southern Mexico: *Tectonophysics*. doi:10.1016/j.tecto.2008.01.014.
- Morales-Gámez, M., Keppie, J.D., Ortega-Rivera, A., Lee, J.W.K., in press, Paleozoic structures in the Xayacatlán area, Acatlán Complex, southern Mexico: transtensional rift- and subduction-related deformation along the margin of Oaxaquia: *International Geology Review*.
- Navarro-Santillan, D., Sour-Tovar, F., Centeno-García E., 2002, Lower Mississippian (Osagean) brachiopods from the Santiago Formation, Oaxaca, Mexico: stratigraphic and tectonic implications: *Journal of South American Earth Sciences*, 15(3), 327-336.
- Ortega-Gutiérrez, F., Elías-Herrera, M., Reyes-Salas, M., Macías-Romo, C., López, R., 1999, Late Ordovician-Early Silurian continental collision orogeny in southern Mexico and its bearing on Gondwana-Laurentia connections: *Geology*, 27, 719-722.
- Pearce, J. A., 1975, Basalt geochemistry used to investigate past tectonic settings on Cyprus: *Tectonophysics*, 25, 41-67.
- Ramos-Arias, M.A., Keppie, J.D., Ortega-Rivera, A., Lee, J.W.K., 2008, Extensional late Paleozoic deformation on the western margin of Pangea, Patlanoaya area, Acatlán Complex, southern Mexico: *Tectonophysics*, 448, 60-78.
- Rollinson, H. R., 1993, *Using Geochemical Data: Evaluation, Presentation, Interpretation*: Longman, UK, 352 p.
- Solari, L. A., Torres-de León, R., Hernández-Pineda, G., Solé, J., Solís-Pichardo, G., Hernández-Treviño, T., 2007, Tectonic significance of Cretaceous-Tertiary magmatic and structural evolution of the northern margin of the Xolapa Complex, Tierra Colorada area, southern Mexico: *Geological Society of America Bulletin*, 119, 1265–1279.
- Sun, S. S., McDonough, W.F., 1989, Chemical and isotopic systematics of oceanic basalts: implications for mantle composition and processes, in Saunders, A.D., Norry, M.J. (eds.), *Magmatism in the Ocean Basins*: Geological Society of London, Special Publication 42, 313-345.
- Talavera-Mendoza, O., Ruiz, J., Gehrels, G. E., Meza-Figueroa, D.M., Vega-Granillo, R., Campa-Uranga, M. F., 2005, U-Pb geochronology of the Acatlán Complex and implications for the Paleozoic paleogeography and tectonic evolution of southern Mexico: *Earth and Planetary Science Letters*, 235, 682-699.
- Tolson, G., 2007, The Chacalapa fault, southern Oaxaca, Mexico, in Alaniz-Álvarez, S.A., Nieto-Samaniego, Á.F. (eds.), *Geology of Mexico: Celebrating the Centenary of the Geological Society of Mexico*: Geological Society of America, Special Paper 422, 343-357, doi: 10.1130/2007.2422(12).
- Vega-Granillo, R., Talavera-Mendoza, O., Meza-Figueroa, D., Ruiz, J., Gehrels, G.E., López-Martínez, M., de la Cruz-Vargas, J.C., 2007, Pressure-temperature-time evolution of Paleozoic high-pressure rocks of the Acatlán Complex (southern Mexico): implications for the evolution of the Iapetus and Rheic Oceans: *Geological Society of America Bulletin*, 119, 1249-1264.
- Winchester, J.A., Floyd, P.A., 1977, Geochemical discrimination of different magma series and their differentiation products using immobile elements: *Chemical Geology*, 20, 325-343.

Manuscript received: July 31, 2008

Corrected manuscript received: September 16, 2008

Manuscript accepted: October 20, 2008

## Palaeozoic structures in the Xayacatlán area, Acatlán Complex, southern Mexico: transtensional rift- and subduction-related deformation along the margin of Oaxaquia

Miguel Morales-Gamez<sup>a</sup>, J. Duncan Keppie<sup>a\*</sup>, James K. W. Lee<sup>b</sup> and Amabel Ortega-Rivera<sup>c</sup>

<sup>a</sup>Departamento de Geología Regional, Instituto de Geología, Universidad Nacional Autónoma de México, CP 04510 México; <sup>b</sup>Department of Geological Sciences and Geological Engineering, Queens University, Kingston, Ontario, K7L3N6, Canada;

<sup>c</sup>Instituto de Geología, Universidad Nacional Autónoma de México, Estación Regional del Noroeste, Apartado Postal 1039, Hermosillo, Sonora 83000, México

(Accepted 13 December 2008)

The Xayacatlán area (eastern Mixteca terrane, southern Mexico) was previously inferred to preserve the Ordovician-Silurian thrust contact between vestiges of the Iapetus Ocean and the para-autochthon bordering Oaxaquia. Detailed remapping indicates that the rocks occur in four vertically-bounded, NS fault blocks. The latter record the following tectonothermal events that post-date Iapetus and occurred along the margins of the Rheic (1) and Pacific (2 and 3) oceans: (1) dextral transtension accompanying intrusion of an NS, tholeiitic dike swarm at ~442 Ma; (2) penetrative, greenschist-facies deformation during the Mississippian related to extrusion of high-pressure rocks; and (3) subgreenschist-facies dextral transtension on NS faults during the generation of Middle Permian fabrics.

**Keywords:** Mexico; structure; geochronology; Acatlán Complex; Oaxaquia

### Introduction

The Xayacatlán area lies in the eastern part of the Acatlán Complex of southern Mexico (Figure 1(a)). It is critical for palaeogeographic reconstructions because it was the type area for the Xayacatlán formation and was inferred to have undergone eclogite facies metamorphism during the Late Ordovician–Early Silurian Acatecan Orogeny produced by closure of the Iapetus Ocean between eastern Laurentia and Oaxaquia (Ortega-Gutiérrez 1975; Ortega-Gutiérrez *et al.* 1999). On the other hand, Keppie and Ramos (1999) proposed that the Acatlán Complex was deposited in the Ordovician-Carboniferous Rheic Ocean, which closed during the amalgamation of Pangea. The latter proposal appeared to have been confirmed by more recent geochronological data that indicated a Mississippian age for the high-pressure metamorphism (Middleton *et al.* 2007; Nance *et al.* 2007). On the other hand, Talavera-Mendoza *et al.* (2005) and Vega-Granillo *et al.* (2007) suggested that the high-pressure rocks formed during three lower Palaeozoic events and detrital zircon data led them to infer that various units of the Acatlán Complex originated in

\*Corresponding author. Email: [duncan@servidor.unam.mx](mailto:duncan@servidor.unam.mx)

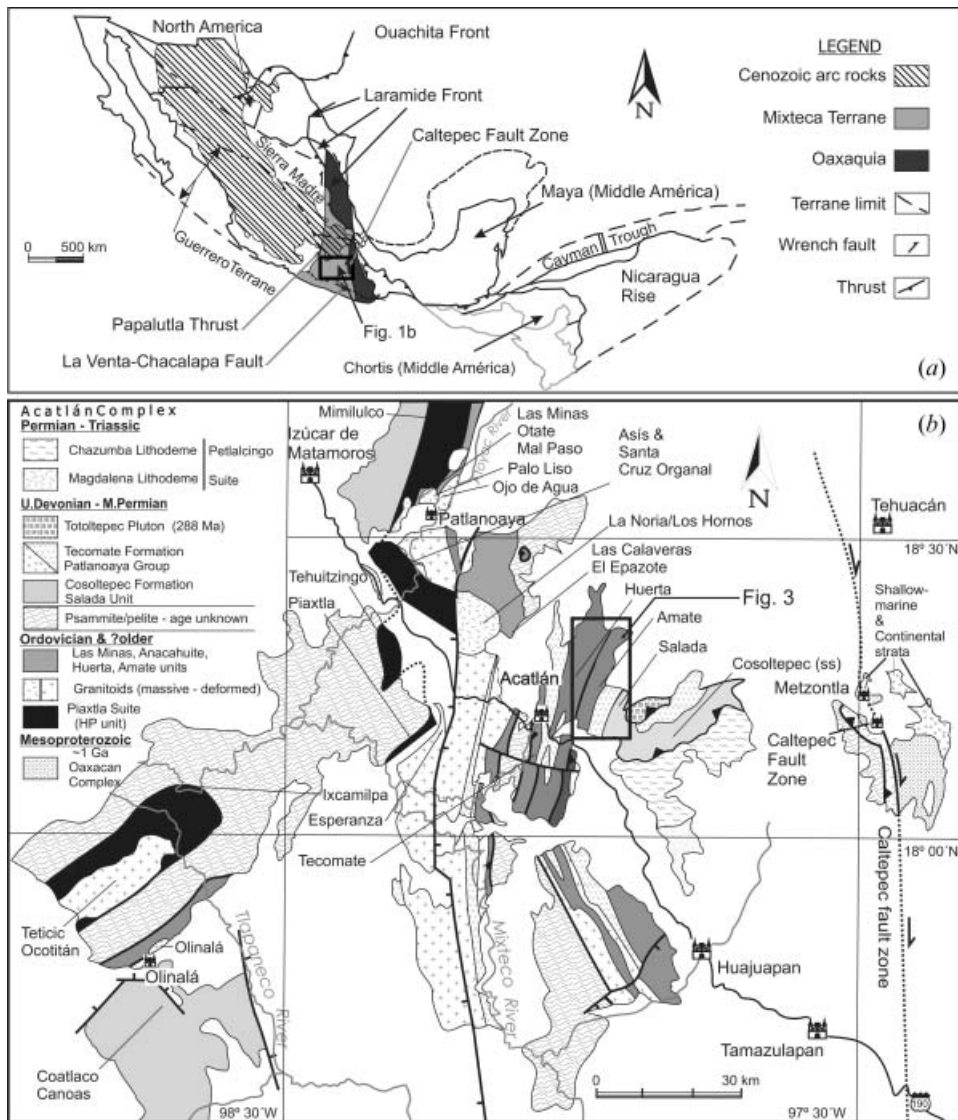


Figure 1. Location of the Xayacatlán map shown on (a) terrane map of Middle America (modified after Keppie 2004), and (b) geological map of the Acatlán Complex (modified after Keppie *et al.* 2008a).

different oceans, for example, the Xayacatlán formation formed in the Iapetus Ocean and associated marginal basins, whereas the Cosoltepec formation originated in the Rheic Ocean. Recently, Keppie *et al.* (2008a) have proposed that whereas the lower Palaeozoic units originated in the Rheic Ocean, the late Palaeozoic record relates to the palaeo-Pacific margin of Pangea. Thus, the age of tectonothermal events and palaeogeography of the Acatlán Complex are currently the subject of considerable debate (Nance *et al.* 2006; Talavera-Mendoza *et al.* 2006). In view of this discussion, a re-examination of the type area of the Xayacatlán formation was essential, the first results of which were presented in Morales-Gámez *et al.* (2008) where the age constraints on the deposition of the various units were presented. This

paper describes the three tectonothermal events that affected the area: (1) ca. 440 Ma transtensional structures found only in rift-related dikes; (2) regional Mississippian structures contemporaneous with extrusion of high-pressure rocks; and (3) Permian transtensional structures. The events are then placed in a palaeogeographic context.

### Acatlán Complex

The Acatlán Complex (Mixteca terrane) is bounded on three sides by faults and shear zones (Figure 1(b)): (1) along its eastern side, the north-trending, Permian, dextral Caltepec fault zone separates it from the ~1 Ga Oaxacan Complex (Elías-Herrera and Ortega-Gutiérrez 2002), which forms the basement of the Oaxacan (Oaxacaqua) terrane (Keppie 2004); (2) to the south, the east-west, Cenozoic, dextral La Venta-Chacalapa Fault (Tolson 2007; Solari *et al.* 2007) juxtaposes it against the Xolapa terrane; and (3) to the west, the NNE-trending, late Mesozoic-early Cenozoic, westerly-vergent Papalutla thrust places the Acatlán Complex on top of the Cretaceous Morelos platform (Cerca *et al.* 2007). The northern boundary of the Mixteca terrane is obscured by Mesozoic-Cenozoic rocks of the Trans-Mexican Volcanic Belt (Gómez-Tuena *et al.* 2007; Figure 1(a)). One group of researchers infers the following geological history for the Acatlán Complex (Figure 2, left hand side): (1) Cambro-Ordovician deposition of the siliciclastic Petlalcingo Group (Magdalena, Chazumba and Cosoltepec formations: Ortega-Gutiérrez *et al.* 1999) and the oceanic Xayacatlán formation [renamed the Piaxtla Group or Suite by

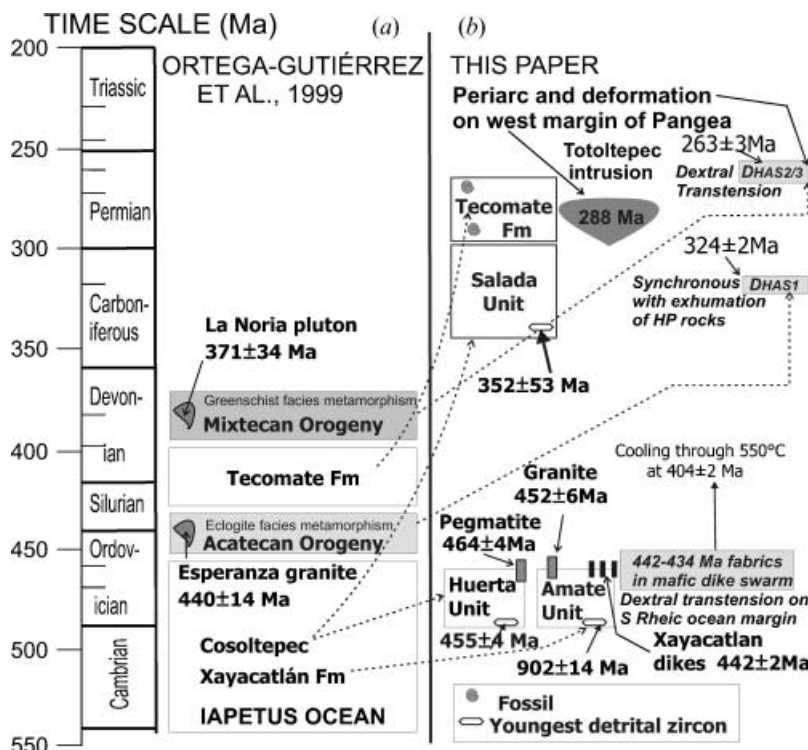


Figure 2. Time-and-Space diagram showing geological record of the Xayacatlán area: (a) after Ortega-Gutiérrez *et al.* (1999); (b) this paper.

Ramírez-Espinosa (2001) and Middleton *et al.* (2007)]; (2) Late Ordovician-Silurian, eclogite facies metamorphism, polyphase deformation and emplacement of the Piaxtla Suite over the greenschist facies Petlalcingo Group during the Acatecan Orogeny (Ortega-Gutiérrez *et al.* 1999), or Taconian-Salinian orogenies (Talavera-Mendoza *et al.* 2005; Vega-Granillo *et al.* 2007): decompression melting is inferred to have produced the megacrystic Esperanza granitoids (Ortega-Gutiérrez *et al.* 1999); (3) Siluro-Devonian deposition of the Tecolate Formation (Ortega-Gutiérrez *et al.* 1999); and (4) deformation and greenschist facies metamorphism during the Late Devonian Mixtecan Orogeny (Ortega-Gutiérrez *et al.* 1999; Sánchez-Zavala *et al.* 2000).

However, recent studies (Malone *et al.* 2002; Keppie *et al.* 2004a, b, 2006, 2008a, b; Murphy *et al.* 2006; Nance *et al.* 2006, 2007; Miller *et al.* 2007; Middleton *et al.* 2007; Morales-Gámez *et al.* 2008; Ramos-Arias *et al.* 2008) have led to a different viewpoint of the geological history (Figure 2: right hand side): (1) Ordovician deposition of rift-passive margin clastic rocks and intrusion of a rift-related, bimodal suite of igneous rocks; (2) latest Devonian-Carboniferous deposition of sedimentary rocks that was broadly synchronous with eclogite facies (HP) metamorphism and polyphase deformation attributed to rapid extrusion of the HP rocks during the Mississippian; (3) Early Permian intrusion of arc-related plutons into periarc sedimentary rocks (including the Tecolate formation) synchronous with low grade polyphase deformation; (4) Late Permian-Triassic deposition of the siliciclastic rocks (Chazumba and Magdalena units) in a foredeep in front of S-vergent thrusts; and (5) Jurassic migmatization associated with polyphase deformation of the Chazumba and Magdalena units.

### Xayacatlán area

Re-examination of the Xayacatlán area has documented the presence of several fault blocks bounded by N–S, vertical faults (Morales-Gámez *et al.* 2008). From west to east these are (Figure 3): (1) the Tizac block, bounded on the east by the Las Ollas fault, in which the Huerta Unit is exposed; (2) the Bravo block, bounded by the Las Ollas and Carrizal faults, where the Amate Unit cut by the Xayacatlán dikes and several thin fault slices of Tecolate formation are exposed; (3) the Estaca block, bounded by the Carrizal and San Jerónimo faults, that contains the Salada Unit over which the Tecolate formation has been thrust; and (4) the Tonahuixtla block, bounded on its west by the San Jerónimo fault, in which the Tecolate formation and Totoltepec intrusion crop out.

The Huerta Unit consists of metapsammites and metapelites polydeformed under greenschist facies metamorphic conditions. This unit was previously assigned to the Cosaltepec Formation (Ortega-Gutiérrez *et al.* 1999; Ramírez-Espinosa 2001), however, cursory re-examination of the type area reveals distinct lithologies and grade of metamorphism. The Huerta Unit is composed of quartz, muscovite, and chlorite with accessory zircons and pyrite, and is cut by numerous quartz veins in the west and pegmatite veins in the east composed of quartz and plagioclase, muscovite and accessory zircon. The youngest detrital zircon from a metapsammite from the western part of the unit has an age of  $455 \pm 4$  Ma with peak populations at ca. 600 Ma and ca. 1–1.2 Ga (Keppie *et al.* 2006). On the other hand, igneous zircons from an intrusive pegmatite in the eastern part of the unit yielded  $464 \pm 4$  Ma age (Morales-Gámez *et al.* 2008). The apparent contradiction between the two age constraints suggests that deposition in the

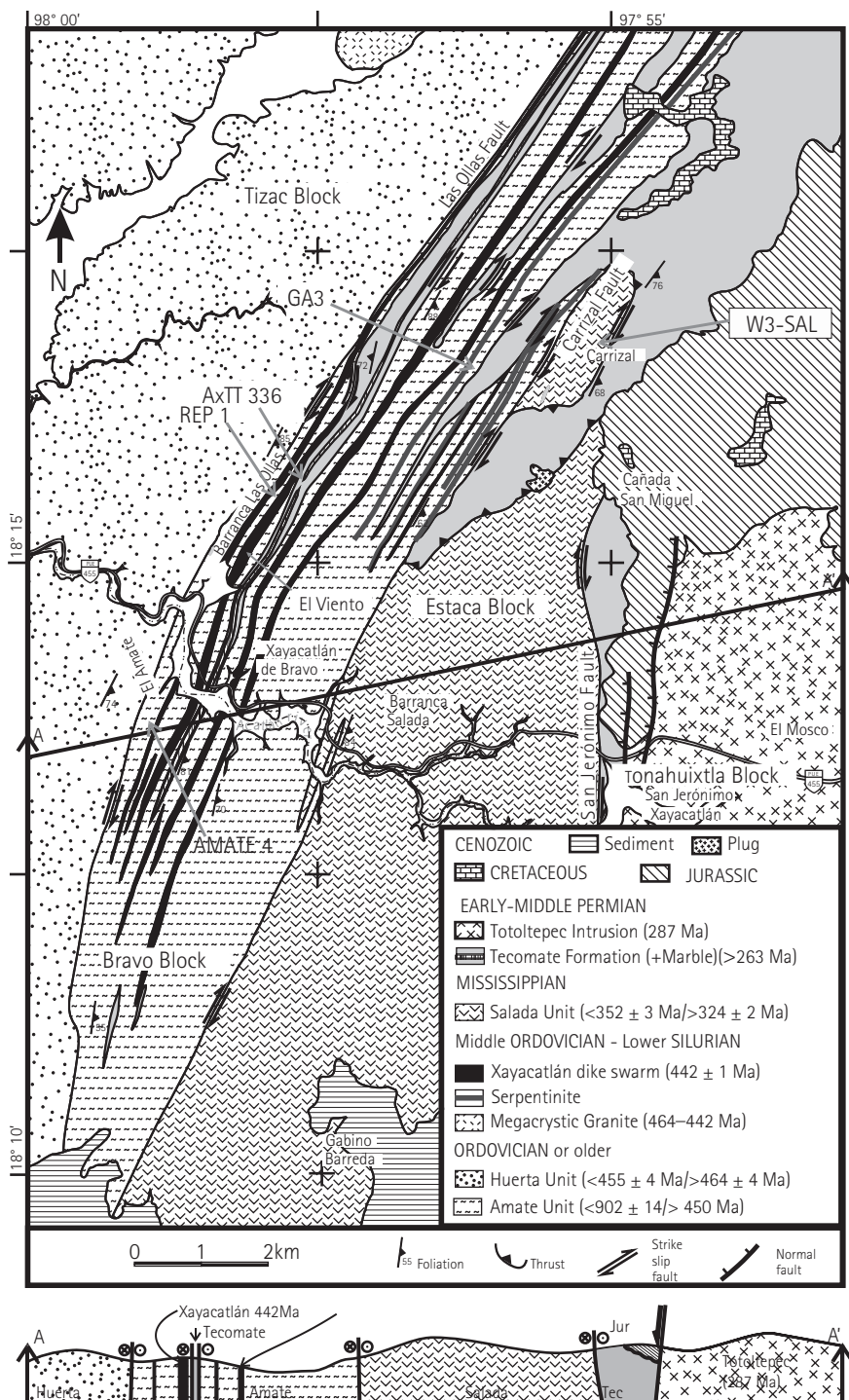


Figure 3. Geological map of the Xayacatlán area showing lower hemisphere stereoplots of structural data and the location of subsequent figures and samples dated by  $^{40}\text{Ar}/^{39}\text{Ar}$  geochronology.

west continued after intrusion of the dated pegmatite. Thus deposition of the Huerta Unit appears to be Ordovician.

The Amate Unit is composed of mainly of meta-arkoses with minor metapelites, containing quartz, plagioclase, hornblende, muscovite, chlorite and accessory zircon and opaque minerals. The metamorphic grade is generally greenschist facies, although adjacent to the thicker mafic dikes the contact metamorphism rises into the amphibolite facies. Deposition of the unit is constrained between the youngest detrital zircon age of  $902 \pm 14$  Ma and cross-cutting granitic dikes dated at  $452 \pm 6$  Ma and  $444 \pm 3$  Ma (LA-ICPMS U-Pb zircon  $^{206}\text{Pb}/^{238}\text{U}$  ages: Morales-Gámez *et al.* 2008). The N-trending mafic dikes range from thick metagabbros through amphibolites to thin sheared and serpentized bodies. The metagabbros consist principally of amphibole and plagioclase showing various degrees of alteration to chlorite and epidote. The amphibolites are fine grained and composed mainly of hornblende and epidote. Pegmatites cut the mafic dikes and are made up of quartz, K-feldspar, and plagioclase variably altered to sericite. A U-Pb, TIMS, concordant zircon age from igneous zircons in the thickest gabbroic dike yielded an age of  $442 \pm 1$  Ma (Keppie *et al.* 2008b). On the other hand, amphibole from a fine grained mafic dike that cuts across the gabbro yielded an  $^{40}\text{Ar}/^{39}\text{Ar}$  plateau age of  $434 \pm 3$  Ma indicating rapid cooling through  $570 \pm 10^\circ\text{C}$  (Keppie *et al.* 2008b).

The Salada Unit is made up of metapsammites and metapelites cut by mafic dikes, all of which are polydeformed and metamorphosed under greenschist facies conditions. The metasedimentary rocks of this unit consists of quartz, muscovite, plagioclase, chlorite, and accessory zircon, epidote and opaque minerals. The youngest concordant detrital zircon yielded a  $^{206}\text{Pb}/^{238}\text{U}$  age of  $352 \pm 3$  Ma and older concordant ages of ca. 434–485 Ma, 511–630 Ma, and 920–1200 Ma (Morales-Gámez *et al.* 2008). This unit was also previously placed within the Cosoltepec Formation (Ortega-Gutiérrez *et al.* 1999; Ramírez-Espinosa 2001), however, it is lithologically and metamorphically distinct.

The Tecomate formation consists of intercalated metapsammites, metapelites, conglomerates, and marble that were polydeformed under lower greenschist facies. In the northern part of the Carrizal block, the Tecomate formation has been thrust over the Salada Unit, whereas in the Bravo block thin fault slices have been sheared into the Amate Unit (Figure 3). The clastic rocks of the Tecomate formation are composed mainly of quartz, muscovite, chlorite and accessory zircon and opaque minerals. Clasts in the conglomerate include granitoids, volcanics, metapsammites, marble and quartz veins. Granitoid pebbles from a metaconglomerate south of the Totoltepec intrusion yielded an age of ca. 290 Ma suggesting derivation from the ca. 288 Ma Totoltepec intrusion (Yañez *et al.* 1991; Keppie *et al.* 2004b). The marble is composed predominantly of calcite with a few quartz crystals. No fossils were recovered from the marbles of the Tecmorate formation in the study area, so their age is inferred by correlation with the type area where latest Pennsylvanian-Early Permian fusilinids have been reported (Keppie *et al.* 2004b).

The Totoltepec intrusion ranges in composition from gabbro (hornblende, plagioclase, epidote, and chlorite) to granite (quartz, K-feldspar, muscovite, plagioclase altered to sericite). Ages obtained from mafic and felsic members of the intrusion yielded zircon ages of ca. 289 Ma (Yañez *et al.* 1991; Keppie *et al.* 2004b). Fabrics in the intrusion have been interpreted in terms of syntectonic intrusion (Malone *et al.* 2002). The intrusion has a calcalkaline geochemistry

suggesting that it forms part of the Permian arc that runs N–S along the backbone of Mexico (Malone *et al.* 2002).

Mesozoic rocks unconformably overlie various units of the Acatlán Complex in the study area (Figure 3). They consist of red conglomerates and sandstones containing Jurassic plant remains (Malone *et al.* 2002) overlain by Cretaceous marine platform limestone. Cenozoic rocks unconformably overlie the Acatlán Complex in the southern part of the study area where they are composed of volcanosedimentary successions. Plugs of presumed Cenozoic age intrude the Salada Unit and Tecomate Formation.

## Structure

The fabrics in the various units are described below using standard abbreviations for the planar and linear structures in each unit. Subscripts use the first letter of the unit followed by a number indicating its place in the sequence of structures, viz  $S_{A2}$  = a planar structure in the Amate Unit attributed to the second set of structures.

### Fabrics in and adjacent to the ca. 442 Ma Xayacatlán mafic dikes ( $S_A$ , $L_X$ and $F_X$ )

The mafic Xayacatlán dikes exhibit amphibolite facies polyphase deformation overprinted by greenschist facies fabrics. In central parts of the thickest gabbro dike (100 m thick), a compositional banding ranging in composition from ultramafic through gabbroic and leucogabbroic to anorthositic is inferred to represent original igneous banding (Keppie *et al.* 2008b). However polyphase deformation is encountered in the margins of this dike. This is most clearly displayed at El Viento on the eastern margin where a N15°E, steeply dipping, mylonitic banding consisting of aligned amphibole is deformed by steeply plunging, asymmetric Z-

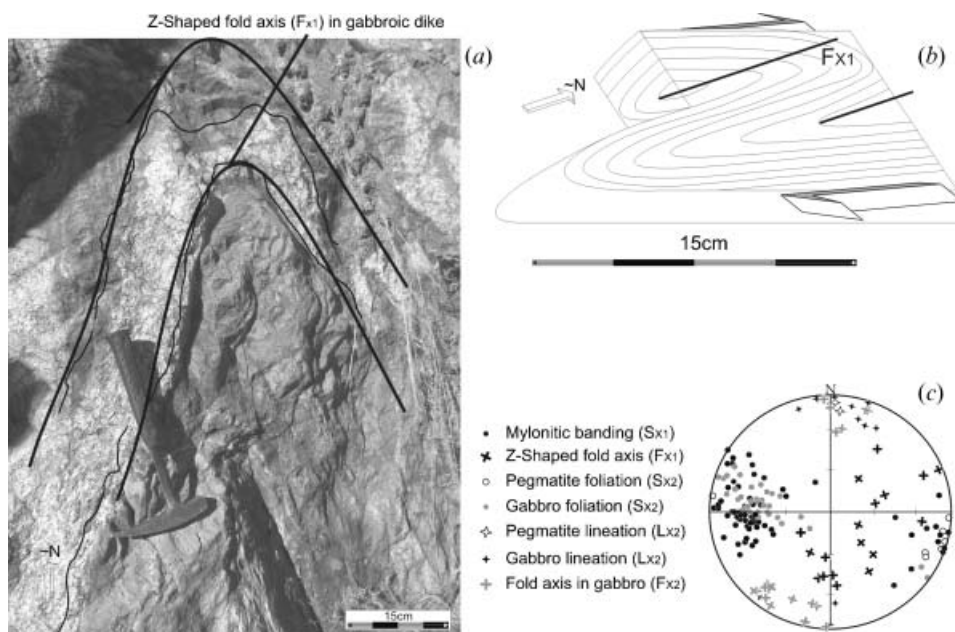


Figure 4. Structure in gabbroic dike at Barranca el Viento: (a) photograph of part of Z-shaped fold; (b) sketch of the same fold; (c) stereoplot of structural data from this outcrop.

shaped folds (Figure 4(a) and (b)). All of these structures are cut by gabbroic dikes that are also folded by steeply plunging, Z-shaped folds with an axial planar foliation defined by aligned amphibole, which is parallel to the main foliation in the host rocks. These dikes are, in turn, cut by pegmatite dikes (Figure 4(c)) that are also folded by steeply plunging, Z-shaped folds with an axial planar cleavage defined by aligned muscovite and stretched quartz that is parallel to the foliation in the host gabbroic rocks. The eastern boundary of this gabbroic dike displays intense greenschist facies shearing along a steeply dipping boundary that juxtaposes marbles of the Tecomate Formation against the gabbro. Fabrics in the Tecumate calcmylonites exhibit a steeply dipping, mylonitic foliation with a subhorizontal stretching lineation that is parallel to the folds axes of sheath folds, all of which formed under lower greenschist facies metamorphic conditions. The asymmetry of all of the amphibolite facies folds together with the subhorizontal amphibole lineation suggests that they formed during dextral shearing.

At one locality in Barranca Las Ollas on the western margin of this same gabbro dike, the mylonitic banding is deformed by a mushroom-type interference pattern with aligned amphibole parallel to the axial planes of both sets of folds (Figure 5(a) and (b)). The first set of folds ( $F_{X1}$ , Figure 5(a) and (b)) in this interference pattern appear to have subhorizontal fold axes trending highly obliquely to the N–S orientation of the gabbro dike. On the other hand, the second set of folds has fold axes ( $F_{X2}$ , Figure 5(a) and (b)) that plunge gently to the NNE parallel to an amphibole mineral lineation ( $L_{X2}$ , Figure 5(b)). Ca. 20 m to the north of this interference pattern, a subhorizontal, 1 m thick, amphibolite dike cuts across all of the amphibolite facies fabrics, and is folded by an open fold with a gently N-plunging fold axis and a steeply dipping axial plane (Figure 5(c) and (d)). This dike, which also has a continental rift tholeiitic geochemistry, has yielded an  $^{40}\text{Ar}/^{39}\text{Ar}$  amphibole plateau age of  $434 \pm 3$  Ma, which indicates cooling through  $\sim 570^\circ\text{C}$  (Keppie *et al.* 2008b) and places a younger limit on the time of development of amphibolite facies fabrics. The ca. 4–11 my interval between the zircon intrusive age and the cooling age suggest that the amphibolite facies fabrics developed during cooling of the intrusion. The geochemistry of the mafic dikes indicates that they are rift-related continental tholeiites (Keppie *et al.* 2008b), and this, combined with the kinematics of the amphibolite facies fabrics, suggests that the dike swarm was intruded during dextral transtensional deformation. A few metres to the west, adjacent to the western contact of the widest gabbro dike, chloritic shear zones also affect the amphibolite facies fabrics.

Contact metamorphism along the western margin of the widest gabbro dike is exhibited by the growth of decussate hornblende, muscovite and biotite, which disappear beyond ca. 10–20 m of the contact where the grade of metamorphism becomes the greenschist facies. These decussate minerals are affected by variable degrees of shearing associated with the growth of chlorite under lower greenschist facies metamorphic conditions.

#### ***Fabrics in the Amate Unit ( $S_A$ , $L_A$ and $F_A$ )***

Bedding is well preserved in the Amate Unit where layers of arkose alternate with quartzite and metapelite. The bedding is generally parallel to a cleavage,  $S_{A1}$ , defined by aligned chlorite and muscovite, which indicate greenschist facies metamorphism. In the contact aureole of the thickest gabbro dike, this cleavage wraps around the amphibole and mica porphyroblasts and feldspar porphyroclasts.

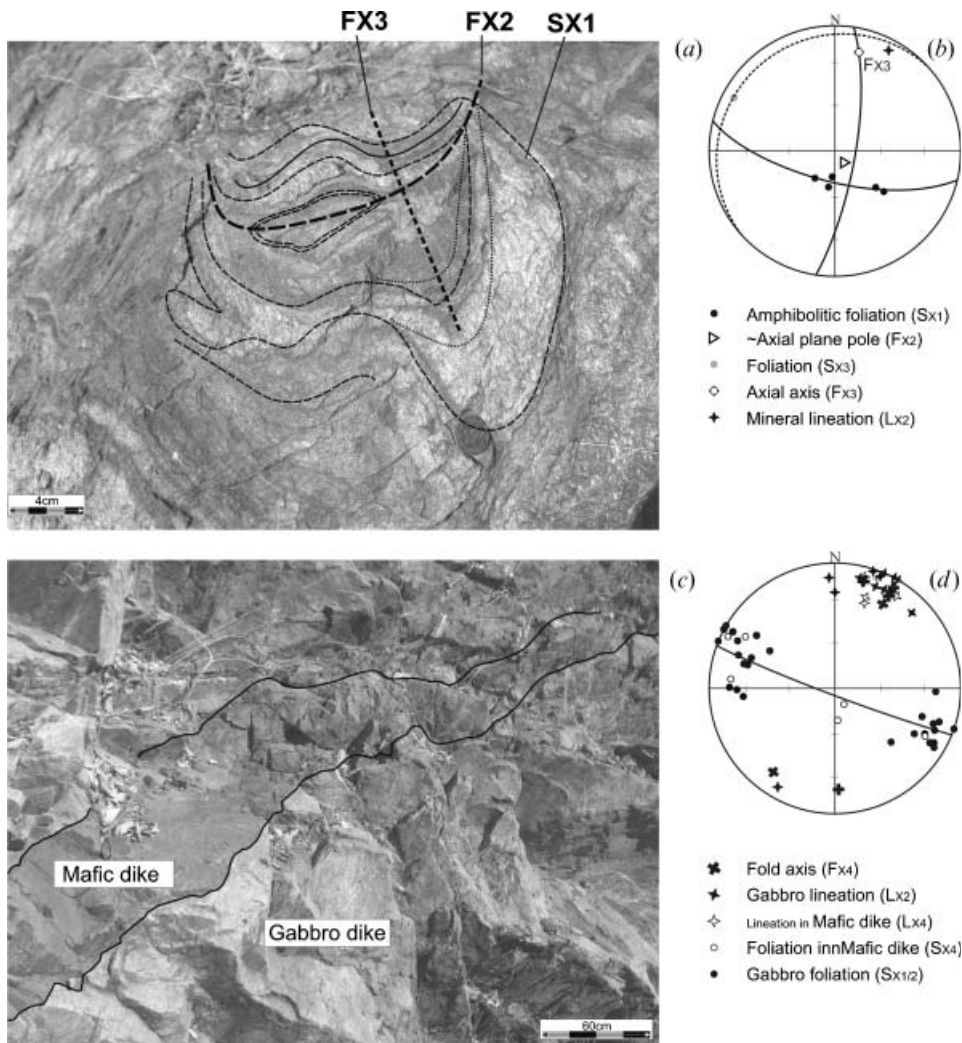


Figure 5. Structure in gabbroic dike at Barranca las Ollas: (a) photograph and (b) stereoplot of mushroom interference patterns in the gabbroic dike; (c) photograph and (d) stereoplot of open fold in mafic dike intruded into gabbroic dike.

Kinematic indicators include bookshelf fabrics, subhorizontal stretching lineations and sigma structures indicative of dextral movements (Figure 6). The  $S_{A1}$  cleavage is deformed by open-tight, NNE–SSW, upright folds with fold axes varying from subvertical to subhorizontal accompanied by a subhorizontal stretching lineation,  $L_{A2}$ , and the development of an axial planar crenulation cleavage,  $S_{A2}$ , in the pelitic lithologies and in the fault zones bounding the Bravo block (Figures 7(a) and (b)). All of these structures are locally deformed by open, N–S upright, subhorizontal folds,  $F_{A3}$ , (Figure 7(c)).

#### **Fabrics in the Huerta and Salada units ( $S_{HS}$ , $L_{HS}$ and $F_{HS}$ )**

The Huerta and Salada units are both deformed by a similar sequence of fabrics involving three sets of structures and so they will be described together. Bedding,  $S_0$ ,

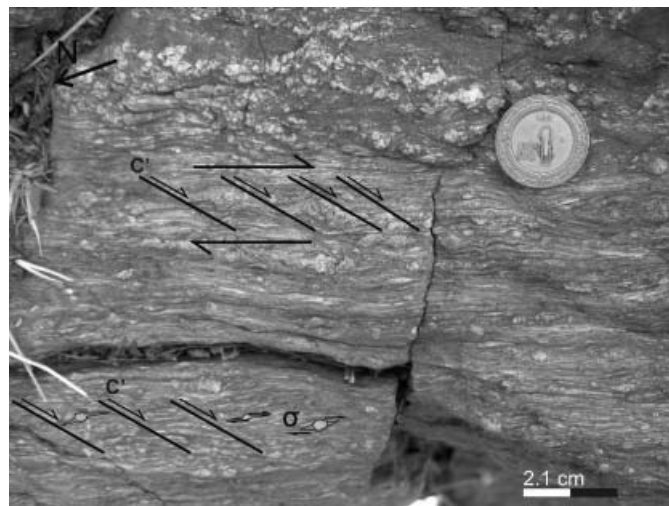


Figure 6. Photograph of bookshelf fabrics and sigma porphyroclasts in the Amate Unit indicating dextral shear in the contact aureole of the gabbroic dike located at Barranca Amate.

in these units is preserved as an alternation of psammitic and pelitic horizons. The first deformational structure is a cleavage,  $S_{HS1}$  (Figures 8(a) and (c)), which varies from a solution cleavage in the psammites to a phyllitic cleavage in the pelites. This cleavage is generally parallel to the bedding in the pelites and is refracted in the psammites. Folds were not observed. It is defined by aligned muscovite and chlorite indicating that this deformation took place under lower greenschist facies conditions.

These latter structures are deformed by a second set of structures that includes isoclinal folds and rare sheath folds ( $F_{HS2}$ ), a cleavage ( $S_{HS2}$ ) (Figures 8(a)–(d), 9(a) and (b)), and a strong stretching lineation defined by stretched quartz ( $L_{HS2}$ ). The  $S_{HS2}$  cleavage varies from a solution cleavage in the psammites to a phyllitic cleavage made up of muscovite, chlorite, phengite, and stretched quartz that is generally a composite cleavage,  $S_{HS1+2}$ . This mineral association indicates deformation under greenschist facies conditions. The cleavage generally strikes N–S with a sub-vertical dip, whereas the lineation is generally subhorizontal (Figures 9(a) and (b)). Fold axial planes are generally steeply dipping whereas fold axes are predominantly subhorizontal.

A third set of structures deforms both  $S_{HS1}$  and  $S_{HS2}$  and produced open-close, N-trending (N25°E to N10°W), upright folds and crenulations with subhorizontal-shallowly N-plunging, fold axes (0–25°N) ( $F_{HS3}$ , Figure 9(b)). Muscovite crystals are folded in the fold hinges, whereas chlorite appears to have recrystallized in short straight segments, suggesting sub-greenschist facies metamorphic conditions.

#### **Fabrics in the Tecomate formation ( $S_T$ , $L_T$ and $F_T$ )**

The Tecomate formation is deformed by two sets of structures. Bedding is clearly preserved in least deformed areas where alternating sandstone, slate/phyllite, conglomerate, and limestone/marble layers are preserved. The bedding is deformed by folds that vary from upright, subhorizontal, open folds to tight-isoclinal, subhorizontal folds (Figure 10) and sheath folds ( $F_{T1}$ ) in shear zones. The N–S, subvertical, axial planar cleavage is defined by muscovite and chlorite,  $S_{T1}$

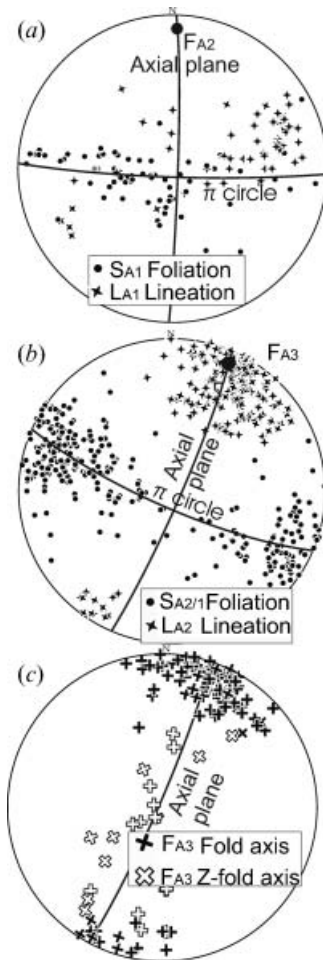


Figure 7. Structural data from the Amate Unit: (a) S<sub>A1</sub> foliation and L<sub>A1</sub> lineation; (b) S<sub>A2/1</sub> composite foliation and L<sub>A3</sub> stretching lineation; (c) F<sub>A3</sub> fold axes in pegmatite dikes intruding the Amate Unit.

(Figures 11(a) and (b)). An associated lineation,  $L_{T1}$ , varies from an intersection lineation to a subhorizontal stretching lineation in shear zones. A study of fold axis orientations and fold asymmetry in the shear zones shows a great circle distribution of fold axes with a change of asymmetry about a shallowly N-plunging line, which is parallel to the local stretching lineation (Figure 11(a)). In vertical shear zones, steeply plunging folds have a Z-shape indicating dextral kinematics. In gently northward dipping shear zones, such as those juxtaposing the Salada Unit with the Tecomate formation, E–W trending  $F_{T1}$  fold axes have an asymmetry indicative of S-vergent thrusting. Measurements of clast shapes in conglomerate were made at two localities, one in a steeply dipping shear zone (Carrizal: Figure 12(a)) and the other in an N-dipping, S-vergent thrust zone (San Juan Chichihualtepec). At both localities, the clasts are prolate spheroids with long axes parallel to the  $L_{T1}$  stretching lineation (Figure 12(b) and (c)). Ratios of long versus short/medium axes vary up to 10:1. Such strain is typical of transtensional deformation (Dewey *et al.* 2006; Venkat-Ramani and Tikoff 2002).

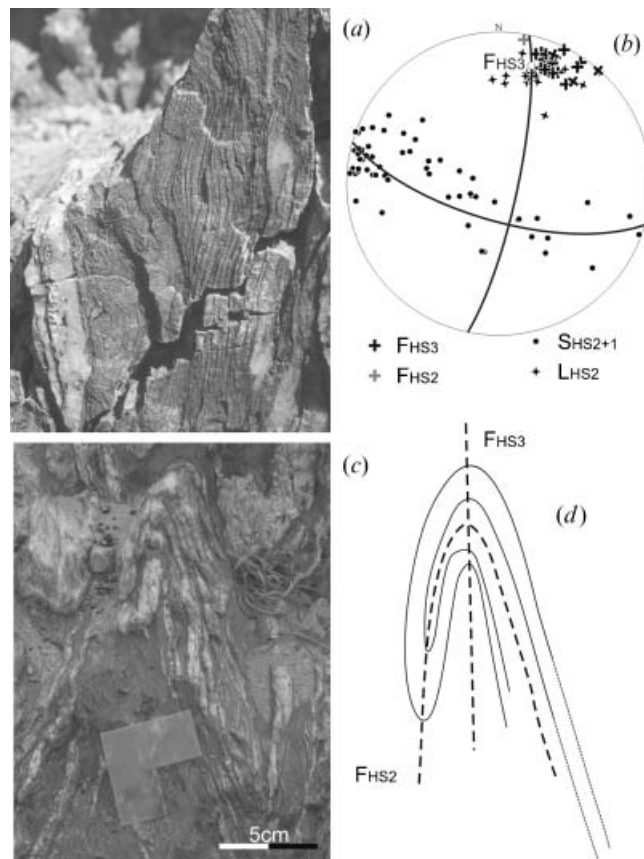


Figure 8. (a) Photograph of folded solution cleavage,  $S_{HS1}$ , in metapsammite of the Huerta Unit; (b) stereoplot of data for the folded Huerta unit; (c) photograph of refolded fold in metapelite of the Huerta Unit; (d) sketch of (c).

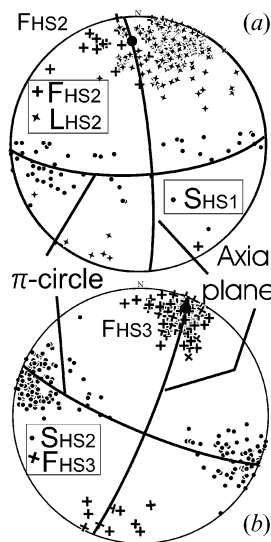


Figure 9. Structural data from the Huerta and the Salada units: (a)  $S_{HS1}$  foliation,  $F_{HS2}$  folds, and  $F_{HS2}$  lineations; (b)  $S_{HS2}$  foliation and  $F_{HS3}$  folds.



Figure 10. Photograph of fabrics in the Tecolate Formation.

The bedding and  $S_{T1}$  cleavage are refolded by NW- to NE-trending upright open folds, crenulations and kink bands ( $F_{T2}$ ) (Figure 11(c)). These folds are associated with the growth of chlorite.

#### **Fabrics in the Totoltepec intrusion ( $S_{Tr}$ )**

The Totoltepec intrusion occurs in the Tonahuixtla block and is faulted against the Tecolate formation along the San Jeronimo Fault. A foliation,  $S_{Tr1}$ , defined by hornblende in the gabbro, and quartz and feldspar in the granite, has a variable orientation (ENE-ESE strike and 60–85°S dip). This variation is attributed to post- $S_{Tr1}$  folding,  $F_{Tr2}$  (Figure 13; Malone *et al.* 2002).

#### **$^{40}\text{Ar}/^{39}\text{Ar}$ geochronology**

##### **Analytical methods**

In the contact aureole of the gabbroic dikes, decussate amphibole (AMATE-GA3/D-644) and decussate muscovite (REP-1/AOR-1016 and AMATE-4/AOR-1018) were separated from hornfelses in the Amate Unit. Additional samples include muscovite, which was separated from a pelitic schist in the Salada Unit (W3-SAL/D-646) and a whole-rock sample of sericitic phyllite of the Tecolate formation (AxTT-366-TCC/D-645). These minerals were pre-treated and concentrated by

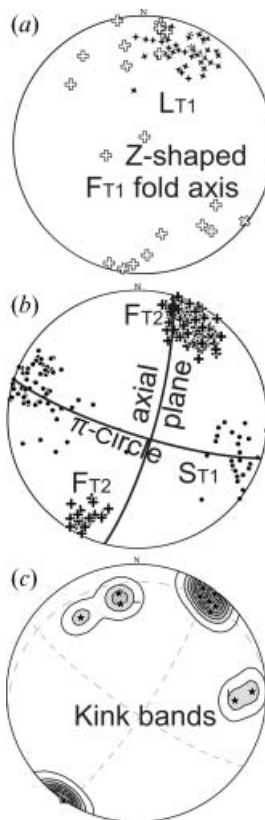


Figure 11. Stereoplots of fabrics in the Tecolate Formation: (a)  $F_{T1}$  fold axes and lineations; (b) Foliation  $S_{T1}$  folded about  $F_{T2}$  fold axes; (c) kink band axes.

standard techniques and later selected by handpicking under a binocular microscope from fractions that ranged in size from 40–60 mesh at the mineral separation laboratory at ERNO, Instituto de Geología, Universidad Nacional Autónoma de México, Hermosillo, Sonora, México. Mineral separates were loaded into Al-foil packets and irradiated together with Hb3gr (1072 Ma) as a neutron-fluence monitor at the McMaster Nuclear Reactor (Hamilton, Ontario).  $^{40}\text{Ar}/^{39}\text{Ar}$  analyses were performed by standard laser step-heating techniques described in detail by Clark *et al.* (1998) at the Geochronology Research Laboratory of Queen's University, Kingston, Ontario, Canada. The data are given in Table 1 and plotted in Figure 14. All data have been corrected for blanks, mass discrimination, and neutron-induced interferences. For the purpose of this paper, a plateau age is obtained when the apparent ages of at least three consecutive steps, comprising a minimum of 39% of the  $^{39}\text{Ar}_k$  released, agree within  $2\sigma$  error with the integrated age of the plateau segment. Errors shown in Table 1 and on the age spectrum represent the analytical precision at  $\pm 2\sigma$ .

### **Results and interpretation**

The decussate amphibole (AMATE-G3) from the Amate Unit in the contact aureole of the widest gabbro dike yielded a plateau age of  $404 \pm 2$  Ma (MSWD=2.2) for 89% of the  $^{39}\text{Ar}$  released, with younger ages (ca. 200–250 Ma) in the lower power

## VERTICAL SURFACE



## HORIZONTAL SURFACE

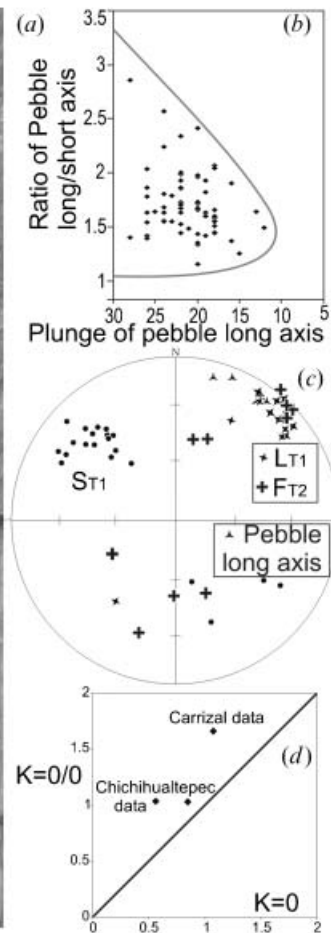


Figure 12. (a) Photograph of strained conglomerate in the Tecomate Formation in the barranca El Carrizal, (b) diagram showing the long/short axes of pebbles versus the plunge of the long axes, (c) stereoplot of the structures, and (d) the strain ellipsoids in the conglomerate shown on a Flynn diagram.

increments attributed to the degassing of minor inclusions as indicated by the different Ca/K ratios (Figure 14(a); Table 1). Although a closure temperature of ca. 530°C results from using a cooling rate of 5°C/My and the actual grain size, the strong cleavage in the rocks has resulted in a much smaller effective diffusion

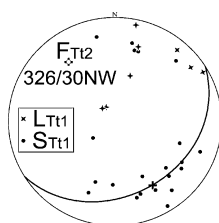


Figure 13. Stereoplot of fabrics in the Totoltepec intrusion.

Table 1.  $^{40}\text{Ar}/^{39}\text{Ar}$  data for samples from the Xayacalán area, Eastern Acatlán Complex, southern Mexico.

Power	36Ar/40Ar	39Ar/40Ar	r	Ca/K	%40Atm	%39Ar	40Ar*/39K	Age	40Ar	39Ar	38Ar	37Ar	36Ar	Blank 40Ar
<b>Amate Unit: AOR-1018/AMATE-4 (18°13.735', 97°58.947') Muscovite</b>														
1.00	0.001254±0.000106	0.055544±0.000668	0.031	0.514	36.99	0.84	11.332±0.587	139.21±6.94	5.915±0.032	0.320±0.003	0.019±0.001	0.047±0.002	0.009±0.001	0.213
2.00	0.000443±0.000056	0.054927±0.000532	0.016	0.918	13.08	1.51	15.820±0.341	191.51±3.92	10.586±0.047	0.575±0.005	0.017±0.001	0.143±0.003	0.007±0.001	0.210
3.00	0.000145±0.000024	0.049581±0.000330	0.006	0.360	4.26	3.30	19.308±0.195	231.12±2.19	25.292±0.066	1.252±0.008	0.023±0.001	0.123±0.003	0.005±0.001	0.204
4.00	0.000075±0.000015	0.047133±0.000244	0.002	0.124	2.21	7.34	20.748±0.144	247.23±1.61	58.966±0.090	2.786±0.014	0.043±0.002	0.095±0.003	0.006±0.001	0.206
5.00	0.000040±0.000012	0.041982±0.000237	0.001	0.074	1.18	9.57	23.537±0.158	278.03±1.73	86.220±0.093	3.633±0.020	0.049±0.003	0.075±0.003	0.005±0.001	0.201
6.00	0.000036±0.000010	0.040536±0.000213	0.001	0.040	1.06	13.81	24.408±0.150	287.54±1.64	128.764±0.139	5.243±0.027	0.071±0.005	0.059±0.004	0.006±0.001	0.200
<7.00	0.000006±0.000024	0.042385±0.000250	0.001	0.192	0.17	63.63	23.552±0.218	278.19±2.39	566.589±0.796	24.149±0.137	0.308±0.027	1.224±0.048	0.006±0.014	0.158
J Value: 0.007079±0.000054 Mass: 22.0 mg. Volume 39K: 37.68×1E-10 cm <sup>3</sup> NTP. Approx. 9.34% K, 1.62% Ca. Integrated Age: 273.28±2.48 Ma.														
Initial 40/36: Linear regression has positive slope. Plateau Age: 278.19±3.10 Ma (63.6% of 39Ar, steps marked by <>).														
<b>Amate Unit: AOR-1016/REP-1 (18°15.508', 97°58.090') Muscovite</b>														
0.75	0.001562±0.000143	0.065730±0.000908	0.023	0.287	46.07	1.14	8.192±0.658	101.58±7.94	5.156±0.028	0.335±0.004	0.012±0.001	0.030±0.002	0.010±0.001	0.102
2	0.000493±0.000034	0.044717±0.000298	0.022	0.183	14.54	3.46	19.108±0.264	228.63±2.97	22.573±0.072	1.012±0.006	0.017±0.001	0.053±0.002	0.013±0.001	0.098
3	0.000177±0.000022	0.038581±0.000252	0.002	0.056	5.22	5.18	24.564±0.236	288.94±2.57	39.143±0.058	1.516±0.010	0.021±0.002	0.027±0.002	0.009±0.001	0.1
4	0.000101±0.000015	0.035137±0.000206	0.002	0.028	2.98	6.13	27.611±0.207	321.75±2.21	50.783±0.074	1.792±0.010	0.025±0.002	0.017±0.002	0.007±0.001	0.1
5	0.000047±0.000011	0.033981±0.000216	0.001	0.02	1.38	28.25	29.022±0.211	336.74±2.24	241.731±0.333	8.261±0.051	0.105±0.009	0.047±0.006	0.013±0.003	0.099
6	0.000041±0.000017	0.035553±0.000219	0.001	0.029	1.2	6.19	27.788±0.222	323.64±2.36	50.695±0.071	1.810±0.011	0.024±0.002	0.018±0.002	0.004±0.001	0.098
7	0.000042±0.000014	0.034752±0.000258	0.001	0.06	1.23	12.26	28.420±0.244	330.36±2.60	102.630±0.142	3.585±0.026	0.048±0.004	0.062±0.004	0.006±0.001	0.1
<8.00	0.000023±0.000045	0.032109±0.000420	0.001	0.1	0.67	37.39	30.934±0.577	356.87±6.04	338.690±0.763	10.935±0.140	0.141±0.027	0.294±0.050	0.010±0.015	0.23
J Value: 0.007071±0.000054 Mass: 21.0 mg Volume 39K: 29.04×1E-10 cm <sup>3</sup> NTP Approx. 7.55% K, 0.50% Ca. Integrated Age: 333.22±3.31 Ma.														
Initial 40/36: Linear regression has positive slope. Plateau Age: 356.87±6.53 Ma (37.4% of 39Ar, steps marked by <>).														
<b>Amate Unit: D-644:AMATE-GA3 (18°16.442', 97°54.852') Amphibole bp</b>														
1.6	0.003209±0.000130	0.006815±0.000186	0.074	3.332	94.66	0.29	7.81±5.60	194.5±132.0	1.815±0.004	0.011±0.000	0.087±0.001	0.009±0.000	0.006±0.000	0.169
1.8	0.002891±0.000200	0.022201±0.000473	0.025	5.145	84.84	0.48	6.80±2.68	170.5±64.0	0.983±0.004	0.018±0.000	0.143±0.001	0.020±0.001	0.003±0.000	0.168
2	0.002663±0.000218	0.028145±0.000525	0.021	4.838	78.3	0.55	7.69±2.30	191.5±54.3	0.917±0.003	0.021±0.000	0.082±0.001	0.022±0.001	0.003±0.000	0.168
2.3	0.002338±0.000089	0.026309±0.000370	0.015	2.456	69.03	1.68	11.75±1.03	285.0±23.0	2.598±0.006	0.065±0.001	0.010±0.000	0.033±0.001	0.007±0.000	0.166
2.5	0.002195±0.000166	0.037157±0.000575	0.015	3.787	64.77	0.91	9.46±1.33	232.9±30.8	1.102±0.004	0.035±0.001	0.005±0.000	0.028±0.001	0.003±0.000	0.167
2.7	0.001584±0.000393	0.062071±0.001198	0.006	5.33	46.71	0.82	8.57±1.89	212.2±44.1	0.669±0.003	0.031±0.001	0.003±0.000	0.035±0.001	0.002±0.000	0.169
3	0.001028±0.000178	0.067350±0.000968	0.009	11.65	30.3	1.48	10.34±0.80	253.1±18.3	1.004±0.003	0.057±0.001	0.007±0.000	0.135±0.001	0.002±0.000	0.168
3.3	0.000347±0.000062	0.058366±0.000482	0.011	9.672	10.2	4.92	15.38±0.34	364.7±7.3	3.372±0.007	0.189±0.001	0.033±0.001	0.371±0.003	0.002±0.000	0.165
<3.50>	0.000187±0.000024	0.055159±0.000410	0.021	7.802	5.5	11.85	17.13±0.18	401.9±3.8	8.340±0.011	0.455±0.003	0.081±0.001	0.719±0.005	0.003±0.000	0.165

Table 1. (Continued.)

Power	36Ar/40Ar	39Ar/40Ar	r	Ca/K	%40Atm	%39Ar	40Ar*/39K	Age	40Ar	39Ar	38Ar	37Ar	36Ar	Blank 40Ar
<3.70>	0.000116±0.000020	0.056196±0.000325	0.023	7.454	3.39	26.1	17.19±0.14	403.2±3.0	17.838±0.020	1.001±0.006	0.166±0.002	1.511±0.010	0.004±0.000	0.166
<3.80>	0.000127±0.000096	0.056700±0.000621	0.006	7.992	3.72	2.4	16.98±0.53	398.7±11.2	1.781±0.004	0.092±0.001	0.016±0.000	0.150±0.002	0.001±0.000	0.168
<4.00>	0.000111±0.000055	0.057258±0.000540	0.009	7.854	3.26	4.22	16.89±0.32	396.9±6.8	2.969±0.006	0.162±0.001	0.029±0.001	0.258±0.002	0.001±0.000	0.165
<4.30>	0.000090±0.000025	0.056873±0.000383	0.019	7.745	2.63	9.43	17.12±0.17	401.7±3.6	6.475±0.008	0.362±0.002	0.059±0.001	0.567±0.004	0.002±0.000	0.166
<4.50>	0.000085±0.000015	0.056203±0.000359	0.035	7.949	2.48	34.85	17.35±0.13	406.5±2.7	23.755±0.022	1.337±0.008	0.227±0.003	2.148±0.015	0.004±0.000	0.166
J Value: 0.014566±0.000042 Mass: 0.0 mg Volume 39K: 3.81×1E-10 cm <sup>3</sup> NTP Approx. % K, % Ca. Integrated Age: 392.01±1.97 Ma.														
Initial 40/36: 312.24±197.11 (MSWD=2.64, isochron between 0.29 and 2.41). Correlation Age: 402.49±8.50 Ma (88.9% of 39Ar, steps marked by >) MSWD 2.204. Plateau Age: 403.73±1.91 Ma (88.9% of 39Ar, steps marked by <). Mod. err. 2.28.														
<b>Tecomate formation: D-645:AxTT-366-TCC (18°15.582', 97°56.223') Sericitic Wr</b>														
1.5	0.002662±0.000248	0.063261±0.001409	0.015	0.192	78.52	2.45	3.37±1.16	86.6±29.2	0.952±0.005	0.058±0.001	0.004±0.001	0.003±0.000	0.003±0.000	0.045
1.7	0.000915±0.000129	0.094448±0.001410	0.008	0.251	26.95	6.1	7.73±0.42	192.5±10.0	1.557±0.006	0.143±0.002	0.003±0.000	0.007±0.001	0.002±0.000	0.044
1.8	0.000497±0.000092	0.083271±0.000931	0.006	0.193	14.64	6.66	10.25±0.35	251.1±8.0	1.918±0.007	0.157±0.002	0.003±0.000	0.006±0.001	0.001±0.000	0.045
1.9	0.000218±0.000063	0.081627±0.000970	0.001	0.104	6.42	9.16	11.46±0.27	278.8±6.0	2.672±0.005	0.213±0.002	0.003±0.000	0.005±0.001	0.001±0.000	0.044
2.1	0.000105±0.000044	0.084269±0.000725	0.001	0.069	3.09	14.49	11.50±0.19	279.6±4.2	4.070±0.009	0.341±0.003	0.005±0.000	0.005±0.001	0.001±0.000	0.044
<2.30>	0.000093±0.000043	0.091014±0.000829	0.001	0.071	2.73	12.62	10.69±0.17	261.2±3.9	3.291±0.007	0.297±0.003	0.004±0.001	0.005±0.001	0.001±0.000	0.044
<2.50>	0.000090±0.000055	0.092211±0.000805	0.001	0.081	2.65	11.6	10.56±0.20	258.2±4.6	2.990±0.008	0.273±0.002	0.004±0.000	0.005±0.001	0.001±0.000	0.044
<2.70>	0.000554±0.000071	0.076948±0.000785	0.008	0.123	16.33	12	10.87±0.30	265.3±6.7	3.694±0.011	0.282±0.003	0.004±0.000	0.007±0.001	0.002±0.000	0.044
<2.90>	0.000101±0.000091	0.089484±0.000936	0	0.123	2.97	11.52	10.84±0.32	264.7±7.3	3.059±0.007	0.271±0.003	0.004±0.001	0.007±0.001	0.001±0.000	0.045
<3.10>	0.000130±0.000060	0.087648±0.001073	0.002	0.136	3.83	10.19	10.97±0.25	267.6±5.6	2.767±0.010	0.240±0.003	0.004±0.000	0.007±0.001	0.001±0.000	0.045
4	0.000300±0.000181	0.074958±0.001276	0.003	1.334	8.84	3.23	12.16±0.75	294.4±16.7	1.052±0.005	0.076±0.001	0.003±0.000	0.019±0.001	0.001±0.000	0.045
J Value: 0.014577mg±0.000042 Mass: 0.0 Volume 39K: 2.34×1E-10 cm <sup>3</sup> NTP Approx. % K, % Ca. Integrated Age: 258.92 ± 2.18 Ma.														
Initial 40/36: 336.02±61.50 (MSWD = 0.98, isochron between 0.00 and 3.00). Correlation Age: 259.53±3.75 Ma (47.7% of 39Ar, steps marked by >) MSWD 2.106. Plateau Age: 263.29±2.66 Ma (57.9% of 39Ar, steps marked by <).														
<b>Salada Unit: D-644:W3-SAL (18°16.952', 97°54.852') Muscovite hp</b>														
1.5	0.001197±0.000357	0.068649±0.001742	0.005	0.015	35.28	0.3	9.42±1.56	232.0±36.1	0.505±0.003	0.032±0.001	0.003±0.000	0.001±0.000	0.001±0.000	0.039
1.7	0.000181±0.000058	0.076936±0.000800	0.001	0.009	5.32	2.13	12.30±0.26	297.5±5.8	2.995±0.009	0.229±0.002	0.009±0.001	0.001±0.000	0.001±0.000	0.04
1.8	0.000093±0.000036	0.075576±0.000688	0	0.007	2.73	3.1	12.87±0.18	310.1±4.1	4.416±0.009	0.332±0.003	0.010±0.001	0.001±0.000	0.001±0.000	0.039
1.9	0.000042±0.000024	0.075572±0.000544	0	0.003	1.23	4.6	13.07±0.13	314.5±3.0	6.531±0.010	0.493±0.003	0.007±0.000	0.001±0.000	0.001±0.000	0.039
2.1	0.000039±0.000013	0.075418±0.000443	0.001	0.003	1.16	11.72	13.11±0.09	315.3±2.1	16.633±0.025	1.257±0.007	0.016±0.001	0.002±0.001	0.001±0.000	0.038
2.2	0.000030±0.000016	0.075410±0.000444	0	0.004	0.89	10.28	13.14±0.10	316.1±2.2	14.585±0.021	1.102±0.006	0.014±0.001	0.002±0.001	0.001±0.000	0.039
2.3	0.000029±0.000014	0.074146±0.000455	0	0.004	0.85	14.74	13.37±0.10	321.2±2.2	21.252±0.027	1.580±0.009	0.020±0.001	0.002±0.001	0.001±0.000	0.039
2.4	0.000024±0.000014	0.074449±0.000433	0	0.001	0.71	13.87	13.34±0.10	320.4±2.1	19.924±0.026	1.487±0.008	0.019±0.001	0.001±0.001	0.001±0.000	0.039
<2.50>	0.000024±0.000018	0.073584±0.000414	0	0.002	0.71	15.95	13.49±0.10	323.8±2.3	23.178±0.027	1.711±0.009	0.021±0.002	0.002±0.001	0.001±0.000	0.039
<2.60>	0.000011±0.000027	0.073893±0.000597	-0.001	0.005	0.32	3.62	13.49±0.16	323.7±3.4	5.261±0.013	0.388±0.003	0.005±0.001	0.001±0.000	0.000±0.000	0.039

Table 1. (Continued.)

Power	36Ar/40Ar	39Ar/40Ar	r	Ca/K	%40Atm	%39Ar	40Ar*/39K	Age	40Ar	39Ar	38Ar	37Ar	36Ar	Blank 40Ar
<2.80	0.000012±0.000017	0.073690±0.000483	0	0.004	0.34	6.62	13.52±0.11	324.5±2.5	9.634±0.015	0.710±0.004	0.009±0.001	0.001±0.000	0.000±0.000	0.039
<3.00	0.000015±0.000016	0.074076±0.000483	0	0.004	0.45	9	13.44±0.11	322.6±2.4	13.004±0.021	0.965±0.006	0.012±0.001	0.002±0.001	0.001±0.000	0.039
<3.20	0.000000±0.000057	0.073592±0.000807	-0.002	0.014	0	1.62	13.59±0.28	325.9±6.0	2.386±0.006	0.174±0.002	0.002±0.000	0.001±0.000	0.000±0.000	0.039
<4.00	0.000000±0.000039	0.074663±0.000836	-0.001	0.026	0.01	2.46	13.39±0.22	321.6±4.8	3.555±0.008	0.264±0.003	0.003±0.000	0.002±0.000	0.000±0.000	0.039

J Value: 0.014571±0.000042 Mass: 0.0 mg Volume 39K: 10.65×1E-10 cm<sup>3</sup> NTP Approx. % K, % Ca. Integrated Age: 319.39±1.18 Ma  
Initial 40/36: Linear regression has positive slope. Correlation Age: MSWD 0.505. Plateau Age: 323.60±1.54 Ma (39.3% of 39Ar, steps marked by <). Mod. err. 1.70

Notes: Atmospheric 40Ar/36Ar = 287.137. Measured volumes are × 1E-10 cm<sup>3</sup>. NTP: normal temperature and pressure. All errors are 2 × standard error. MSWD: mean square of weighted deviates.

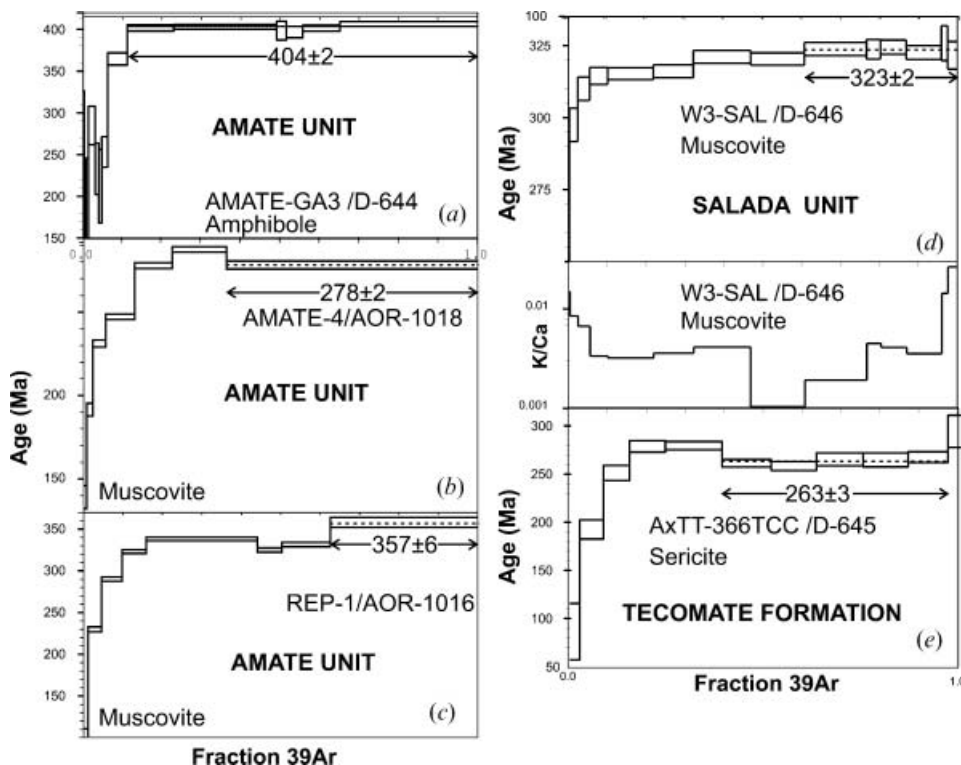


Figure 14.  $^{40}\text{Ar}/^{39}\text{Ar}$  spectra for: (a–c) contact aureole decussate minerals in the contact aureole of the thickest gabbro dike: (a) amphibole, and (b, c) muscovite, (d) muscovite from the Salada Unit, (e) whole-rock sericitic phyllite from the Tecolate Formation.

dimension and a correspondingly lower closure temperature of ca.  $480^\circ\text{C}$ . The ca. 404 Ma age is ca. 30 My younger than the  $434 \pm 3$  Ma plateau age for cooling through  $570^\circ\text{C}$  recorded by amphibole in the adjacent gabbro (Keppie *et al.* 2008b). This difference is attributed to a difference in composition and grain size.

Decussate muscovite (REP-1 and AMATE-4) from the Amate Unit in the contact aureole of the same gabbro dike also yielded discordant spectra (Figures 14(b) and (c); Table 1). Whereas they both have young ages (ca. 100–230 Ma) in the lowest power increments, one increases to an age of  $357 \pm 6$  Ma whereas the other gave  $278 \pm 2$  Ma in the highest power increments. Calculations using the grain size and a cooling rate of  $5^\circ\text{C}/\text{My}$  for the ca. 360 and 280 Ma ages indicate that these probably represent minimum ages for cooling through ca.  $370$ – $380^\circ\text{C}$ .

Muscovite (W3-SAL) defining the  $S_{\text{HSI}}$  cleavage in the Salada Unit yielded discordant data with apparent ages that increase from ca. 232 Ma to a  $324 \pm 2$  Ma plateau ( $\text{MSWD} = 0.51$ ) in the highest six power increments for 39% of the  $^{39}\text{Ar}$  released (Figure 14(d); Table 1). Using an average grain size of 0.8 mm. suggests that this age represents a minimum age for cooling through ca.  $400^\circ\text{C}$ .

A whole-rock, sericitic phyllite (AxTT-366-TCC) of the Tecolate Formation yielded a partially discordant spectrum in which five steps define a plateau with an apparent age of  $263 \pm 3$  Ma (= 58% of the total  $^{39}\text{Ar}$  released,  $\text{MSWD} = 2.1$ ). These steps generally have the lowest  $^{40}\text{Ar}$  atmospheric contamination and the Ca/K and Cl/K ratios are consistent with Ar release from sericite. Thus, the ca. 263 Ma age

probably dates the tectonothermal event that produced the cleavage in the Tecomate Formation. The apparent ages of the lower temperature steps appear to be correlated with Ar released from other phases in the rocks and are not considered to be geologically significant.

### Correlation and age constraints for Late Palaeozoic fabrics

Using the geometry of the structure in the various units along with U/Pb geochronology and  $^{40}\text{Ar}/^{39}\text{Ar}$  data, the following correlations can be made:

- (1)  $F_{T1} \equiv F_{HS2} \equiv F_{A2}$ , and  $F_{T2} \equiv F_{HS3} \equiv F_{A3}$ , respectively. The age of the phyllitic cleavage in the Tecomate formation appears to be given by  $263 \pm 3$  Ma (Figure 14(e)), i.e. close to the Middle-Late Permian boundary. This is consistent with the  $314\text{--}282$  Ma ages of granitic pebbles recovered from a conglomerate in the Tecomate to the southeast of the study area, which is also cut by the  $S_{T1}$  cleavage (Keppie *et al.* 2004b). Migmatization along the Caltepec fault zone dated at  $276 \pm 1$  Ma (Elías-Herrera and Ortega-Gutiérrez 2002) is within error the same as the  $278 \pm 2$  Ma age recorded by muscovite adjacent to the Las Ollas fault suggesting that it may have been active at this time with hot fluids flowed along the fault, a precursor of the  $F_{T1}$  deformation. The  $F_{T2}$  folds have not been recorded in the Matzitzi Formation that unconformably overlies Caltepec fault zone (Elías-Herrera and Ortega-Gutiérrez 2002). This is inconsistent with the Leonardian age reported for the Matzitzi Formation (Weber 1997), but is compatible with its reassignment to the Late Permian (Centeno-García *et al.* 2008). Thus,  $F_{T1}$  and  $F_{T2}$ , and their correlatives, appear to be constrained within the Middle Permian.
- (2)  $F_{HS1} \equiv F_{A1}$ . The difference in the intensity of this deformation in the Huerta/Salada versus Amate units is inferred to result from competency differences where the arkoses of the Amate Unit are more competent. The  $324 \pm 2$  Ma plateau age for muscovite defining the  $S_{S1}$  cleavage in the Salada Unit (Figure 14(d)) provides a mid-Upper Mississippian age for this deformation. This is consistent with the  $352 \pm 3$  Ma age of the youngest detrital zircon recovered from the Salada Unit (Morales-Gámez *et al.* 2008), and the fact that the Permian Tecomate formation does not record this deformation. The correlation of the structures in the Huerta and Amate units with those in the Salada Unit suggests that the  $F_{H1}$  and  $F_{A1}$  structures are also Upper Mississippian in age. A younger limit is provided by the fact that the  $F_{HS1}$  deformation is not recorded in the Tecomate formation. These structures are contemporaneous with the earliest,  $347 \pm 3$  Ma deformation reported in the Patlanoaya area in the northern part of the Acatlán Complex (Ramos-Arias *et al.* 2008).

### Conclusions

Three periods of deformation are recorded in the Xayacatlán area, ca. 442 Ma (ca. Ordovician-Silurian boundary), Mississippian, and Middle Permian. The ca. 442 Ma structures are only to be found in an N–S tholeiitic dike swarm that cuts the Amate Unit. The rift-related nature of the dike swarm together with the kinematics of the structures suggests that they formed during a period of dextral transtension constrained between the time of intrusion of the dikes ( $442 \pm 2$  Ma) and the hornblende cooling age ( $434 \pm 3$  Ma; Figure 15; Keppie *et al.* 2008b). Initiation of

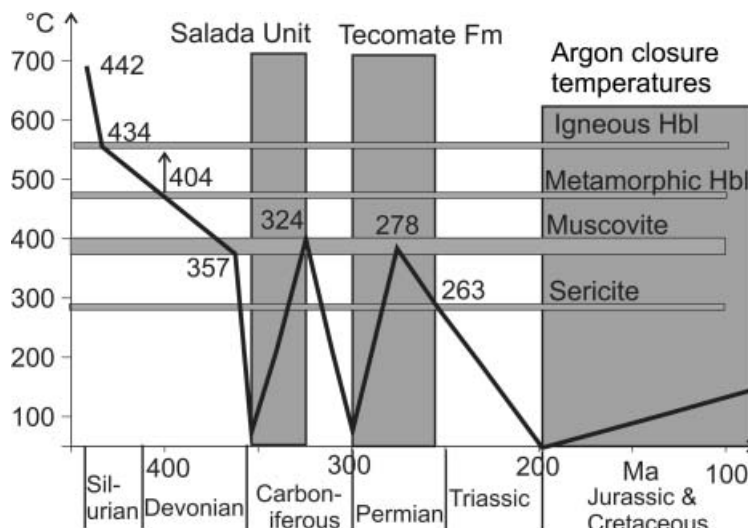


Figure 15. Temperature versus Time graph using  $^{40}\text{Ar}/^{39}\text{Ar}$  data to constrain events in the Xayacatlán area.

rifting appears to have started somewhat earlier at ca. 464 Ma with the intrusion of granitic dikes and pegmatites (Morales-Gámez *et al.* 2008), which are inferred to be felsic members of a bimodal suite (Keppie *et al.* 2008b). Thus, this tectonothermal event appears to be extensional rather than recording an orogenic event, the Acatecan Orogeny (Ortega-Gutiérrez *et al.* 1999, Talavera-Mendoza *et al.* 2005; Vega-Granillo *et al.* 2007). Furthermore, an extensional event is more consistent with rifting on the southern margin of the Rheic Ocean than closing of the Iapetus Ocean (Figure 16(A); Keppie *et al.* 2008a).

The synchronicity of the Mississippian deformation in the Xayacatlán and Patlanoaya areas suggests that the mechanism of deformation may be similar. The deformation has been linked to extrusion of high-pressure rocks derived from upper plate material by subduction erosion (Keppie *et al.* 2008a). The appearance of Mid-Continent fauna, a shallow water fauna in the USA, in the Mississippian rocks of the adjacent Oaxaquia terrane (Navarro-Santillan *et al.* 2002) suggests that Pangea had amalgamated by this time. This suggests that the Mississippian structure in the Xayacatlán area were developed on the western margin of Pangea (Figure 16(B)).

The Middle Permian age of the dextral transtensional deformation in the Tecomate formation confirms previous results that concluded that the structures were not Siluro-Devonian (Sánchez-Zavala *et al.* 2000), but Permian (Keppie *et al.* 2004b). This deformation is broadly synchronous with the development of a Permian magmatic arc that extends along the backbone of Mexico (Torres *et al.* 1999; Keppie *et al.* 2008a), and suggests that the arc formed in a dextral transtensional environment that may have been due to oblique convergence between the paleo-Pacific and western Pangea.

### Acknowledgements

We would like to acknowledge a Papiit grant (IN100108-3), a CONACyT grant (CB-2005-1: 24894) to JDK and AOR that facilitated the fieldwork and  $^{40}\text{Ar}/^{39}\text{Ar}$

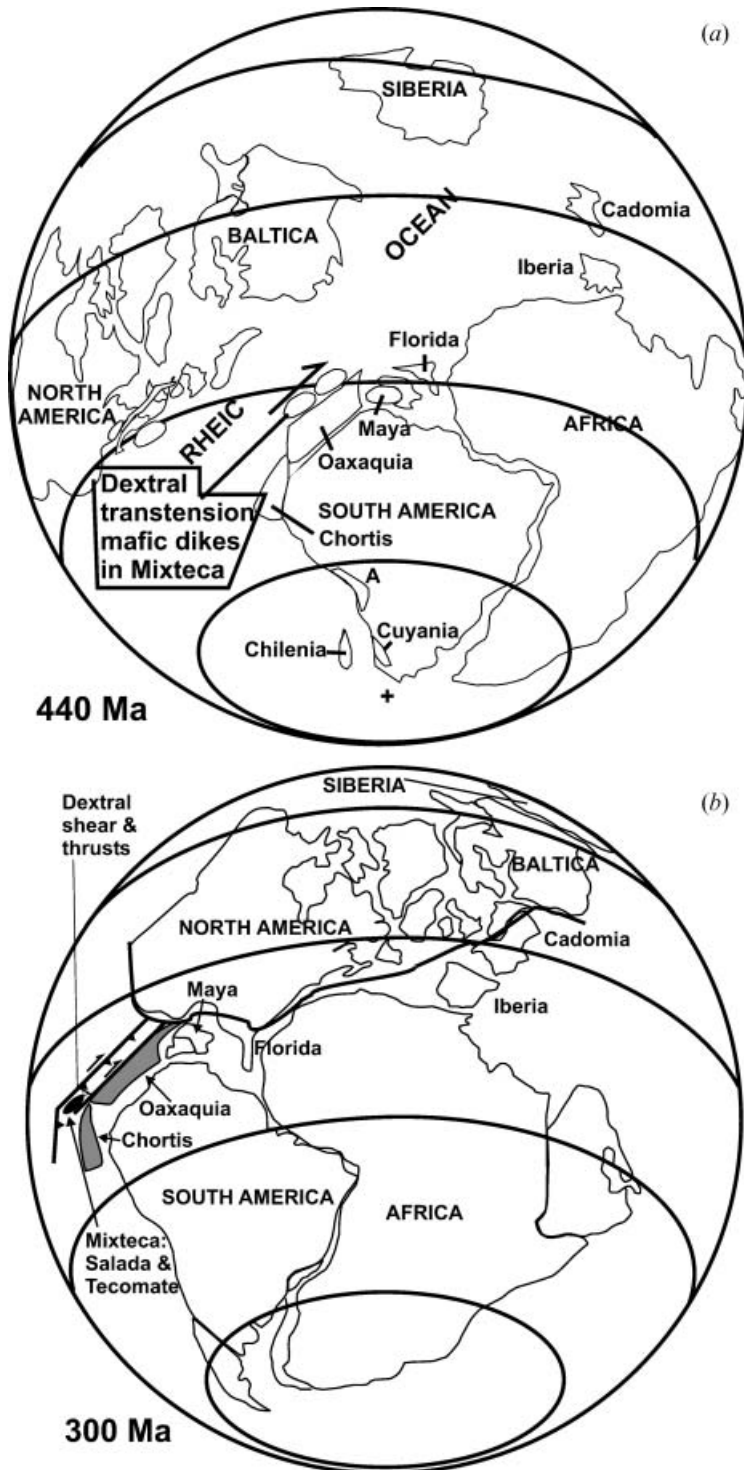


Figure 16. Palaeogeographic reconstructions for: (A) Ordovician-Silurian boundary at ca. 440 Ma (modified after Keppie 2004); and (B) Permo-Carboniferous reconstruction showing the Carboniferous extrusion and Middle Permian transtensional arc development on the western margin of Pangea (modified after Keppie *et al.* 2008a).

analyses, a CONACyT scholarship to MMG, and NSERC Discovery and Major Facilities Access grants to JKWL Doug Archibald is also thanked for his able assistance in the  $^{40}\text{Ar}/^{39}\text{Ar}$  laboratory.

## References

- Centeno-García, E., Mendoza-Rosales, C., and Silva-Romo, G., 2008, Sedimentología de la Formación Matzitzí (Paleozoico Superior) y significado de sus componentes volcánicos, región de Los Reyes Metzontla-San Luis Atolotitlán, Estado de Puebla: Revista Mexicana de Ciencias Geológicas (in press).
- Cerca, M., Ferrari, L., López-Martínez, M., Martiny, B., and Iriondo, A., 2007, Late Cretaceous shortening and early Tertiary shearing in the central Sierra Madre del Sur, southern Mexico: Insights into the evolution of the Caribbean–North American plate interaction: *Tectonics*, v. 26, TC3007, doi:10.1029/2006TC001981.
- Clark, A.H., Archibald, D.A., Lee, A.W., Farrar, E., and Hodgson, C.J., 1998, Laser Probe  $^{40}\text{Ar}/^{39}\text{Ar}$  ages of early- and Late-stage alteration assemblages, Rosario porphyry copper-molybdenum deposit, Collahuasi District, I Region, Chile: *Economic Geology*, v. 93, p. 326–337.
- Dewey, J.F., Robb, L., and Van Schalkwyk, L., 2006, Did Bushmanland extensionally unroof Namaqualand?: *Precambrian Research*, v. 150, p. 173–182.
- Elías-Herrera, M., and Ortega-Gutiérrez, F., 2002, Caltepec fault zone: An Early Permian dextral transpressional boundary between the Proterozoic Oaxacan and Paleozoic Acatlán complexes, southern Mexico, and regional implications: *Tectonics*, v. 21, no. (3), 1013, doi: 10.1029/200TC001278.
- Gómez-Tuena, A., Langmuir, C.H., Goldstein, S.L., Straub, S.M., and Ortega-Gutiérrez, F., 2007, Geochemical evidence for slab-melting in the Trans-Mexican Volcanic Belt: *Journal of Petrology*, v. 48, no. (3), p. 537–562.
- Keppie, J.D., 2004, Terranes of Mexico revisited: A 1.3 billion year odyssey: *International Geology Review*, v. 46, p. 765–794.
- Keppie, J.D., and Ramos, V.S., editors, 1999, *Odyssey of terranes in the Iapetus and Rheic Oceans during the Paleozoic*, in *Laurentia–Gondwana Connections Before Pangea*: Geological Society of America Special Paper, v. 336, p. 267–276.
- Keppie, J.D., Nance, R.D., Powell, J.T., Mumma, S.A., Dostal, J., Fox, D., Muise, J., Ortega-Rivera, A., Miller, B.V., and Lee, J.W.K., 2004a, Mid-Jurassic tectonothermal event superposed on a Paleozoic geological record in the Acatlán Complex of southern Mexico: hotspot activity during the breakup of Pangea: *Gondwana Research*, v. 7, p. 239–260.
- Keppie, J.D., Sandberg, C.A., Miller, B.V., Sánchez-Zavala, J.L., Nance, R.D., and Poole, F.G., 2004b, Implications of latest Pennsylvanian to Middle Permian paleontological and U–Pb SHRIMP data from the Tecolate Formation to re-dating tectonothermal events in the Acatlán Complex, southern Mexico: *International Geology Review*, v. 46, p. 745–754.
- Keppie, J.D., Nance, R.D., Fernández-Suárez, J., Storey, C.D., Jeffries, T.E., and Murphy, J.B., 2006, Detrital zircon data from the eastern Mixteca terrane, southern Mexico: evidence for an Ordovician-Mississippian continental rise and a Permo-Triassic clastic wedge adjacent to Oaxaquia: *International Geology Review*, v. 48, p. 97–111.
- Keppie, J.D., Dostal, J., Murphy, J.B., and Nance, R.D., 2008a, Synthesis and tectonic interpretation of the westernmost Paleozoic Variscan orogen in southern Mexico: from rifted Rheic margin to active Pacific margin: *Tectonophysics*, v. 461, p. 277–290.
- Keppie, J.D., Dostal, J., Miller, B.V., Ramos-Arias, M.A., Morales-Gámez, M., Nance, R.D., Murphy, J.B., Ortega-Rivera, A., Lee, J.W.K., Housh, T., and Cooper, P., 2008b, Ordovician-earliest Silurian rift tholeiites in the Acatlán Complex, southern Mexico: Evidence of rifting on the southern margin of the Rheic Ocean: *Tectonophysics*, v. 461, p. 130–156.

- Malone, J.W., Nance, R.D., Keppie, J.D., and Dostal, J., 2002, Deformational history of part of the Acatlán Complex: Late Ordovician-Early Silurian and Early Permian orogenesis in southern Mexico: *Journal of South American Earth Sciences*, v. 15, p. 511–524.
- Middleton, M., Keppie, J.D., Murphy, J.B., Miller, B.V., and Nance, R.D., 2007, P-T-t constraints on exhumation following subduction in the Rheic Ocean: Eclogitic Asis Lithodeme, Piaxtla Suite, Acatlán Complex, southern Mexico, in Linnemann, U., Nance, R.D., Zulaf, G., and Kraft, P., eds., *The evolution of the Rheic Ocean: From Avalonian-Cadomian active margin to Alleghenian-Variscan collision*: Geological Society of America, Special Paper 423, p. 489–509.
- Miller, B.V., Dostal, J., Keppie, J.D., Nance, R.D., Ortega-Rivera, A., and Lee, J.W.K., 2007, Ordovician calc-alkaline granitoids in the Acatlán Complex, southern Mexico: geochemical and geochronological data and implications for tectonic of the Gondwanan margin of the Rheic Ocean, in Linnemann, U., Nance, R.D., Zulaf, G., and Kraft, P., eds., *The Evolution of the Rheic Ocean: From Avalonian-Cadomian Active Margin to Alleghenian-Variscan Collision*: Geological Society of America Special Paper, v. 423, p. 465–475.
- Morales-Gámez, M., Keppie, J.D., and Norman, M., 2008, Ordovician-Silurian rift-passive margin on the Mexican margin of the Rheic Ocean overlain by Permian periarc rocks: evidence from the Acatlán Complex, southern Mexico: *Tectonophysics*, v. 461, p. 291–310.
- Murphy, J.B., Keppie, J.D., Nance, R.D., Miller, B.V., Dostal, J., Middleton, M., Fernández-Suárez, J., and Jefferies, T.E., 2006, Geochemistry and U-Pb protolith ages of eclogitic rocks of the Asis Lithodeme, Piaxtla Suite, Acatlán Complex, southern Mexico: Tectono-thermal activity along the southern margin of the Rheic Ocean: *Journal of the Geological Society (London)*, v. 163, p. 683–695.
- Nance, R.D., Miller, B.V., Keppie, J.D., Murphy, J.B., and Dostal, J., 2006, Acatlán Complex, southern Mexico: Record spanning the assembly and breakup of Pangea: *Geology*, v. 34, p. 857–860.
- Nance, R.D., Fernández-Suárez, J., Keppie, J.D., Storey, C., and Jeffries, T.E., 2007, Provenance of the Granjeno Schist, Ciudad Victoria, Mexico: Detrital zircon U-Pb age constraints and implications for Paleozoic paleogeography, in Linnemann, U., Nance, R.D., Zulaf, G., and Kraft, P., eds., *The evolution of the Rheic Ocean: From Avalonian-Cadomian active margin to Alleghenian-Variscan collision*: Geological Society of America, Special Paper 423, p. 437–452.
- Navarro-Santillan, D., Sour-Tovar, F., and Centeno-García, E., 2002, Lower Mississippian (Osagean) brachiopods from the Santiago Formation, Oaxaca, Mexico: Stratigraphic and tectonic implications: *Journal of South American Earth Sciences*, v. 15, no. (3), p. 327–336.
- Ortega-Gutiérrez, F., 1975, The pre-Mesozoic geology of the Acatlán area, south Mexico: [PhD thesis]: Leeds, Leeds University, 166 p.
- Ortega-Gutiérrez, F., Elías-Herrera, M., Reyes-Salas, M., Macias-Romo, C., and López, R., 1999, Late Ordovician-Early Silurian continental collision orogeny in southern Mexico and its bearing on Gondwana-Laurentia connections: *Geology*, v. 27, p. 719–722.
- Ramírez-Espinosa, J., 2001, Tectono-magmatic evolution of the Paleozoic Acatlán Complex in southern Mexico, and its correlation with the Appalachian system: [PhD thesis]: Tucson, AZ, University of Arizona, 170 p.
- Ramos-Arias, M.A., Keppie, J.D., Ortega-Rivera, A., and Lee, J.W.K., 2008, Extensional late Paleozoic deformation on the western margin of Pangea, Patlanoaya area, Acatlán Complex, southern Mexico: *Tectonophysics*, v. 448, p. 60–76.
- Sánchez-Zavala, J.L., Ortega-Gutiérrez, F., and Elías-Herrera, M., 2000, La orogenia Mixteca del Devónico del complejo Acatlán, sur de México: GEOS Unión Geofísica Mexicana, *Boletín Informativo Época II*, v. 20, no. (3), p. 321–322.
- Solari, L.A., Torres de León, R., Hernández Pineda, G., Solé, J., Solís-Pichardo, G., and Hernández-Treviño, T., 2007, Tectonic significance of Cretaceous-Tertiary magmatic

- and structural evolution of the northern margin of the Xolapa Complex, Tierra Colorado area, southern Mexico: Geological Society of America Bulletin, v. 119, p. 1265–1279.
- Talavera-Mendoza, O., Ruiz, J., Gehrels, G.E., Meza-Figueroa, D.M., Vega-Granillo, R., and Campa-Uranga, M.F., 2005, U–Pb geochronology of the Acatlán Complex and implications for the Paleozoic paleogeography and tectonic evolution of southern Mexico: *Earth and Planetary Science Letters*, v. 235, p. 682–699.
- Talavera-Mendoza, O., Ruiz, J., Gehrels, G.E., Meza-Figueroa, D.M., Vega-Granillo, R., and Valencia, V.A., 2006, Reply to comment on ‘U–Pb geochronology of the Acatlán Complex and implications for the Paleozoic paleogeography and tectonic evolution of southern Mexico’ by Talavera *et al.*: *Earth and Planetary Science Letters*, v. 245, p. 476–480.
- Tolson, G., 2007, The Chacalapa Fault, southern Oaxaca, Mexico, in Nieto-Samaniego, A.F., ed., *Geology of Mexico, Celebrating the Centenary of the Geological Society of Mexico*: Geological Society of America Special Paper, v. 422, p. 343–357.
- Torres, R., Ruiz, J., Patchett, P.J., and Grajales-Nishimura, J.M., 1999, Permo-Triassic continental arc in eastern Mexico, tectonic implications for reconstructions of southern North America, in Bartolini, C., Wilson, J.L., and Lawton, T.F., eds., *Mesozoic Sedimentary and Tectonic History of North-central Mexico*: Geological Society of America Special Paper, v. 340, p. 191–196.
- Vega-Granillo, R., Talavera-Mendoza, O., Meza-Figueroa, D., Ruiz, J., Gehrels, G.E., López-Martínez, M., and de La Cruz-Vargas, J.C., 2007, Pressure-temperature-time evolution of Paleozoic high-pressure rocks of the Acatlán Complex (southern Mexico): Implications for the evolution of the Iapetus and Rheic Oceans: *Geological Society of America Bulletin*, v. 119, p. 1249–1264.
- Venkat-Ramani, M., and Tikoff, B., 2002, Physical models of transtensional folding: *Geology*, v. 30, p. 523–526.
- Weber, R., 1997, How old is the Triassic flora of Sonora and Tamaulipas and news on Leonardian flora in Puebla and Hidalgo, Mexico: *Revista Mexicana de Ciencias Geológicas*, v. 14, p. 225–243.
- Yañez, P., Ruiz, J., Patchett, P.J., Ortega-Gutiérrez, F., and Gehrels, G.E., 1991, Isotopic studies of the Acatlan complex, southern Mexico: implications for North American tectonics: *Geological Society of America Bulletin*, v. 103, p. 817–827.



# Ordovician–earliest Silurian rift tholeiites in the Acatlán Complex, southern Mexico: Evidence of rifting on the southern margin of the Rheic Ocean

J. Duncan Keppie <sup>a,\*</sup>, Jaroslav Dostal <sup>b</sup>, Brent V. Miller <sup>c</sup>, M.A. Ramos-Arias <sup>a</sup>,  
Miguel Morales-Gámez <sup>a</sup>, R. Damian Nance <sup>d</sup>, J. Brendan Murphy <sup>e</sup>,  
Amabel Ortega-Rivera <sup>f</sup>, J.W.K. Lee <sup>h</sup>, T. Housh <sup>g</sup>, P. Cooper <sup>b</sup>

<sup>a</sup> Departamento de Geología Regional, Instituto de Geología, Universidad Nacional Autónoma de México, 04510 México D.F., México

<sup>b</sup> Department of Geology, St. Mary's University, Halifax, Nova Scotia, Canada B3H 3C3

<sup>c</sup> Department of Geology and Geophysics, Texas A&M University, College Station, Texas 77843, USA

<sup>d</sup> Department of Geological Sciences, 316 Clippinger Laboratories, Ohio University, Athens, Ohio 45701, USA

<sup>e</sup> Department of Earth Sciences, St. Francis Xavier University, Antigonish, Nova Scotia, Canada B2G 2W5

<sup>f</sup> Instituto de Geología, Universidad Nacional Autónoma de México, Estación Regional del Noroeste, Apartado Postal 1039, Hermosillo, Sonora 83000, México

<sup>g</sup> Department of Geology, Queen's University, Kingston, Ontario, Canada K7L3NG

<sup>h</sup> Department of Geological Sciences, 1 University Station, C-1100, The University of Texas, Austin, Texas 78712-0254, USA

Received 14 May 2007; received in revised form 31 October 2007; accepted 26 January 2008

Available online 7 February 2008

## Abstract

The Acatlán Complex of southern Mexico is a vestige of a Paleozoic Ocean inferred to be either the Cambro-Ordovician Iapetus and/or the Ordovician-Carboniferous Rheic oceans. Ordovician granitoids in the complex have been interpreted as either the products of dehydration melting, arc or rift magmatism, however, the geochemistry of felsic rocks is inconclusive. The geochemistry of a recently discovered, major, Ordovician–earliest Silurian mafic igneous suite associated with these granitoids is critical to defining the tectonic setting of the igneous event, and to paleogeographic reconstructions. Such data from three areas in the Acatlán Complex (Xayacatlán, Patlanoaya, and Cuauhtle) document tholeitic, within-plate characteristics with a source in either primitive mantle or mantle previously modified by subduction-related magmatism possibly combined with crustal contamination. This, combined with their occurrence as a dike swarm intruding rift-passive margin clastic sedimentary rocks, indicates rifting of a continental margin. Mafic dikes at Xayacatlán yielded a concordant U–Pb TIMS zircon age of  $442 \pm 1$  Ma and a  $^{40}\text{Ar}/^{39}\text{Ar}$  hornblende plateau age of  $434 \pm 3$  Ma. The age of mafic magmatism at other localities is defined by the ages of associated granitoids intruded at ca. 461 Ma and by the age of the youngest detrital zircon in the host rocks:  $496 \pm 25$  Ma at Patlanoaya. Previously published age data suggest that this igneous event may have started earlier at  $478 \pm 5$  Ma (Early Ordovician). Although the life spans of the Iapetus and Rheic oceans overlap during the Ordovician, subduction and collision characterize the former, whereas the latter was in a rift–drift mode. Thus, this Ordovician–earliest Silurian magmatism is more consistent with rifting along the southern margin of the Rheic Ocean. Initiation of rifting at ca. 480 Ma is contemporaneous with separation of peri-Gondwanan terranes, such as Avalonia and Carolina, from Amazonia–Oaxaquia. Subsequent rifting may be analogous to Mesozoic–Cenozoic western North America where transtensional deformation is related to dispersal of terranes (e.g. Baja California and Cretaceous Baja British Columbia) leading to a gradual collapse of the inboard continental margin.

© 2008 Elsevier B.V. All rights reserved.

**Keywords:** Acatlán Complex; Mexico; Ordovician; Geochemistry; Geochronology; Rifting

## 1. Introduction

\* Corresponding author. Tel.: +52 555 622 4290.

E-mail address: [duncan@servidor.unam.mx](mailto:duncan@servidor.unam.mx) (J.D. Keppie).

The Mixteca terrane of southern Mexico is made up of the Acatlán Complex (Fig. 1a) and records the vestiges of a Paleozoic

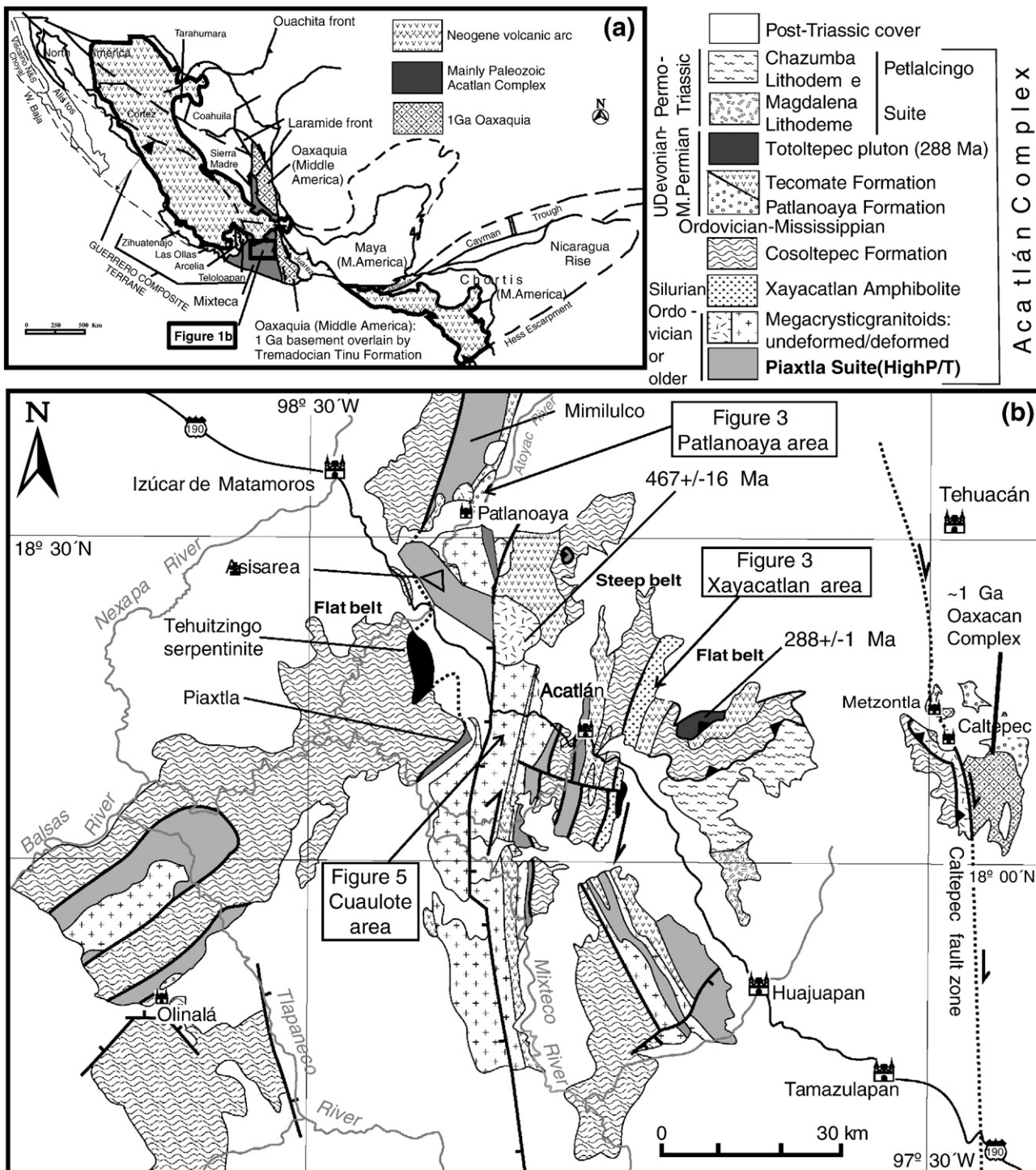


Fig. 1. (a) Terrane map of Mexico (after Keppe, 2004) showing the location of the Acatlán Complex and (b) geological map of the Acatlán Complex (modified after Ortega-Gutiérrez et al., 1999) showing the locations of Figs 3, 4 and 5.

ocean that has been variously ascribed to either the Iapetus Ocean (Ortega-Gutiérrez et al., 1999), the Rheic Ocean (Keppe and Ramos, 1999), or the Baie Verte Seaway, Iapetus and Rheic oceans (Talavera-Mendoza et al., 2005; Vega-Granillo et al., 2007). Critical to this debate is the origin of ubiquitous Ordovician megacrystic granitoids in the complex. These granitoids were previously interpreted to be the result of either dehydration melting (Ortega-Gutiérrez et al., 1999) or arc

magmatism (Talavera-Mendoza et al., 2005; Vega-Granillo et al., 2007), however, Miller et al. (2007) indicate that their calc-alkaline characteristics could result from either arc magmatism or melting of a calc-alkaline source. Some of the granitoids are associated with retrograde eclogite facies rocks of the Piaxtla Suite (Esperanza granitoids and Xayacatlán Formation) that have been interpreted as ophiolites. The high pressure (HP) metamorphism in the Piaxtla Suite has been interpreted in

terms of subduction, followed by exhumation that triggered dehydration melting, during the late Ordovician to Early Silurian ( $440 \pm 14$  Ma; U–Pb lower intercept zircon age of the type Esperanza granitoid: Ortega-Gutiérrez et al., 1999). Although Vega-Granillo et al. (2007) argue for three, Ordovician–Silurian, periods of HP metamorphism, all direct dating of both eclogite and blueschist facies metamorphism in the Piaxtla Suite has so far yielded Mississippian ages (Middleton et al., 2007; Elías-Herrera et al., 2007; Keppie et al., submitted for publication), and so cannot be genetically related to the Ordovician granitoids. Furthermore, some rocks that were included in the Piaxtla Suite, such as the type area of the Xayacatlán Formation, do not appear to have undergone eclogite facies metamorphism (Morales-Gámez et al., 2008). On the other hand, mafic igneous rocks associated with these granitoids indicate a bimodal suite intruded during Ordovician rifting of a continental margin and form the topic of this paper. These data are fundamental to Paleozoic continental reconstructions in this paper and Keppie et al. (2008).

## 2. Geological setting

The Acatlán Complex is juxtaposed on its eastern side against the ~1 Ga Oaxacan Complex of the Oaxaquia terrane (Fig. 1b) along a Permian dextral flower structure where syntectonic migmatites have yielded an age of  $276 \pm 1$  Ma, i.e. Early Permian (Elías-Herrera and Ortega-Gutiérrez, 2002). The ~1 Ga rocks of southern and central Mexico belong to the Middle American microcontinent (Keppie et al., 2004a,b), which was fringed by Paleozoic passive margin and oceanic sequences, one of which is the Acatlán Complex (Fig. 1a).

Knowledge of the geological history of the Acatlán Complex has undergone rapid changes in recent years largely due to a rapidly improving geochronological and fossil database

(Ortega-Gutiérrez et al., 1999; Elías-Herrera and Ortega-Gutiérrez, 2002; Vachard and Flores de Dios, 2002; Keppie et al., 2004a,b, 2006; Sánchez-Zavala et al., 2004; Talavera-Mendoza et al., 2005; Nance et al., 2006, 2007; Murphy et al., 2006; Miller et al., 2007; Middleton et al., 2007; Elías-Herrera et al., 2007; Vega-Granillo et al., 2007; Morales-Gámez et al., 2008; Ramos-Arias et al., 2008). As these changes have been recently reviewed by Nance et al. (2006, 2007, submitted for publication), and Keppie et al. (2008) only a summary of the revised geological history is presented here (Fig. 2):

- (1) Ordovician deposition of a rift-passive margin sequence accompanied by intrusion of megacrystic granitoids with a source in ca. 1 Ga basement, probably the Oaxacan Complex;
- (2) Latest Devonian–Triassic events on the western margin of Pangea:
  - (i) Latest Devonian (Strunian)–Middle Permian deposition of periacr rocks;
  - (ii) Latest Devonian–Mississippian exhumation of blueschist-eclogitic rocks, dehydration migmatization and polyphase deformation of the high pressure rocks during E–W extension that juxtaposes them with low grade cover rocks;
  - (iii) Permian intrusion of arc-related plutons;
  - (iv) Permo-Triassic dextral, N–S shearing accompanied by S-vergent thrusting triggering the deposition of a clastic wedge;
- (3) Mesozoic deposition of a shelf-clastic wedge sequence followed by deposition of Cenozoic arc-related rocks.

In this paper, we present geochronological and geochemical data for several Ordovician mafic igneous suites and associated host rocks, which indicate that they are a rift-related suite

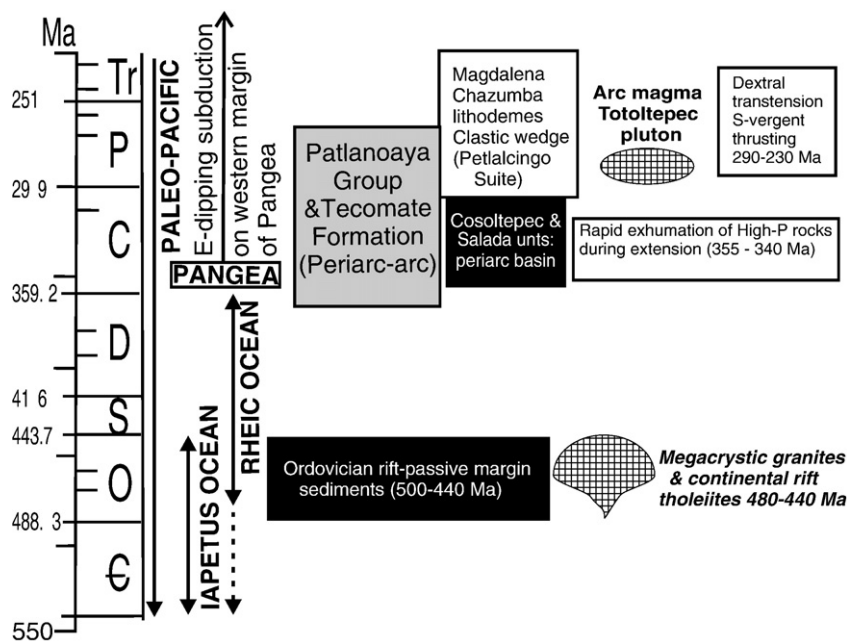


Fig. 2. Time and space diagram showing the geological history of the Acatlán Complex.

temporally connected with intrusion of megacrystic granitoids. Our data are then applied to Ordovician paleogeographic reconstructions, in which rifting is more compatible with

opening of the Rheic Ocean than closing of the Iapetus Ocean and Baie Verte Seaway (see also Nance et al., 2006, 2007, submitted for publication; Keppe et al., 2008).

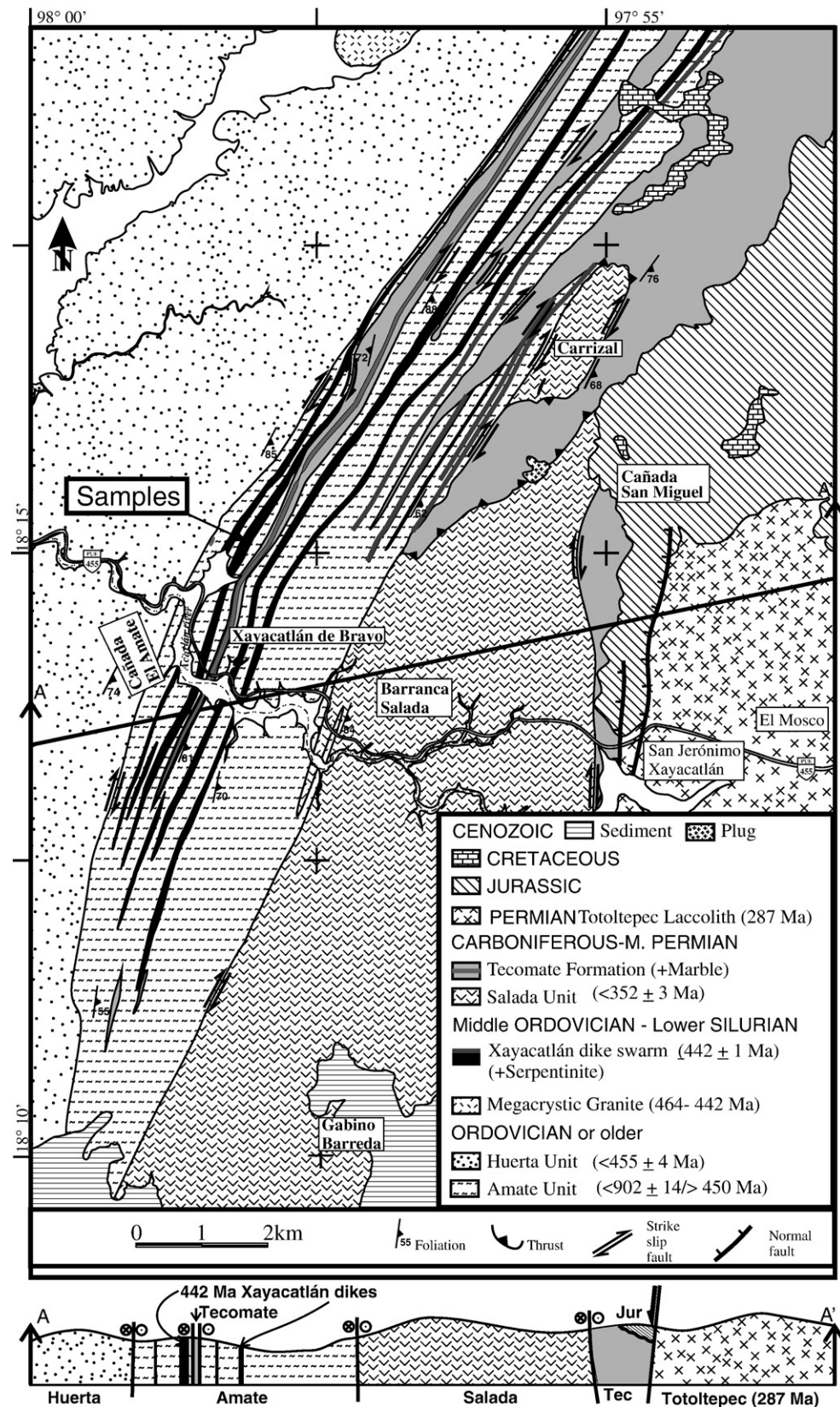


Fig. 3. Geological map of the Xayacatlán area showing sample locations.

## 2.1. Xayacatlán area

In the Xayacatlán area, a fault block exposes metaigneous and metasedimentary rocks (Fig. 3). The mafic metaigneous units (originally designated part of the Xayacatlán Formation by Ortega-Gutiérrez, 1975) consist of a dike swarm of vertical, N–S trending, amphibolites and amphibolitic gabbros that have been variably affected by retrograde metamorphism resulting in chlorite schists and serpentinites (Fig. 3). In view of this, the metaigneous component has been redesignated as the Xayacatlán dike swarm, whereas the metasedimentary rocks are included in a new unit, the Amate Unit (Morales-Gámez et al., 2008). The widest dike (~100 m) contains the least altered rocks. It consists predominantly of a coarse grained, foliated amphibolitic gneiss and is layered with bands varying from ultramafic through amphibolitic to leucogabbroic (mainly plagioclase). The gneiss is intruded by deformed mafic and felsic sheets that also contain the foliation present in the amphibolitic gneiss. These dikes intrude clastic metasedimentary rocks metamorphosed under greenschist facies conditions

that rise to amphibolite facies in contact aureoles (Morales-Gámez et al., 2008).

This fault block is bounded to the west by pelites and psammites (Ordovician Huerta Unit), and to the east by interbedded pelite and psammite intruded by mafic volcanic rocks (Carboniferous Salada Unit) (Fig. 3). The Huerta and Amate units are intruded by pegmatites and granite dikes that range in age from ca. 464 to 442 Ma (Morales-Gámez et al., 2008). The Permo-Carboniferous Tecolate Formation is thrust over and sliced into the central fault block (Fig. 3). All of the rocks show evidence of dextral shearing under greenschist facies metamorphic conditions that induced grain-size reduction.

The fresh amphibolitic gabbros of the widest dike of the Xayacatlán dike swarm consist almost exclusively of amphibole and plagioclase ( $An_{15-20}$ ) with accessory opaques. The amphibole is brownish green to brown hornblende, with distinct pleochroism. Its elongated crystals range in size usually from 0.1 mm to ~3 mm. Amphiboles from various types of amphibolites and amphibolitic gneisses show no significant differences in composition. Thus, variations within a single sample are similar to the variations among the various types of amphibolite. The amphibole mainly corresponds to magnesio-hornblende to edenite (Fig. 4). The composition is typical of amphibole from amphibolite facies rocks and resembles amphibole of the Dalradian metamorphic suites (i.e. medium pressure–medium temperature: Fig. 4d). The mineral assemblage is partially altered to the retrograde greenschist facies assemblage of tremolite–chlorite–calcite. Amphibole is locally replaced by tremolite whereas plagioclase is replaced by fine-grained sericite. The ultramafic bands consist almost entirely of amphibole, whereas the leucocratic bands consist mainly of plagioclase. The granitic sheets contain quartz, K-feldspar, and accessory minerals.

## 2.2. Patlanoaya area

In the Patlanoaya area (Fig. 5) fossiliferous, uppermost Devonian–Middle Permian rocks (Patlanoaya Group) and unconformably underlying Ojo de Agua Unit (meta-pelites intruded by rare mafic sheets) are faulted against the Mal Paso Unit (low grade sandstone, conglomerate, and slate) (Ramos-Arias et al., 2008). The Mal Paso Unit is cut by the  $461 \pm 2$  Ma megacrystic Palo Liso granite (concordant U–Pb zircon age: Miller et al., 2007). The Palo Liso granite is bordered along its western margin by a thin mafic selvage inferred to be the first stage of intrusion by a stoping mechanism. It consists of plagioclase (albite), hornblende, epidote, chlorite, sericite, calcite, and haematite. The western side of the Palo Liso granite is inferred to be intrusive into clastic rocks of the Otate Unit consisting mainly of low grade psammites and pelites. This latter unit rests unconformably upon the Las Minas Unit, which is made up of low grade psammitic rocks with thin pelitic interbeds that are cut by a mafic dike swarm (Ramos-Arias et al., 2008). The youngest detrital zircon in the Las Minas Unit is  $496 \pm 25$  Ma (see below and Fig. 5), thus bracketing its deposition and intrusion of the mafic dikes within the Ordovician. The Las Minas Unit lies above an easterly dipping listric shear zone, below which is a deformed megacrystic

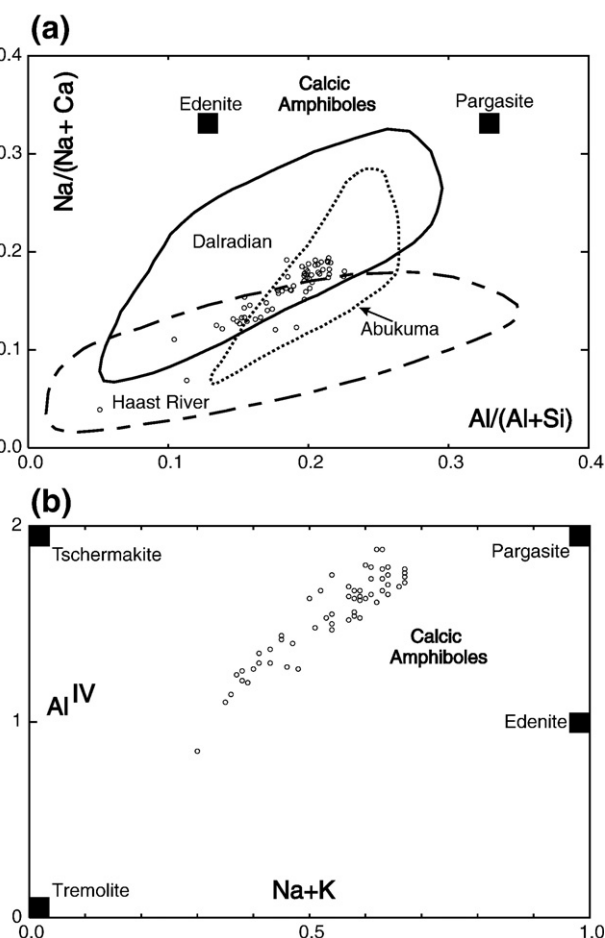


Fig. 4. Analyses of calcic amphiboles from the Xayacatlán gabbroic dike plotted on: (a)  $Na/(Na+Ca)$  versus  $Al/(Al+Si)$ ; envelopes show the composition for medium-pressure and low-pressure amphiboles from Dalradian (Scotland), Haast River (New Zealand) and Abukuma (Japan), respectively (Laird and Albee, 1981; Caredda et al., 2001); and (b) the  $Al^{IV}$  versus  $(Na+K)$  atoms plot (after Caredda et al., 2001); solid squares represent amphibole-end members.

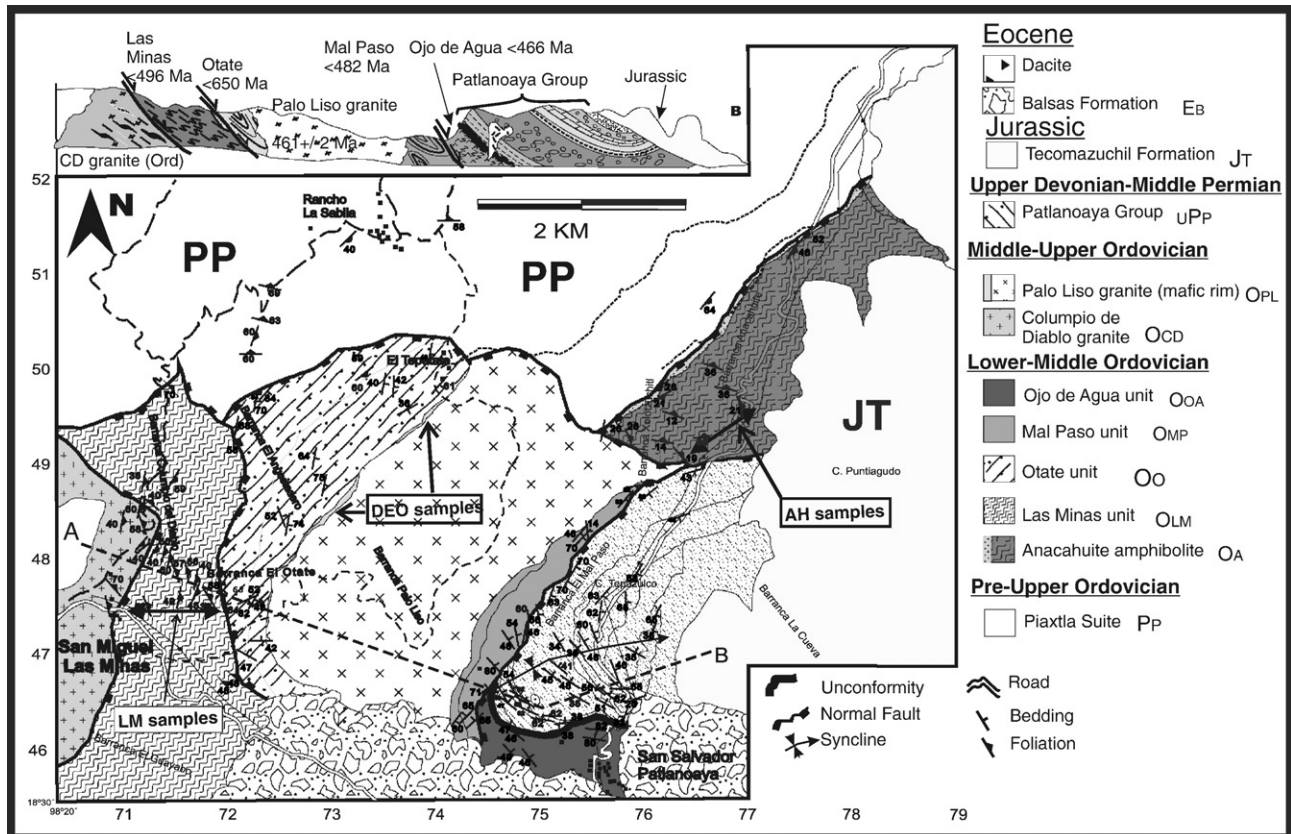


Fig. 5. Geological map of the Patlanoaya area showing sample locations.

granite: a leucogranite dike inferred to have emanated from this granite cuts the Las Minas Unit. A nearby dike has yielded a mean  $^{206}\text{Pb}/^{238}\text{U}$  LA-ICPMS zircon age of  $460 \pm 9$  Ma (Vega-Granillo, 2006). The mafic minor intrusives in the Las Minas Unit generally contain aligned chlorite, quartz, altered plagioclase, and opaques occasionally accompanied by muscovite, amphibole and apatite. The dominant foliation is defined by

amphibole and chlorite. This assemblage suggests lower greenschist facies metamorphic conditions, a conclusion consistent with the quartz–muscovite–chlorite association in the host metasedimentary rocks.

An amphibolite (Anacahuite Amphibolite) is in fault contact with the all of the low grade units to the south (Fig. 5). It is cut by deformed megacrystic granite sheets, also inferred to be

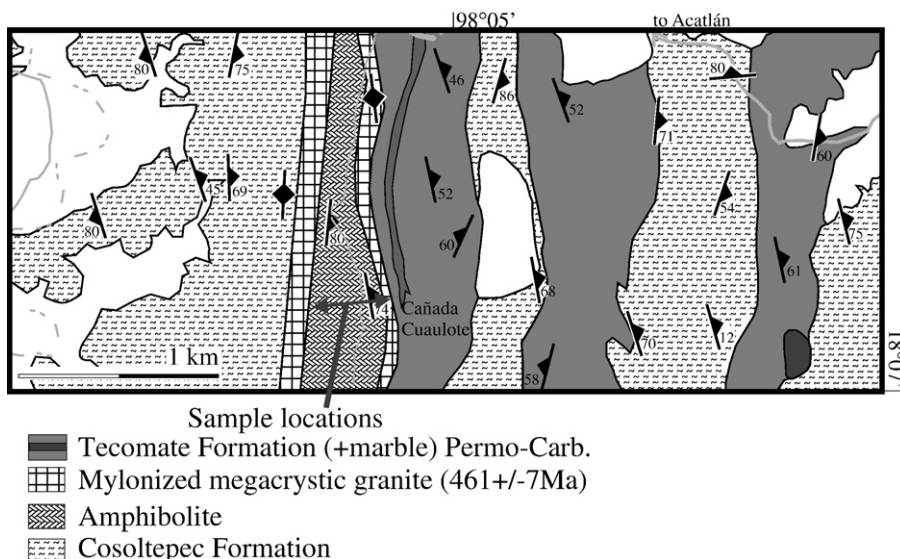


Fig. 6. Geological map of the Cuauilate area showing sample locations.

comagmatic with the other Ordovician megacrystic granites. The Anacahuite Amphibolite consists mainly of aligned blue-green amphibole defining a prominent foliation, plagioclase, epidote, and quartz, with accessory titanite and opaque minerals. It also contains occasional relict pyroxene and plagioclase phenocrysts, with biotite, and chlorite generally localized along kink bands. This mineral assemblage indicates peak metamorphic conditions reached upper greenschist to lower amphibolite facies.

### 2.3. Cuaujote area

In the Cañada el Cuaujote (Fig. 6), low grade, strongly to mildly deformed, nearly vertical and N–S striking pelites, psammites, marbles and conglomerates of the Tecomate Formation lie disconformably upon a deformed megacrystic granite dated at  $461 \pm 7$  Ma (mean of 13  $^{206}\text{Pb} / ^{238}\text{U}$  LA-ICPMS zircon analyses: Talavera-Mendoza et al., 2005). This granite cuts foliated amphibolites, which have been correlated with the Xayacaltán Formation by Ortega-Gutiérrez et al. (1999). The youngest detrital zircons in the Tecomate Formation yielded LA-ICPMS ages of  $\sim 455 \pm 5$  Ma (Sánchez-Zavala et al., 2004), suggesting that they were derived from the underlying granite: this is consistent with the presence of granite pebbles at the base of the Tecomate Formation. The amphibolite consists mainly of amphibole with minor plagioclase, biotite, chlorite and opaques minerals, whereas the mylonitic granitic rocks are made up of quartz, feldspar, biotite and accessory minerals.

## 3. U–Pb geochronology

### 3.1. Analytical methods

One amphibolitic gneiss sample was collected from the widest Xayacatlán dike for U–Pb analysis (XAY-3; Fig. 3). The sample was crushed and zircons were separated using standard techniques (e.g., Ratajeski et al., 2001). Zircon grains were carefully hand-picked in an effort to select clear, well-faceted,

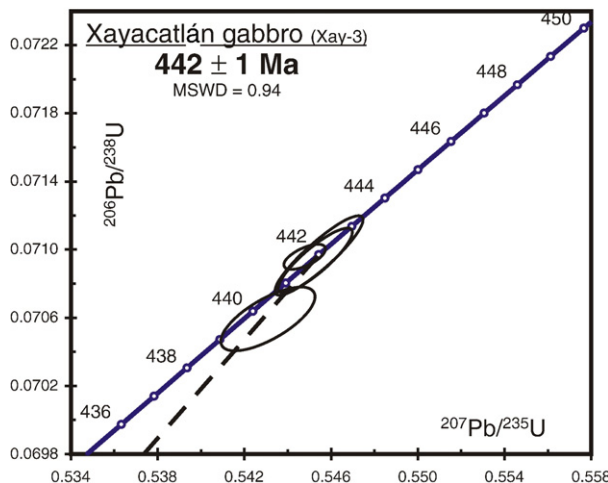


Fig. 7. U–Pb TIMS data from zircons amphibolitic gneiss sample XAY-3 of the Xayacatlán Suite plotted on a concordia diagram.

Table 1  
U–Pb TIMS zircon analyses from the Xayacatlán dike

Analysis#, fraction (number of grains)	Weight (mg) <sup>a</sup>	Total <sup>a</sup> U (mg)	Total <sup>b</sup> Pb (pg)	U (ppm)	Pb (ppm)	Atomic ratios		Ages (Ma)		Rho <sup>c</sup>								
						$^{206}\text{Pb} / ^{238}\text{U}$	$^{206}\text{Pb} / ^{235}\text{U}$	$^{207}\text{Pb} / ^{238}\text{U}$	$^{207}\text{Pb} / ^{235}\text{U}$									
<i>Xayacatlán granite (sample XAY-3; N18°15'.150, W97°58.287)</i>																		
1) Medium prismatic (1)	0.001	1.68	113.0	1.61	1678	113	4719	20.899	0.07096	0.270	0.54541	0.303	0.05575	0.132	441.9	442.0	442.3	0.90
2) Large prismatic (1)	0.001	2.80	218.8	1.60	2802	219	7919	4.493	0.07095	0.085	0.54477	0.144	0.05569	0.112	441.9	441.6	439.9	0.63
3) Large prismatic (1)	0.001	3.20	254.3	1.75	3205	254	8313	4.107	0.07093	0.220	0.54524	0.256	0.05575	0.127	441.8	441.9	442.4	0.87
4) Flat hexagonal (1)	0.001	1.41	115.3	1.34	1407	115	4744	3.422	0.07058	0.218	0.54306	0.327	0.05580	0.234	439.7	440.4	444.4	0.70

<sup>a</sup> Weight estimated from measured grain dimensions and assuming density = 4.67 g/cm<sup>3</sup>, ~20% uncertainty affects only U and Pb concentrations.

<sup>b</sup> Corrected for fractionation (0.12 ± 0.08% amu — Faraday-Daly; 0.20 ± 0.1% amu — Daly) and spike.

<sup>c</sup> Corrected for fractionation, blank, and initial common Pb.

<sup>d</sup> ID-TIMS errors are 2-sigma.

<sup>e</sup>  $^{207}\text{Pb} / ^{235}\text{U} - ^{206}\text{Pb} / ^{238}\text{U}$  correlation coefficient of Ludwig (1989).

acicular grains without inclusions or obvious inherited cores. These grains are commonly interpreted as igneous phenocrysts. Selected zircon grains were mounted in epoxy, polished, imaged in cathodoluminescence and photographed under reflected light, then gold-coated prior to analysis.

As the mafic rocks in the Patlanoaya area do not contain zircon, their age may be bracketed between the youngest detrital zircon in the host rock and the age of cross-cutting granitic rocks. One psammite sample from each of the Las Minas, Ocate, Mal Paso, and Ojo de Agua units was collected for LA-ICPMS U–Pb analyses of their detrital zircon populations at the University of Texas at Austin, Texas (Fig. 5). Procedures used are described in Jones and Connelly (2006). In quoting the ages obtained, the  $^{206}\text{Pb}/^{238}\text{U}$  age is used for ages  $<1000$  Ma, whereas the  $^{207}\text{Pb}/^{206}\text{Pb}$  ages are used for those  $>1000$  Ma.

### 3.2. Results

The four analyses of the amphibolitic gneiss from the widest Xayacatlán dike (XAY-3: N18°15.150, W97°58.287) yielded two concordant results with an age of  $442 \pm 1$  Ma (Fig. 7; Table 1), which is interpreted as the time of intrusion.

158 analyses of detrital zircon ages from the psammite sample of the Las Minas Unit (LM-10: N18°31.070', W98°19.649') range from  $432 \pm 21$  Ma to  $3067 \pm 42$  Ma (Table 2) with age probability peaks at  $\sim 600$  Ma, 900 Ma, 1200 Ma, and 1550 Ma (Fig. 8a). The youngest concordant zircon has a  $^{206}\text{Pb}/^{238}\text{U}$  age of  $496 \pm 25$  Ma, which provides an older limit for the time of deposition.

127 analyses of detrital zircons from the Ocate sandstone sample (OT-1: N18°31.087', W98°18.956') range from  $649 \pm 28$  Ma (the youngest concordant zircon) to  $1619 \pm 49$  Ma (Table 2) with age probability peaks at  $\sim 980$  Ma, and 1210 Ma (Fig. 8b). The  $\sim 650$  Ma age provides an older limit for the time of deposition, however, as it lies unconformably upon the Las Minas Unit it must have been deposited after  $496 \pm 25$  Ma.

71 analyses of detrital zircons from semipelitic schist of the Mal Paso Unit (SSP-1: N18°30.667', W98°17.778') range from  $389 \pm 18$  Ma to  $1586 \pm 28$  Ma (Table 2) with age probability peaks at  $\sim 520$  Ma,  $\sim 750$  Ma, and 1200 Ma (Fig. 8c). As none of the analyses is exactly concordant, the three youngest  $^{206}\text{Pb}/^{238}\text{U}$  ages with overlapping errors were averaged to give an age of  $482 \pm 25$  Ma.

59 analyses of detrital zircons from siltstone of the Ojo de Agua Unit (SSP-2: N18°31.827', W98°16.620') range from  $452 \pm 23$  Ma to  $1987 \pm 47$  Ma (Table 2) with age probability peaks at  $466 \pm 25$  Ma,  $\sim 700$  Ma, and 1100 Ma (Fig. 8d). The youngest probability peak is taken to provide an older limit on the time of deposition.

### 3.3. Provenance of detrital zircons

All of the detrital zircon samples have peaks between 900 and 1200 Ma (Fig. 8), which, since they coincide with the tectonothermal events in the adjacent Oaxacan Complex, indicate a local source (Keppe et al., 2001, 2003; Solari et al., 2003). The younger zircons show age peaks that vary

from one unit to another: (a) the ca. 600 Ma peak in the Las Minas Unit is absent in the unconformably overlying Ocate Unit; (b) a ca. 700–750 Ma peak is present in both the Mal Paso and Ojo de Agua units; and (c) a ca. 520 Ma peak is only present in the Mal Paso Unit. These contrasts suggest somewhat different sources for each of the units, which corroborate their separation into different map units. The source of the Neoproterozoic zircons is inferred to have been either in Brasiliano and/or Pan-African orogens in northwestern Gondwana (Amazonia, northwest Africa, Florida and Yucatan basements) or in Avalonia and Carolina that are inferred to have separated from Oaxaca in the early Ordovician (Keppe, 2004). There are also a few concordant ages between 800 and 900 Ma in each of these units (Table 2), whose provenance may only be found in the Goiás magmatic arc presently lying on the eastern side of Amazonia (Keppe et al., 2008).

## 4. $^{40}\text{Ar}/^{39}\text{Ar}$ geochronology

### 4.1. Analytical methods

Amphibole was separated from a sample of an amphibolite dike cutting the thickest Xayacatlán amphibolitic gneiss dike (XAY-13: N18°15.150, W97°58.275; Fig. 3). It was pre-treated and concentrated by standard techniques and then amphibole was selected by handpicking under a binocular microscope from fractions that ranged in size from 40 to 60 mesh at the mineral separation laboratory at UNICIT-Universidad Nacional Autónoma de México, Campus-Juriquilla, Querétaro, Qro. Mineral separates were loaded into Al-foil packets and irradiated together with Hb3GR as a neutron-fluence monitor at the McMaster Nuclear Reactor (Hamilton, Ontario, Canada).  $^{40}\text{Ar}/^{39}\text{Ar}$  analyses were performed by standard laser step-heating techniques described in detail by Clark et al. (1998) at the Geochronology Research Laboratory of Queen's University, Kingston, Ontario, Canada. The data are given in Table 3 and plotted in Fig. 9. All data have been corrected for blanks, mass discrimination, and neutron-induced interferences. For the purposes of this paper, a plateau age is obtained when the apparent ages of at least three consecutive steps, comprising a minimum of 70% of the  $^{39}\text{Ar}_k$  released, agree within  $2\sigma$  error with the integrated age of the plateau segment. Errors shown in Table 3 and on the age spectrum and isotope-correlation diagrams represent the analytical precision at  $\pm 2\sigma$ .

### 4.2. Results

The Xayacatlán amphibole yielded discordant data with a plateau age of  $434 \pm 3$  Ma in the two upper temperature steps representing 73% of the  $^{39}\text{Ar}$  released (Fig. 9, Table 3). The lower temperature increments show progressively younger ages stepping down to  $\sim 250$ – $210$  Ma. Using the grain size of the analyzed amphiboles and a  $25$  °C/my cooling rate, we estimate that the ca. 434 Ma plateau age represents a closure temperature of  $570 \pm 10$  °C (Harrison et al., 1985). On the other hand, the ca. 250–200 Ma age probably represents a subsequent thermal perturbation.

Table 2

U–Pb LA-ICPMS zircon analyses from psammites in the Patlanoaya area

Sample analysis	$^{207}\text{Pb}^*/^{206}\text{Pb}^*$	$\pm t\sigma$	$^{207}\text{Pb}^*/^{235}\text{U}$	$\pm t\sigma$	$^{206}\text{Pb}^*/^{238}\text{U}$	$\pm t\sigma$	Hg-Corr	$^{206}\text{Pb}^*/^{204}\text{Pb}$	$^{207}\text{Pb}^*/^{235}\text{U}$	age (Ma)	$\pm t\sigma$ (95% Conf)	$^{206}\text{Pb}^*/^{238}\text{U}$	age (Ma)	$\pm t\sigma$ (95% Conf)	$^{207}\text{Pb}^*/^{206}\text{Pb}^*$	age (Ma)	$\pm t\sigma$ (95% Conf)	% discord.	Rho
<i>LM-10</i>																			
A01	0.0818	0.0022	1.747	0.114	0.1549	0.0085	15,288		1026		$\pm 42$	928		$\pm 47$	1240		$\pm 52$	10.51	0.8922
A02	0.0608	0.0017	0.804	0.051	0.0958	0.0050	8045		599		$\pm 28$	590		$\pm 29$	633		$\pm 61$	1.52	0.8516
A03	0.1767	0.0059	7.395	0.639	0.3035	0.0209	27,414		2160		$\pm 77$	1709		$\pm 104$	2622		$\pm 56$	-15.60	0.8870
A04	0.0813	0.0022	1.730	0.112	0.1544	0.0085	18,772		1020		$\pm 42$	926		$\pm 47$	1228		$\pm 52$	10.16	0.8932
A05	0.0949	0.0025	2.295	0.169	0.1754	0.0112	10,500		1211		$\pm 52$	1042		$\pm 61$	1526		$\pm 50$	-15.54	0.9058
A06	0.0884	0.0025	1.197	0.079	0.0982	0.0053	1697		799		$\pm 37$	604		$\pm 31$	1392		$\pm 54$	32.38	0.7982
A07	0.1496	0.0040	5.911	0.474	0.2865	0.0197	14,104		1963		$\pm 70$	1624		$\pm 99$	2342		$\pm 46$	-12.48	0.9181
A08	0.0640	0.0018	1.138	0.087	0.1290	0.0084	5601		771		$\pm 41$	782		$\pm 48$	741		$\pm 61$	-1.35	0.9061
A09	0.0906	0.0026	2.525	0.190	0.2022	0.0124	3227		1279		$\pm 55$	1187		$\pm 66$	1437		$\pm 55$	-6.12	0.9123
A10	0.0658	0.0020	1.095	0.072	0.1207	0.0064	5969		751		$\pm 35$	735		$\pm 37$	799		$\pm 63$	2.20	0.8670
A11	0.0583	0.0016	0.677	0.042	0.0843	0.0043	5881		525		$\pm 26$	522		$\pm 26$	539		$\pm 62$	0.63	0.8357
A12	0.0644	0.0017	0.872	0.052	0.0982	0.0050	22,082		637		$\pm 28$	604		$\pm 29$	756		$\pm 56$	5.48	0.8519
A13	0.0729	0.0021	1.428	0.094	0.1421	0.0077	7999		901		$\pm 39$	856		$\pm 44$	1011		$\pm 57$	5.17	0.8873
A14	0.0814	0.0021	1.651	0.106	0.1471	0.0080	35,636		990		$\pm 41$	885		$\pm 45$	1231		$\pm 52$	11.90	0.8879
A15	0.1167	0.0031	4.380	0.337	0.2722	0.0179	20,753		1709		$\pm 64$	1552		$\pm 91$	1907		$\pm 47$	-5.86	0.9301
A16	0.0810	0.0028	1.947	0.164	0.1744	0.0118	4724		1097		$\pm 56$	1036		$\pm 65$	1221		$\pm 67$	-5.39	0.9019
A17	0.0506	0.0032	0.566	0.054	0.0812	0.0042	1461		455		$\pm 35$	503		$\pm 25$	221		$\pm 148$	-9.48	0.6341
A18	0.0555	0.0022	0.818	0.065	0.1069	0.0065	3515		607		$\pm 36$	655		$\pm 38$	432		$\pm 87$	-7.32	0.8547
A19	0.0631	0.0030	1.241	0.154	0.1426	0.0143	1911		819		$\pm 70$	860		$\pm 80$	712		$\pm 101$	-4.68	0.9100
A20	0.1232	0.0033	4.365	0.337	0.2569	0.0169	8796		1706		$\pm 64$	1474		$\pm 87$	2003		$\pm 47$	-10.15	0.9207
A21	0.0582	0.0018	1.100	0.099	0.1371	0.0105	2774		753		$\pm 48$	828		$\pm 59$	537		$\pm 68$	-9.04	0.9248
A22	0.0962	0.0026	3.960	0.349	0.2986	0.0230	7985		1626		$\pm 72$	1684		$\pm 114$	1552		$\pm 50$	1.60	0.9538
A23	0.0610	0.0017	1.018	0.065	0.1210	0.0064	6951		713		$\pm 33$	736		$\pm 37$	640		$\pm 59$	-3.16	0.8884
A24	0.0722	0.0031	1.371	0.108	0.1378	0.0074	3021		877		$\pm 46$	832		$\pm 42$	991		$\pm 88$	5.36	0.8212
A25	0.0958	0.0026	2.519	0.188	0.1908	0.0122	9497		1278		$\pm 54$	1126		$\pm 66$	1543		$\pm 50$	-11.72	0.9128
A28	0.0788	0.0022	1.610	0.106	0.1483	0.0081	6236		974		$\pm 41$	891		$\pm 45$	1166		$\pm 54$	9.30	0.8877
A29	0.0588	0.0017	0.678	0.041	0.0837	0.0041	7257		526		$\pm 25$	518		$\pm 25$	560		$\pm 61$	1.52	0.8255
A30	0.0690	0.0025	1.547	0.151	0.1626	0.0127	1757		949		$\pm 60$	971		$\pm 70$	899		$\pm 75$	-2.27	0.9158
A31	0.0610	0.0016	0.852	0.056	0.1013	0.0057	7703		626		$\pm 31$	622		$\pm 33$	640		$\pm 58$	0.62	0.8752
A32	0.0912	0.0024	2.301	0.160	0.1831	0.0108	13,524		1213		$\pm 49$	1084		$\pm 59$	1450		$\pm 50$	-10.68	0.9068
A33	0.0567	0.0027	0.624	0.051	0.0799	0.0042	1190		493		$\pm 32$	496		$\pm 25$	479		$\pm 104$	-0.58	0.7107
A34	0.0772	0.0022	2.913	0.265	0.2735	0.0216	6319		1385		$\pm 69$	1559		$\pm 109$	1128		$\pm 56$	5.44	0.9575
A35	0.0593	0.0016	0.701	0.044	0.0856	0.0046	7656		539		$\pm 27$	530		$\pm 27$	580		$\pm 60$	1.80	0.8443
A36	0.0608	0.0019	0.851	0.076	0.1014	0.0076	2003		625		$\pm 42$	623		$\pm 44$	633		$\pm 68$	0.37	0.8912
A37	0.0832	0.0023	2.877	0.246	0.2507	0.0186	7884		1376		$\pm 64$	1442		$\pm 96$	1274		$\pm 53$	2.63	0.9487
A38	0.0848	0.0022	1.937	0.130	0.1657	0.0095	19,451		1094		$\pm 45$	988		$\pm 52$	1310		$\pm 51$	10.68	0.9012
A39	0.1873	0.0049	9.000	0.815	0.3485	0.0275	5791		2338		$\pm 83$	1927		$\pm 131$	2719		$\pm 43$	-10.28	0.9280
A40	0.0813	0.0022	1.685	0.109	0.1502	0.0081	11,227		1003		$\pm 41$	902		$\pm 46$	1230		$\pm 53$	11.15	0.8872
A41	0.0400	0.0134	0.563	0.244	0.1021	0.0067	332		453		$\pm 159$	627		$\pm 39$	-352		$\pm 866$	-27.66	0.9550
A42	0.0595	0.0020	0.690	0.047	0.0841	0.0044	2578		533		$\pm 28$	521		$\pm 26$	585		$\pm 73$	2.31	0.8014
B01	0.0534	0.0041	0.510	0.053	0.0693	0.0034	1633		418		$\pm 36$	432		$\pm 21$	346		$\pm 175$	-3.09	0.9369
B02	0.0811	0.0022	1.853	0.125	0.1656	0.0093	8167		1065		$\pm 44$	988		$\pm 52$	1225		$\pm 54$	7.75	0.9005
B03	0.0608	0.0025	0.801	0.060	0.0955	0.0049	1250		598		$\pm 34$	588		$\pm 29$	633		$\pm 90$	1.59	0.7740
B04	0.0620	0.0022	0.875	0.064	0.1024	0.0058	2177		639		$\pm 35$	628		$\pm 34$	675		$\pm 76$	1.64	0.8359
B05	0.0962	0.0025	2.422	0.168	0.1827	0.0107	30,428		1249		$\pm 50$	1082		$\pm 58$	1551		$\pm 50$	-14.21	0.9019
B06	0.0595	0.0018	0.745	0.047	0.0908	0.0047	5296		565		$\pm 27$	560		$\pm 28$	586		$\pm 64$	0.89	0.8374
B07	0.0957	0.0078	2.028	0.262	0.1537	0.0100	629		1125		$\pm 88$	922		$\pm 56$	1542		$\pm 153$	22.06	0.6510
B08	0.0813	0.0043	1.635	0.143	0.1458	0.0080	3493		984		$\pm 55$	877		$\pm 45$	1230		$\pm 104$	12.13	0.7704
B09	0.0849	0.0024	1.988	0.136	0.1697	0.0096	5030		1111		$\pm 46$	1011		$\pm 53$	1314		$\pm 54$	-9.58	0.8975
B10	0.2322	0.0061	12.111	1.070	0.3783	0.0287	18,512		2613		$\pm 83$	2068		$\pm 134$	3067		$\pm 42$	-12.20	0.9153
B11	0.0618	0.0019	0.919	0.058	0.1079	0.0053	3058		662		$\pm 31$	661		$\pm 31$	666		$\pm 67$	0.16	0.8436
B12	0.1169	0.0031	4.241	0.302	0.2631	0.0158	8396		1682		$\pm 58$	1506		$\pm 80$	1909		$\pm 48$	-7.14	0.9192
B13	0.0813	0.0021	1.849	0.114	0.1649	0.0086	21,649		1063		$\pm 41$	984		$\pm 48$	1229		$\pm 52$	8.02	0.8959
B14	0.0818	0.0022	2.006	0.129	0.1778	0.0097	19,446		1117		$\pm 43$	1055		$\pm 53$	1241		$\pm 52$	-5.29	0.9064
B15	0.0590	0.0016	0.921	0.061	0.1131	0.0064	7865		663										

B21	0.0629	0.0036	0.923	0.083	0.1064	0.0058	1248	664	±44	652	±34	705	±121	1.85	0.7288
B22	0.0603	0.0017	0.816	0.049	0.0982	0.0049	11,330	606	±27	604	±29	613	±60	0.33	0.8522
B23	0.0754	0.0022	1.602	0.117	0.1541	0.0095	3924	971	±46	924	±53	1078	±59	5.04	0.9015
B24	0.1366	0.0037	5.224	0.373	0.2774	0.0166	37,266	1857	±61	1578	±84	2184	±48	-10.62	0.9087
B25	0.0801	0.0022	1.966	0.131	0.1781	0.0098	4391	1104	±45	1057	±54	1198	±55	-3.97	0.9045
B26	0.0597	0.0020	0.767	0.047	0.0932	0.0044	8978	578	±27	575	±26	593	±72	0.66	0.8053
B27	0.0795	0.0023	1.877	0.123	0.1713	0.0092	7557	1073	±44	1019	±50	1184	±58	-4.89	0.8929
B28	0.0813	0.0021	1.860	0.114	0.1660	0.0087	28,379	1067	±41	990	±48	1228	±51	7.77	0.8972
B29	0.0738	0.0019	1.393	0.082	0.1369	0.0068	20,821	886	±35	827	±39	1036	±53	7.13	0.8793
B30	0.0772	0.0022	1.989	0.141	0.1867	0.0108	3706	1112	±48	1104	±59	1127	±58	-0.60	0.9130
B31	0.0648	0.0019	1.057	0.064	0.1182	0.0058	5826	732	±32	720	±33	769	±62	1.64	0.8602
B32	0.0804	0.0024	2.090	0.146	0.1886	0.0106	7676	1146	±48	1114	±57	1206	±60	-2.35	0.9039
B33	0.0798	0.0022	1.964	0.152	0.1786	0.0119	4634	1103	±52	1059	±65	1191	±56	-3.66	0.9205
B34	0.0701	0.0019	1.635	0.105	0.1692	0.0091	7252	984	±41	1008	±50	932	±56	2.12	0.9103
B35	0.0964	0.0026	2.323	0.157	0.1748	0.0102	17,213	1219	±48	1038	±56	1555	±51	-16.88	0.8929
B36	0.0794	0.0023	1.949	0.132	0.1779	0.0098	6091	1098	±45	1056	±54	1183	±57	-3.56	0.9031
B37	0.0661	0.0018	1.243	0.078	0.1364	0.0071	5647	820	±35	824	±40	809	±57	-0.50	0.8920
B38	0.0619	0.0017	0.931	0.055	0.1091	0.0053	7738	668	±29	668	±31	669	±60	0.05	0.8605
B39	0.0598	0.0024	1.130	0.084	0.1371	0.0076	3287	768	±40	828	±43	596	±86	-7.29	0.8662
B40	0.0736	0.0020	1.690	0.111	0.1665	0.0094	14,816	1005	±42	993	±52	1030	±54	1.17	0.9121
C01	0.0609	0.0017	0.817	0.047	0.0973	0.0047	9339	606	±26	598	±27	637	±59	1.37	0.8448
C02	0.0819	0.0022	2.075	0.139	0.1837	0.0105	20,192	1141	±46	1087	±57	1243	±51	-4.21	0.9137
C03	0.1344	0.0035	5.170	0.388	0.2790	0.0180	8727	1848	±64	1586	±91	2156	±46	-9.79	0.9200
C04	0.0578	0.0024	0.756	0.064	0.0949	0.0062	2174	572	±37	584	±36	523	±92	-2.12	0.8289
C05	0.0662	0.0018	1.264	0.079	0.1385	0.0071	6534	830	±35	836	±40	811	±58	-0.81	0.8897
C06	0.0590	0.0019	0.905	0.057	0.1113	0.0055	4097	655	±30	680	±32	568	±70	-3.73	0.8509
C07	0.0778	0.0022	1.907	0.133	0.1778	0.0104	6034	1084	±46	1055	±57	1142	±55	-2.41	0.9122
C08	0.0819	0.0063	1.783	0.201	0.1578	0.0087	1096	1039	±73	945	±48	1244	±150	10.01	0.6777
C09a	0.0506	0.0036	0.533	0.050	0.0764	0.0036	2361	434	±33	474	±22	224	±165	-8.54	0.4867
C09b	0.0581	0.0030	0.736	0.061	0.0919	0.0047	1136	560	±36	567	±28	534	±113	-1.12	0.7124
C10	0.1237	0.0033	4.554	0.322	0.2669	0.0160	18,926	1741	±59	1525	±82	2011	±47	-8.65	0.9172
C11	0.0737	0.0024	1.542	0.102	0.1517	0.0079	4394	947	±41	910	±44	1034	±66	4.04	0.8710
C12	0.0813	0.0022	1.943	0.124	0.1734	0.0092	13,095	1096	±43	1031	±51	1228	±53	-5.81	0.8999
C13	0.0811	0.0023	1.874	0.121	0.1675	0.0089	5743	1072	±43	999	±49	1224	±55	7.34	0.8941
C14	0.0726	0.0021	1.748	0.138	0.1746	0.0118	7499	1026	±51	1037	±65	1003	±59	0.92	0.9243
C15	0.0986	0.0033	3.333	0.272	0.2451	0.0158	2857	1489	±64	1413	±82	1599	±63	-3.38	0.9132
C16	0.0847	0.0023	2.100	0.139	0.1798	0.0100	12,217	1149	±46	1066	±55	1309	±52	-6.95	0.9058
C17	0.0929	0.0025	2.416	0.161	0.1887	0.0106	20,079	1247	±48	1114	±58	1485	±50	-10.41	0.9042
C18	0.0952	0.0025	2.298	0.148	0.1750	0.0095	6914	1212	±46	1040	±52	1532	±50	-15.91	0.8901
C19a	0.0778	0.0026	1.853	0.139	0.1728	0.0104	3389	1065	±50	1028	±57	1141	±66	-3.29	0.8961
C19b	0.0714	0.0036	1.691	0.151	0.1718	0.0097	1520	1005	±57	1022	±53	968	±104	1.48	0.8432
C20	0.0584	0.0016	0.767	0.048	0.0952	0.0050	6478	578	±27	586	±29	546	±61	-1.41	0.8582
C21	0.0704	0.0019	1.321	0.088	0.1362	0.0078	8967	855	±38	823	±44	939	±56	3.87	0.8941
C22	0.0604	0.0017	0.968	0.058	0.1162	0.0058	7110	687	±30	709	±34	617	±59	-3.04	0.8774
C23	0.0776	0.0022	1.588	0.099	0.1485	0.0076	7853	966	±39	892	±43	1136	±56	8.18	0.8783
C24	0.0584	0.0016	0.860	0.055	0.1068	0.0057	5292	630	±30	654	±33	543	±62	-3.73	0.8758
C25	0.0730	0.0020	1.596	0.100	0.1586	0.0083	7786	969	±39	949	±46	1014	±56	2.10	0.8965
C26	0.0730	0.0020	1.400	0.084	0.1391	0.0070	10,439	889	±36	839	±40	1015	±54	5.91	0.8815
C27	0.0613	0.0017	1.328	0.090	0.1570	0.0091	8712	858	±39	940	±51	651	±58	-8.73	0.9208
C28	0.0866	0.0023	2.358	0.157	0.1974	0.0111	17,563	1230	±47	1162	±60	1352	±51	-4.72	0.9140
C29	0.0546	0.0039	0.843	0.095	0.1120	0.0074	1192	621	±53	684	±43	396	±162	-9.27	0.7674
C30	0.0577	0.0018	1.052	0.070	0.1321	0.0071	4174	730	±35	800	±40	520	±67	-8.77	0.8926
C31	0.0772	0.0021	2.338	0.193	0.2197	0.0160	8624	1224	±59	1280	±85	1126	±54	2.95	0.9447
C32	0.0781	0.0021	1.625	0.099	0.1508	0.0077	11,463	980	±38	906	±43	1150	±53	8.20	0.8856
C33	0.0796	0.0021	1.876	0.121	0.1710	0.0093	14,896	1073	±43	1018	±51	1186	±53	-5.02	0.9045
C34	0.0651	0.0018	1.231	0.080	0.1371	0.0076	8044	815	±36	828	±43	777	±58	-1.68	0.8993
C35	0.0728	0.0020	1.420	0.086	0.1414	0.0071	8895	897	±36	852	±40	1009	±56	5.25	0.8814
C36	0.0841	0.0026	1.843	0.136	0.1590	0.0099	8764	1061	±48	951	±55	1295	±59	11.57	0.8923
C37	0.0797	0.0031	2.167	0.175	0.1972	0.0118	2405	1170	±56	1160	±63	1189	±76	-0.68	0.8920
D01	0.0604	0.0018	0.944	0.058	0.1134	0.0056	5023	675	±30	692	±32	617	±64	-2.52	0.8624
D02	0.0583	0.0022	0.987	0.138	0.1227	0.0152	2364	697	±71	746	±87	542	±84	-6.56	0.9355
D03	0.0706	0.0019	1.243	0.074	0.1278	0.0063	9407	820	±33	775	±36	945	±56	5.81	0.8705

(continued on next page)

Table 2 (continued)

Sample analysis	$^{207}\text{Pb}^*/^{206}\text{Pb}^*$	$\pm t\sigma$	$^{207}\text{Pb}^*/^{235}\text{U}$	$\pm t\sigma$	$^{206}\text{Pb}^*/^{238}\text{U}$	$\pm t\sigma$	Hg-Corr	$^{206}\text{Pb}^*/^{204}\text{Pb}$	$^{207}\text{Pb}^*/^{235}\text{U}$	age (Ma)	$\pm t\sigma$ (95% Conf)	$^{206}\text{Pb}^*/^{238}\text{U}$	age (Ma)	$\pm t\sigma$ (95% Conf)	$^{207}\text{Pb}^*/^{206}\text{Pb}^*$	age (Ma)	$\pm t\sigma$ (95% Conf)	% discord.	Rho
<i>LM-10</i>																			
D04	0.0883	0.0024	2.435	0.165	0.2000	0.0115	42,506	1253		±49	1175		±62	1389		±52	–5.25	0.9134	
D05	0.0802	0.0022	1.845	0.117	0.1668	0.0089	10,782	1062		±42	995		±49	1203		±53	6.75	0.8977	
D06	0.0614	0.0031	0.868	0.069	0.1026	0.0050	1688	635		±37	630		±29	653		±110	0.79	0.7190	
D07	0.0794	0.0024	2.283	0.172	0.2085	0.0127	3737	1207		±53	1221		±68	1182		±60	0.82	0.9198	
D08	0.0629	0.0017	0.933	0.054	0.1076	0.0052	10,053	669		±29	659		±31	706		±58	1.64	0.8602	
D09	0.0584	0.0017	0.779	0.047	0.0967	0.0047	4764	585		±27	595		±27	546		±65	–1.67	0.8389	
D10	0.0892	0.0024	2.585	0.188	0.2102	0.0130	6521	1296		±53	1230		±69	1408		±53	–4.05	0.9215	
D11	0.0732	0.0028	1.415	0.097	0.1402	0.0070	4256	895		±41	846		±40	1021		±76	5.90	0.8337	
D12	0.1715	0.0045	7.598	0.564	0.3213	0.0202	24,167	2185		±67	1796		±99	2573		±44	–11.50	0.9100	
D13	0.0554	0.0027	0.762	0.060	0.0997	0.0050	1727	575		±34	613		±29	429		±109	–6.12	0.7623	
D14	0.0558	0.0018	0.641	0.040	0.0833	0.0040	2433	503		±25	516		±24	446		±71	–2.47	0.8034	
D15	0.0815	0.0023	1.961	0.128	0.1745	0.0093	6671	1102		±44	1037		±51	1233		±56	–5.75	0.8944	
D16	0.0767	0.0020	1.591	0.097	0.1504	0.0077	14,304	967		±38	903		±43	1115		±53	7.06	0.8892	
D17	0.1255	0.0033	4.289	0.296	0.2479	0.0146	38,330	1691		±57	1428		±75	2035		±46	–12.63	0.9085	
D18	0.0601	0.0019	0.788	0.048	0.0950	0.0045	4303	590		±27	585		±26	608		±68	0.81	0.8170	
D19	0.0597	0.0019	0.886	0.057	0.1076	0.0055	4551	644		±30	659		±32	592		±68	–2.27	0.8539	
D20	0.0660	0.0036	1.426	0.134	0.1567	0.0095	1900	900		±56	939		±53	806		±115	–4.13	0.8380	
D21	0.0594	0.0017	0.681	0.040	0.0832	0.0039	4745	528		±24	515		±23	583		±63	2.46	0.8070	
D22	0.0778	0.0031	1.863	0.141	0.1737	0.0094	3480	1068		±50	1032		±52	1142		±80	–3.14	0.8616	
D23	0.0650	0.0017	1.146	0.070	0.1278	0.0066	11,493	776		±33	776		±38	776		±57	0.00	0.8862	
D24	0.0655	0.0022	1.289	0.087	0.1427	0.0074	3694	841		±38	860		±42	792		±70	–2.19	0.8736	
D25	0.1164	0.0031	4.013	0.279	0.2501	0.0147	16,659	1637		±57	1439		±76	1901		±47	–9.00	0.9149	
D26	0.0803	0.0022	1.818	0.116	0.1641	0.0088	8715	1052		±42	980		±49	1205		±53	7.37	0.8958	
D27	0.0598	0.0017	0.898	0.058	0.1089	0.0058	4947	651		±31	666		±34	596		±63	–2.39	0.8702	
D28	0.0619	0.0034	0.924	0.079	0.1083	0.0056	1434	665		±42	663		±33	670		±118	0.23	0.7324	
D29	0.0574	0.0018	0.707	0.043	0.0894	0.0042	3311	543		±26	552		±25	506		±71	–1.61	0.8093	
D30	0.0812	0.0022	2.058	0.146	0.1837	0.0109	4789	1135		±48	1087		±59	1227		±54	–3.76	0.9134	
D31	0.0652	0.0018	1.203	0.080	0.1339	0.0077	9007	802		±37	810		±44	780		±58	–0.97	0.9003	
D32	0.0781	0.0021	1.876	0.127	0.1743	0.0099	8410	1073		±45	1035		±55	1149		±54	–3.24	0.9108	
D33	0.0819	0.0021	1.985	0.129	0.1758	0.0097	19,604	1111		±44	1044		±53	1243		±51	–5.77	0.9074	
D34	0.0812	0.0021	3.018	0.238	0.2696	0.0186	17,792	1412		±60	1539		±94	1226		±52	4.19	0.9512	
<i>SSP-1</i>																			
A01	0.0836	0.0013	3.131	0.195	0.2717	0.0166	10,809	1440		±48	1550		±84	1283		±31	3.59	0.9661	
A03	0.0860	0.0019	3.124	0.201	0.2634	0.0159	2268	1439		±49	1507		±81	1338		±43	2.46	0.9494	
A04	0.0584	0.0027	0.969	0.103	0.1203	0.0115	1640	688		±53	732		±66	546		±103	–6.03	0.8960	
A05	0.0980	0.0015	3.597	0.220	0.2663	0.0159	10,087	1549		±49	1522		±81	1585		±28	–0.98	0.9608	
A06	0.0563	0.0019	0.674	0.038	0.0869	0.0045	3343	523		±23	537		±27	464		±73	–2.57	0.8156	
A07	0.0617	0.0017	0.745	0.040	0.0876	0.0043	2278	565		±23	542		±25	662		±61	4.39	0.8198	
A08	0.0689	0.0013	1.426	0.078	0.1500	0.0077	3447	900		±33	901		±43	897		±40	–0.12	0.9261	
A09	0.0566	0.0016	0.529	0.029	0.0679	0.0034	2264	431		±19	423		±21	474		±62	1.89	0.7928	
A10	0.0754	0.0011	1.843	0.124	0.1773	0.0117	27,811	1061		±44	1052		±64	1079		±30	–0.73	0.9586	
A12	0.0575	0.0010	0.657	0.035	0.0828	0.0042	5108	513		±21	513		±25	511		±39	–0.08	0.8926	
A13	0.0528	0.0025	0.453	0.026	0.0622	0.0029	1345	379		±18	389		±18	321		±107	–2.48	0.5794	
A14	0.0782	0.0013	2.388	0.145	0.2214	0.0129	4904	1239		±43	1289		±68	1153		±34	2.59	0.9556	
A15 (all)	0.0588	0.0054	0.843	0.068	0.1040	0.0057	1340	621		±37	638		±33	561		±201	–2.62	0.5173	
A15 (core)	0.0689	0.0060	1.070	0.090	0.1127	0.0067	820	739		±44	688		±39	895		±181	7.32	0.5585	
A15 (rim?)	0.0543	0.0022	0.612	0.056	0.0817	0.0067	1683	485		±35	506		±40	382		±90	–4.32	0.8567	
A17	0.0796	0.0012	2.178	0.130	0.1985	0.0115	9574	1174		±41	1167		±62	1186		±30	–0.44	0.9548	
A19	0.0795	0.0014	2.154	0.125	0.1964	0.0111	10,277	1166		±40	1156		±60	1185		±36	–0.68	0.9443	
A20	0.0951	0.0020	2.008	0.112	0.1531	0.0083	8360	1118		±38	918		±46	1531		±39	21.78	0.9010	
A22	0.0590	0.0017	0.819	0.046	0.1006	0.0052	2560	607		±26	618		±30	568		±64	–1.73	0.8535	
A24	0.0571	0.0014	0.739	0.043	0.0938	0.0050	2214	562		±25	578		±29	496		±55	–2.82	0.8748	
A26	0.0564	0.0018	0.736	0.050	0.0947	0.0059	2862	560		±29	583		±35	467		±69	–3.95	0.8693	
A28	0.0547	0.0021	0.602	0.036	0.0798	0.0041	1601	478		±23	495		±25	400		±87	–3.33	0.7674	
B01	0.0828	0.0012	2.276	0.154	0.1994	0.0132	8471	1205		±48	1172		±71	1264		±29	–2.18	0.9602	
B02	0.0534	0.0031	0.733	0.247	0.0995	0.0303	1333	558		±145	611		±178	346		±133	–8.72	0.9540	
B05	0.0874	0.0013	3.417	0.209	0.2835	0.0171	31,288	1508		±48	1609		±86	1370		±28	3.03	0.9679	
B06	0.0559	0.0013	0.774	0.046	0.1004	0.0055	2816	582		±26	617		±32	447		±53	–5.69	0.8937	
B07	0.0813	0.0013	3.036	0.205	0.2707	0.0178	8015	1417		±52	1544		±90	1230		±33	4.19	0.9676	
B08	0.0627	0.0043	1.101	0.087	0.1272	0.0079	1204	754		±42	772		±45	700		±145	–2.37	0.7620	

B09	0.0576	0.0015	0.755	0.048	0.0950	0.0057	2926	571	±28	585	±33	515	±56	-2.42	0.8856
B10a	0.0618	0.0044	0.726	0.051	0.0852	0.0044	1243	554	±30	527	±26	666	±154	5.10	0.4797
B10b	0.0582	0.0022	1.073	0.067	0.1337	0.0076	6290	740	±33	809	±43	538	±84	-8.47	0.8722
B11c	0.0804	0.0013	2.268	0.134	0.2047	0.0118	8009	1202	±42	1200	±63	1206	±32	-0.12	0.9523
B13	0.0827	0.0013	2.532	0.150	0.2220	0.0129	12,997	1281	±43	1292	±68	1263	±31	0.58	0.9568
B14	0.0582	0.0018	0.969	0.054	0.1207	0.0062	3657	688	±28	735	±35	538	±66	-6.35	0.8758
B16	0.0571	0.0017	1.013	0.061	0.1286	0.0071	2305	710	±31	780	±40	495	±65	-8.95	0.8952
B17	0.0575	0.0015	0.944	0.055	0.1190	0.0065	5266	675	±29	725	±37	511	±59	-6.91	0.8966
C01	0.0558	0.0026	0.878	0.053	0.1141	0.0058	1929	640	±29	696	±33	445	±104	-8.13	0.7996
C02	0.0657	0.0266	0.785	0.189	0.0867	0.0058	3802	588	±107	536	±34	796	±851	9.78	0.8870
C03	0.0580	0.0017	0.897	0.054	0.1122	0.0063	3103	650	±29	686	±36	530	±66	-5.15	0.8782
C05	0.0601	0.0016	0.840	0.048	0.1013	0.0051	1484	619	±26	622	±30	608	±56	-0.47	0.8674
C06	0.0749	0.0016	1.857	0.110	0.1799	0.0101	3119	1066	±39	1066	±55	1065	±43	0.03	0.9323
C07	0.0592	0.0010	0.661	0.033	0.0809	0.0039	11,706	515	±20	502	±23	576	±38	2.72	0.8827
C08	0.0668	0.0024	1.228	0.087	0.1333	0.0085	2022	814	±40	807	±49	832	±76	0.83	0.8772
C09	0.0828	0.0013	1.855	0.098	0.1626	0.0084	21,819	1065	±35	971	±47	1264	±30	9.70	0.9358
C10	0.0800	0.0013	1.973	0.116	0.1790	0.0103	8387	1106	±40	1061	±56	1196	±31	-3.74	0.9481
C11	0.0578	0.0014	0.597	0.035	0.0749	0.0041	1919	475	±23	466	±24	521	±55	2.01	0.8429
C12	0.0810	0.0012	2.420	0.142	0.2167	0.0124	11,550	1249	±42	1264	±66	1221	±30	0.87	0.9576
C13	0.0603	0.0015	0.650	0.045	0.0783	0.0049	1626	509	±28	486	±29	613	±55	4.71	0.8643
C14	0.0778	0.0012	2.105	0.142	0.1961	0.0129	9012	1150	±46	1154	±70	1143	±31	0.27	0.9597
C15	0.0578	0.0019	0.575	0.032	0.0722	0.0036	1906	461	±21	449	±21	523	±72	2.72	0.7618
C16	0.0776	0.0012	2.214	0.131	0.2070	0.0119	6888	1186	±41	1213	±63	1136	±31	1.63	0.9564
C17	0.0791	0.0021	2.535	0.178	0.2323	0.0154	3701	1282	±51	1347	±81	1176	±52	3.00	0.9422
C18	0.0638	0.0042	1.003	0.072	0.1140	0.0064	1275	706	±37	696	±37	736	±140	1.38	0.7000
C20	0.0577	0.0023	0.772	0.049	0.0970	0.0055	2663	581	±28	597	±32	519	±86	-2.67	0.8189
C21	0.0580	0.0013	0.962	0.059	0.1202	0.0066	1661	684	±30	732	±38	530	±51	-6.52	0.9119
C22	0.0855	0.0014	3.463	0.224	0.2939	0.0185	8271	1519	±51	1661	±92	1326	±31	3.89	0.9688
C23	0.0568	0.0026	0.646	0.039	0.0825	0.0040	1239	506	±24	511	±24	483	±100	-1.02	0.7067
C24	0.0775	0.0025	1.501	0.160	0.1404	0.0141	1991	931	±65	847	±80	1135	±64	9.91	0.9246
C25	0.0806	0.0014	2.274	0.133	0.2047	0.0115	5906	1204	±41	1200	±62	1211	±35	-0.24	0.9470
C26	0.0578	0.0014	0.723	0.044	0.0906	0.0051	2604	552	±26	559	±30	524	±52	-1.24	0.8828
C27 (all)	0.0589	0.0021	0.684	0.042	0.0843	0.0045	1752	529	±25	522	±27	563	±77	1.49	0.7969
C27 (core)	0.0609	0.0021	0.703	0.053	0.0837	0.0055	1234	540	±31	518	±33	634	±74	4.23	0.8345
C27 (rim?)	0.0572	0.0018	0.746	0.052	0.0946	0.0060	2299	566	±30	583	±35	500	±68	-2.85	0.8708
C28	0.0715	0.0011	2.043	0.124	0.2073	0.0123	9291	1130	±41	1214	±66	972	±31	4.88	0.9612
C29	0.0801	0.0012	2.617	0.156	0.2369	0.0138	7495	1305	±44	1371	±72	1200	±30	2.91	0.9615
C30	0.0804	0.0052	1.047	0.128	0.0945	0.0088	348	728	±63	582	±52	1206	±128	25.00	0.7404
<i>SSP-2</i>															
A01	0.1221	0.0032	4.638	0.375	0.2756	0.0193	16,627	1756	±68	1569	±97	1987	±47	-6.92	0.9320
A02	0.0836	0.0022	2.211	0.175	0.1919	0.0132	11,120	1185	±55	1132	±72	1283	±52	-3.84	0.9294
A03	0.0848	0.0022	2.055	0.145	0.1758	0.0104	11,013	1134	±48	1044	±57	1310	±51	-7.89	0.9099
A04	0.0844	0.0023	1.832	0.127	0.1574	0.0091	16,203	1057	±45	942	±51	1302	±54	12.16	0.8929
A06	0.1068	0.0028	4.449	0.424	0.3021	0.0258	15,035	1722	±79	1702	±128	1746	±48	-0.55	0.9547
A07	0.0574	0.0019	0.792	0.066	0.1000	0.0068	3349	592	±38	615	±40	508	±73	-3.61	0.8775
A09	0.0899	0.0024	2.629	0.220	0.2122	0.0155	7755	1309	±62	1240	±83	1423	±51	-4.09	0.9355
A10	0.1627	0.0050	4.535	0.438	0.2021	0.0172	5431	1737	±80	1187	±92	2484	±51	-46.59	0.8839
A11	0.0679	0.0019	1.265	0.093	0.1351	0.0085	8990	830	±42	817	±49	865	±57	1.61	0.9066
A12	0.0730	0.0020	1.255	0.090	0.1246	0.0074	4819	826	±40	757	±42	1015	±57	9.06	0.8828
A13	0.0625	0.0023	1.126	0.087	0.1307	0.0074	2757	766	±41	792	±42	690	±77	-3.30	0.8695
A14	0.0767	0.0020	1.958	0.142	0.1851	0.0115	15,222	1101	±49	1095	±62	1114	±53	-0.50	0.9251
A15	0.0750	0.0021	1.852	0.138	0.1792	0.0111	6807	1064	±49	1063	±61	1067	±56	-0.13	0.9200
A16	0.0555	0.0044	0.759	0.114	0.0991	0.0085	836	573	±66	609	±50	433	±175	-5.92	0.7779
A17	0.0552	0.0018	0.933	0.072	0.1227	0.0072	3000	669	±38	746	±41	420	±75	-10.24	0.8891
A18	0.0791	0.0021	1.862	0.130	0.1707	0.0100	10,869	1068	±46	1016	±55	1175	±53	-4.74	0.9104
A19	0.0733	0.0019	1.570	0.113	0.1553	0.0097	19,651	959	±44	931	±54	1024	±53	3.02	0.9152
A20	0.0765	0.0144	1.006	0.274	0.0954	0.0063	268	707	±139	587	±37	1108	±377	20.36	0.9573
A23	0.0757	0.0023	1.752	0.130	0.1678	0.0097	2959	1028	±48	1000	±54	1088	±62	-2.61	0.8988
A24	0.0740	0.0020	1.374	0.092	0.1347	0.0074	7034	878	±39	814	±42	1041	±55	7.78	0.8852
A25	0.0748	0.0020	1.592	0.107	0.1542	0.0088	23,792	967	±42	925	±49	1064	±53	4.57	0.9054
A27	0.0435	0.0044	0.077	0.011	0.0129	0.0008	1024	76	±10	83	±5	-138	±250	-8.40	0.6826
A28	0.0758	0.0020	2.123	0.174	0.2032	0.0147	14,612	1156	±57	1193	±79	1089	±53	2.25	0.9416

(continued on next page)

Table 2 (continued)

Sample analysis	$^{207}\text{Pb}^*/^{206}\text{Pb}^*$	$\pm t\sigma$	$^{207}\text{Pb}^*/^{235}\text{U}$	$\pm t\sigma$	$^{206}\text{Pb}^*/^{238}\text{U}$	$\pm t\sigma$	Hg-Corr	$^{206}\text{Pb}^*/^{204}\text{Pb}$	$^{207}\text{Pb}^*/^{235}\text{U}$	age (Ma)	$\pm t\sigma$ (95% Conf)	$^{206}\text{Pb}^*/^{238}\text{U}$	age (Ma)	$\pm t\sigma$ (95% Conf)	$^{207}\text{Pb}^*/^{206}\text{Pb}^*$	age (Ma)	$\pm t\sigma$ (95% Conf)	% discord.	Rho
<i>SSP-2</i>																			
A29	0.0760	0.0020	1.565	0.119	0.1494	0.0098	8389	956		$\pm 47$	898		$\pm 55$	1094		$\pm 54$	6.53	0.9121	
B01	0.0810	0.0022	1.915	0.133	0.1714	0.0099	5876	1086		$\pm 46$	1020		$\pm 55$	1222		$\pm 54$	-6.08	0.9059	
B02	0.0547	0.0029	0.878	0.082	0.1164	0.0072	2692	640		$\pm 45$	710		$\pm 42$	399		$\pm 118$	-9.88	0.8281	
B03	0.0900	0.0024	3.797	0.311	0.3059	0.0212	7003	1592		$\pm 66$	1720		$\pm 105$	1426		$\pm 51$	3.25	0.9525	
B04	0.0789	0.0022	2.293	0.196	0.2108	0.0158	8049	1210		$\pm 60$	1233		$\pm 84$	1169		$\pm 54$	1.32	0.9422	
B05	0.0623	0.0021	0.931	0.077	0.1084	0.0074	3482	668		$\pm 40$	664		$\pm 43$	685		$\pm 70$	0.73	0.8812	
B06	0.0628	0.0022	0.951	0.079	0.1098	0.0071	2054	678		$\pm 41$	672		$\pm 41$	701		$\pm 76$	1.02	0.8652	
B08	0.0615	0.0018	1.117	0.096	0.1317	0.0097	3436	762		$\pm 46$	798		$\pm 56$	657		$\pm 62$	-4.52	0.9216	
B09	0.0654	0.0020	1.055	0.073	0.1171	0.0066	7185	732		$\pm 36$	714		$\pm 38$	787		$\pm 64$	2.50	0.8714	
B10	0.0772	0.0021	1.869	0.130	0.1755	0.0104	16,709	1070		$\pm 46$	1042		$\pm 57$	1127		$\pm 53$	-2.38	0.9164	
B12	0.0832	0.0022	2.283	0.175	0.1989	0.0130	8169	1207		$\pm 54$	1170		$\pm 70$	1275		$\pm 52$	-2.51	0.9282	
B13	0.0585	0.0036	0.701	0.069	0.0869	0.0048	1620	540		$\pm 41$	537		$\pm 28$	549		$\pm 135$	0.42	0.6501	
B14	0.0774	0.0021	1.980	0.160	0.1856	0.0131	12,477	1109		$\pm 55$	1098		$\pm 71$	1130		$\pm 54$	-0.84	0.9321	
B15	0.0796	0.0021	2.532	0.193	0.2308	0.0150	12,332	1281		$\pm 56$	1339		$\pm 78$	1186		$\pm 53$	2.71	0.9395	
B16	0.0751	0.0020	1.668	0.115	0.1612	0.0093	5844	996		$\pm 44$	963		$\pm 52$	1070		$\pm 54$	3.43	0.9082	
B17	0.0565	0.0020	0.778	0.056	0.0998	0.0054	3113	584		$\pm 32$	613		$\pm 32$	472		$\pm 78$	-4.75	0.8400	
B18	0.0733	0.0022	1.777	0.147	0.1758	0.0122	4662	1037		$\pm 54$	1044		$\pm 67$	1022		$\pm 60$	0.59	0.9241	
B19	0.0708	0.0020	1.209	0.079	0.1238	0.0067	8866	805		$\pm 36$	752		$\pm 39$	952		$\pm 57$	6.94	0.8752	
B21	0.0573	0.0018	0.590	0.040	0.0747	0.0039	3267	471		$\pm 25$	464		$\pm 23$	501		$\pm 71$	1.35	0.7900	
B22	0.0732	0.0020	1.229	0.080	0.1218	0.0065	9695	814		$\pm 36$	741		$\pm 37$	1019		$\pm 57$	9.84	0.8673	
B23	0.0727	0.0020	1.395	0.092	0.1391	0.0077	9977	887		$\pm 39$	839		$\pm 44$	1007		$\pm 55$	5.63	0.8915	
B24	0.0577	0.0016	0.578	0.036	0.0726	0.0038	7374	463		$\pm 23$	452		$\pm 23$	518		$\pm 61$	2.44	0.8155	
B25	0.0777	0.0021	1.676	0.115	0.1564	0.0091	14,023	999		$\pm 44$	937		$\pm 51$	1140		$\pm 53$	6.72	0.9038	
B26	0.0898	0.0027	2.488	0.191	0.2008	0.0125	4280	1269		$\pm 56$	1180		$\pm 67$	1422		$\pm 58$	-5.98	0.9095	
B28	0.1158	0.0030	4.602	0.402	0.2881	0.0222	12,926	1750		$\pm 73$	1632		$\pm 111$	1893		$\pm 47$	-3.81	0.9436	
B29	0.0892	0.0024	2.497	0.181	0.2029	0.0125	13,223	1271		$\pm 53$	1191		$\pm 67$	1410		$\pm 50$	-5.28	0.9216	
<i>OT-1</i>																			
A01	0.0914	0.0025	2.739	0.179	0.2173	0.0120	11,114	1339		$\pm 49$	1267		$\pm 64$	1456		$\pm 52$	-4.09	0.9127	
A02	0.0828	0.0022	1.922	0.111	0.1683	0.0083	26,399	1089		$\pm 39$	1003		$\pm 46$	1264		$\pm 51$	-8.20	0.8901	
A03	0.0789	0.0021	1.703	0.098	0.1566	0.0075	10,957	1010		$\pm 37$	938		$\pm 42$	1169		$\pm 54$	7.67	0.8802	
A05	0.0728	0.0023	1.463	0.087	0.1458	0.0069	5355	915		$\pm 36$	878		$\pm 39$	1007		$\pm 64$	4.30	0.8589	
A06	0.0795	0.0021	1.714	0.096	0.1564	0.0075	49,982	1014		$\pm 36$	937		$\pm 42$	1185		$\pm 52$	8.25	0.8835	
A07	0.0805	0.0023	2.132	0.149	0.1919	0.0114	6864	1159		$\pm 48$	1132		$\pm 62$	1210		$\pm 57$	-1.95	0.9135	
A08	0.0798	0.0027	1.653	0.102	0.1502	0.0073	7683	991		$\pm 39$	902		$\pm 41$	1192		$\pm 67$	9.82	0.8437	
A09	0.0833	0.0027	2.019	0.128	0.1759	0.0089	6735	1122		$\pm 43$	1044		$\pm 49$	1276		$\pm 64$	-6.78	0.8718	
A10	0.0844	0.0022	1.924	0.110	0.1653	0.0080	28,611	1089		$\pm 38$	986		$\pm 44$	1302		$\pm 52$	10.46	0.8824	
A11	0.0796	0.0026	2.094	0.137	0.1909	0.0100	17,303	1147		$\pm 45$	1126		$\pm 54$	1186		$\pm 65$	-1.49	0.8907	
A12	0.0770	0.0067	1.579	0.171	0.1488	0.0071	7347	962		$\pm 67$	894		$\pm 40$	1121		$\pm 174$	7.60	0.5399	
A13	0.0798	0.0025	1.774	0.108	0.1613	0.0079	9699	1036		$\pm 40$	964		$\pm 44$	1191		$\pm 63$	7.46	0.8652	
A14	0.0823	0.0022	1.912	0.111	0.1685	0.0082	13,881	1085		$\pm 39$	1004		$\pm 45$	1252		$\pm 53$	-7.74	0.8856	
A15	0.0797	0.0023	1.746	0.104	0.1588	0.0079	16,023	1026		$\pm 39$	950		$\pm 44$	1190		$\pm 57$	7.93	0.8784	
A16	0.0997	0.0026	2.930	0.185	0.2131	0.0114	31,612	1390		$\pm 48$	1245		$\pm 61$	1619		$\pm 49$	-8.88	0.9049	
A17	0.0813	0.0023	1.804	0.104	0.1609	0.0077	37,047	1047		$\pm 38$	962		$\pm 43$	1230		$\pm 56$	8.88	0.8739	
A18	0.0893	0.0024	2.231	0.136	0.1812	0.0094	23,432	1191		$\pm 43$	1074		$\pm 51$	1411		$\pm 52$	-9.86	0.8923	
A19	0.0784	0.0029	1.939	0.135	0.1795	0.0095	4691	1095		$\pm 47$	1064		$\pm 52$	1157		$\pm 75$	-2.52	0.8697	
E01	0.0872	0.0024	2.853	0.230	0.2373	0.0166	5403	1370		$\pm 61$	1373		$\pm 86$	1365		$\pm 54$	0.13	0.9387	
E02	0.0728	0.0036	1.918	0.186	0.1911	0.0134	5070	1087		$\pm 65$	1127		$\pm 72$	1009		$\pm 100$	2.78	0.8876	
E03	0.0831	0.0025	1.669	0.205	0.1456	0.0170	3798	997		$\pm 78$	876		$\pm 95$	1273		$\pm 60$	13.77	0.9367	
E04a	0.0595	0.0019	0.869	0.057	0.1059	0.0057	7700	635		$\pm 31$	649		$\pm 33$	586		$\pm 68$	-2.14	0.8598	
A20	0.0803	0.0025	1.958	0.125	0.1769	0.0091	7451	1101		$\pm 43$	1050		$\pm 50$	1204		$\pm 62$	-4.36	0.8837	
E04b	0.0587	0.0018	0.739	0.073	0.0913	0.0083	8651	562		$\pm 42$	563		$\pm 49$	555		$\pm 66$	-0.29	0.9070	
E05	0.0597	0.0020	0.733	0.066	0.0891	0.0072	9870	559		$\pm 38$	550		$\pm 42$	594		$\pm 73$	1.56	0.8784	
E06a	0.0836	0.0025	1.600	0.140	0.1388	0.0110	3866	970		$\pm 55$	838		$\pm 62$	1283		$\pm 58$	15.75	0.9043	
E06b	0.0832	0.0024	1.828	0.120	0.1593	0.0087	9490	1055		$\pm 43$	953		$\pm 49$	1274		$\pm 56$	10.77	0.8863	
E06c	0.0824	0.0028	1.724	0.133	0.1518	0.0096	4540	1018		$\pm 50$	911		$\pm 54$	1254		$\pm 67$	11.69	0.8762	
E07	0.0822	0.0026	2.807	0.231	0.2476	0.0170	8808	1357		$\pm 62$	1426		$\pm 88$	1251		$\pm 62$			

E12	0.0841	0.0041	1.763	0.148	0.1520	0.0086	1457	1032	±55	912	±48	1296	±95	13.15	0.7970
E13	0.0789	0.0023	2.058	0.150	0.1891	0.0117	9204	1135	±50	1116	±63	1171	±57	-1.36	0.9185
E14a	0.0760	0.0070	1.338	0.173	0.1276	0.0078	1363	862	±75	774	±45	1095	±186	11.33	0.5688
E14b	0.0685	0.0025	1.342	0.099	0.1421	0.0081	1645	864	±43	857	±46	883	±76	0.87	0.8691
E15	0.0809	0.0029	1.957	0.154	0.1754	0.0109	4607	1101	±53	1042	±60	1220	±72	-5.16	0.8871
E16	0.0953	0.0028	2.625	0.191	0.1998	0.0121	6529	1308	±53	1174	±65	1534	±55	-9.32	0.9043
E17a	0.0780	0.0025	1.934	0.155	0.1798	0.0120	5804	1093	±54	1066	±66	1146	±65	-2.17	0.9111
E17b	0.0775	0.0025	1.749	0.123	0.1636	0.0091	3440	1027	±45	977	±51	1134	±65	5.08	0.8834
E17c	0.0803	0.0026	1.833	0.147	0.1655	0.0113	4381	1057	±53	987	±62	1206	±64	7.12	0.9031
E18	0.0489	0.0249	0.533	0.318	0.0790	0.0057	313	434	±211	490	±34	141	±1194	-11.60	0.9366
E20b	0.0794	0.0023	2.056	0.131	0.1878	0.0099	11,919	1134	±43	1109	±54	1182	±58	-1.86	0.9012
E22a	0.0796	0.0027	2.030	0.134	0.1849	0.0094	4980	1125	±45	1094	±51	1188	±67	-2.47	0.8796
E22b	0.0784	0.0022	1.987	0.146	0.1837	0.0118	4702	1111	±50	1087	±64	1158	±55	-1.86	0.9220
E23	0.0783	0.0025	2.082	0.151	0.1929	0.0116	7080	1143	±50	1137	±63	1155	±62	-0.43	0.9109
E24a	0.1096	0.0030	3.975	0.294	0.2631	0.0170	8459	1629	±60	1506	±87	1792	±49	-4.86	0.9278
E24b	0.0747	0.0022	2.239	0.150	0.2175	0.0121	8856	1193	±47	1269	±64	1059	±58	3.98	0.9249
E25a	0.0800	0.0042	2.415	0.215	0.2188	0.0126	2283	1247	±64	1276	±67	1198	±103	1.53	0.8626
E25b	0.0824	0.0030	2.200	0.170	0.1937	0.0117	2449	1181	±54	1141	±63	1255	±72	-2.81	0.8923
E26	0.0840	0.0024	2.325	0.153	0.2007	0.0111	7167	1220	±47	1179	±59	1293	±55	-2.71	0.9110
E27	0.0692	0.0035	1.564	0.120	0.1640	0.0081	3427	956	±48	979	±45	904	±104	-2.34	0.8177
E28a	0.0822	0.0027	2.469	0.174	0.2177	0.0122	4112	1263	±51	1270	±65	1251	±64	0.38	0.9085
E28b	0.0823	0.0024	2.172	0.166	0.1915	0.0126	5079	1172	±53	1130	±68	1252	±58	-3.08	0.9189
E29	0.0795	0.0117	1.922	0.348	0.1753	0.0099	1616	1089	±121	1042	±54	1185	±290	-4.10	0.9727
E30	0.0816	0.0026	2.088	0.140	0.1857	0.0101	8623	1145	±46	1098	±55	1235	±64	-3.63	0.8908
E31	0.0849	0.0027	2.398	0.182	0.2049	0.0126	1601	1242	±54	1202	±67	1313	±62	-2.57	0.9097
E32	0.0845	0.0025	2.756	0.239	0.2365	0.0184	21,716	1344	±65	1369	±96	1304	±58	1.14	0.9425
E33	0.0766	0.0031	1.668	0.113	0.1581	0.0078	7950	997	±43	946	±43	1110	±81	5.35	0.8318
E34a	0.0805	0.0024	1.923	0.117	0.1731	0.0086	6357	1089	±41	1029	±47	1210	±58	-5.33	0.8829
E34b	0.0761	0.0030	1.705	0.115	0.1625	0.0079	3060	1010	±43	971	±44	1097	±79	4.08	0.8403
E35	0.0731	0.0038	1.398	0.123	0.1388	0.0086	1182	888	±52	838	±48	1016	±106	6.01	0.8097
E36a	0.0819	0.0037	2.068	0.158	0.1832	0.0098	3319	1138	±52	1084	±53	1243	±88	-4.30	0.8443
E36b	0.0840	0.0037	2.130	0.265	0.1839	0.0197	1473	1159	±86	1088	±107	1293	±86	-5.62	0.9208
E37	0.0797	0.0029	2.143	0.194	0.1951	0.0149	3907	1163	±63	1149	±81	1189	±72	-0.96	0.9184
E38	0.0803	0.0022	2.107	0.140	0.1902	0.0108	8725	1151	±46	1123	±59	1205	±54	-2.09	0.9150
E39	0.0844	0.0025	2.046	0.125	0.1759	0.0088	10,262	1131	±42	1044	±48	1301	±58	-7.61	0.8798
E40	0.0826	0.0025	2.035	0.125	0.1786	0.0089	8906	1127	±42	1059	±48	1260	±60	-5.73	0.8807
E41	0.0952	0.0025	2.806	0.179	0.2137	0.0116	18,826	1357	±48	1249	±62	1533	±50	-6.51	0.9095
E42	0.0833	0.0023	1.868	0.108	0.1626	0.0078	21,004	1070	±38	971	±43	1277	±54	10.15	0.8754
E43a	0.0739	0.0027	1.448	0.091	0.1421	0.0068	4474	909	±38	856	±38	1039	±74	6.14	0.8303
E43b	0.0714	0.0020	1.614	0.118	0.1640	0.0106	6532	976	±46	979	±59	969	±58	-0.33	0.9190
E43c	0.0714	0.0020	1.360	0.078	0.1382	0.0066	10,573	872	±33	834	±37	969	±59	4.51	0.8673
E44	0.0802	0.0029	2.062	0.149	0.1865	0.0106	3110	1136	±49	1102	±58	1202	±70	-2.59	0.8870
E45a	0.0846	0.0028	2.101	0.134	0.1801	0.0090	5686	1149	±44	1067	±49	1307	±64	-6.85	0.8712
E45b	0.0841	0.0029	2.155	0.228	0.1860	0.0177	3543	1167	±73	1100	±96	1294	±67	-5.23	0.9311
E46	0.0821	0.0043	2.105	0.192	0.1859	0.0122	3583	1150	±63	1099	±66	1248	±102	-3.95	0.8532
E47	0.0763	0.0022	1.826	0.110	0.1736	0.0086	8616	1055	±39	1032	±47	1103	±58	-2.02	0.8920
E48	0.0985	0.0027	3.515	0.254	0.2588	0.0161	7927	1531	±57	1484	±83	1596	±51	-1.84	0.9301
F01	0.0785	0.0022	1.915	0.113	0.1769	0.0087	8335	1086	±39	1050	±48	1159	±56	-3.06	0.8934
F02	0.0867	0.0024	2.901	0.203	0.2426	0.0147	16,028	1382	±53	1400	±76	1355	±52	0.77	0.9330
F03	0.0799	0.0025	2.083	0.151	0.1892	0.0115	3419	1143	±50	1117	±62	1193	±62	-1.92	0.9078
F04	0.0813	0.0027	2.110	0.180	0.1882	0.0139	3467	1152	±59	1112	±75	1228	±66	-3.00	0.9173
F05	0.0821	0.0023	2.987	0.230	0.2639	0.0178	6607	1404	±58	1510	±91	1248	±54	3.68	0.9465
F06	0.0953	0.0030	2.619	0.170	0.1994	0.0103	6634	1306	±48	1172	±55	1533	±60	-9.38	0.8778
F07	0.0766	0.0039	1.837	0.154	0.1738	0.0103	3166	1059	±55	1033	±56	1112	±101	-2.22	0.8407
F08	0.0825	0.0022	1.980	0.114	0.1742	0.0085	16,357	1109	±39	1035	±47	1256	±52	-6.56	0.8922
F09	0.0818	0.0024	2.229	0.146	0.1977	0.0106	4692	1190	±46	1163	±57	1240	±59	-1.83	0.9031
F10	0.0877	0.0042	2.366	0.199	0.1958	0.0119	3010	1232	±60	1153	±64	1375	±92	-5.64	0.8538
F11	0.0685	0.0029	1.316	0.088	0.1394	0.0064	2262	853	±39	841	±36	883	±89	1.36	0.8039
F12	0.0837	0.0025	2.109	0.128	0.1827	0.0091	9338	1152	±42	1082	±50	1286	±57	-5.66	0.8870
F13	0.0844	0.0042	1.999	0.161	0.1717	0.0096	2447	1115	±54	1022	±53	1302	±96	-8.65	0.8170
F14	0.0691	0.0074	1.317	0.169	0.1382	0.0069	1190	853	±74	834	±39	903	±220	2.27	0.9644
F15	0.0717	0.0024	1.496	0.097	0.1514	0.0077	2135	929	±40	909	±43	977	±69	2.22	0.8652
F16	0.0647	0.0086	1.141	0.175	0.1279	0.0062	898	773	±83	776	±35	764	±280	-0.40	0.9600

(continued on next page)

Table 2 (continued)

Sample analysis	$^{207}\text{Pb}^*/^{206}\text{Pb}^*$	$\pm t\sigma$	$^{207}\text{Pb}^*/^{235}\text{U}$	$\pm t\sigma$	$^{206}\text{Pb}^*/^{238}\text{U}$	$\pm t\sigma$	Hg-Corr	$^{206}\text{Pb}^*/^{204}\text{Pb}$	$^{207}\text{Pb}^*/^{235}\text{U}$	age (Ma)	$\pm t\sigma$ (95% Conf)	$^{206}\text{Pb}^*/^{238}\text{U}$	age (Ma)	$\pm t\sigma$ (95% Conf)	$^{207}\text{Pb}^*/^{206}\text{Pb}^*$	age (Ma)	$\pm t\sigma$ (95% Conf)	% discord.	Rho
<i>OT-1</i>																			
F17	0.0824	0.0030	1.870	0.126	0.1647	0.0086	2425		1071		$\pm 45$	983		$\pm 48$	1254		$\pm 70$	8.94	0.8563
F18	0.0604	0.0047	0.883	0.083	0.1060	0.0047	2823		643		$\pm 45$	649		$\pm 28$	619		$\pm 169$	-1.03	0.4941
F19	0.0764	0.0029	1.823	0.124	0.1730	0.0087	2049		1054		$\pm 45$	1029		$\pm 48$	1105		$\pm 75$	-2.18	0.8620
F20	0.0789	0.0023	1.841	0.109	0.1693	0.0082	32,703		1060		$\pm 39$	1008		$\pm 45$	1169		$\pm 59$	-4.84	0.8796
F21	0.0810	0.0026	2.566	0.177	0.2299	0.0125	2881		1291		$\pm 50$	1334		$\pm 65$	1221		$\pm 64$	2.05	0.9116
F22a	0.0745	0.0064	2.002	0.239	0.1949	0.0106	1153		1116		$\pm 81$	1148		$\pm 57$	1056		$\pm 172$	2.12	0.7410
F22b	0.0775	0.0070	2.087	0.260	0.1953	0.0112	2816		1145		$\pm 86$	1150		$\pm 60$	1134		$\pm 180$	0.38	0.7300
F23	0.0738	0.0047	1.705	0.152	0.1675	0.0084	2612		1010		$\pm 57$	998		$\pm 46$	1037		$\pm 130$	1.22	0.7581
F24	0.0630	0.0046	1.216	0.118	0.1400	0.0071	1318		808		$\pm 54$	844		$\pm 40$	709		$\pm 157$	-4.32	0.7088
F25a	0.0717	0.0055	1.856	0.194	0.1876	0.0094	1693		1066		$\pm 69$	1108		$\pm 51$	979		$\pm 157$	3.10	0.7488
F25b	0.0776	0.0025	2.095	0.141	0.1959	0.0106	5196		1147		$\pm 46$	1153		$\pm 57$	1136		$\pm 64$	0.40	0.9022
F26	0.0776	0.0034	2.013	0.147	0.1880	0.0097	4360		1120		$\pm 50$	1111		$\pm 53$	1138		$\pm 87$	-0.69	0.8528
F27a	0.0810	0.0022	2.030	0.123	0.1818	0.0094	18,289		1126		$\pm 41$	1077		$\pm 51$	1221		$\pm 54$	-3.95	0.9003
F27b	0.0798	0.0023	2.016	0.148	0.1833	0.0120	12,090		1121		$\pm 50$	1085		$\pm 65$	1191		$\pm 56$	-2.82	0.9198
F28	0.0819	0.0021	1.987	0.124	0.1761	0.0096	47,106		1111		$\pm 42$	1046		$\pm 53$	1242		$\pm 51$	-5.70	0.9059
F29	0.0795	0.0025	1.853	0.112	0.1690	0.0081	4923		1064		$\pm 40$	1007		$\pm 45$	1185		$\pm 62$	-5.43	0.8705
F30	0.0753	0.0031	1.638	0.117	0.1579	0.0084	4264		985		$\pm 45$	945		$\pm 47$	1076		$\pm 83$	4.26	0.8444
F31	0.0736	0.0043	1.569	0.133	0.1547	0.0077	968		958		$\pm 53$	927		$\pm 43$	1030		$\pm 118$	3.34	0.7626
F32	0.0726	0.0040	1.750	0.143	0.1748	0.0087	1897		1027		$\pm 53$	1039		$\pm 48$	1002		$\pm 112$	0.98	0.8044
F33	0.0986	0.0035	3.010	0.206	0.2214	0.0115	6194		1410		$\pm 52$	1289		$\pm 61$	1598		$\pm 66$	-6.79	0.8762
F34	0.0816	0.0023	2.145	0.132	0.1908	0.0097	4791		1164		$\pm 43$	1126		$\pm 52$	1235		$\pm 56$	-2.77	0.8993
F35	0.0695	0.0028	1.364	0.092	0.1424	0.0070	3107		874		$\pm 39$	858		$\pm 39$	913		$\pm 84$	1.82	0.8275
F36	0.0676	0.0027	1.274	0.084	0.1367	0.0066	3482		834		$\pm 38$	826		$\pm 38$	856		$\pm 83$	0.97	0.8266
F37	0.0794	0.0021	1.803	0.101	0.1647	0.0078	12,013		1047		$\pm 37$	983		$\pm 43$	1182		$\pm 53$	6.49	0.8856
F38	0.0813	0.0024	2.015	0.120	0.1799	0.0087	7698		1121		$\pm 40$	1066		$\pm 47$	1228		$\pm 58$	-4.49	0.8845
F39	0.0702	0.0027	1.431	0.093	0.1479	0.0069	1932		902		$\pm 39$	889		$\pm 39$	934		$\pm 79$	1.44	0.8355
F40	0.0762	0.0030	1.807	0.122	0.1719	0.0083	2789		1048		$\pm 44$	1023		$\pm 46$	1101		$\pm 79$	-2.25	0.8484

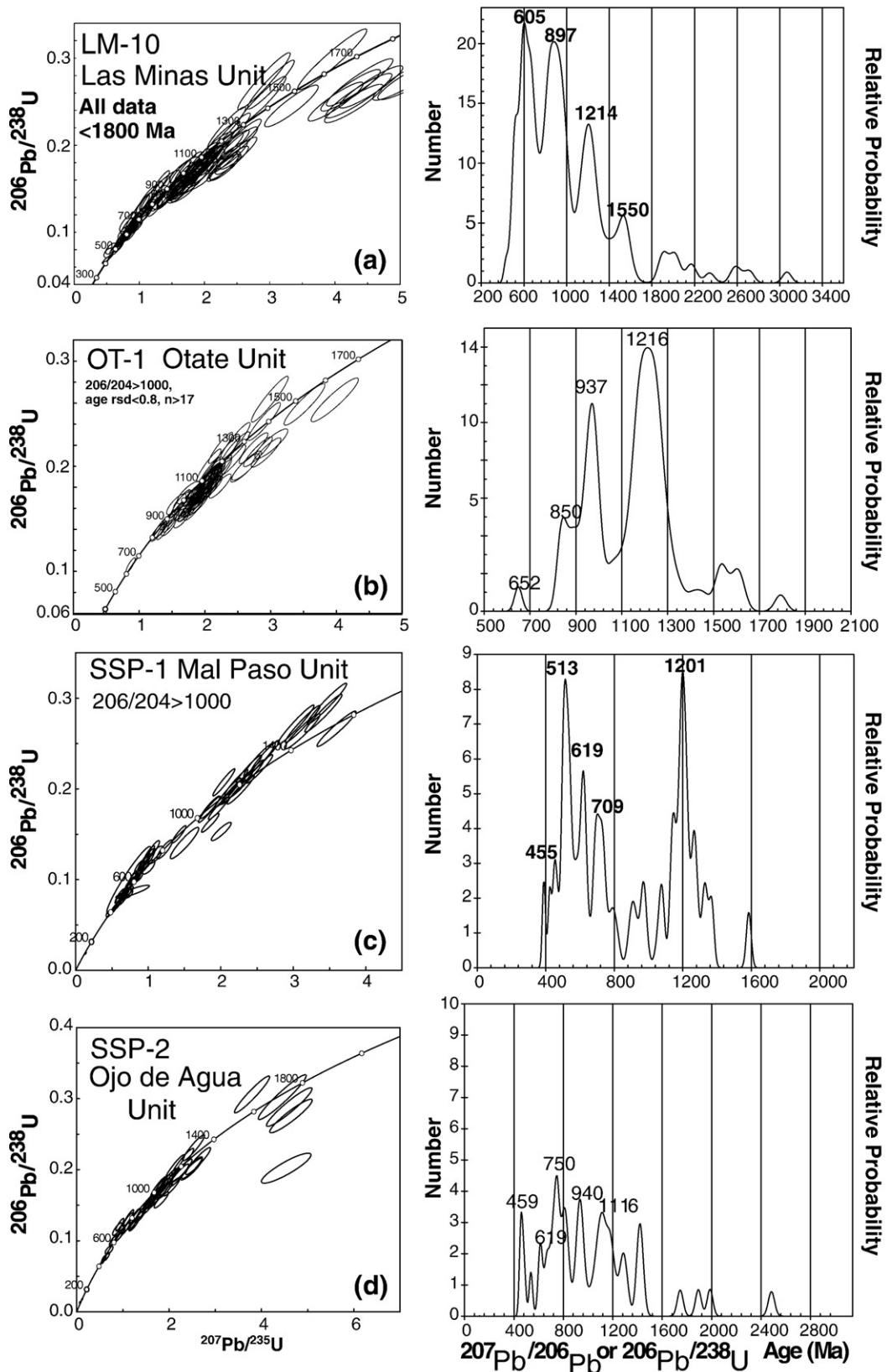


Fig. 8. U-Pb LA-ICPMS zircon analyses in psammitic samples from the Patlanoaya area plotted on concordia and histogram diagrams: (a) Las Minas Unit; (b) Ocate Unit; (c) Mal Paso Unit, and (d) Ojo de Agua Unit.

Table 3  
 $^{40}\text{Ar}/^{39}\text{Ar}$  analyses of hornblende from the Xayacatlán mafic dike

AOR-R590: XAY13 Amph 40/60

Steps	Laser power (Watts)	Isotope volumes					Isotope correlation data									
		$^{40}\text{Ar}$	$^{39}\text{Ar}$	$^{38}\text{Ar}$	$^{37}\text{Ar}$	$^{36}\text{Ar}$	Ca/K	Cl/K	% $^{40}\text{Ar}$ atm	f	$^{39}\text{Ar}$	$^{40}\text{Ar}^*/^{39}\text{ArK}$	Age	$^{36}\text{Ar}/^{40}\text{Ar}$	$^{39}\text{Ar}/^{40}\text{Ar}$	r
1	2.50	3.225±0.039	0.078±0.002	0.007±0.001	0.065±0.002	0.006±0.000	3.652	0.012	55.05	3.63	18.733±1.747	230.19±20.16	0.001864±0.000131	0.023976±0.000730	0.079	
2	4.00	1.114 0.007	0.048 0.001	0.002 0.001	0.032 0.001	0.001 0.000	2.882	0.001	8.65	2.21	21.180 1.725	258.21 19.59	0.000293 0.000236	0.043127 0.001184	0.003	
3	5.00	1.692 0.014	0.076 0.002	0.004 0.001	0.097 0.002	0.001 0.000	5.604	0.004	3.99	3.52	21.469 1.255	261.48 14.23	0.000135 0.000171	0.044718 0.001124	0.006	
4	6.00	6.722 0.025	0.237 0.003	0.012 0.001	0.508 0.005	0.002 0.000	9.478	0.007	3.56	11.10	27.623 0.524	329.94 5.72	0.000121 0.000050	0.034911 0.000428	0.032	
5	6.50	4.669 0.013	0.136 0.002	0.007 0.001	0.268 0.003	0.001 0.000	8.669	0.008	1.81	6.38	33.923 0.840	397.44 8.83	0.000061 0.000066	0.028946 0.000449	0.024	
6**	7.00	31.556 0.038	0.831 0.006	0.043 0.001	1.601 0.015	0.003 0.000	8.483	0.008	1.49	39.16	37.698 0.300	436.70 3.08	0.000051 0.000016	0.026131 0.000193	0.128	
7**	7.50	26.891 0.031	0.722 0.005	0.039 0.001	1.624 0.015	0.003 0.000	9.917	0.009	1.08	34.01	37.151 0.338	431.06 3.49	0.000037 0.000021	0.026628 0.000210	0.117	
Total/average		75.61±0.071	2.108±0.009	0.106±0.003	9.981±0.023	0.013±0.001	8.692	0.007		100.00	37.443±0.101	403.78±1.27				

Footnotes: Isotope production ratios.

( $^{40}\text{Ar}/^{39}\text{Ar}$ )K=0.0302.

( $^{37}\text{Ar}/^{39}\text{Ar}$ )Ca=1416.4306.

( $^{36}\text{Ar}/^{39}\text{Ar}$ )Ca=0.3952.

Ca/K=1.83 × ( $^{37}\text{Ar}$ Ca/ $^{39}\text{Ar}$ K).

J=0.007265±0.000028.

Volume  $^{39}\text{Ar}$ K=21.08.

Integrated date=403.78±2.53.

Plateau date=434.08±2.76.

% $^{39}\text{Ar}$ K for PA=73.17.

Isotope correlation date=262.75±65.54.

Initial  $^{40}\text{Ar}/^{36}\text{Ar}$  ratio=257.95±544.57.

MSWD=0.04.

% $^{39}\text{Ar}$ K for CA=9.35.

## 5. Geochemistry

### 5.1. Analytical techniques

Forty-seven samples were collected during a detailed investigation of the freshest dike in the Xayacatlán dike swarm (Fig. 3), 9 samples of the Anacahuite Amphibolite (Fig. 5), 8 samples from the mafic dikes in the Las Minas Unit (Fig. 6), 3 samples from the mafic selvage of the Palo Liso granite, and 9 samples in the Cuauhté area (Fig. 7). The samples were analyzed by the X-ray fluorescence technique for major and several trace elements (Rb, Sr, Ba, Zr, Nb, Y, Zn, V, Cr and Ni) in the Nova Scotia Regional Geochemical Centre at Saint Mary's University, Halifax, Nova Scotia, Canada. Additional trace elements (La, Ce, Pr, Nd, Sm, Eu, Gd, Tb, Dy, Er, Tm, Yb, Lu, Nb, Th and Hf) were determined by inductively-coupled plasma-mass spectrometer (ICP-MS) in 13 selected samples in the Geochemical laboratory of the Ontario Geological Survey in Sudbury, Canada. The precision and accuracy of the ICP-MS and X-ray fluorescence data were reported by Ayer and Davis (1997) and Dostal et al. (1986, 1994), respectively. Analytical errors are generally <5 rel.%. The analyses of the samples are given in Table 4. Minerals in the Xayacatlán dike were analyzed at the Department of Earth Sciences of Dalhousie University (Halifax, Nova Scotia, Canada) using a JEOL Superprobe 733 equipped with four wavelength-dispersive spectrometers and one energy-dispersive spectrometer, and operated with a beam current of 15 kV at 5 nA.

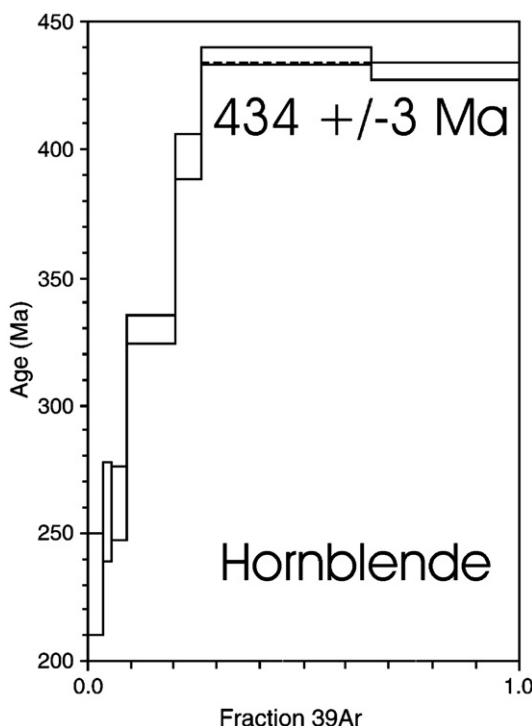


Fig. 9.  $^{40}\text{Ar}/^{39}\text{Ar}$  data from hornblende in an amphibolitic sheet cutting the thickest Xayacatlán dike plotted on incremental release spectrum.

### 5.2. Results

All of the rocks have been affected to a varying degree by secondary processes, which modified the chemical composition of these rocks. For example, variable contents of LOI (up to 5.1 wt.% in the Anacahuite Amphibolite and up to 6.8 wt.% in Las Minas mafic rocks) are largely due to secondary processes (Table 4). Alteration has also changed the alkali elements in some samples as shown by the variations of the  $\text{Na}_2\text{O}/\text{K}_2\text{O}$  ratio that range from about 5 to 20 in the Anacahuite samples and up to 100 in the Las Minas samples. The most highly altered samples were omitted from further consideration. The concentrations of most major elements, high-field-strength elements (HFSE), rare earth elements (REE), Th and transition elements in the remaining samples were probably not significantly remobilized and are thought to reflect the primary magmatic distribution.

### 5.3. Xayacatlán dike swarm

The rocks are distinctly bimodal with a strong predominance of mafic over felsic types (Table 4). The mafic rocks, with  $\text{SiO}_2$  ranging between 46 and 55 wt.% (LOI-free), are variable in their composition, although they display a tholeiitic fractionation trend (Fig. 10). They can be subdivided into three distinct groups (Fig. 11). Rocks of the *first group*, which plot predominantly in the field of high-Mg tholeiitic rocks on the  $\text{Al}-\text{Mg}-\text{Ti}$  diagram (Fig. 11), have high Mg# ( $\text{MgO}/[\text{MgO} + \text{FeO}^*]$  in mole%) (0.68–0.73) and elevated Cr (250–650 ppm) and Ni (70–150 ppm) abundances (Table 4). Cr and Ni positively correlate with MgO ranging between 10 to 14 wt.%. On the other hand, the rocks have relatively low abundances of incompatible trace elements such as Zr, P and rare earth elements (REE), which, like Ti, show negative correlation with Mg#. Their Ti/V ratios are low (20–25) compared to the other two groups. Their chondrite-normalized REE patterns display a minor light REE enrichment relative to heavy REE with  $(\text{La/Yb})_n \sim 4–7$  (Fig. 12a). The HREE part of the pattern is horizontal. The REE patterns of all these rocks are sub-parallel but their total abundances increase with differentiation. The chemical characteristics of these rocks are consistent with the relicts of cumulate textures. It appears that the rocks represent a mixture of cumulate minerals containing interstitial liquids of tholeiitic affinities.

The rocks of the *second group* (Fig. 11) have Mg# between 0.66 and 0.60 and high contents of Cr (700–1200 ppm) and Ni (180–350 ppm) (Table 4). On the other hand, they have relatively low contents of  $\text{Al}_2\text{O}_3$  (<14%) and low  $\text{Al}_2\text{O}_3/\text{CaO}$  (1–2), but high Ti/V (25–32). They have variable contents of MgO (9–14%), which shows a positive correlation with Cr, Ni and CaO. The rocks probably represent pyroxene dominated cumulates derived from a tholeiitic basaltic parent.

The rocks of the *third group* include mafic types with variable proportions of plagioclase bands or rocks rich in plagioclase. The rocks have relatively low Mg# (0.53–0.60), MgO (5–10%), Cr (~200 ppm) and Ni (20–120 ppm) but high  $\text{Al}_2\text{O}_3$  (15–22%) (Table 4). Their REE patterns (Fig. 12b),

Table 4  
Chemical analyses of samples from the Acatlán Complex

Sample	XAYA-26	XAYA-33	XAYA-34	XAYA-37	XAYA-40	XAYA-48	XAYA-06	XAYA-08	XAYA-19	XAYA-30	XAYA-29	XAYA-39	XAYA-42	XAYA-44	XAYA-4G	XAYA-10
SiO <sub>2</sub> (wt.%)	48.36	47.79	46.96	47.21	48.49	48.33	49.70	49.16	47.03	49.79	47.19	46.56	50.85	48.32	77.39	72.71
TiO <sub>2</sub>	0.60	0.37	0.60	0.38	0.55	0.66	1.02	1.15	0.94	0.71	1.08	0.83	1.64	1.01	0.09	0.07
Al <sub>2</sub> O <sub>3</sub>	16.40	16.19	14.18	16.76	14.92	15.06	10.96	11.65	10.19	10.19	21.45	16.63	14.73	19.99	11.80	15.48
Fe <sub>2</sub> O <sub>3</sub>	8.30	7.24	9.23	7.73	8.75	9.78	13.07	13.54	13.85	12.21	8.73	11.44	10.82	8.20	1.69	0.81
MnO	0.14	0.12	0.15	0.13	0.15	0.16	0.25	0.25	0.28	0.25	0.13	0.20	0.20	0.14	0.03	0.00
MgO	9.84	9.93	12.15	10.37	10.68	10.97	10.27	10.52	13.07	11.53	5.64	8.07	6.97	5.57	0.65	0.14
CaO	9.79	10.94	9.68	11.46	8.91	8.78	8.90	8.82	9.71	9.95	7.10	8.70	9.19	7.64	5.16	0.42
Na <sub>2</sub> O	0.75	0.81	0.60	0.46	0.73	0.75	1.05	1.48	0.95	1.19	1.96	1.59	2.72	2.73	2.03	8.26
K <sub>2</sub> O	3.41	2.74	2.59	2.79	3.28	3.36	1.05	1.05	1.19	1.38	4.11	2.49	1.73	3.28	0.77	0.53
P <sub>2</sub> O <sub>5</sub>	0.11	0.08	0.09	0.09	0.11	0.13	0.05	0.05	0.03	0.05	0.29	0.02	0.23	0.28	0.04	0.06
LOI	2.39	2.30	2.72	2.64	2.65	2.79	2.19	2.43	2.54	2.53	3.10	2.45	1.78	3.12	1.10	0.56
Total	100.10	98.51	98.94	100.01	99.22	100.76	98.51	100.11	99.78	99.78	100.78	98.98	100.86	100.28	100.75	99.05
Mg#	70.13	73.09	72.28	72.65	70.74	68.96	60.88	60.61	65.14	65.16	56.13	58.28	56.06	57.36	43.24	25.50
Cr (ppm)	309	255	451	303	320	320	935	840	1141	955	104	251	101	123	18	8
Ni	82	69	109	82	78	97	277	181	349	320	79	51	54	84	6	1
Co	37	36	47	37	42	46	59	59	61	49	33	49	33	43	2	2
V	159	110	160	114	151	186	189	217	177	146	181	197	256	173	19	13
Cu	48	65	77	55	101	122	18	17	7	5	5	31	2	11	5	22
Zn	65	76	72	66	72	89	148	157	173	149	93	112	104	91	22	11
Rb	87	75	63	74	82	78	21	21	24	29	110	61	88	34	26	21
Ba	1052	767	689	756	1004	1012	176	237	257	288	1184	762	594	832	276	296
Sr	96	104	56	98	73	114	100	112	58	61	347	179	208	294	147	65
Ga	16	13	13	13	16	18	22	21	21	20	29	24	15	25	20	10
Ta	0.22		0.2		0.4	0.3					0.63	0.34	1.23	0.63	0.34	0.05
Nb	3.7	1.8	2.6	1.9	3.9	5.0	21.0	29.0	24.0	16.0	14.2	6.6	20.7	14.2	2.8	1.9
Hf	2.21	1.30	1.80	1.40	2.10	2.10					6.41	3.70	3.30	5.85	3.90	4.36
Zr	82	44	55	46	64	64	232	154	127	103	238	147	132	213	128	170
La	18.6	13.0	15.4	12.5	19.0	18.7	24.0	23.0	20.0	17.0	27.8	18.6	23.6	30.2	30.8	36.0
Ce	44.8	26.3	33.4	26.4	48.2	49.7					68.4	47.6	53.0	77.6	58.1	67.6
Pr	5.38	3.32	4.39	3.37	5.82	6.54					9.52	6.76	6.59	11.10	7.07	7.72
Nd	20.4	13.6	18.9	13.9	22.0	26.9	51.0	57.0	44.0	36.0	41.1	28.2	26.1	47.6	25.4	28.2
Sm	4.04	2.77	3.98	2.85	4.30	5.44					8.79	6.01	5.65	10.70	4.35	4.15
Eu	1.00	0.73	0.97	0.75	1.08	1.24					1.75	1.47	2.29	1.83	1.17	1.54
Gd	3.59	2.49	3.53	2.43	3.64	4.35					7.72	5.10	5.87	9.32	3.14	2.75
Tb	0.526	0.363	0.524	0.371	0.537	0.641					1.160	0.761	0.977	1.430	0.426	0.285
Dy	3.06	2.11	3.06	2.16	3.14	3.66					6.69	4.32	5.97	8.10	2.12	1.11
Ho	0.618	0.436	0.617	0.437	0.644	0.729					1.320	0.877	1.240	1.580	0.399	0.170
Er	1.77	1.25	1.79	1.22	1.85	2.13					3.69	2.45	3.61	4.46	1.16	0.34
Tm	0.251	0.174	0.252	0.176	0.266	0.299					0.514	0.362	0.521	0.617	0.175	0.050
Yb	1.63	1.13	1.60	1.16	1.76	1.97					3.19	2.37	3.36	3.86	1.24	0.30
Lu	0.239	0.167	0.238	0.169	0.264	0.292					0.454	0.358	0.496	0.537	0.187	0.050

Table 4 (continued)

Sample	AH-1	AH-4	AH-5	AH-6	AH-7	AH-8	AH-9	AH-2	AH-3	LM-1	LM-3	LM-5	LM-6	LM-7	LM-2	LM-8	LM-9
SiO <sub>2</sub> (wt.%)	46.06	47.00	48.76	47.72	46.81	45.39	46.00	48.12	48.41	46.50	47.89	65.82	45.63	39.19	48.18	45.92	46.35
TiO <sub>2</sub>	2.62	2.29	2.48	2.50	2.28	3.65	1.97	2.82	2.06	2.33	0.70	2.33	1.56	2.00	2.57	1.77	
Al <sub>2</sub> O <sub>3</sub>	14.42	13.24	12.30	14.11	13.17	12.39	11.65	12.40	12.86	14.36	13.82	14.46	13.19	10.31	13.95	12.92	14.02
Fe <sub>2</sub> O <sub>3</sub>	14.11	12.69	12.58	14.16	12.03	16.69	11.82	14.16	11.95	14.36	15.03	6.24	14.59	12.62	14.19	15.12	13.05
MnO	0.19	0.18	0.20	0.19	0.17	0.23	0.20	0.21	0.17	0.23	0.26	0.14	0.25	0.29	0.21	0.25	0.22
MgO	6.01	8.05	4.67	6.18	7.05	5.25	6.79	5.75	8.19	7.02	6.12	3.07	5.77	11.52	6.79	5.97	6.87
CaO	11.07	11.39	11.18	10.25	11.75	10.36	11.96	10.47	11.21	7.79	7.26	0.56	8.94	11.47	10.23	8.51	10.04
Na <sub>2</sub> O	1.72	2.11	4.17	2.98	2.70	2.90	3.50	2.91	2.57	2.30	0.06	2.56	1.38	0.01	1.30	2.09	0.91
K <sub>2</sub> O	0.25	0.31	0.21	0.31	0.29	0.00	0.22	0.60	0.34	0.12	0.74	2.47	0.04	0.01	0.07	0.02	0.05
P <sub>2</sub> O <sub>5</sub>	0.26	0.24	0.27	0.25	0.22	0.38	0.20	0.30	0.21	0.20	0.22	0.15	0.23	0.18	0.19	0.25	0.16
LOI	3.31	2.17	2.57	2.09	2.28	1.18	5.12	2.65	1.99	4.97	6.19	2.80	6.76	13.64	3.74	6.70	6.56
Total	100.01	99.66	99.39	100.74	98.76	98.42	99.42	100.38	99.96	99.91	99.92	98.97	99.11	100.80	100.85	100.32	100.00
Mg#	45.76	55.68	42.37	46.36	53.72	38.38	53.22	44.57	57.58	49.19	44.64	49.35	43.92	64.38	48.66	43.88	51.04
Cr (ppm)	121	248	50	47	219	31	197	90	265	255	63	37	48	706	106	58	106
Ni									53	24	1	11	587	37	11	33	
Co	56	53	45	58	49	47	47	53	50	65	64	25	64	84	59	65	63
V	330	293	336	356	307	451	275	337	270	310	359	85	325	230	321	346	266
Cu									166	24	12	160	13	161	185	158	
Zn									102	138	102	128	110	92	115	136	
Rb									10	30	94	10	9	10	10	10	
Ba									627	159	398	10	46	25	10	10	
Sr	353	295	297	317	309	270	184	280	268	373	715	46	561	380	415	354	525
Ga								0.0	0.0	18	23	17	20	17	20	21	19
Ta								1.34	0.93					0.54	0.68	0.49	
Nb	18.0	18.0	18.0	18.0	16.0	26.0	13.0	22.6	15.4	10.0	12.0	14.0	14.0	11.0	9.3	11.7	8.3
Hf								4.80	3.50					3.40	4.40	3.10	
Zr	172	152	160	161	143	224	124	194	138	124	193	173	178	135	134	170	119
La								18.30	13.50	19.00	23.00	33.00	20.00	5.00	8.85	11.80	9.40
Ce								44.80	32.10					22.20	29.80	22.80	
Pr								6.12	4.41			0.00	0.00	0.00	3.26	4.32	3.20
Nd								27.70	20.20	20.00	21.00	24.00	22.00	10.00	16.20	21.20	15.20
Sm								6.70	4.95					4.70	5.92	4.19	
Eu								2.06	1.66					1.62	2.01	1.44	
Gd								6.87	5.14					5.63	6.96	5.01	
Tb								1.05	0.79					0.94	1.15	0.83	
Dy								6.05	4.48					5.94	7.07	5.13	
Ho								1.14	0.85					1.22	1.44	1.06	
Er								3.09	2.26					3.52	4.17	3.00	
Tm								0.410	0.307					0.494	0.582	0.420	
Yb								2.51	1.89					3.14	3.66	2.66	
Lu								0.349	0.264					0.461	0.527	0.396	

(continued on next page)

Table 4 (continued)

Sample	CEC-1	CEC-2	CEC-3	CEC-4	CEC-5	CEC-6	CEC-7	CEC-8	CEC-9	DEO-1	DEO-2	DEO-4
SiO <sub>2</sub> (wt.%)	47.85	47.96	47.98	48.10	47.33	57.22	75.44	72.03	71.54	48.10	49.55	47.79
TiO <sub>2</sub>	1.18	2.40	2.64	2.57	2.57	1.17	0.82	0.86	0.89	2.31	2.67	2.00
Al <sub>2</sub> O <sub>3</sub>	12.81	13.92	13.55	13.52	13.38	13.89	12.81	12.10	12.56	14.25	13.36	14.36
Fe <sub>2</sub> O <sub>3</sub>	10.78	12.05	12.94	12.47	13.68	10.20	3.98	4.79	5.09	13.88	14.32	13.47
MnO	0.19	0.15	0.17	0.17	0.18	0.10	0.17	0.08	0.08	0.15	0.16	0.27
MgO	9.48	7.36	5.85	6.80	5.87	3.60	1.24	1.07	1.34	4.80	5.14	6.01
CaO	13.42	9.41	11.03	10.02	10.17	7.36	0.58	1.37	0.86	5.03	4.69	10.16
Na <sub>2</sub> O	1.33	2.70	2.90	2.63	2.88	2.27	3.33	2.68	2.66	4.32	4.49	2.01
K <sub>2</sub> O	0.20	0.59	0.27	0.52	0.27	0.31	1.45	2.33	2.79	0.66	0.72	1.35
P <sub>2</sub> O <sub>5</sub>	0.09	0.26	0.28	0.27	0.28	0.18	0.06	0.12	0.14	0.32	0.29	0.20
LOI	1.90	2.93	2.09	3.16	2.38	2.72	1.49	2.02	2.11	5.16	3.48	1.72
Total	99.23	99.72	99.70	100.23	98.99	99.03	101.38	99.45	100.06	98.98	98.87	99.33
Mg#	63.52	54.74	47.24	51.92	45.94	41.14	38.16	30.67	34.27	40.65	41.55	46.91
Cr (ppm)	648	370	218	252	154	104	12	14	133	88	113	70
Ni	125	135	93	111	79	46	16	5	369	61	69	60
Co	45	62	62	61	65	54	36	33	32	53	77	67
V	284	337	365	341	356	224	62	61	77	276	332	365
Cu	61	101	63	67	57	45	82	27	32	118	123	187
Zn	100	93	108	109	122	100	74	66	68	128	132	108
Rb	4	11	2	8	0	15	84	93	111	8	8	24
Ba	38	84	68	60	84	72	229	408	581	339	380	352
Sr	186	291	368	249	301	299	102	65	80	168	72	368
Ga	19	23	24	23	25	19	13	14	17	20	22	24
Ta	0.35		1.15			0.64		1.28		0.90	1.06	0.69
Nb	6.0	16.0	21.1		14.0	11.0	37.0	22.5	40.0	21.6	24.5	12.4
Hf	1.68		3.80			3.04		6.52		5.15	5.40	3.23
Zr	63	151	157	141	164	135	465	346	497	227	245	128
La	3.71		12.66			14.59		26.13		20.01	22.18	8.41
Ce	8.96		29.40			30.87		52.30		43.43	47.76	19.56
Pr	1.36		4.07			4.03		6.57		5.78	6.35	2.87
Nd	6.67		18.99			17.55		25.83		25.22	27.46	13.54
Sm	2.11		4.74			4.13		5.14		5.90	6.16	3.85
Eu	0.85		1.68			1.23		1.18		1.75	1.83	1.33
Gd	3.04		5.74			4.88		5.43		6.83	7.06	5.07
Tb	0.53		0.85			0.77		0.84		1.11	1.14	0.83
Dy	3.31		5.20			5.03		5.31		6.81	6.90	5.39
Ho	0.61		0.85			0.87		0.97		1.21	1.24	0.97
Er	1.66		2.24			2.49		2.82		3.28	3.41	2.73
Tm	0.236		0.302			0.366		0.432		0.470	0.481	0.373
Yb	1.45		1.84			2.39		2.94		3.02	3.22	2.34
Lu	0.225		0.260			0.376		0.438		0.423	0.441	0.358

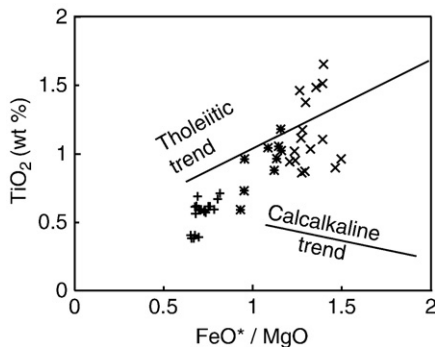


Fig. 10. Mafic rocks from the Xatacatlán dikes plotted on the  $\text{FeO}_{\text{tot}}/\text{MgO}$  versus  $\text{TiO}_2$ (wt %) diagram. Symbols: group 1 (+), group 2 (\*) and group 3 (x). Vectors for tholeiitic and calc-alkaline trends are after Miyashiro (1974).

which have  $(\text{La}/\text{Yb})_n$  ranging between 4 and 5, show either a negative or a positive Eu anomaly, indicating a role for feldspar during fractionation. As these rocks frequently occur in the same bodies as the other two groups and it appears that they represent variably differentiated gabbroic bodies.

From the field observation as well as from overall chemistry, it appears that the rocks are genetically related and most likely they represent variably differentiated tholeiitic gabbroic intrusions. The rocks are partially cumulates. All these rocks show negative Nb-Ta and Ti anomalies on the mantle-normalized plots (Fig. 13a and b), indicating that they were derived either from subcontinental lithospheric mantle or were affected by crustal contamination. From the data in hand, it is difficult to discriminate between these two possibilities, and both processes may have participated.

The felsic rocks are granitic with >72%  $\text{SiO}_2$ , but have highly variable compositions characterized by low  $\text{K}_2\text{O}$  (<1%) and variable  $\text{Na}_2\text{O}$  (2–8%) contents (Table 4). Their REE

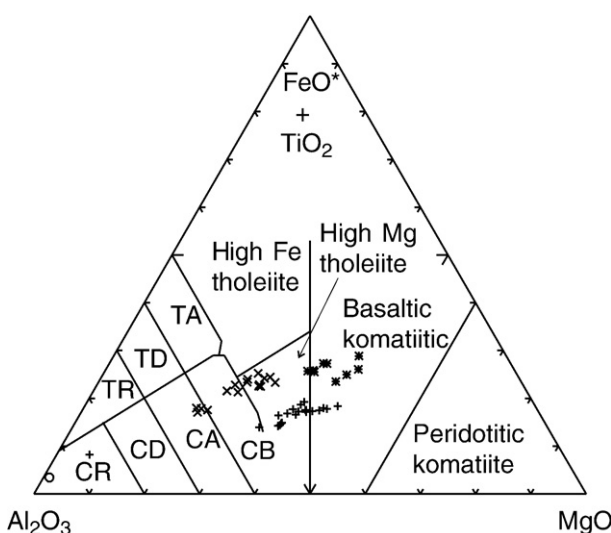


Fig. 11. Classification of the mafic rocks from Xatacatlán dikes using a Jensen (1976) cation plot. Symbols: group 1 (+), group 2 (\*) and group 3 (x). Fields: TA = tholeiitic andesite; TD = tholeiitic dacite; TR = tholeiitic rhyolite; CB = calc-alkaline basalt; CA = calc-alkaline andesite; CD = calc-alkaline dacite; CR = calc-alkaline rhyolite.

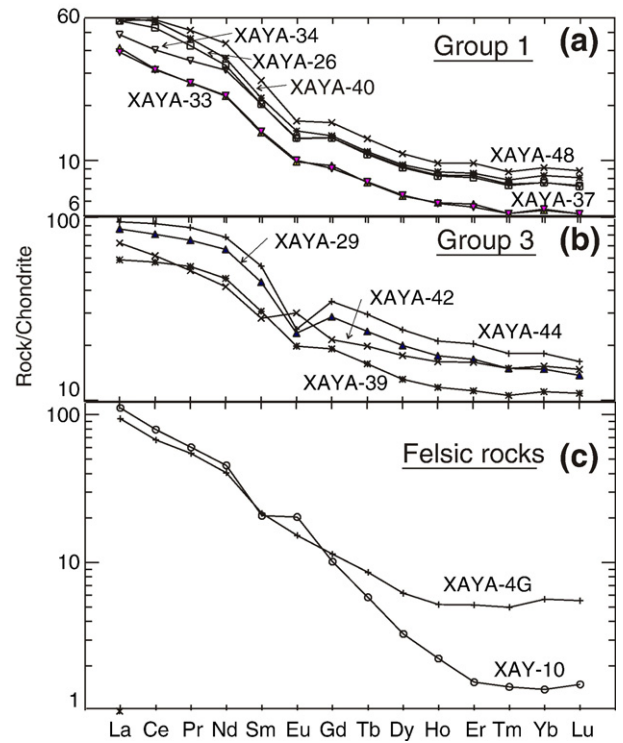


Fig. 12. Chondrite-normalized rare earth element abundances in the metaigneous rocks of: (a) Xayacatlán mafic rocks of group 1; (b) Xayacatlán mafic rocks of group 3; (c) Xayacatlán felsic rocks. Normalizing values are after Sun and McDonough (1989).

patterns are strongly enriched in light REE relative to HREE with patterns showing either no Eu anomaly or a positive Eu anomaly (Fig. 12c). The HREE segment of the patterns is horizontal. The mantle-normalized trace element patterns show a distinct enrichment in Th but negative anomalies of Nb, Ta and Ti, a shape similar to that of continental crust (Fig. 13c). The felsic rocks do not appear to be directly related to the mafic rocks and probably represent crustal partial melts possibly induced by the rising mafic magma.

#### 5.4. Patlanoaya area

The Anacahuite Amphibolite is characterized by low  $\text{SiO}_2$  contents (in the range of 47 to 51 wt.%; LOI-free) and variable Mg #, mostly between 0.58 and 0.38. According to  $\text{Zr}/\text{TiO}_2$  versus  $\text{SiO}_2$  relationship (Fig. 14a, Table 4), they are sub-alkaline basalts. The increase of Ti, Fe and V with fractionation for roughly constant  $\text{SiO}_2$  (Table 4) is characteristic of the tholeiitic suites. However, compared to typical tholeiitic suites, the rocks have higher Nb/Y ratio (Fig. 14b) suggesting mildly alkaline affinities. The rocks are typical within-plate basalts (Figs. 15 and 16).

The Las Minas minor intrusive rocks are also basaltic in composition with  $\text{SiO}_2$  ranging between 49 and 51 wt.% and Mg# between 0.51 and 0.44. They display the tholeiitic fractionation trends of increasing Ti, Fe and V with  $\text{FeO}^*/\text{MgO}$  (Fig. 17b). However, compared to the Anacahuite Amphibolite, the rocks have low Nb/Y (Fig. 14b), which is characteristic of

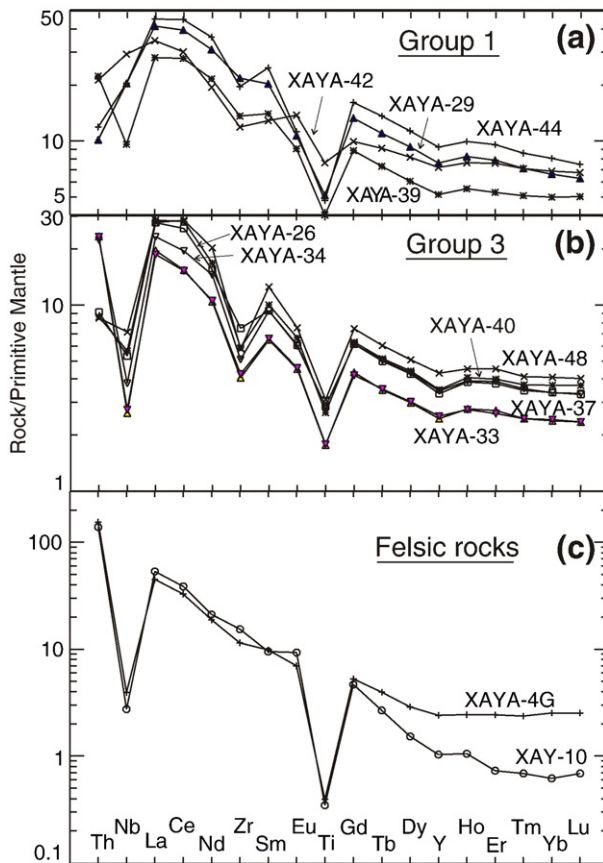


Fig. 13. Mantle-normalized incompatible trace element abundances in the metagranitic rocks of: (a) Xayacatlán mafic rocks of group 1; (b) Xayacatlán mafic rocks of group 3; (c) Xayacatlán felsic rocks. Normalizing values are after Sun and McDonough (1989).

sub-alkaline suites. They also show features of within-plate basalts (Figs. 15 and 16), and although both suites are compositionally similar, there are subtle differences between them (Table 4). In addition, the two groups show differences in the shape of both chondrite-normalized REE patterns and the mantle-normalized trace element plots (Figs. 18a and b, 19a and b). The Las Minas rocks have gently sloping REE patterns with  $(La/Yb)_n \sim 1.7\text{--}2.2$  and  $(Gd/Yb)_n \sim 1.5$  (Fig. 18b). The Anacahuite Amphibolites have distinctly more fractionated patterns with  $(La/Yb) \sim 4.4$  and  $(Gd/Yb)_n \sim 2.2$ . (Fig. 18a). Although mantle-normalized trace element patterns of both suites do not show negative anomalies of HFSE, the plots of Anacahuite rocks are more fractionated and peak at Nb-Ta (Fig. 19a and b). The rocks of both suites are characterized by low Th/La ratio ( $<0.12$ ), indicating that they were not significantly affected by crustal contamination. Likewise the mantle-normalized patterns without Nb-Ta depletion imply that their mantle sources were not modified by subduction processes.

Rocks of the mafic rim on the western margin of the Palo Liso granite (DEO samples) are also sub-alkaline basalts (Fig. 14a) with  $\text{SiO}_2$  ranging from 49 to 52% (LOI-free) and Mg# varying between 0.40 and 0.47. They are tholeiitic (Fig. 17) with within-plate characteristics (Figs. 15 and 16). Their REE patterns show a gentle slope with  $(La/Yb)_n \sim 2\text{--}4.2$

and  $(La/\text{Sm})_n \sim 1.2\text{--}2.0$  (Fig. 18c), and their mantle-normalized trace element patterns have no Nb-Ta and Ti anomalies (Fig. 19c). The mafic rim rocks are probably primitive continental tholeiites derived from a mantle that was not modified by subduction processes and the rocks were not affected by crustal contamination. As these mafic rocks form part of the Palo Liso granite, they resolve the tectonic setting of intrusion as within-plate and rift-related (c.f. Miller et al., 2007).

### 5.5. Cuaulote area

The rocks in the Cañada el Cuaulote (CEC samples) represent a bimodal suite of sub-alkaline basalts with  $\text{SiO}_2$  between 49 and 50 wt.% and Mg# between 0.46 and 0.64. The basaltic rocks are tholeiitic (Fig. 14A) and their trace element distribution shows typical within-plate characteristics (Figs. 15 and 16). Assuming that the magmatic major element composition was not significantly modified, the rocks have norms corresponding to olivine tholeiites. A decrease of Mg, Cr and Ni with increasing of differentiation suggests that the rocks were affected by crystallization of clinopyroxene and olivine. The

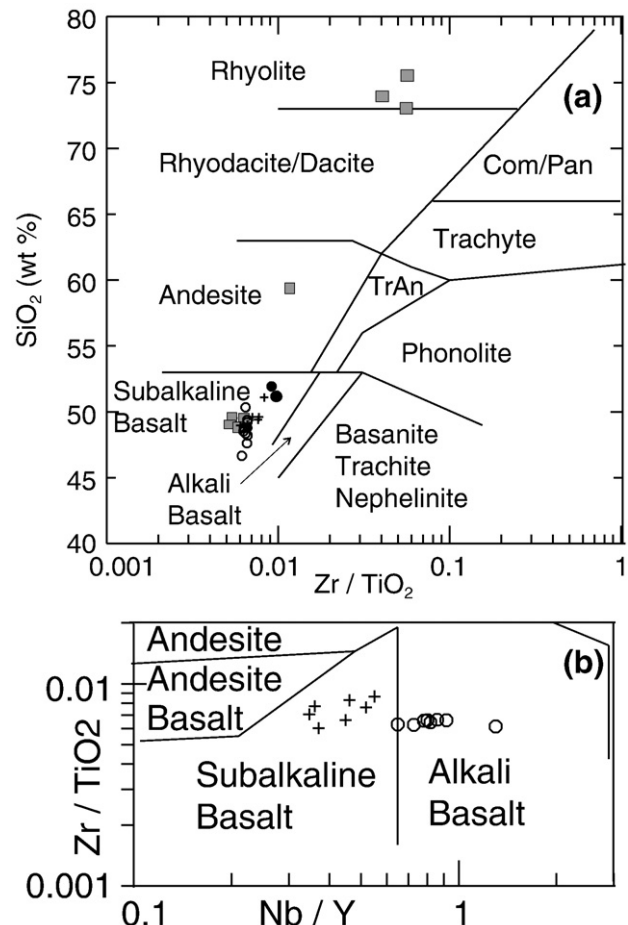


Fig. 14. Rocks from the Patlanoaya and Cuaulote areas plotted on: (a)  $\text{Zr}/\text{TiO}_2$  versus  $\text{SiO}_2$  diagram of Winchester and Floyd (1977); and (b)  $\text{Zr}/\text{TiO}_2$  versus  $\text{Nb}/\text{Y}$  diagram of Winchester and Floyd (1977). Abbreviations: Com/Pan = Comendite/Pantellerite; TrAn = trachyandesite. Patlanoaya area: Anacahuite (○), Las Minas (+) and mafic selvage of the Palo Liso granite (filled circle); and Cuaulote area (grey square).

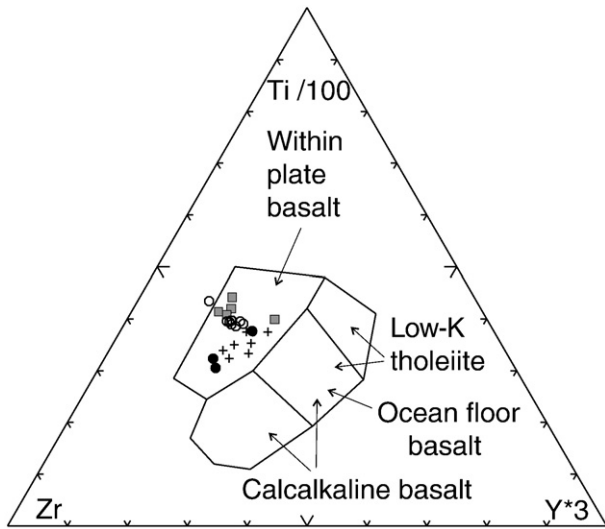


Fig. 15. Mafic rocks from the Patlanoaya and Cuauolote areas plotted on the Ti–Zr–Y tectonic discrimination diagram of Pearce and Cann (1973). Patlanoaya area: Anacahuite (○), Las Minas (+) and mafic selvage of the Palo Liso granite (filled circle); and Cuauolote area (grey square).

rocks have relatively horizontal chondrite-normalized REE patterns with  $(\text{La/Yb})_n \sim 1.5\text{--}4$  and  $(\text{La/Sm})_n 1\text{--}1.5$  (Fig. 18d). Their mantle-normalized trace element patterns do not show Nb–Ta and Ti anomalies (Fig. 19d).

The mylonized granitic samples have  $\text{SiO}_2 \sim 73\text{--}75$  wt.%; and are peraluminous with  $\text{Al}_2\text{O}_3/\text{CaO} + \text{Na}_2\text{O} + \text{K}_2\text{O} > 1$  and  $\text{Al}_2\text{O}_3/\text{Na}_2\text{O} + \text{K}_2\text{O} > 1$ . Their REE patterns are fractionated with  $(\text{La/Yb})_n \sim 5.5$  and  $(\text{La/Sm})_n \sim 2.8$  and show minor negative Eu anomalies (Fig. 18d).

## 6. Tectonic implications

The geochronological and geochemical data presented here indicate the presence of a widespread bimodal igneous event during the Ordovician. The Xayacatlán amphibolitic dikes were intruded at  $442 \pm 1$  Ma as layered tholeiitic gabbros with the primary mineralogy quickly converted to plagioclase and amphibole, which cooled through ca.  $570^\circ\text{C}$  by ca. 434 Ma. The bimodal Palo Liso diabase-granite was intruded 20 my years earlier, at  $461 \pm 2$  Ma (Miller et al., 2007), and the mafic rocks are primitive, within-plate tholeiites. Similarly, the Las Minas mafic dikes and the Anacahuite Amphibolite are within-plate tholeiites intruded either before or synchronously with a

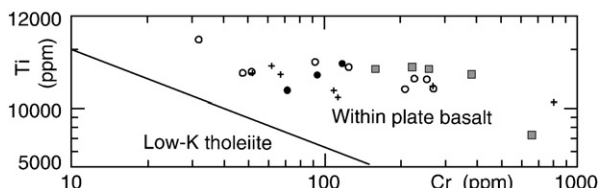


Fig. 16. Mafic rocks from the Patlanoaya and Cuauolote areas plotted on the Ti (ppm) versus Cr (ppm) plot of Pearce (1975). Patlanoaya area: Anacahuite (○), Las Minas (+) and mafic selvage of the Palo Liso granite (filled circle); and Cuauolote area (grey square). Compositional fields for island arc tholeiites and within-plate basalts are also shown.

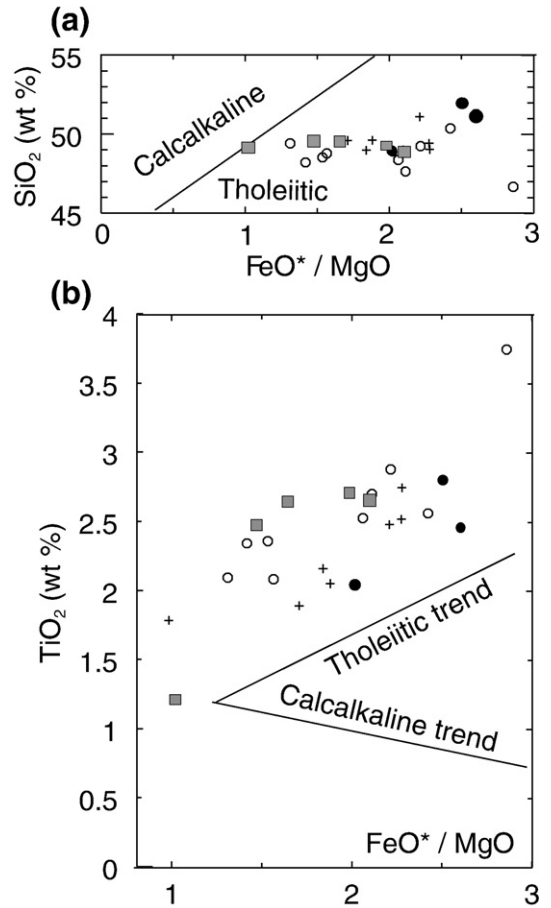


Fig. 17. Mafic rocks from the Patlanoaya and Cuauolote areas plotted on: (a) the  $\text{FeO}_{\text{tot}}/\text{MgO}$  versus  $\text{SiO}_2$  diagram, and (b)  $\text{FeO}_{\text{tot}}/\text{MgO}$  versus  $\text{TiO}_2$  diagram. Patlanoaya area: Anacahuite (○), Las Minas (+) and mafic selvage of the Palo Liso granite (filled circle); and (b) Cuauolote area (grey square). Vectors for tholeiitic and calc-alkaline trends are after Miyashiro (1974).

$460 \pm 9$  Ma nearby cross-cutting leucogranite dike (Vega-Granillo, 2006). The similarity of the Las Minas mafic rocks and the mafic selvage of the Palo Liso granite suggests that they are part of the same magmatic event. An older age limit for intrusion of the Las Minas dikes is provided by the  $496 \pm 25$  Ma age of the youngest concordant detrital zircon. Furthermore, the mafic rocks in the bimodal suite at Cuauolote are within-plate tholeiites intruded at  $461 \pm 7$  Ma (U–Pb age of the megacrystic granite: Talavera-Mendoza et al., 2005). The Xayacatlán dikes are distinct from the other suites in showing negative Nb, Ta and Ti anomalies attributable to either crustal contamination or derivation from subcontinental mantle previously modified by arc magmatism.

The dike swarm character of the minor intrusions in the Xayacatlán and Patlanoaya areas suggests that they were intruded during rifting. This rifting lasted from ca. 461 to 442 Ma, but may have started earlier at  $478 \pm 5$  Ma, the oldest dated granite of this suite (Talavera-Mendoza et al., 2005). This timing is more consistent with rifting associated with opening the Rheic Ocean because the Iapetus Ocean was being subducted throughout the Ordovician culminating in its complete closure at the end of the Ordovician. That the rocks

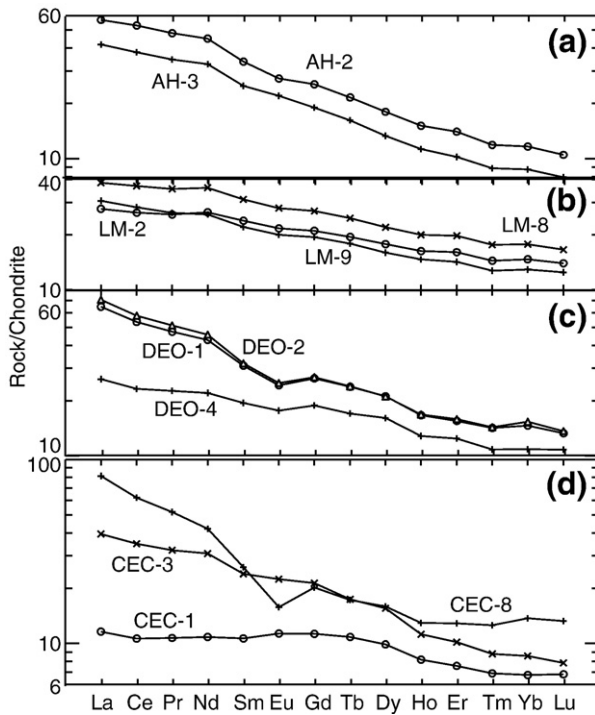


Fig. 18. Chondrite-normalized rare earth element abundances in the metaigneous rocks from the Patlanoaya and Cualote areas: (a) Anacahuite Amphibolite; (b) Las Minas; (c) mafic selvage of Palo Liso granite; and (d) Cuaulote rocks. Normalizing values are after Sun and McDonough (1989).

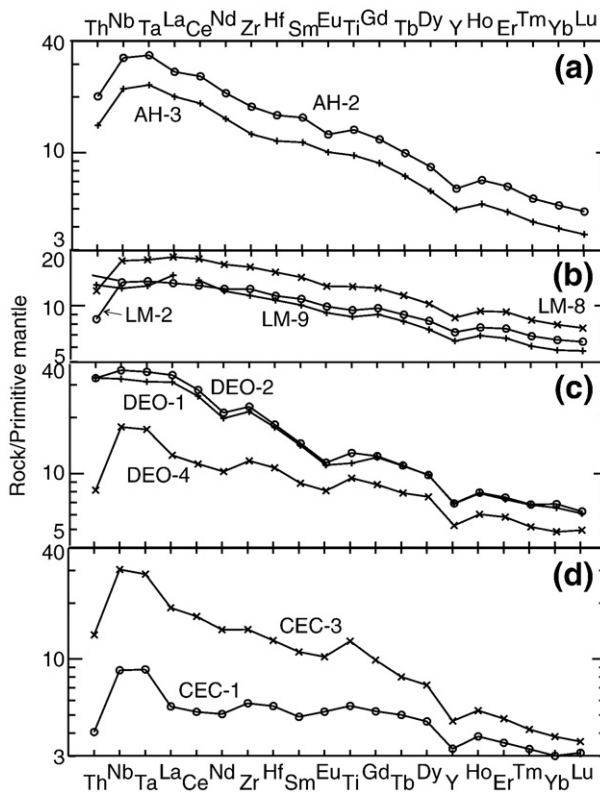


Fig. 19. Mantle-normalized incompatible trace element abundances in the metaigneous rocks from the Patlanoaya and Cuaulote areas: (a) Anacahuite Amphibolite; (b) Las Minas; (c) mafic selvage of Palo Liso granite; and (d) Cuaulote rocks. Normalizing values are after Sun and McDonough (1989).

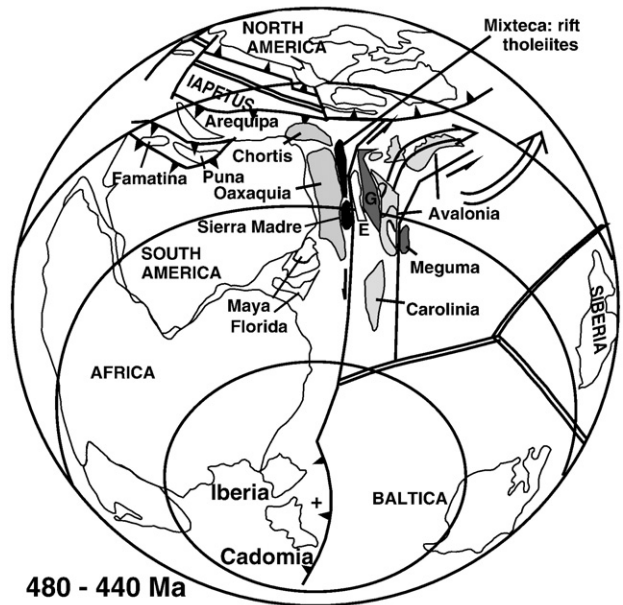


Fig. 20. Paleogeographic reconstruction at 460 Ma showing the location of the Xayacatlán Suite on the rifted margin of Oaxaquia (modified after Keppe, 2004).

were formed along the southern margin of the Rheic Ocean is indicated by the ages of the detrital zircon populations, because, although most can be derived from either Laurentia or Gondwana, a source for the 800–900 Ma suite can only be found in the Goiás magmatic arc that lies east of Amazonia (Fig. 20, see also Keppe et al., 2008). Furthermore, initiation of rifting at ca. 480 Ma is contemporaneous with the separation of peri-Gondwanan terranes, such as Avalonia and Carolina, from Gondwana during opening of the Rheic Ocean (e.g. Keppe, 2004). The prolonged nature of the rifting, however, is enigmatic, but it may have been related to the development of a transtensional margin similar to that inboard of Baja California and Cretaceous Baja British Columbia, where collision of mid-oceanic ridges with the trench produced a transform/transtensional margin. Furthermore, removal of Avalonia and Carolina with opening of the Rheic Ocean may have led to gradual collapse of the rifted margin.

The ~250–200 Ma thermal perturbation experienced by the Xayacatlán dike swarm was probably due to the deformation at greenschist facies that juxtaposed fault blocks containing the Xayacatlán dikes and their country rocks with the neighbouring units during the Permo-Triassic (Malone et al., 1999; Keppe et al., 2006).

### Acknowledgements

We would like to thank two anonymous reviewers for constructive comments. We also acknowledge funding from a Papiit grant (IN103003) and a CONACyT grant (CB-2005-1: 24894) to JDK and AOR that facilitated the fieldwork and  $^{40}\text{Ar}/^{39}\text{Ar}$  analyses, an NSF grant (EAR 0308105) and an Ohio University 1804 Award to RDN, NSF grant (EAR-0308437) to BVM and NSERC Discovery grants to JBM and JD.

## References

- Ayer, J.A., Davis, D.W., 1997. Neoarchean evolution of differing convergent margin assemblages in the Wabigoon Subprovince: geochemical and geochronological evidence from the Lake of the Woods greenstone belt, Superior Province, Northwestern Ontario. *Precambrian Research* 81, 155–178.
- Careddu, A.M., Cruciani, G., Franceschelli, M., Carcangiu, G., 2001. Amphibole evolution in ultramafic amphibolites from NE Sardinia, Italy: In: Cidu, R. (Ed.), *Water–Rock Interaction 2001*, pp. 685–688. Sweets & Zeitlinger, Balkema Publishers, Lisse, The Netherlands.
- Clark, A.H., Archibald, D.A., Lee, A.W., Farrar, E., Hodgson, C.J., 1998. Laser probe  $^{40}\text{Ar}/^{39}\text{Ar}$  ages of early- and late-stage alteration assemblages, Rosario porphyry copper-molybdenum deposit, Collahuasi District, I Region, Chile. *Economic Geology* 93, 326–337.
- Dostal, J., Baragar, W.R.A., Dupuy, C., 1986. Petrogenesis of the Natkusiak continental basalts, Victoria Island, N.W.T. *Canadian Journal of Earth Sciences* 23, 622–632.
- Dostal, J., Dupuy, C., Caby, R., 1994. Geochemistry of the Neoproterozoic Tilemsi belt of Iforas (Mali, Sahara): a crustal section of an oceanic island arc. *Precambrian Research* 65, 55–69.
- Elías-Herrera, M., Ortega-Gutiérrez, F., 2002. Caltepec fault zone: an Early Permian dextral transpressional boundary between the Proterozoic Oaxacan and Paleozoic Acatlán complexes, southern Mexico, and regional implications. *Tectonics* 21 (3) 10.1029/200TC001278.
- Elías-Herrera, M., Ortega-Gutiérrez, F., Sánchez-Zavala, J.L., Iriondo, A., Ortega-Rivera, A., 2007. Conflicting stratigraphic and geochronological data from the Acatlán Complex: “Ordovician” granite intrude metamorphic and sedimentary rocks of Devonian–Permian age. *Eos Transactions AGU* 88 (23) Joint Assembly Suppl., Abstract T41A-12.
- Harrison, T.M., Duncan, I., McDougall, I., 1985. Diffusion of  $^{40}\text{Ar}$  in biotite: temperature, pressure, and compositional effects. *Geochimica Cosmochimica Acta* 49, 2461–2468.
- Jensen, L.S., 1976. A New Cation Plot for Classifying Subalkalic Volcanic Rocks. Ontario Division of Mines, p. 22. MP 66.
- Jones III, J.V., Connolly, J.N., 2006. Proterozoic tectonic evolution of the Sangre de Cristo Mountains, southern Colorado, U.S.A. *Rocky Mountain Geology* 41, 79–116.
- Keppie, J.D., 2004. Terranes of Mexico revisited: a 1.3 billion year odyssey. *International Geology Review* 46, 765–794.
- Keppie, J.D., Ramos, V.S., 1999. Odyssey of terranes in the Iapetus and Rheic Oceans during the Paleozoic. In: Ramos, V.S., Keppie, J.D. (Eds.), *Laurentia–Gondwana Connections before Pangea*: Boulder, Colorado. Geological Society of America Special Paper, 336, pp. 267–276.
- Keppie, J.D., Dostal, J., Ortega-Gutiérrez, F., López, R., 2001. A Grenvillian arc on the margin of Amazonia: evidence from the southern Oaxacan Complex, southern Mexico. *Precambrian Research* 112, 165–181.
- Keppie, J.D., Dostal, J., Cameron, K.L., Solari, L.A., Ortega-Gutiérrez, F., López, R., 2003. Geochronology and geochemistry of Grenvillian igneous suites in the northern Oaxacan Complex, southern Mexico: tectonic implications. *Precambrian Research* 120, 365–389.
- Keppie, J.D., Nance, R.D., Powell, J.T., Mumma, S.A., Dostal, J., Fox, D., Muise, J., Ortega-Rivera, A., Miller, B.V., Lee, J.W.K., 2004a. Mid-Jurassic tectonothermal event superposed on a Paleozoic geological record in the Acatlán Complex of southern Mexico: hotspot activity during the breakup of Pangea. *Gondwana Research* 7, 239–260.
- Keppie, J.D., Sandberg, C.A., Miller, B.V., Sánchez-Zavala, J.L., Nance, R.D., Poole, F.G., 2004b. Implications of latest Pennsylvanian to Middle Permian paleontological and U–Pb SHRIMP data from the Tecolate Formation to re-dating tectonothermal events in the Acatlán Complex, southern Mexico. *International Geology Review* 46, 745–754.
- Keppie, J.D., Nance, R.D., Fernández-Suárez, J., Storey, C.D., Jeffries, T.E., Murphy, J.B., 2006. Detrital zircon data from the eastern Mixteca terrane, southern Mexico: evidence for an Ordovician–Mississippian continental rise and a Permo-Triassic clastic wedge adjacent to Oaxaquia. *International Geology Review* 48, 97–111.
- Keppie, J.D., Dostal, J., Murphy, J.B., Nance, R.D., 2008. Synthesis and tectonic interpretation of the westernmost Paleozoic Variscan orogen in southern Mexico: from rifted Rheic margin to active Pacific margin. *Tectonophysics*.
- Keppie, J.D., Nance, R.D., Murphy, J.B., Miller, B.V., Dostal, J., Ortega-Rivera, A., submitted for publication. Comment on paper by Vega-Granillo et al., 2007, Pressure–temperature–time evolution of high pressure rocks of the Acatlán Complex (southern Mexico): implications for the evolution of the Iapetus and Rheic oceans. *GSA Bulletin*, v. 119, p. 1249–1264.
- Laird, J., Albee, A.L., 1981. Pressure, temperature and time indicators in mafic schists: their application to reconstructing the polymetamorphic history of Vermont. *American Journal of Science* 281, 127–175.
- Ludwig, K.B., 1989. Pb dat: a Computer Program for Processing Raw Pb–U–Th Isotopic Data: U.S. Geological Survey Open File 88-667.
- Malone, J.W., Nance, R.D., Keppie, J.D., Dostal, J., 2002. Deformational history of part of the Acatlán Complex: Late Ordovician–Early Silurian and Early Permian orogenesis in southern Mexico. *Journal of South American Earth Sciences* 15, 511–524.
- Middleton, M., Keppie, J.D., Murphy, J.B., Miller, B.V., Nance, R.D., 2007. P–T–t constraints on exhumation following subduction in the Rheic Ocean: eclogitic Asis Lithodeme, Piaxtla Suite, Acatlán Complex, southern Mexico. In: Linnemann, U., Nance, R.D., Zulauf, G., Kraft, P. (Eds.), *The Geology of Peri-Gondwana: The Avalonian–Cadomian Belt, Adjoining Cratons and the Rheic Ocean*. Geological Society of America, Special Paper, Vol. 23, pp. 489–509.
- Miller, B.V., Dostal, J., Keppie, J.D., Nance, R.D., Ortega-Rivera, A., Lee, J.K.W., 2007. Ordovician calc-alkaline granitoids in the Acatlán Complex, southern Mexico: geochemical and geochronologic evidence for either rifting or subduction along the Gondwanan margin of the Rheic Ocean. In: Linnemann, U., Nance, R.D., Zulauf, G., Kraft, P. (Eds.), *The Geology of Peri-Gondwana: The Avalonian–Cadomian Belt, Adjoining Cratons and the Rheic Ocean*. Geological Society of America, Special Paper, Vol. 423, pp. 465–475.
- Miyashiro, A., 1974. Volcanic rock series in island arcs and active continental margins. *American Journal of Science* 274, 321–355.
- Morales-Gámez, M., Keppie, J.D., Norman, M., 2008. Ordovician–Silurian rift-passive margin on the Mexican margin of the Rheic Ocean overlain by Permian periarc rocks: evidence from the Acatlán Complex, southern Mexico. In: Pereira, M.F., Bozkurt, E., Quesada, C., Strachan, R. (Eds.), *The foundations and birth of the Rheic Ocean: Avalonian–Cadomian orogenic processes and Early Palaeozoic rifting at the north-Gondwana margin*. *Tectonophysics*.
- Murphy, J.B., Keppie, J.D., Nance, R.D., Miller, B.V., Dostal, J., Middleton, M., Fernández-Suárez, J., Jeffries, T.E., 2006. Geochemistry and U–Pb protolith ages of eclogitic rocks of the Asis Lithodeme, Piaxtla Suite, Acatlán Complex, southern Mexico: tectonothermal activity along the southern margin of the Rheic Ocean. *Journal of the Geological Society (London)* 163, 683–695.
- Nance, R.D., Miller, B.V., Keppie, J.D., Murphy, J.B., Dostal, J., 2006. Acatlán Complex, southern Mexico: record spanning the assembly and breakup of Pangea. *Geology* 34, 857–860.
- Nance, R.D., Fernández-Suárez, J., Keppie, J.D., Storey, C., Jeffries, T.E., 2007. Provenance of the Granjeno Schist, Ciudad Victoria, Mexico: detrital zircon U–Pb age constraints and implications for Paleozoic paleogeography. In: Linnemann, U., Nance, R.D., Zulauf, G., Kraft, P. (Eds.), *The Geology of Peri-Gondwana: The Avalonian–Cadomian Belt, Adjoining Cratons and the Rheic Ocean*. Geological Society of America, Special Paper, Vol. 23, pp. 437–452.
- Nance, R.D., Keppie, J.D., Miller, B.V., Murphy, J.B., Dostal, J., submitted for publication. Palaeozoic palaeogeography of Mexico: constraints from detrital zircon age data, in *Geological Society of London Special Publication*.
- Ortega-Gutiérrez, F., 1975, The Pre-Mesozoic geology of the Acatlán area, south Mexico: Ph.D. thesis, Leeds University, U.K. 166 p.
- Ortega-Gutiérrez, F., Elías-Herrera, M., Reyes-Salas, M., Macías-Romo, C., López, R., 1999. Late Ordovician–Early Silurian continental collision orogeny in southern Mexico and its bearing on Gondwana–Laurentia connections. *Geology* 27, 719–722.
- Pearce, J.A., 1975. Basalt geochemistry used to investigate past tectonic environments on Cyprus. *Tectonophysics* 25, 41–67.
- Pearce, J.A., Cann, J.R., 1973. Tectonic setting of basic volcanic rocks determined using trace element analyses. *Earth Planetary Science Letters* 19, 290–300.
- Ramos-Arias, M.A., Keppie, J.D., Ortega-Rivera, A., Lee, J.W.K., 2008. Extensional late Paleozoic deformation on the western margin of Pangea,

- Patlanoaya area, Acatlán Complex, southern Mexico. In: Pereira, M.F., Bozkurt, E., Quesada, C., Strachan, R. (Eds.), The foundations and birth of the Rheic Ocean: Avalonian-Cadomian orogenic processes and Early Palaeozoic rifting at the north-Gondwana margin. *Tectonophysics*.
- Ratajeski, K., Glazner, A.F., Miller, B.V., 2001. Geology and geochemistry of mafic to felsic plutonic rocks in the Cretaceous intrusive suite of Yosemite Valley, California. *Geological Society of America Bulletin* 113, 1486–1502.
- Sánchez-Zavala, J.L., Ortega-Gutiérrez, F., Keppe, J.D., Jenner, G.A., Belousova, E., 2004. Ordovician and Mesoproterozoic zircon from the Tecolate Formation and Esperanza granitoid, Acatlán Complex, southern Mexico: local provenance in the Acatlán and Oaxacan complexes. *International Geology Review* 46, 1005–1021.
- Solari, L.A., Keppe, J.D., Ortega-Gutiérrez, F., Cameron, K.L., López, R., Hames, W.E., 2003. 990 Ma and 1,100 Ma Grenvillian tectonothermal events in the northern Oaxacan Complex, southern Mexico: roots of an orogen. *Tectonophysics* 365, 257–282.
- Sun, S.S., McDonough, W.F., 1989. Chemical and isotopic systematics of oceanic basalts: implications for mantle composition and processes. In: Saunders, A.D., Norry, M.J. (Eds.), *Magmatism in the Ocean Basins*. Geological Society of London, Special Publication, 42, pp. 313–345.
- Talavera-Mendoza, O., Ruiz, J., Gehrels, G.E., Meza-Figueroa, D.M., Vega-Granillo, R., Campa-Uranga, M.F., 2005. U–Pb geochronology of the Acatlán Complex and implications for the Paleozoic paleogeography and tectonic evolution of southern Mexico. *Earth and Planetary Science Letters* 235, 682–699.
- Vachard, D., Flores de Dios, A., 2002. Discovery of latest Devonian/earliest Mississippian microfossils in San Salvador Patlanoaya (Puebla, Mexico): biogeographic and geodynamic consequences. *Compté Rendu Geoscience* 334, 1095–1101.
- Vega-Granillo, R., 2006. Petrología, termobarometría y análisis estructural en la región del Complejo Acatlán, Puebla, México: implicaciones tectónicas: Tesis doctorado, Universidad Nacional Autónoma de México, 334 p.
- Vega-Granillo, R., Talavera-Mendoza, O., Meza-Figueroa, D., Ruiz, J., Gehrels, G.E., López-Martínez, M., de La Cruz-Vargas, J.C., 2007. Pressure–temperature–time evolution of Paleozoic high-pressure rocks of the Acatlán Complex (southern Mexico): implications for the evolution of the Iapetus and Rheic Oceans. *Geological Society of America Bulletin* 119, 1249–1264.
- Winchester, J.A., Floyd, P.A., 1977. Geochemical discrimination of different magma series and their differentiation products using immobile elements. *Chemical Geology* 20, 325–343.

## **Discusión de resultados**

### **Terminología**

La ausencia de metamorfismo en facies de eclogita en el área de Xayacatlán imposibilita la inclusión de las unidades de esta área en la Suite Piaxtla, no obstante, el término Xayacatlán está inextricablemente vinculado a la suite Piaxtla (*e.g.* Vega-Granillo *et al.*, 2007 y referencias *In*). Por lo cual se ha introducido el nombre de Unidad Amate para las rocas meta-sedimentarias previamente incluidas en la Formación Xayacatlán (Ortega-Gutiérrez, 1975), y que afloran en el área de estudio.

Las diferencias en edad y litología de las unidades Huerta y Salada, las cuales fueron previamente asignadas a la Formación Cosoltepec (Ortega-Gutiérrez, 1975), sugieren la introducción de una nueva nomenclatura para las rocas meta-sedimentarias que afloran en la zona de estudio. Un ejemplar en la sección tipo de la Formación Cosoltepec proporcionó una población de circones de edad similar a los de la Unidad Salada. Sin embargo, la edad U-Pb más joven reportada para la Formación Cosoltepec es de ~376 Ma (datos discordantes: Talavera-Mendoza *et al.*, 2005), y esta edad es un poco más vieja que la de 352 Ma en la unidad Salada. Ambas unidades, Salada y Cosoltepec tipo, contienen lentes ígneos máficos y parecen ser continuos en la dirección NNE-SSW, sin embargo la falta de una cartografía completa no permite confirmar su continuidad. Por lo cual se mantiene la unidad Salada como una unidad distinta de la Cosoltepec tipo.

### **Edad y procedencia de los circones**

La parte oeste del depósito de la Unidad Huerta es constreñido por circones detríticos de  $455 \pm 4$  Ma (Keppie *et al.*, 2006), y en una muestra colectada ~10 kilómetros al oeste de un ejemplar de pegmatita, cuya edad de intrusión es de  $464 \pm 4$  Ma, la cual cortan a esta unidad meta-sedimentaria. Las edades son similares dentro del error analítico y sugieren una depositación síncrona con la intrusión. En este sentido el depósito de las rocas en la parte este de la unidad son cortadas por pegmatitas que quizás son más viejas que ~455 Ma. Las múltiples fases de deformación de la unidad probablemente significa que este problema no puede ser determinado por cartografía adicional: en todo caso se requiere de dataciones adicionales de circones detríticos. Sin embargo, el depósito de la unidad tuvo lugar durante el Ordovícico.

El depósito de la Unidad Amate se considera posterior a  $902 \pm 14$  Ma, con base en el circón detrítico concordante más joven encontrado en esta unidad, y una edad previa a  $442 \pm 1$  Ma, la cual corresponde a la edad de intrusión del enjambre de diques Xayacatlán. La ausencia de edades neoproterozoicas en la Unidad Amate, pero presentes en la unidad Huerta, sugieren que ambas unidades son de edades diferentes o que la procedencia de sus circones es distinta. Las edades más tardías son, aparentemente, las unidades ordovícicas en el área de Patlanoaya y en la Formación Tecomate (Sánchez-Zavala *et al.*, 2004), sin embargo, no se puede descartar una diferencia en el tiempo de depósito.

Las unidades Huerta y Amate tienen poblaciones de circones entre 900-1300 Ma, mientras que en la Unidad Huerta se tienen además poblaciones de  $\sim 460$  Ma y dentro del rango de  $\sim 510$ -640 Ma. Las poblaciones de 900-1300 Ma tienen una procedencia del vecino Complejo Oaxaqueño, el cual proporciona un rango semejante de edades de 920 Ma a 1300 Ma (Keppie *et al.*, 2003; Solari *et al.*, 2003; Ortega-Obregón *et al.*, 2003). Los circones detríticos de  $\sim 460$  Ma se considera que tienen una procedencia local, probablemente derivados de los granitoides del Complejo Acatlán (Sánchez-Zavala *et al.*, 2004; Talavera-Mendoza *et al.*, 2005; Miller *et al.*, 2007). Mientras que para los circones detríticos con edades dentro del rango de  $\sim 510$ -640 Ma se interpreta una fuente distal, probablemente localizada en el basamento de la península de Yucatán, los orógenos brasiliano de Amazonia o Avalonia (los cuales fueron separados de Oaxaquía/Amazonia a  $\sim 480$  Ma) (Keppie, 2004; Keppie *et al.*, 2006; Nance *et al.*, 2006).

En la Unidad Salada el límite más antiguo para el tiempo de depósito es proporcionado por una edad de  $352 \pm 3$  Ma en circones detríticos, y el límite más joven es  $324 \pm 2$  Ma (edad de  $^{40}\text{Ar}/^{39}\text{Ar}$  en la muscovita asociada al clivaje). La Formación Tecomate está en contacto tectónico con la Unidad Salada, sin embargo, ambas litologías son marcadamente diferentes y las rocas datadas en la Formación Tecomate son del Pensilvánico tardío-Pérmico medio (Keppie *et al.*, 2004a). No obstante, es litológicamente distinta a las unidades Chazumba Permo-Triásica y Magdalena, las cuales tienen poblaciones de circones detríticos más jóvenes (Keppie *et al.*, 2006) lo cual implica que la Unidad Salada es misisípica.

La unidad Salada presenta poblaciones más tardías que contienen circones de  $\sim 352$  Ma. Como dichas edades (353-346 Ma) han sido registradas en los circones de las

eclogitas de la Suite Piaxtla, en la parte central del Complejo Acatlán (Middleton *et al.*, 2007; Elías-Herrera *et al.*, 2007), donde se ha relacionado con la exhumación de las rocas de subducción, se considera una fuente local como probable. Sin embargo, para este tiempo Pangea estaba amalgamada y en este sentido fuentes distales son posibles también.

### Circones en las rocas meta-ígneas

Las rocas graníticas más jóvenes datadas en el área de Xayacatlán, están dentro de un rango de  $464 \pm 4$  Ma a  $447 \pm 3$  Ma, y este rango es próximo a la edad de  $442 \pm 1$  Ma del enjambre de diques gabróicos que cortan a la Unidad Amate. Como los diques gabróicos y pegmatitas también cortan a los diques máficos, esto indica que el magmatismo del área de Xayacatlán está dentro del rango de ~464 Ma a ~442 Ma. Las rocas ígneas que afloran en el área de estudio están por lo tanto asociadas a un magmatismo bimodal y los diques máficos tienen una composición de toleitas continentales, y al parecer forman parte de un amplio evento magmático ocurrido dentro del rango de ~480–440 Ma en el Complejo Acatlán.

La Unidad Huerta parece haber sido depositada durante el mismo intervalo de tiempo y así, es probable que represente un ambiente de rift en la margen de Oaxaca. Se ha inferido que el complejo Oaxaca subyació al complejo Acatlán durante el Ordovícico (Keppie *et al.*, 2004); una interpretación que es consistente con los circones heredados en las pegmatitas que cortan a la Unidad Huerta. Esta misma interpretación puede aplicarse para la Unidad Amate, sin embargo, probablemente ésta sea más vieja.

### Geoquímica del enjambre de diques Xayacatlán

El enjambre de diques de Xayacatlán tiene una composición bimodal, con un fuerte predominio de las rocas máficas sobre las félsicas. Las rocas máficas tienen una composición de SiO<sub>2</sub> entre 46 y 55 % en peso (LOI-libre), son variables en su composición, a pesar que muestran una tendencia a la fracción toleítica. Estas rocas pueden dividirse en tres grupos distintivos.

Las rocas del primer grupo caen dentro del campo de las toleitas de alto Mg en el diagrama Al-Mg-Ti, tienen un alto contenido de Mg# ( $MgO/[MgO+FeO^*]$  % molar) (0.68-0.73), elevado Cr (259-650 ppm) y abundante Ni (70-150 ppm). El Cr y Ni se

correlacionan positivamente con el MgO en un rango entre 10 a 14 % en peso. Por otra parte, las rocas de este grupo tienen una abundancia relativa de elementos traza incompatibles como es el Zr, P y elementos de las tierras raras (REE) que, como el Ti, muestran una correlación negativa con Mg#. Su relación de Ti/V es baja (20-25) comparadas con las de los otros dos grupos. Los patrones REE normalizados a condritas muestran un menor enriquecimiento de las REE ligeras con relación a las REE pesadas con  $(La/Yb)_n \sim 4-7$ . La parte de las REE pesadas de los patrones es horizontal, los patrones de REE de todas las rocas son subparalelas, pero su abundancia total se incrementa con la diferenciación. Las características químicas de las rocas consisten de relictos de texturas cumulares. Al parecer las rocas representan una mezcla de minerales cumulares contenidos en el líquido intersticial de afinidad toleítica.

Las rocas del segundo grupo tienen Mg# entre 0.66 y 0.60, altos contenidos de Cr (700-1200 ppm) y Ni (180-350 ppm). En otras palabras, tienen bajos contenido de  $Al_2O_3$  (<14%) y bajo  $Al_2O_3/CaO$  (1-2), pero una relación alta de Ti/V (25-32). Las rocas de este grupo tienen contenidos variables de MgO (9-14%), los cuales muestran una correlación positiva de Cr, Ni y CaO. Las rocas probablemente representan cúmulos dominados por piroxenos derivados de una fuente basáltica toleítica parental.

Las rocas del tercer grupo incluyen diques máficos con bandas de plagioclasas. Las rocas tienen un contenido bajo de MgO# (0.53-0.60), MgO (5-10%), Cr (~200 ppm) y Ni (20-120 ppm) pero un alto contenido de  $Al_2O_3$  (15-22%). Sus patrones de REE, tienen  $(La/Yb)_n$  en un rango entre 4 y 5, y muestra cada uno anomalías negativas o positivas de Eu, indicando un rol del feldespato durante la fraccionación. Como este tipo de rocas frecuentemente ocurren en los dos grupos, lo cual puede representar una diferenciación variable de los cuerpos gabróicos.

Los resultados de campo y la química indican que las rocas están genéticamente relacionadas, probablemente, a una diferenciación de las intrusiones gabróicas toleíticas. Las rocas son parcialmente cumulares. Todas las rocas muestran anomalías negativas de Nb-Ta y Ti en los gráficos de manto normalizado, indicando que fueron derivadas tanto del manto litosférico subcontinental o bien fueron afectadas por contaminación cortical. Por medio de los datos disponibles es difícil discriminar entre esas dos posibilidades y ambos procesos pudieron haber ocurrido.

## **Geoquímica de las rocas graníticas**

Las rocas félasicas tienen un porcentaje >72 de SiO<sub>2</sub>, pero tienen una composición variable caracterizada por bajo K<sub>2</sub>O (<1%) y contenidos variables de Na<sub>2</sub>O (2-8%). Sus patrones de REE están enriquecidos en REE ligeras con relación a las REE pesadas, y no muestran anomalías positivas o negativas de Eu. Los segmentos en REE pesadas tiene patrones horizontales. Los patrones de elementos traza en manto normalizado muestran enriquecimiento distintivo de Th pero anomalías negativas de Nb, Ta y Ti, de forma similar a los de la corteza continental. Las rocas félasicas no parecen estar directamente relacionadas a las rocas máficas y probablemente representan fusión parcial de corteza, inducida probablemente por la elevación del magma máfico.

## **Geoquímica de los diques toleíticos en la unidad Salada**

Los diques, emplazados en la unidad Salada, tienen una composición correspondiente a basaltos sub-alcalinos con SiO<sub>2</sub> (base volátil libre) con un rango entre 47.5 y 51.5 de % en peso y Mg# (=Mg/Mg+Fe<sub>tot</sub>) entre 0.40 y 0.60, mostrando características toleíticas. De acuerdo a su composición normativa, las rocas son en su mayoría toleitas de olivino. La abundancia de Cr y Ti es típica de toleitas relacionadas a rift. Los patrones de REE normalizados a condrita, en la mayoría de las muestras de rocas, evidencian un menor empobrecimiento de REE ligeras y sus patrones son similares a los MORB tipo N con (La/Sm)n principalmente ~0.5-0.6. La concentración absoluta de los REE varía un poco, pero la forma de los patrones permanece la misma; esas variaciones son consistentes con la cristalización fraccionada a baja presión.

Los patrones de los elementos traza, normalizados al manto, de las rocas máficas emplazadas en la Unidad Salada, son relativamente planos sin empobrecimiento en Nb con relación a La y Th, lo que sugiere que las rocas no han sido modificadas por fluidos relacionados a subducción, y que las rocas no fueron significativamente contaminadas por material cortical. La ausencia de una anomalía de Nb y una baja relación de Th/La sugiere una fuente astenosférica, sin alguna supra-subducción impuesta o contaminación cortical. Los contenidos altos de Ti y Cr también indican una formación en un ambiente de arco. Las características geoquímicas sugieren que las rocas están relacionadas a basaltos de ambiente de a rift o toleitas emplazadas en el continente en una corteza adelgazada, sin

una contaminación cortical significativa, esto último es más probable, es decir que los diques máficos hayan intrusiónado rocas clásticas derivadas del continente.

Los diques toléticos carboníferos relacionados a rift en el área de Xayacatlán pueden ser correlacionados con basaltos intraplaca, lavas basálticas almohadilladas toléticas relacionadas a rift, intercaladas con rocas metasedimentarias clásticas (unidad Coatlaco), localizadas en la parte oeste del Complejo Acatlán y cuyas edades obtenidas en circones detríticos son de  $357 \pm 35$  Ma (Grodzicki *et al.*, 2008).

El depósito de las unidades Salada y Coatlaco fue también contemporáneo con el depósito del Grupo Patlanoaya, el cual, a su vez, fue contemporáneo con la exhumación y deformación de las rocas de alta presión (Ramos-Arias *et al.*, 2008) y la deformación más temprana en la unidad Salada. Esta deformación ha sido relacionada a la extrusión de las rocas de alta presión dentro de la placa superior por encima de una zona de subducción activa (Keppie *et al.*, 2008a).

### **Geocronología $^{40}\text{Ar}$ - $^{39}\text{Ar}$**

Los resultados obtenidos en un anfíbol de los diques de Xayacatlán proporcionan datos discordantes con edades de meseta de  $434 \pm 3$  Ma. Usando el tamaño de grano de los anfíboles analizados y considerando una tasa de enfriamiento de  $25^\circ\text{C}$ , lo cual representa una temperatura de cierre de  $570 \pm 10^\circ\text{C}$  (Harrison *et al.*, 1985). Las edades ca 250-200 Ma representan probablemente una perturbación térmica subsecuente. La perturbación térmica experimentada por el enjambre de dique Xayacatlán, probablemente se debió a la deformación que acompañó al metamorfismo en facies de esquitos verde, la cual yuxtapuso al bloque Bravo, que contiene al enjambre de diques Xayacatlán y sus rocas encajonantes, con los bloques Tizac y Estaca durante el Permo-Triásico (Malone *et al.*, 2002; Keppie *et al.*, 2006).

La muestra (AMATE-G3) obtenida en la unidad Amate en anfíboles, con textura decusada en la aureola de contacto con los diques Xayacatlán, muestran una edad de meseta  $^{40}\text{Ar}/^{39}\text{Ar}$  de  $404 \pm 2$  Ma. Ésta edad se relaciona con una temperatura de cierre ca.  $530^\circ\text{C}$ , tomando en cuenta una tasa de enfriamiento de  $5^\circ\text{C/año}$ . Sin embargo, el fuerte clivaje en las rocas resulta tener una difusión efectiva menor y una temperatura de cierre más baja ca.  $480^\circ\text{C}$ . La edad ~404 Ma es ~30 millones de años más joven que la edad de

meseta de  $434 \pm 3$  Ma, en la cual se ha calculado un enfriamiento a partir de  $570^{\circ}\text{C}$ , esta diferencia es atribuida a la diferencia en la composición y al tamaño de grano.

En la Unidad Amate en la aureola de contacto, en donde la muscovita muestra una textura decusada, se tomaron los ejemplares (REP-1 y AMATE-4). Y los cuales proporcionaron una meseta  $^{40}\text{Ar}/^{39}\text{Ar}$  con espectro discordante. Mientras que ambas muscovitas tienen edades jóvenes (*ca.* 100-230 Ma), para los incrementos de poder inferiores. Los incrementos superiores proporcionan una edad de  $357 \pm 6$  Ma para REP-1, mientras que para AMATE-4 tiene una edad de  $278 \pm 2$  Ma. Se calculó una tasa de enfriamiento de  $5^{\circ}\text{C/M}$  años para las edades de 360 y 280 Ma, lo cual indica que dichas edades probablemente representan edades de enfriamiento de *ca.*  $370\text{-}380^{\circ}\text{C}$ .

En la Unidad Salada de la muestra de muscovita (W3-SAL), la cual define al clivaje,  $S_{HS1}$ , se obtuvieron datos que muestran edades aparentes que se incrementan desde *ca.* 232 Ma a  $324 \pm 2$  Ma. Usando un promedio de tamaño de grano de 0.8 mm, se sugiere que esta edad representa un mínimo para un enfriamiento desde los  $400^{\circ}\text{C}$ .

La roca total, filita sericítica (AxTT-366-TCC) de la Formación Tecomate proporcionó un espectro parcialmente discordante y define una meseta con una edad aparente de  $263 \pm 3$  Ma. Los incrementos generalmente tienen una contaminación baja de  $^{40}\text{Ar}$  atmosférico y las relaciones Ca/K y Cl/K son consistentes con el Ar liberado de la sericita. Así la edad *ca.* 263 Ma., probablemente data un evento tectonotérmico que produjo el clivaje en la Formación Tecomate. Las edades aparentes de los pasos de las temperaturas bajas parecen correlacionarse con la liberación de Ar durante las otras fases de deformación en las rocas y no se considera que tenga un significado geológico.

### **Correlación y límites de las edad en las fábricas de las rocas paleozoicas tardías**

Las fábricas paleozoicas registradas en las rocas Huerta/Salada y Tecomate se consideran como:  $F_{T1}=F_{HS2}=F_{A2}$ , y  $F_{T2}=F_{HS3}=F_{A3}$ , y la edad del clivaje filítico en la Formación Tecomate es de  $263 \pm 3$  Ma, *i.e.* cercano al límite Pérmico medio-tardío. Esta edad es consistente con el rango de edades de 314-282 Ma de los guijarros graníticos recuperados de un meta-conglomerado de la Formación Tecomate, al sureste del área de estudio, el cual es cortado por el clivaje  $S_{T1}$  (Keppie *et al.* 2004b). La migmatización, a lo largo de la falla de Caltepec, datada en  $276 \pm 1$  Ma (Elías-Herrera y Ortega-Gutiérrez

2002) está dentro del mismo error que la edad de  $278 \pm 2$  Ma registrada en la muscovita adyacente a la falla Las Ollas, sugiriendo que ésta pudo haber sido activada durante este mismo tiempo con fluidos calientes fluyendo a lo largo de la falla, y fue un precursor de la deformación  $F_{T1}$ . Los pliegues  $F_{T2}$  no han sido registrados en la Formación Matzitzi que sobreyace discordantemente a la zona de falla de Caltepec  $276 \pm 1$  Ma (Elías-Herrera y Ortega-Gutiérrez, 2002). Esto es inconsistente con la edad leonardiana reportada para la Formación Matzitzi (Weber, 1997), pero es compatible con la edad Pérmico tardío (Centeno-García *et al.*, 2008), así,  $F_{T1}$  y  $F_{T2}$  y sus correlativos, parecen constreñirse al Pérmico medio.

Las fábricas registradas en las unidades Huerta y Amate se consideran como:  $F_{HS1}=F_{A1}$  y se asume que la diferencia en la intensidad de la deformación entre las unidades Huerta/Salada contra Amate se debe a la diferencia de competencia entre estas unidades, siendo la Unidad Amate la más competente de las tres. La edad de meseta en  $^{40}\text{Ar}/^{39}\text{Ar}$  de  $324 \pm 2$  Ma, para la muscovita definida por el clivaje  $S_{S1}$  en la unidad Salada, indica una edad del Misisípico medio-superior para esta etapa de deformación. La cual es consistente con la edad de  $352 \pm 3$  obtenida en los circones detríticos más jóvenes registrados en la Unidad Salada. La edad Misisípico medio-superior se corrobora con el hecho de que la Formación Tecomate del Pérmico no registró esta deformación. La correlación de las estructuras en las unidades Huerta y Amate con aquellas de la unidad Salada sugiere que las estructuras  $F_{HS1}$  y  $F_{A1}$  son también del Misisípico superior. Estas estructuras son contemporáneas con las edades más tempranas de la deformación,  $347 \pm 3$  Ma, reportadas en el área de Patlanoaya en la parte norte del Complejo Acatlán (Ramos-Arias *et al.* 2008).

### **Correlación de las rocas máficas ordovícias de Xayacatlán, Patlanoaya y Cuaujote**

Los datos geocronológicos y geoquímicos presentados en este trabajo indican la presencia de un evento ígneo bimodal durante el Ordovícico en las rocas del Complejo Acatlán. Las rocas del enjambre de diques Xayacatlán intrusionaron a los  $442 \pm 1$  Ma, como capas de gabros toleíticos, con una mineralogía primaria convertida rápidamente a plagioclasa y anfíbol. La diabasa granítica bimodal Palo Liso fue intrusionada 20 m.a. (millones de años) de años más temprano, a los  $461 \pm 2$  Ma (Miller *et al.*, 2007), las rocas máficas son consideradas como toleitas intraplaca. En este sentido, los diques máficos

Las Minas y la anfibolita Anacahuite son toleitas intraplaca intrusionadas cada una antes o simultáneamente por un dique leucogranítico ca 460±9 Ma (Vega-Granillo, 2006).

La similitud de las rocas máficas de Las Minas y de las rocas máficas del granito Palo Liso sugiere que son parte de un mismo evento magmático. Un límite más viejo para la intrusión de los diques Las Minas es proporcionado por una edad de 496±25 Ma para los circones detríticos concordantes más jóvenes. Las rocas máficas bimodales en el área de Cuauhtépetl son toleitas intraplaca intrusionadas a los 461±7 Ma (edades U-Pb de los granitos megacristalinos: Talavera-Mendoza *et al.*, 2005). Los diques Xayacatlán son distintos de los otros conjuntos al mostrar anomalías negativas de Nb, Ta y Ti atribuidas cada a una contaminación cortical o derivación del manto subcontinental previamente modificado por magmatismo de arco.

El hecho de que las rocas se hayan formado a lo largo de la margen sur del océano Rhéico está indicado por las edades de las poblaciones de los circones detríticos, porque, si bien también pudo ser derivado de Laurentia o Gondwana. La fuente para el conjunto de 800-900 Ma puede ser localizada en el arco magmático Goiás que yació al este de Amazonia. No obstante, el inicio del rifting ca 480 Ma es contemporáneo con la separación de los terrenos peri-gondwánicos, Avalonia y Carolinia, desde Gondwana durante la apertura del océano Rhéico (*e.g.* Keppie, 2004). La naturaleza prolongada del rifting, sin embargo, es enigmática, pero esta puede estar relacionada al desarrollo de una margen transtensional similar a la del borde de Baja California actual y de Baja Columbia Británica del Cretácico, donde la colisión de dorsales centro oceánicas con la trinchera produjo una margen transforme/transtensional. Sin embargo, la remoción de Avalonia y Carolinia con la apertura del océano Rhéico pudo haber llevado a un gradual colapso de la margen “rifteada”.

## **Conclusiones**

Las etapas de deformación identificadas en el área de Xayacatlán son tres a partir de los ~442 Ma (ca del límite Ordovícico-Silúrico), Misisípico y Pérmico medio. Las estructuras *ca* 442 Ma están registradas únicamente en los enjambres de diques toleíticos ~N-S que cortan a la unidad Amate. La naturaleza asociada a rift de los diques, junto con la cinemática de las estructuras, sugiere que el enjambre de diques Xayacatlán se formó durante el periodo de transtensión, constreñido entre el tiempo de intrusión de los diques (442±2 Ma) y la edad de enfriamiento de la hornblenda (434±3 Ma).

El rift parece haber iniciado *ca.* 464 Ma o mas temprano a 480 Ma con la intrusión de diques graníticos y pegmatitas, los cuales se han inferido como los miembros félscico de un conjunto bimodal (Keppie *et al.* 2008b). Así, este evento tectonotérmico es extensional más que registrar un evento orogénico (*i.e.* orogenia Acateca: Ortega-Gutiérrez *et al.* 1999, Talavera-Mendoza *et al.* 2005; Vega-Granillo *et al.* 2007).

El conjunto de margen continental asociado a rift, inferido para todas las rocas ordovícicas (y posiblemente más antiguas), es más consistente con un depósito a lo largo de la margen sur del océano Rhéico durante su deriva, dado que el océano Iapetus se cerró durante el Ordovícico y estuvo rodeado por márgenes activas. No obstante, todos los circones detríticos en las unidades Huerta y Amate pudieron haber procedido de Oaxaquia y Amazonia, por lo tanto los circones neo-proterozoicos son menos compatibles con una procedencia de Laurentia.

La previamente denominada Formación Cosoltepec (Ortega-Gutiérrez *et al.*, 1999, Ramírez-Espinosa, 2001, Talavera-Mendoza *et al.*, 2005) en el área de estudio fue separada en dos miembros: Unidad Huerta y Unidad Salada. En el caso de la Unidad Huerta, la edad de depósito se considera, de acuerdo a los datos obtenidos, haber ocurrido durante el Ordovícico. La Unidad Salada cuya edad es carbonífera y no ordovícica como se había previamente considerado, en esta unidad los circones detríticos muestran edades de *ca.* 352 Ma y el clivaje más temprano está datado en *ca.* 323 Ma.

La edad carbonífera de la unidad Salada sugiere que su depósito fue contemporáneo con las partes más viejas del Grupo Patlanoaya del Devónico tardío-Pérmico temprano (Vachard *et al.*, 2000), las cuales fueron síncronas con la deformación extensional y con una subducción buzando hacia el este (Ramos-Arias *et al.*, 2008; Keppie *et al.*, 2008a),

así como con las rocas de la Unidad Coatlaco (Grodzicki *et al.*, 2008). La sincronización de la deformación misisípica en las áreas de Xayacatlán y Patlanoaya sugiere que el mecanismo de deformación pudo haber sido similar en ambas áreas. La deformación ha sido vinculada a la extrusión de rocas de alta presión derivadas de material de la placa superior por erosión-subducción (Keppie *et al.* 2008a). La deformación temprana desarrollada en facies de esquistos verdes en las unidades Salada, Amate y Huerta es del Carbonífero (*ca.* 323 Ma, más que del Ordovícico-Silúrico. Esta deformación estuvo asociada a un evento extensivo durante la extrusión de rocas de alta presión.

Los diques toleíticos carboníferos en el área de Xayacatlán se correlacionan con los basaltos almohadillados toleíticos intercalados con las rocas clásticas metasedimentarias en la parte oeste del Complejo Acatlán (Unidad Coatlaco), las cuales proporcionan una edad de *ca.* 357 Ma en circones detríticos (Grodzicki *et al.*, 2008). Posiblemente es al mismo tiempo de deposición de la Formación Cosoltepec en el área tipo (~352Ma datos discordantes: Talavera-Mendoza *et al.*, 2005).

La ubicación posterior del terreno Mixteca tuvo lugar en la margen pacífica de Pangea, esto significa que las toleitas relacionadas a rift del carbonífero en la Unidad Salada son contemporáneas con la deformación y extrusión de las rocas de alta presión, en un ambiente de margen activa, mas consistente con una localización en la margen oeste de Pangea, al sur de la zona de sutura de Laurentia-Gondwana (Elias-Herrera y Ortega-Gutiérrez, 2002; Keppie *et al.*, 2008a). Se concluye que las estructuras misisípicas en el área de Xayacatlán fueron desarrolladas en el margen oeste de Pangea.

Talavera-Mendoza *et al.* (2005) y Vega-Granillo *et al.* (2007) colocan al terreno Mixteca en la zona de sutura colisional entre el sur de Laurentia y Gondwana. Esta colisión tuvo lugar en el Misisípico y es sugerida por la presencia de fauna Meso-Continental (EUA) de mares someros en la Formación Santiago, La cual yace sobre el Complejo Oaxaqueño de 1~ Ga en el adyacente terreno Oaxaquia (Navarro-Santillan *et al.*, 2002). No obstante que la presencia de rocas carboníferas de intraplaca y toleitas relacionadas a rift, puede explicarse por medio de un colapso gravitacional durante una orogenia colisional. Ésta resulta ser inconsistente con los datos paleomagnéticos, los cuales indican que durante el Pérmico, el terreno Mixteca yació aproximadamente en una posición relativa, similar a la actual con relación a Laurentia (Alva-Valdivia *et al.*, 2002).

La Formación Tecomate que sobreyace a la Unidad Salada fue síncrona con un magmatismo de arco (Torres *et al.*, 1999), incluyendo al lacolito de Totoltepec. El hecho que las rocas de la Formación Tecomate se hayan formado en la margen oeste de Pangea está indicado por la fauna meso-continental (EUA), cuyos fósiles encontrados en las rocas son de edad misisípica (Keppie *et al.*, 2004).

La edad del Pérmico medio de la deformación transtensional destral en la Formación Tecomate permite concluir que las estructuras fueron no silúrico-devónicas (Sánchez-Zavala *et al.* 2000), pero si pérmicas (Keppie *et al.* 2004b). Además se concluye que el arco se formó en un ambiente transtensional destral, que pudo haber sido debido a la convergencia oblicua entre el Paleo-Pacífico y el oeste de Pangea (Torres *et al.* 1999; Keppie *et al.* 2008a).

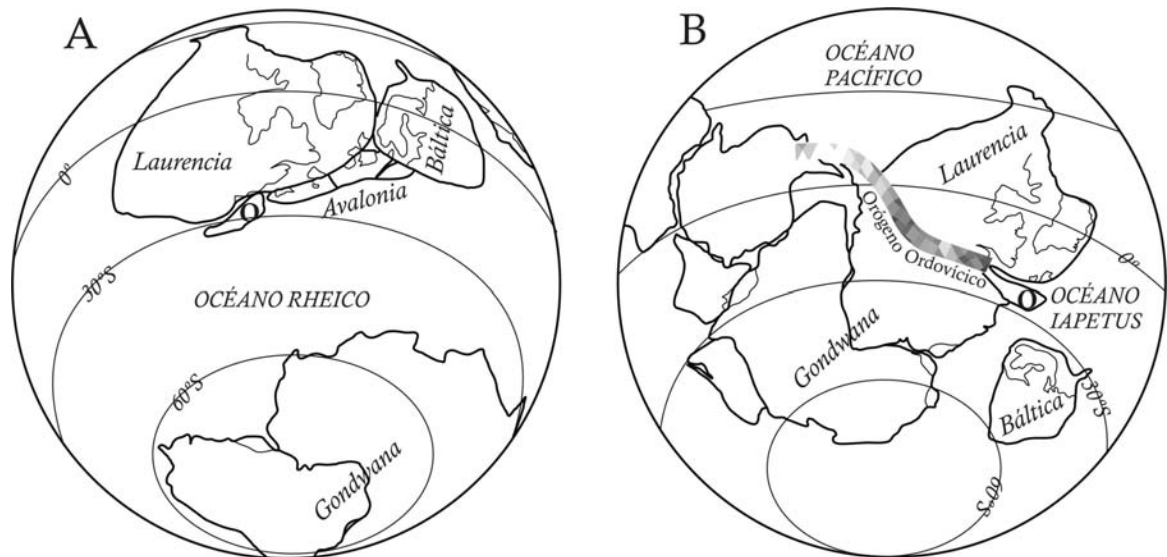


**Figura 1-C. Depósito de sedimentos en el océano Iapetus, (A) cerrado por el acoplamiento de terrenos peri-gonwánicos y deformados durante el cierre de este océano (Keppie, 2004), y (B) cerrado por la colisión de Laurentia contra Gondwana durante el Ordovícico medio-tardío, en ambos casos el Complejo Acatlán se forma en una sutura colisional (Ortega-Gutiérrez *et al.*, 1999).**

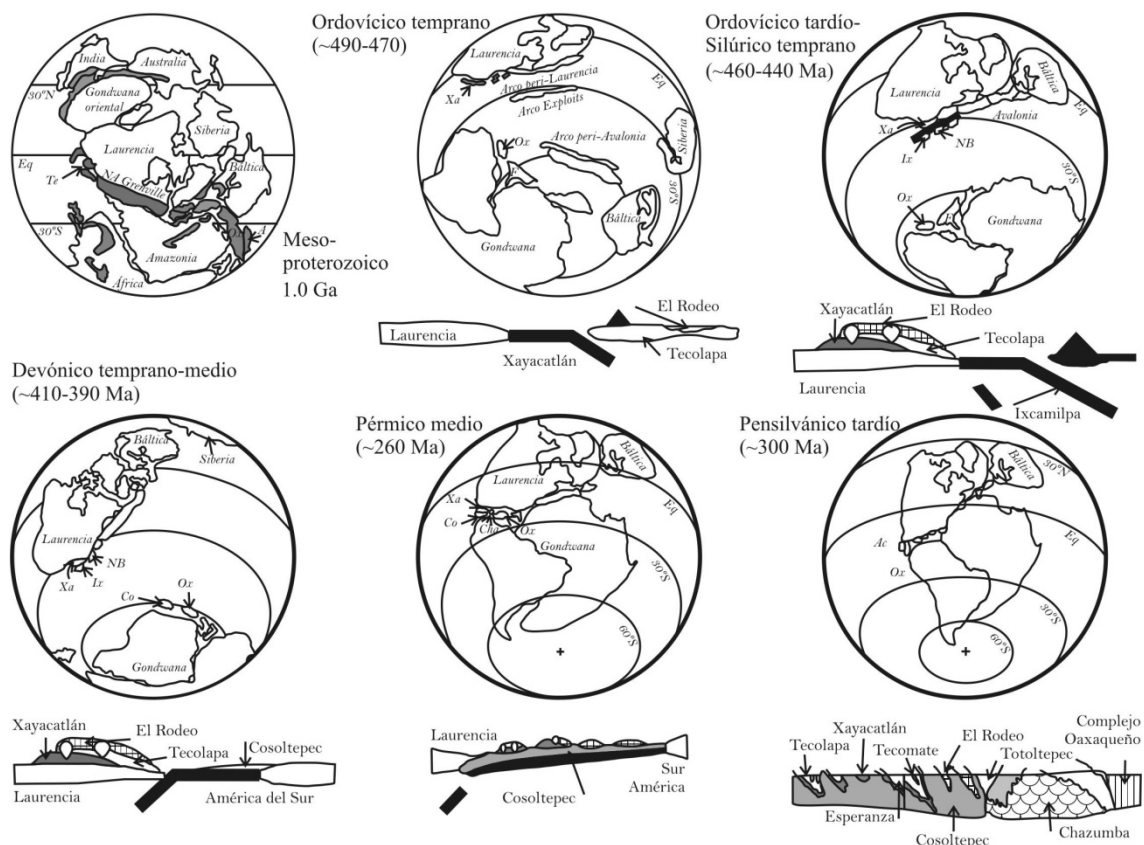


**Figura 2-C** Talavera-Mendoza *et al.* 2005, superior y Vega-Granillo *et al.* (2007), inferior. En ambos modelos se propone que los eventos de deformación, registrados en las rocas del Complejo Acatlán, están asociados a procesos de colisión y que estos ocurrieron tanto en los océanos Iapetus y Rhéico durante una evolución tectónica compleja durante el Paleozoico.

Los datos presentados en este trabajo indican un conjunto tectónico asociado a un rift continental, tanto para las unidades ordovícicas, así como para las carboníferas y un magmatismo bimodal durante la transtensión del Ordovícico, estos datos resultan inconsistentes con los conjuntos tectónicos asociados a colisión (Figuras 1C y 2C). Pero son compatibles con el modelo propuesto en la figura 3C (b), el cual consiste de un magmatismo bimodal asociado a transtensión 480-440 Ma. Por lo tanto se concluye que: las rocas de la región de Xayacatlán están asociadas a la evolución tectónica en el sur del océano Rhéico durante el Paleozoico, más que con la asociada al Precámbrico océano Iapetus.

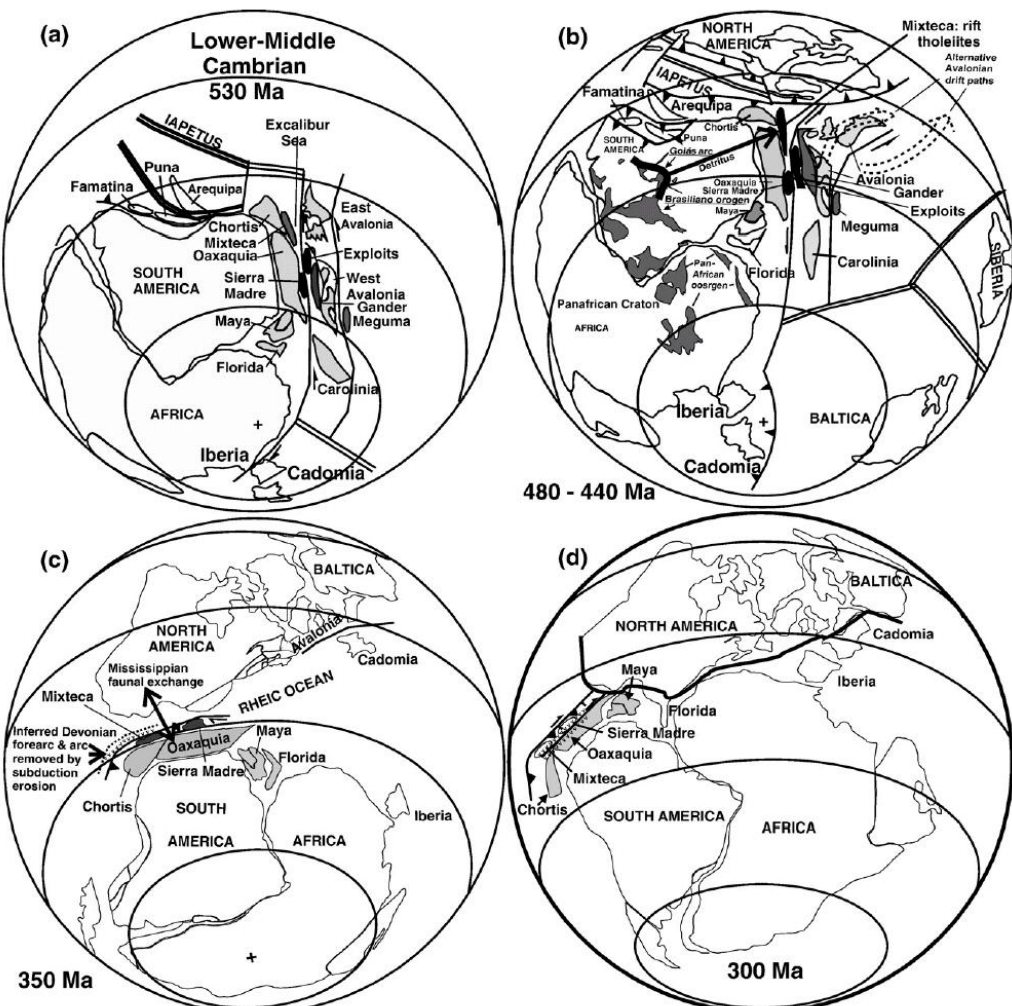


**Figura 3-C. Keppie *et al.* (2008a)** propusieron un modelo paleogeográfico en el cual sugieren que la sedimentación de las rocas del Complejo Acatlán, ocurrió tanto en los océanos Rhéico y Paleopacífico en diferentes etapas y una tectónica extensional durante el Ordovícico y Misísípico, respectivamente.

Finalmente la Unidad Salada y la Formación Tecolate parecen ser síncronas con un arco magmático permo-triásico desarrollado en la margen oeste de Pangea en el Paleo-pacífico 350-300 Ma (Figura 3-C (c) y (d)).

## Referencias

- Alsop, G.I. and Holdsworth, R.E . 2004a. Shear zone folds: records of flow perturbation or structural inheritance? In: Alsop, G.I., Holdsworth, R.E., McCaffrey, K.J.W. and Hand, M. (Editors) Flow Processes in Faults and Shear Zones. Geological Society, London, Special Publications, 224, 177-199. 379 pp.
- Alsop, G.I. and Holdsworth, R.E . 2004b. Shear zones - an introduction and overview. In: Alsop, G.I., Holdsworth, R.E., McCaffrey, K.J.W. and Hand, M. (Editors) Flow Processes in Faults and Shear Zones. Geological Society, London, Special Publications, 224, 1-9. 379 pp.
- Alva-Valdivia, L.M., Goguitchaichvili, A., Grajales, M., Flores de Dios, A., Urrutia-Fucugauchi, J., Rosales C., Morales, J., 2002, Further constraints for Permo-Carboniferous magnetostratigraphy: case study of the sedimentary sequence from San Salvador-Patlanoaya (Mexico): Compte Rendus Geoscience, 334, 1-7.
- Bozkurt E., Pereira M.F., Strachan R. y Quesada C., 2008, Evolution of the Rheic Ocean, Editorial, In: Pereira M.F., Bozkurt E., Strachan R., and Quesada C. (Eds.), The Foundations and Birth of the Rheic Ocean: Avalonian–Cadomian Orogenic Processes and Early Palaeozoic Rifting at the Northern Gondwana Margin. Tectonophysics 461, 1-8.
- Campa, M.F., and Coney, P.J., 1983. Tectono-stratigraphic terranes and mineral distributions in Mexico. Canadian Journal of Earth Science 20, 1040–1051.
- Centeno García E, Mendoza-Rosales CC, Silva Romo G., 2009, Sedimentología de la Formación Matzitzi (Paleozoico superior) y significado de sus componentes volcánicos, región de Los Reyes Metzontla-San Luis Atolotitlán, Estado de Puebla. Revista Mexicana de Ciencias Geológicas 26, 1:18-36.
- Centeno-García E., Guerrero-Suastegui M., and Talavera-Mendoza O., 2008, The Guerrero Composite Terrane of western Mexico: collision and subsequent rifting in a supra-subduction zone. In: Amy Draut, Peter Clift, and Dave Scholl, (eds) Formation and applications of the sedimentary record in arc collision zones, GSA Special Paper 436.
- Cerca M., Ferrari L., López-Martínez M., Martiny, B., & Iriondo, A. 2007. Late Cretaceous shortening and early Tertiary shearing in the central Sierra Madre del Sur, southern

Mexico: insights into the initiation of the Caribbean-North American plate boundary. Tectonics 26, TC3007.

De Cserna, Z., 1965, Reconocimiento geológico en la Sierra Madre del Sur de México entre Chilpancingo y Acapulco, Estado de Guerrero: UNAM. Instituto de Geología. Boletín 62, 76p.

Elías-Herrera, M., and Ortega-Gutiérrez, F., 2002, Caltepec fault zone: An Early Permian dextral transpressional boundary between the Proterozoic Oaxacan and Paleozoic Acatlán complexes, southern Mexico, and regional implications: Tectonics, v. 21, no. (3), 1013, doi: 10.1029/2000TC001278.

Elías-Herrera, M., Macías-Romo, C., Ortega-Gutiérrez, F., Sánchez-Zavala, J.L., Iriondo, A., Ortega-Rivera, A., 2007. Conflicting stratigraphic and geochronologic data from the Acatlán Complex: “Ordovician” granites intrude metamorphic and sedimentary rocks of Devonian–Permian age. Eos Transactions of the American Geophysical Union 88 (23) Joint Assembly Supplement, Abstract T41A-12.

Gómez-Tuena A., Orozco-Esquivel M.T., Ferrari L., 2005, Petrogénesis ígnea de la Faja Volcánica Transmexicana. Boletín de la Sociedad Geológica Mexicana. Volumen Conmemorativo del Centenario. Temas Selectos de la Geología Mexicana. TÓMO LVII Núm 3 227-283.

Grodzicki, K.R., Nance, J.D., Keppie, J.D., Dostal, J., Murphy, J.B., 2008, Structural, geochemical and geochronological analysis of metasedimentary and metavolcanic rocks of the Coatlaco area, Acatlán Complex, southern Mexico . In: Pereira M.F., Bozkurt E., Strachan R., and Quesada C. (Eds.). The Foundations and Birth of the Rheic Ocean: Avalonian–Cadomian Orogenic Processes and Early Palaeozoic Rifting at the Northern Gondwana, Tectonophysics 461 311-323.

Harrison, T.M., Duncan, I., McDougall, I., 1985. Diffusion of  $^{40}\text{Ar}$  in biotite: temperature, pressure, and compositional effects. Geochimica Cosmochimica Acta 49, 2461–2468.

Hinojosa-Prieto, H.R., Nance, R.D., Keppie, J.D., Dostal, J.V., Ortega-Rivera, A., Lee, J.K.W., 2008, Ordovician and Late Paleozoic-Early Mesozoic tectonothermal history of the La Noria area, northern Acatlán Complex, southern Mexico: Record of convergence in the Rheic and paleo-Pacific Oceans. In: Pereira M.F., Bozkurt E., Strachan R., and Quesada

C. (Eds.), The Foundations and Birth of the Rheic Ocean: Avalonian–Cadomian Orogenic Processes and Early Palaeozoic Rifting at the Northern Gondwana, *Tectonophysics* 461 324–342.

Keppie J.D., Dostal J., Miller B.V., Ramos-Arias M.A., Morales-Gámez M., Nance R.D., Murphy J.B., Ortega-Rivera A., Lee J.W.K., Housh T., Cooper P., 2008b, Ordovician–earliest Silurian rift tholeiites in the Acatlán Complex, southern Mexico: Evidence of rifting on the southern margin of the Rheic Ocean. In: Pereira M.F., Bozkurt E., Strachan R., and Quesada C. (Eds.), The Foundations and Birth of the Rheic Ocean: Avalonian–Cadomian Orogenic Processes and Early Palaeozoic Rifting at the Northern Gondwana Margin. *Tectonophysics* 461, 130–156.

Keppie, J.D., y Ramos, V.S., 1999. Odyssey of terranes in the Iapetus and Rheic Oceans during the Paleozoic. In: Keppie, J.D., Ramos, V.A. (Eds.), Laurentia–Gondwana Connections Before Pangea. Geological Society of America Special Paper, vol. 336, pp. 267–276.

Keppie, J.D., 2004. Terranes of Mexico revisited: a 1.3 billion year odyssey. *International Geology Review* 46, 765–794.

Keppie, J.D., Dostal, J., Cameron, K.L., Solari, L.A., Ortega-Gutiérrez, F., López, R., 2003. Geochronology and geochemistry of Grenvillian igneous suites in the northern Oaxacan Complex, southern Mexico: tectonic implications. *Precambrian Research* 120, 365–389.

Keppie, J.D., Dostal, J., Murphy, J.B., and Nance, R.D., 2008a, Synthesis and tectonic interpretation of the westernmost Paleozoic Variscan orogen in southern Mexico: from rifted Rheic margin to active Pacific margin: In: Pereira M.F., Bozkurt E., Strachan R., and Quesada C. (Eds.), The Foundations and Birth of the Rheic Ocean: Avalonian–Cadomian Orogenic Processes and Early Palaeozoic Rifting at the Northern Gondwana Margin. *Tectonophysics*. 461, 277–290.

Keppie, J.D., Nance, R.D., Fernández-Suárez, J., Storey, C.D., Jeffries, T.E., and Murphy, J.B., 2006, Detrital zircon data from the eastern Mixteca terrane, southern Mexico: evidence for an Ordovician-Mississippian continental rise and a Permo-Triassic clastic wedge adjacent to Oaxaquia: *International Geology Review*, 48, p. 97–111.

Keppie, J.D., Nance, R.D., Powell, J.T., Mumma, S.A., Dostal, J., Fox, D., Muise, J., Ortega-Rivera, A., Miller, B.V., Lee, J.W.K., 2004b. Mid-Jurassic tectonothermal event

- superposed on a Paleozoic geological record in the Acatlán Complex of southern Mexico: hotspot activity during the breakup of Pangea. *Gondwana Research* 7, 239–260.
- Keppie, J.D., Sandberg, C.A., Miller, B.V., Sánchez-Zavala, J.L., Nance, R.D., and Poole, F.G., 2004a, Implications of latest Pennsylvanian to Middle Permian paleontological and U–Pb SHRIMP data from the Tecolate Formation to re-dating tectonothermal events in the Acatlán Complex, southern Mexico: *International Geology Review*, 46, p. 745–753.
- Linnemann, U., 2003. Sedimentation and geotectonic setting of the basin development of Saxo-Thuringia (Neoproterozoic–Lower Carboniferous). In: Linnemann, U. (Ed.), *Das Saxothuringikum-Abriss der präkambrischen und paläozoischen Geologie von Sachsen und Thüringen*, vol. 48/49. *Geologica Saxonica*, pp. 71–110.
- Malone, J.W., Nance, R.D., Keppie, J.D., Dostal, J., 2002. Deformational history of part of the Acatlán Complex: Late Ordovician–Early Silurian and Early Permian orogenesis in southern Mexico. *Journal of South American Earth Sciences* 15, 511–524.
- Matte, P., 2001. The Variscan collage and orogeny (480–290 Ma) and the tectonic definition of the Armorica microplate: a review. *Terra Nova* 13, 122–128.
- McCausland P.J.A., Vander Voo R., Hall C.M., 2007, Circum-Iapetus paleogeography of the Precambrian-Cambrian transition with a new paleomagnetic constraint from Laurentia, *Precambrian Research* 156, 125–152.
- Meza-Figueroa, D.M., Ruiz, J., Talavera-Mendoza, O., Ortega-Gutiérrez, F., 2003, Tectonometamorphic evolution of the Acatlán Complex eclogites (southern Mexico), *Canadian Jouurnal of Earth Sciences*. 40 27–44.
- Middleton, M., Keppie, J.D., Murphy, J.B., Miller, B.V., Nance, R.D., Ortega-Rivera, A., Lee, J.K.W., 2007. P–T–t constraints on exumation following subduction in the Rheic Ocean from eclogitic rocks in the Acatlán Complex of southern Mexico. In: Linnemann, U., Nance, R.D., Kraft, P., Zulauf, G. (Eds.), *The Evolution of the Rheic Ocean: From Avalonian–Cadomian Active Margin to Alleghenian–Variscan Collision*. Geological Society of America Special Paper, 423, 489–509.
- Miller, B.V., Dostal, J., Keppie, J.D., Nance, R.D., Ortega-Rivera, A., and Lee, J.W.K., 2007. Ordovician calc-alkaline granitoids in the Acatlán Complex, southern Mexico:

geochemical and geochronological data and implications for tectonic of the Gondwanan margin of the Rheic Ocean. In: Linnemann, U., Nance, R.D., Zulaf, G., Kraft, P. (Eds.), The Evolution of the Rheic Ocean: From Avalonian–Cadomian Active Margin to Alleghenian–Variscan Collision. Geological Society of America Special Paper, 423, 465–475.

Morales-Gámez M., Keppie J.D., Lee J.W.K., Ortega-Rivera A., 2009, Paleozoic structures in the Xayacatlán area, Acatlán Complex, southern Mexico: transtensional rift- and subduction-related deformation along the margin of Oaxaquia: International Geology Review. 51, 279-303.

Morales-Gámez, M. Keppie J.D., y Dostal J., 2009, Carboniferous tholeiitic dikes in the Salada unit, Acatlán Complex, southern Mexico: a record of extension on the western margin of Pangea Revista Mexicana de Ciencias Geológicas, v. 26, núm. 1, 2009, p. 133-142.

Morales-Gámez, M., Keppie, J. D., Norman, M., 2008, Ordovician-Silurian rift-passive margin on the Mexican margin of the Rheic Ocean overlain by Permian periarc rocks: evidence from the Acatlán Complex, southern Mexico. In: Pereira M.F., Bozkurt E., Strachan R., and Quesada C. (Eds.), The Foundations and Birth of the Rheic Ocean: Avalonian–Cadomian Orogenic Processes and Early Palaeozoic Rifting at the Northern Gondwana Margin. Tectonophysics. 461, 291-310.

Murphy, J.B., Fernández-Suárez, J., Keppie, J.D., Jeffries, T.E., 2004. Contiguous rather than discrete Paleozoic histories for the Avalon and Meguma terranes based on detrital zircon data. Geology 32, 585–588.

Murphy, J.B., Keppie, J.D., Nance, R.D., Miller, B.V., Dostal, J., Middleton, M., Fernández-Suárez, J., and Jefferies, T.E., 2006, Geochemistry and U–Pb protolith ages of eclogitic rocks of the Asis Lithodeme, Piaxtla Suite, Acatlán Complex, southern Mexico: Tectonothermal activity along the southern margin of the Rheic Ocean: Journal of the Geological Society (London), v. 163, 683–695.

Nance, R.D., Miller, B.V., Keppie, J.D., Murphy, J.B., and Dostal, J., 2006, Acatlán Complex, southern Mexico: Record spanning the assembly and breakup of Pangea: Geology, 34, p. 857–860.

- Nance, R.D., Miller, B.V., Keppie, J.D., Murphy, J.B., Dostal, J., 2007. Vestige of the Rheic Ocean in North America: the Acatlán Complex of southern México. In: Linnemann, U., Nance, R.D., Zulaf, G., Kraft, P. (Eds.), *The Evolution of the Rheic Ocean: From Avalonian–Cadomian Active Margin to Alleghenian–Variscan Collision*. Geological Society of America Special Paper, vol. 423, pp. 437–452.
- Navarro-Santillan, D., Sour-Tovar, F., Centeno-Garcia, E., 2002, Lower Mississippian (Osagean) brachiopods from the Santiago Formation, Oaxaca, Mexico: stratigraphic and tectonic implications. *Journal of South American Earth Sciences* 15, 327–336.
- Ortega-Gutiérrez F., 1978, Estratigrafía del Complejo Acatlán en la Mixteca Baja, Estados de Puebla y Oaxaca. *Revista Mexicana de Ciencias Geológicas*. 2, 112-131.
- Ortega-Gutiérrez F., Ruiz J., Centeno-García E., 1995, Oaxaquia, a Proterozoic microcontinent accreted to North America during the late Paleozoic, *Geology*, 23, 12, 1127-1130.
- Ortega-Gutiérrez, F., 1975. The pre-Mesozoic geology of the Acatlán area, south Mexico: Ph.D. thesis, Leeds University, U.K. 166 pp.
- Ortega-Gutiérrez, F., 1993, Tectonostratigraphic analysis and significance of the Paleozoic Acatlán Complex of southern México, in Ortega-Gutiérrez, F., et al., eds., First circum-Pacific and circum-Atlantic terrane conference, Guanajuato, México: México, D.F., Universidad Nacional Autónoma de México, Instituto de Geología, p. 54–60.
- Ortega-Gutiérrez, F., Elias-Herrera, M., Reyes-Salas, M., Macias-Romo, C., López, R., 1999. Late Ordovician–Early Silurian continental collision orogeny in southern Mexico and its bearing on Gondwana–Laurentia connections. *Geology* 27, 719–722.
- Ortega-Obregón, C., Keppie, J.D., Solari, L.A., Ortega-Gutiérrez, F., Dostal, J., López, R., Ortega-Rivera, A., Lee, J.W.K., 2003. Geochronology and geochemistry of the ~917 Ma, calc-alkaline Etla granitoid pluton (Oaxaca, southern México): evidence of post-Grenvillian subduction along the northern margin of Amazonia. *International Geology Review* 45, 596–610.
- Pereira M.F., Aparaiz A., Silva J.B., Chichorro M., 2008, Tectonothermal analisys of high-temperature mylonitization in the Coimbra-Córdoba shear zone (SW Iberian Massif, Ouguela tectonic unit, Portugal): Evidencie of intra-continental transcurrent transport

during the amalgamation of Pangea. In: Pereira M.F., Bozkurt E., Strachan R., and Quesada C. (Eds.), *The Foundations and Birth of the Rheic Ocean: Avalonian–Cadomian Orogenic Processes and Early Palaeozoic Rifting at the Northern Gondwana Margin*. Tectonophysics 461, 378–394.

Pérez-Gutiérrez R., Solari L.A., Gómez-Tuena A., and Martens U., 2009, Mesozoic geologic evolution of the Xolapa migmatitic complex nort of Acapulco, southern Mexico: implication for paleogeographic reconstructions. *Revista Mexicana de Ciencias Geológicas*. 26, 1, 201–221.

Ramírez-Espinosa, J., 2001, Tectono-magmatic evolution of the Paleozoic Acatlán Complex in southern Mexico, and its correlation with the Appalachian system: Unpubl. Ph.D. thesis, University of Arizona, 170 p.

Ramírez-Espinosa, J., Ruiz, J., and Gehrels, G., 2002, Procedencia Pan-Africana en la sedimentación de la Formación Cosoltepec del Complejo Acatlán: Evidencia del margen pasivo oriental del Iapetus en el sur de México: *Actas Instituto Nacional de Geoquímica*, v. 8, no. 1, p. 181–182.

Ramos-Arias, M.A., Keppie, J.D., Ortega-Rivera, A., and Lee, J.W.K., 2008, Extensional late Paleozoic deformation on the western margin of Pangea, Patlanoaya area, Acatlán Complex, southern Mexico. *Tectonophysics*, v. 448, p. 60–76.

Riller, U., Ratschbacher, L., and Frisch, W., 1992, Left-lateral transtension along the Tierra Colorada deformation zone, northern margin of the Xolapa magmatic arc of southern Mexico: *Journal of South American Earth Sciences*, 5, 237–249.

Sánchez-Zavala, J.L., Ortega-Gutiérrez, F., Elías-Herrera, M., 2000. La orogenia Mixteca del Devónico del complejo Acatlán, sur de México. *GEOS Unión Geofísica Mexicana, Boletín Informativo Época II*, 20, No. 3, 321–322.

Sánchez-Zavala, J.L., Ortega-Gutiérrez, F., Keppie, J.D., Jenner, G.A., Belousova, E., Macías-Romo, C., 2004. Ordovician and Mesoproterozoic zircons from the Tecolate Formation and Esperanza granitoids, Acatlán Complex, southern Mexico: local provenance in the Acatlán and Oaxacan complexes. *International Geology Review* 46, 1005–1021.

Sedlock, R. L., Ortega-Gutiérrez, F., and Speed, R. C., 1993, Tectonostratigraphic terranes and tectonic evolution of Mexico: Geological Society of America Special Paper 278, 153 p.

Servicio Geológico Mexicano, 2001, Carta Geológico-Minera Orizaba E14-6 Veracruz, Puebla y Oaxaca.

Solari, L.A., Keppie, J.D., Ortega-Gutiérrez, F., Cameron, K.L., Lopez, R., Hames, W.E., 2003. 990 Ma and 1,100 Ma Grenvillian tectonothermal events in the northern Oaxacan Complex, southern Mexico: roots of an orogen. *Tectonophysics* 365, 257–282.

Solari, L.A., Torres de León, R., Hernández Pineda, G., Solé, J., Solís-Pichardo, G., and Hernández-Treviño, T., 2007, Tectonic significance of Cretaceous-Tertiary magmatic 302 M. and structural evolution of the northern margin of the Xolapa Complex, Tierra Colorada area, southern Mexico: *Geological Society of America Bulletin*, v. 119, p. 1265–1279.

Talavera-Mendoza, O., Ruiz, J., Gehrels, G.E., Meza-Figueroa, D.M., Vega-Granillo, R., and Campa-Uranga, M.F., 2005, U–Pb geochronology of the Acatlaán Complex and implications for the Paleozoic paleogeography and tectonic evolution of southern Mexico: *Earth and Planetary Science Letters*, v. 235, p. 682–699.

Tolson G., 1996, Un catálogo de indicadores cinemáticos en rocas cizalladas, GEOS, Época II, 16, 1, 1-9.

Tolson, G., 2007, The Chacalapa Fault, southern Oaxaca, Mexico, in Nieto-Samaniego, A.F., ed., *Geology of Mexico, Celebrating the Centenary of the Geological Society of Mexico*: Geological Society of America Special Paper, v. 422, p. 343–357.

Torres, R., Ruíz, J., Patchett, P.J., Grajales-Nishimura, J.M., 1999. Permo-Triassic continental arc in eastern Mexico; tectonic implications for reconstructions of southern North America. In: Bartolini, C., Wilson, J.L., Lawton, T.F. (Eds.), *Mesozoic Sedimentary and Tectonic History of north-central Mexico*: Boulder, CO. Geological Society of America, Spec. Paper. 340, pp. 191–196.

Vachard, D., and Flores de Dios, A., 2002, Discovery of latest Devonian/earliest Mississippian microfossils in San Salvador Patlanoaya (Puebla, Mexico); biogeographic and geodynamic consequences: *Compte Rendu Geoscience*, v. 334, p. 1095–1101.

Vachard, D., Flores de Dios, A., Pantoja, J., Buitrón, B.E., Arellano, J., Grajales, M., 2000. Les fusulines du Mexique, une revue biostratigraphique et paléogéographique. *Geobios* 33, 655–679.

Vega-Granillo, R., 2006, Petrología, termobarometría y análisis estructural en la región NW del Complejo Acatlán, Puebla, México: Implicaciones tectónicas, Ph.D. thesis, 344 pp., UNAM, México.

Vega-Granillo, R., Calmus T., Meza-Figueroa D., Ruiz J., Talavera-Mendoza O., and López-Martínez M., 2009, Structural and tectonic evolution of the Acatlán Complex, southern Mexico: Its role in the collisional history of Laurentia and Gondwana, *Tectonics*, 28, TC4008, doi:10.1029/2007TC002159.

Vega-Granillo, R., Talavera-Mendoza, O., Meza-Figueroa, D., Ruiz, J., Gehrels, G.E., López-Martínez, M., de La Cruz-Vargas, J.C., 2007. Pressure–temperature–time evolution of Paleozoic high-pressure rocks of the Acatlán Complex (southern Mexico): implications for the evolution of the Iapetus and Rheic Oceans. *Geological Society of America Bulletin* 119, 1249–1264.

Weber, R., 1997. How old is the Triassic flora of Sonora and Tamaulipas and news on Leonardian flora in Puebla and Hidalgo, Mexico. *RevistaMexicana de Ciencias Geológicas* 14, 225–243.

Yañez, P., Ruiz, J., Patchett, J.P., Ortega-Gutiérrez, F., and Gehrels, G.E., 1991. Isotopic studies of the Acatlán Complex, southern Mexico: implications for Paleozoic North American tectonics. *Geological Society of America Bulletin* 103, 817–828.